Abstract

Title of Document:	Activation, Multiple-Bond Cleavage, and Fixation of Small Molecules Employing Group 6 Cyclopentadienyl, Amidinate (CpAm) Complexes
	Brendan L. Yonke, Doctor of Philosophy, 2012
Directed By:	Professor Lawrence R. Sita Department of Chemistry and Biochemistry University of Maryland, College Park, MD, 20742

Small molecules (e.g. N_2, CO_2, N_2O) represent potential cheap and abundant chemical feedstocks. Despite the use of small molecules in various biosynthetic pathways, relatively few synthetic processes for the commercial utilization of small molecules exist. To investigate potential catalytic and stoichiometric methods for the activation, multiple-bond cleavage, and fixation of small molecules, Group 6 cyclopentadienyl, amidinate (CpAm) dinitrogen and multiple metal-ligand bonded complexes were investigated.

Provided the weak activation of N_2 in Group 6 dinitrogen complexes, these complexes were found to serve as M(II, d^4) and M(IV, d^2) synthons for the respective formation of Group 6 bis(carbonyl), bis(isocyanide), as well as mononuclear oxo and imido complexes. Moreover, a general route to Group 6 CpAm imido complexes of variable substitution was demonstrated upon the reaction of Group 6 CpAm dichloride complexes **48** and **49**, respectively, with lithium amides, for steric amidinate deprotonation followed amido-imido tautomerization.

Utilizing the synthesized mononuclear oxo and imido complexes various catalytic atom transfer reactions were demonstrated with their mechanistic details elucidated. These catalytic processes include the first ever oxygen atom transfer (OAT) reactions involving early transition metals including the synthesis of isocyanates from N_2O and isocyanides, light-mediated degenerate OATs between CO_2 and CO, and light-mediated non-degenerate OATs involving N_2O and CO. Likewise, thermal-mediated nitrogen atom transfer (NAT) reactions were shown for the synthesis of isocyanates from organic azides (N_3R) and CO. Key to this observed reactivity was the ability of multiply bonded metal ligands to undergo reaction with adjacent Lewis acidic ligands with this reactivity having been found to likewise facilitate interligand silyl group transfer in π-loaded Group 6 CpAm oxo trimethylsilyl imido complexes.

Despite direct utilization of the small molecules N_2O and CO_2 in OAT reactions, NAT reactions were found to require the use of organic azides. Therefore, in an effort to directly utilize N_2 in NAT reactions, a novel photolytic N-N cleavage process was devised for the Group 6 dinitrogen complexes **52** and **53**. This novel phot$_o$lytic N-N cleavage represents the first time a ligand set has been shown to facility distinctly different N-N cleavage mechanisms for N_2 bound to different metals.

Layman Abstract

The Earth's atmosphere is composed of various gases like nitrogen and carbon dioxide. Provided the abundance of these gases, biological systems (e.g. bacteria, plants) have evolved different means of utilizing these gases for the production of chemicals that are needed to sustain life. Key to these biological processes is the ability to produce the needed chemicals without having to expend substantial amounts of energy. In this research, we take inspiration from this biological utilization of atmospheric gases by using organometallic transition metal complexes for the production of commercially relevant chemicals without the input of large amounts of energy. In practice, this process involved the removal of individual atoms from these gases followed by the transfer of the excised atoms to organic molecules. To facilitate this process, novel methods for both the removal of atoms from gases and the transfer of these atoms to organic molecules were devised. Significant achievements include the production of chemicals used to make polymers and pesticides as well as the use of gases that are responsible for global warming.

Activation, Multiple-Bond Cleavage, and Fixation of Small Molecules Employing Group 6 Cyclopentadienyl, Amidinate (CpAm) Complexes

By

Brendan Louis Yonke

Dissertation submitted to the Faculty of the Graduate School of the
University of Maryland, College Park, in partial fulfillment
of the requirements for the degree of
Doctor of Philosophy
2012

Advisory Committee:

Professor Lawrence R. Sita (Chair)
Professor Philip DeShong
Professor Bryan W. Eichhorn
Professor Andrei N. Vedernikov
Professor Nam S. Wang

This thesis is dedicated to my loving wife and family. Without their love and support I would not have been able to complete this thesis.

Acknowledgements

I would like to thank my advisor, Professor Lawrence R. Sita, for his guidance during my doctoral studies at the University of Maryland. During my four years of research, he provided me with invaluable advice and offered me the opportunity to grow and mature as a scientist and individual. As a mentor he has allowed me pursue novel research programs and provided me with encouragement to persevere when my ideas didn't work. I am forever indebted to him for the assistance he provided me during my time at the University of Maryland.

I want to extend my thanks to my thesis committee members, Dr. Philip DeShong, Dr. Bryan W. Eichhorn, and Dr. Andrei N. Vedernikov. While at the University of Maryland, I had the privilege to have all of them serve as my teachers and mentors. Their graduate chemistry classes formed the basis of my chemical knowledge and their insights into chemistry have been invaluable to the ideas and theories of my own doctoral research. I would also like to thank Dr. Nam Sun Wang for graciously serving as the Dean's Representative on my thesis committee.

I would like to thank Dr. Yui-fai Lam, Dr. Yinde Wang, Dr. Peter Zavalij, and Dr. Yue Li for assisting me with countless NMR, mass spectroscopy, and X-Ray diffraction experiments. Their expertise has enabled all of my experiments and their advice and insights have been invaluable to my research.

I want to thank Dr. Janice Ruett-Robey and Mrs. Natalia White. Both were instrumental in my reception of the Graduate Assistance in Areas of National Need (GAANN) Fellowship during my fourth year of graduate school. This financial support allowed me to focus on research in my final year of school, facilitating some of the most significant discoveries of my doctoral research.

I wish to thank all of the current and former members of the Sita Group: Monisha Paris, Mary Walker, Daniel Redman, Xiaohang Liu, Emily Trunkley, Rennisha Wickham, Jia Wei, Wonseok Hwang, Andrew Keane, Cathryn Gail Blakley, Wesley Farrell, Kaitlyn Crawford, Dr. Jonathan Reeds, Dr. Phil Fontaine, and Dr. Masakazu Hirotsu. Collectively, they have provided me with countless suggestions for my research and helped me persevere through the toughest times in graduate school. It has been wonderful to work with and alongside such smart and driven people without whom I would have not been able to accomplish anything.

Finally, I would like to thank all of my close friends and family, especially my wife Megan. They have supported me through the best times and the worst times my entire life. They have encouraged me to pursue my dreams and I could not have done any of this without them.

Table of Contents

List of Tables

List of Figures

List of Schemes

List of Abbreviations

d	days
eq	equivalents
h	hours
^{i}Pr	*iso*-propyl
LAH	lithium aluminum hydride
Me	methyl
Na/Hg	sodium amalgam
nBu	n-butyl
Ph	phenyl
R	alkyl substituent
RT	room temperature
TMS	trimethylsilyl
^{t}Bu	*tert*-butyl
xs	excess

Chapter 1: Small Molecule Activation, Cleavage, and Fixation

1.1 Bioinspiration of Small Molecule Cleavage and Activation

Small molecules like dinitrogen (N_2) (78%), oxygen (O_2) (21%), and carbon dioxide (CO_2) (0.04%) represent the most abundant components of Earth's atmosphere. As a result, these small molecules have the potential to serve as cheap abundant chemical feedstocks for the synthesis of fine and commodity chemicals. Nonetheless, while O_2 has found widespread use through aerobic oxidation chemistry, other abundant small molecules, like N_2 and CO_2 have found substantially fewer applications in chemical processes.[1] Despite this paucity, biological processes have evolved to utilize these abundant small molecules in biosynthetic processes like nitrogen fixation and the Calvin Cycle. Therefore, the development of processes capable of converting small molecules like N_2 into useful organic compounds has been an area of intense academic interest for the past fifty years.

Currently, N_2 is converted into ammonia (NH_3), the primary chemical feedstock for the incorporation of nitrogen into fine and commodity chemicals, by the Haber Bosch process through reaction with hydrogen (H_2), $N_2\,(g) + 3\,H_2\,(g) \rightarrow 2\,NH_3\,(g)$, at extreme temperatures (600 – 800 K) and pressures (500 atm). The extreme temperatures for this process are needed to facilitate the dissociation of N_2 (BDE_{N2} = 945 kcal/mol) on the surface of an iron, ruthenium, or alloyed catalyst. While high temperatures are needed to facilitate N_2 dissociation, the enthalpy for the reaction of N_2 with H_2 to form NH_3, ΔH = -10.97 kcal/mol, is outweighed by entropic factors at high temperatures. Therefore, extreme reaction pressures are needed to shift this reaction to completion and facilitate higher more practical catalytic rates of turnover.[2]

Contrasting these extreme reaction conditions for the Haber Bosch process, biological systems have developed significantly less energy intensive routes to the synthesis of NH_3 through processes that occur at ambient temperature and atmospheric pressure. Therefore, substantial effort has been extended to understand the mechanism of N_2 fixation in biological systems. The most widely studied nitrogenase enzyme is the molybdenum iron (Mo/Fe) nitrogenase. This enzyme is composed of two components, an iron sulfur cluster containing iron protein and a molybdenum iron protein. For this enzyme, the iron protein is believed to mediate electron transfer from more ubiquitous external biological reductants to the molybdenum iron protein for the subsequent reduction of substrates in the enzyme active site.[3] The result is the reduction of N_2 to NH_3 in an ATP-hydrolysis dependent pathway according to the equation $N_2 + 18\ H^+ + 8\ e^{-1} + 16\ ATP \rightarrow 2\ NH_3 + H_2 + 16\ ADP + 16\ P_i$. The reduction of N_2 in this process is believed to occur through sequential reduction and protonation steps ultimately leading to the formation of NH_3. Of significant importance to the characterization of this nitrogenase is the structural characterization of the Mo/Fe nitrogenase active site, which was recently revised in 2011, as detailed in Figure 1.[4]

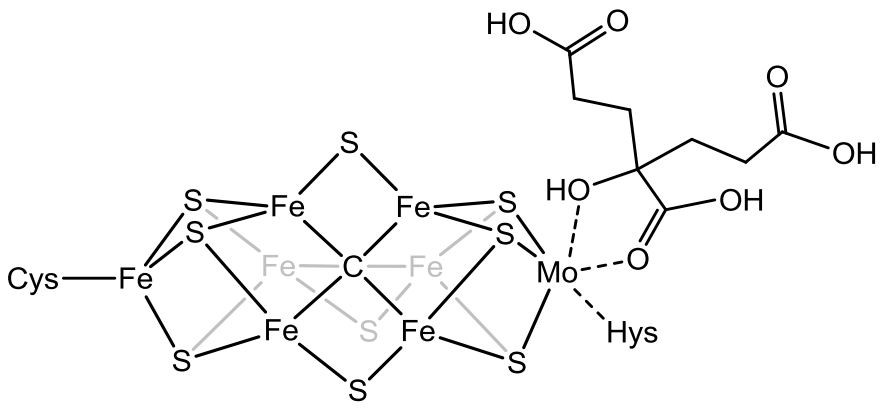

Figure 1: Structure of the molybdenum iron nitrogenase active site and the associated amino acid and homocitrate ligands.

Yet, despite structural characterization of the active site as well as determination of the requirements for the production of NH_3 from N_2, there remains no empirical evidence for the mechanism of nitrogenase catalytic activity (e.g. small molecule activation, bond breaking, M-N bond reactivity). As a result, various groups have sought to undertake fundamental studies on the possible mechanisms of N_2 reduction to NH_3 at ambient temperatures and pressures. Although informed by the structure of the Mo/Fe nitrogenase enzyme, these studies encompass a wide range of methods for the binding, multiple-bond cleavage, and fixation of N_2 provided the observation of different metals (e.g. Mo, V, Fe) and structural diversity of naturally occurring nitrogenase enzymes.[5]

1.2 Dinitrogen Activation and Fixation in Organometallic Complexes

Dinitrogen complexes are typically synthesized through the reduction of high valent transition metal complexes (e.g. halides) in the presence of N_2 using reducing agents (e.g. Na, Mg, K, Li, Zn). For these complexes the activation and fixation of N_2 in

organometallic complexes is characterized by three basic steps, the binding and activation of N_2, the ability to react either multiple N-N or M-N bonds, and the release of nitrogen containing products from the metal center. Provided the weak σ-donor and π-acceptor nature of N_2, stable binding and activation of N_2 by organometallic complexes requires back donation by the metal center into the π* molecular orbitals of N_2. Such binding requires the presence of available d electrons on the metal center and preferably a supporting ligand framework (e.g. sulfides) that undergoes π-donation to the metal center for increased electron density at the metal center in analogy to the observed Mo/Fe nitrogenase active site.[6] The result of this back donation is a dinitrogen ligand of decreased bond order that can assume various potential N_2 binding motifs, depicted in Figure 2, with the extent of N_2 activation characterized by the N-N bond length, as determined by X-Ray crystallography, in comparison to analogous N_xH_y compounds (e.g. N_2 having a bond order of three where d(N-N) = 1.098 Å, *trans*-diazene, N_2H_2, having a bond order of 2 where d(N-N) = 1.247 Å, hydrazine, N_2H_4, having a bond order of 1 where d(N-N) =1.470 Å).[7]

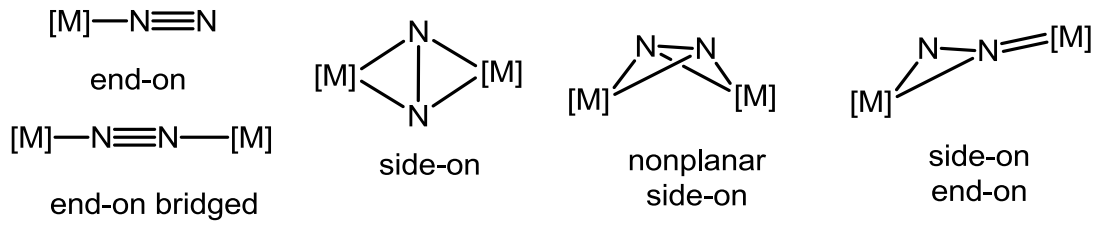

Figure 2: Potential dinitrogen binding motifs to transition metal centers.

Of these known N_2 binding motifs, the end-on and end-on bridged dinitrogen binding modes are the most commonly observed. In the case of the end-on binding mode, end-on dinitrogen ligands almost uniformly exhibit N-N bond lengths of ~1.10 A, while

the end-on bridged and side-on bridged motifs can exhibit a range of N-N bond lengths as well as respective MNN angles and MNNM dihedral angles depending on the extent of N_2 activation and the nature of metal center and supporting ligand framework. Moreover in theoretical studies, the side-on dinitrogen binding motif is proposed to only be viable for transition metals in the lower left corner of the Periodic Table.[8]

1.3 Mononuclear Dinitrogen Activation and Fixation

In an effort to determine the potential binding site for N_2 in the Mo/Fe nitrogenase active site, isolated nitrogenase was reacted with the isoelectronic cyanide (CN^-) ligand with this ligand having been found to coordinate to the molybdenum metal center of the molybdenum iron protein as determined by extended X-Ray absorption fine structure (EXAFS) studies.[9] Seeking to mimic the proposed nitrogenase binding mode for N_2, mononuclear dinitrogen complexes have been studied as a possible means of achieving nitrogenase activity with discrete organometallic complexes. In research pioneered by Hidai and co-workers, end-on dinitrogen complexes, *trans*-$[M(N_2)_2(dppe)_2]$ (**1**) where M = Mo and W, exhibiting nucleophilic reactivity at the β-nitrogen of the dinitrogen ligand could be reacted with electrophiles (e.g. H^+, aldehydes, acyl chloride) for the formation of terminal hydrazido complexes.[10] In the case of the hydrazido complexes trans-$[MF(NNH_2)(dppe)_2][BF_4]$ (**2**) where M = Mo and W, derived from the reaction of **1** with HBF_4, these complexes were found to undergo condensation reactions with 2,5-dimethoxytetrahydrofuran to yield the pyrrolylimido complexes, *trans*-$[MF(NNCH{=}CHCH{=}CH)(dppe)_2]$ $[BF_4]$ (**3**), where M = Mo and W. The reaction of **3**

with lithium aluminum hydride (LAH) was subsequently found to reductively eliminate pyrrole and ammonia for the production of a tetrahydride complex $M(H)_4(dppe)_2$ (**4**) capable of reforming the dinitrogen complexes, **1**, in an atmosphere of N_2 under photolytic conditions.[11] Collectively, these results demonstrated the first stoichiometric synthetic method for the activation and fixation of N_2 as depicted in Scheme 1.

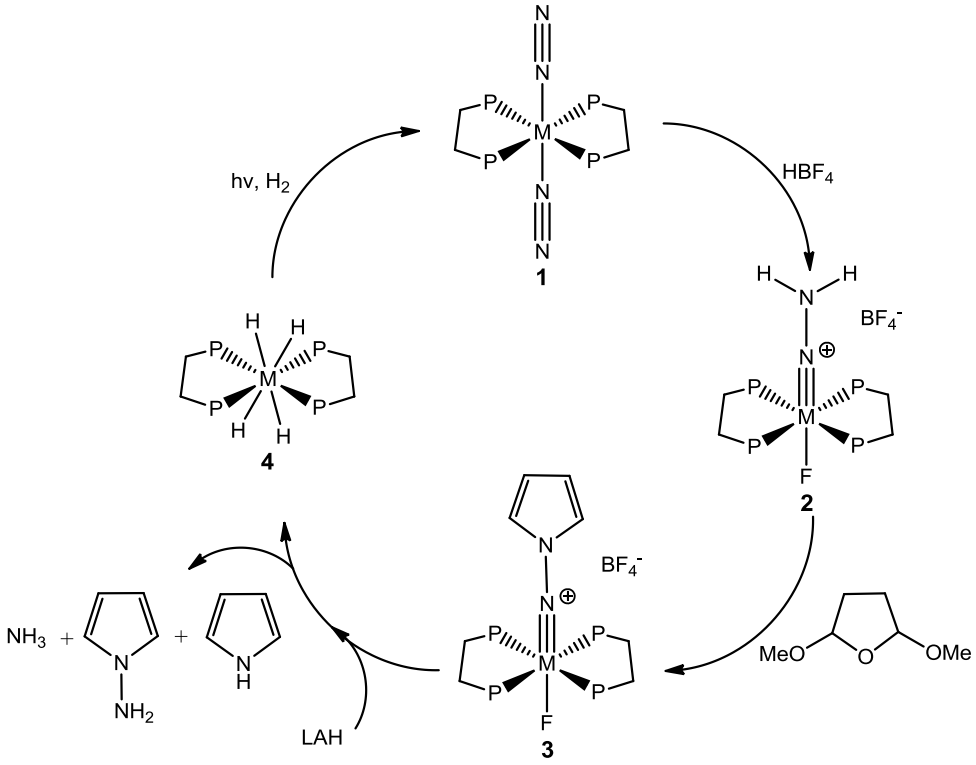

Scheme 1: Stoichiometric cycle for the formation of pyrrole and ammonia from dinitrogen.

Further proving the versatility of end-on mononuclear complexes, Hidai and co-workers have shown that the related end-on complex *cis*-$[W(N_2)_2(PMe_2Ph)_4]$ (**5**) could be reacted with $[RuCl(dppp)_2]X$ (**6**), where X = PF_6, BF_4, and OTf, in the presence of H_2 for the formation of NH_3. Provided the established ability of **6** to react with H_2 for the reversible formation of the weakly acidic complex, $[RuCl(\eta^2\text{-}H_2)(dppp)_2]X$ (**7**), and the

observation of the hydride complex $[RuCl(H)(dppp)_2]X$ (**8**) from the reaction of **5** and **6** under an H_2 atmosphere, NH_3 is presumed to result from the nucleophilic attack of **5** on **7**. Although similarly stoichiometric in nature, this research served as a proof of concept that N_2 could be reacted with H_2 for the formation of NH_3, in analogy to the Haber-Bosch process, through the use of discrete organometallic complexes.[11]

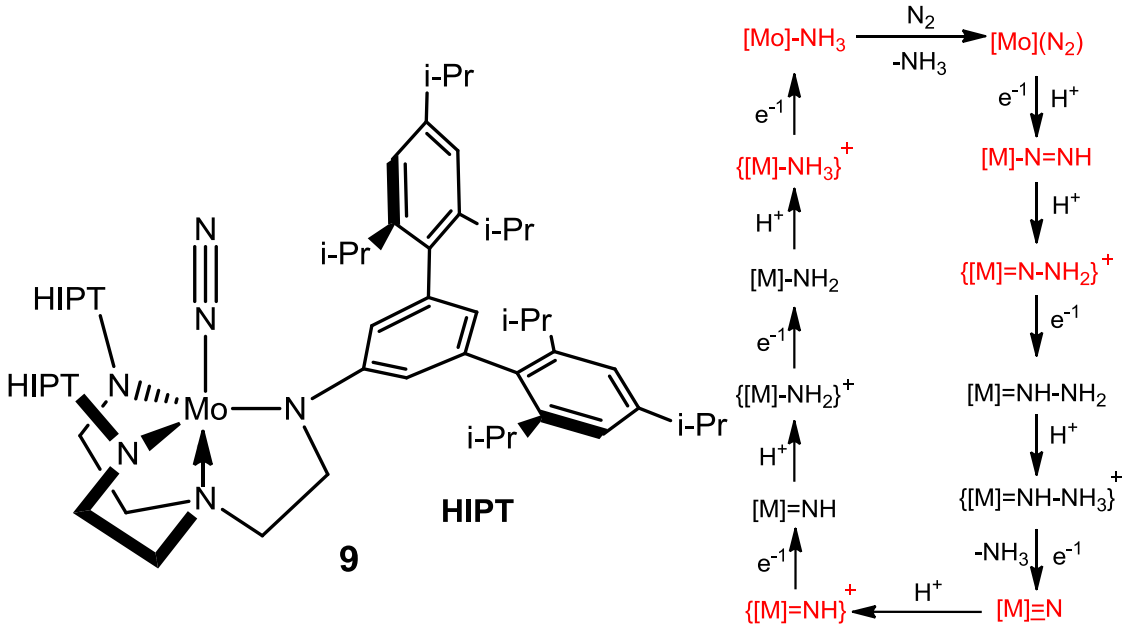

Figure 3: Proposed catalytic cycle for the reduction of dinitrogen to ammonia using [lutidinium] $[BAr^F]$ and Cp^*_2Cr with proposed intermediate complexes that have been isolated and characterized indicated in red.

Furthering the reduction of N_2 using mononuclear dinitrogen complexes, Schrock and co-workers' research on the trisamidoamine ligand, $[(RNCH_2CH_2)N]^{3-}$, has found that mononuclear, $[(RNCH_2CH_2)N]Mo(N_2)$, versus dinuclear, $\{[(RNCH_2CH_2)N]Mo\}_2(\mu\text{-}\eta^1\text{:}\eta^1\text{-}N_2)$ dinitrogen complexes could be synthesized using the bulky hexaisopropylterphenyl (HIPT) substituent (R = 3,5-(2,4,6-$^i Pr_3C_6H_2)_2C_6H_3$).[12] When the mononuclear complex [HIPTN3N]Mo(N_2) (**9**) was reacted with [lutidinium][BAr^F] and

decamethylchromocene (Cp^*_2Cr) in heptane this complex was found to produce 7-8 equivalents of NH_3, a catalytic efficiency of ~65%. The catalytic reduction of N_2 by **9** is proposed to occur through a series of protonation and reduction steps, similar to the proposed reactivity of the Mo/Fe nitrogenase, as supported by the isolation, characterization, and independent synthesis of proposed catalytic intermediates, as seen in Figure 3, some of which were likewise found to be catalytically competent. In order to achieve turnover a fine balance of the solubility of the proton source, [lutidinium][BAr^F], along with the gradual addition of the reducing agent, Cp^*_2Cr, was required to prevent short-circuiting of the catalytic cycle through the formation of H_2. Here, the bulk of the aryl substituents for the triamidoamine ligand were found to be critical to the shielding of the metal center for the prevention of metal hydride formation while also allowing protic reagents sufficient access to the active site and helping to maintain the solubility of proposed salt intermediates.

1.4 Multinuclear Dinitrogen Activation and Fixation

Despite the ability to synthesize NH_3 through sequential protonation and reduction reactions involving the mononuclear trisamidoamine system reported by Schrock and co-workers, efforts to optimize this catalytic system have failed to yield increased catalytic turnover. Therefore, various groups have sought to investigate non-biomimetic methods for the activation of N_2 including the use multinuclear complexes.[14]

1.4.1 Activation and Cleavage of Dinitrogen in Molybdenum Trisamido Complexes

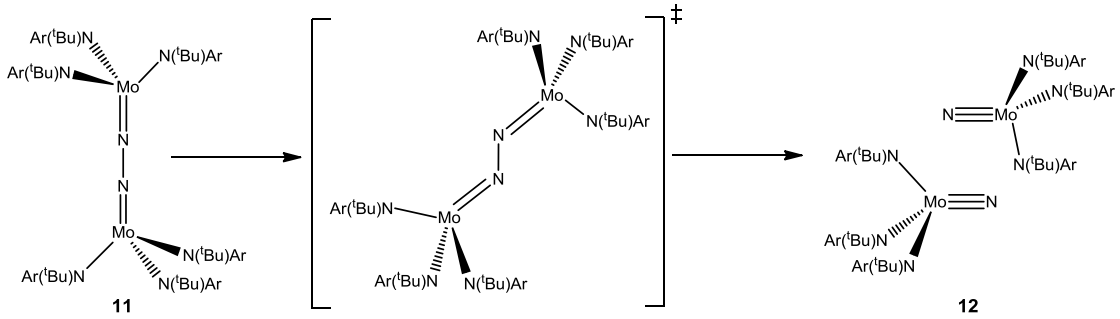

Scheme 2: Thermal cleavage of dinitrogen in trisamido complexes reported by Cummins and co-workers.

Of principle importance for the multinuclear activation of N_2 is the molybdenum trisamido complex, $Mo[N(^tBu)Ar]_3$ (**10**), where Ar = 3,5-$C_6H_3Me_2$. In the presence of N_2, **10** was found to bind N_2 for the formation of an end-on bridged complex, $\{Mo[N(^tBu)Ar]_3\}_2(\mu\text{-}\eta^1\text{:}\eta^1\text{-}N_2)$ (**11**), that thermally cleaves the final N-N bond of the dinitrogen ligand for the formation of two equivalents of the mononuclear nitrido complex $NMo[N(^tBu)Ar]_3$ (**12**) as shown in Scheme 2.[15] Here, the observed reactivity of **11** is of substantial importance as it represents the first demonstration of N_2 cleavage at ambient temperatures through the use of discrete organometallic complexes. Like the related mononuclear trisamidoamine complex **9**, the reactivity of this related system is believed to be facilitated by the bulky amido ligands that preclude the dimerization of **10** as well as **12** through steric shielding while providing N_2 access to the metal center. In analyzing the rate for the thermal cleavage of **11** to **12**, Eyring analysis of this process determined the activation parameters for cleavage to be $\Delta H^{\ddagger} = 23.3 \pm 0.3$ kcal/mol and $\Delta S^{\ddagger} = 2.9 \pm 0.8$ kcal/mol K. These parameters appear to be in good agreement with a

'zig-zag' transition state predicted by Morokuma and co-workers that facilitates the conversion of the open shell complex **11** having a triplet state to the closed shell complex **12** having a singlet state.[16]

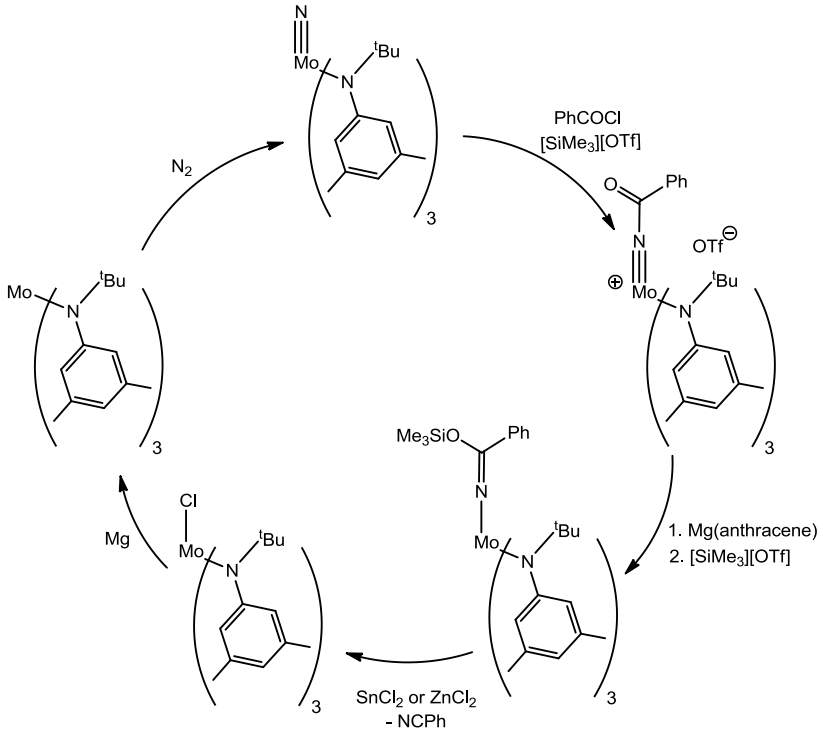

Scheme 3: Synthetic path for the regeneration of the trisamido complex **10** from the nitrido trisamido complex **12** reported by Cummins and co-workers.

Having demonstrated the first thermal cleavage of N_2 at ambient temperature, Cummins and co-workers sought to develop methods for nitrogen atom transfer to regenerate the trisamido complex, **10**, for binding and cleaving additional equivalents of N_2. Although initial results demonstrated quantitative irreversible nitrido transfer from the related nitrido trisalkoxide complex $NMo(O^tBu)_3$ (**13**) to **10** for the formation of **12**, the analogous trisalkoxide $Mo(O^tBu)_3$ (**14**) was found to be incapable of cleaving N_2 in the absence of **10** while also being subject to self-dimerization.[17] Nevertheless, a novel stoichiometric synthetic cycle for the regeneration of **10** through the conversion of the

nitrido ligand to a nitrile has been reported with this cycle shown in Scheme 3.[18] Key aspects of this synthetic cycle include the reaction of **12** with an acyl chloride in the presence of trimethylsilyl triflate ([TMS][OTf]) as a Lewis acid catalyst as well as the cleavage of M-N bonds though the reaction of an anionic keto-imido complex with [TMS][OTf].

1.4.2 Activation and Cleavage of Dinitrogen in Group 4 and 5 Amido Phosphine Complexes

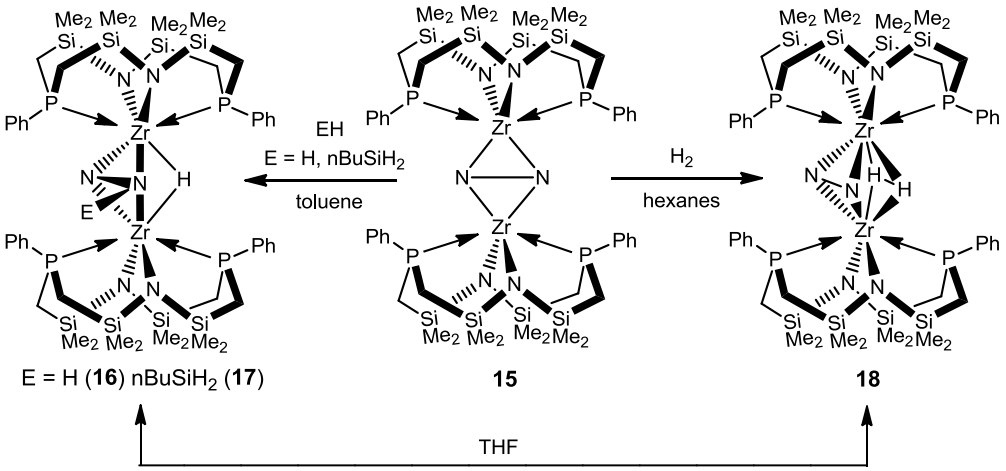

Scheme 4: Reaction of a side-on dinitrogen ligand with hydrogen reported by Fryzuk and co-workers.

The harsh reaction conditions required for nitrogen atom transfers involving **12** demonstrate the inherent strength of M-N bonds for early transition metals following N_2 cleavage. As a means of removing this potential energetic barrier to catalytic turnover, various groups have sought to develop strategies by which N_2 activation could be used to directly perform N_2 fixation reactions involving mild reagents and conditions. In order to

achieve this goal, N_2 binding motifs that place a significant amount of electron density on the nitrogen atoms are desired. In research by Fryzuk and co-workers, a side-on dinitrogen complex $\{Zr[P_2N_2]\}_2(\mu\text{-}\eta^2\text{:}\eta^2\text{-}N_2)$ (**15**), where $[P_2N_2]^{2-}$ is the macrocyclic amido phosphine ligand $PhP(CH_2SiMe_2NSiMe_2CH_2)_2PPh$, was found to exhibit a N-N bond length, 1.43(1) Å, that is nearly equal to the N-N bond length of hydrazine. The reaction of this complex in toluene with either H_2 or n-butyl silane ($nBuSiH_3$) was found to yield nitrogen functionalized complexes having a bridging hydride ligand, $\{Zr[P_2N_2]\}_2(\mu\text{-}\eta^2\text{:}\eta^2\text{-}N_2E)(\mu\text{-}H)$, where E = H (**16**) and $nBuSiH_2$ (**17**). Moreover, repeat of the reaction of **15** with H_2 in hexane was found to provide an intermediate complex, $\{Zr[P_2N_2]\}_2(\mu\text{-}\eta^2\text{:}\eta^2\text{-}N_2)(\mu\text{-}\eta^2\text{:}\eta^2\text{-}H_2)$ (**18**), having nonplanar side-on dinitrogen and hydrogen ligands, which in an THF solution appears to be in reversible equilibrium with **16** through the nucleophilic attack of the side-on dinitrogen ligand on the coordinated hydrogen ligand. This observed reactivity of **15** with H_2 is of significance in that it represents the first reported reaction of N_2 with H_2 in discrete organometallic complexes.[19]

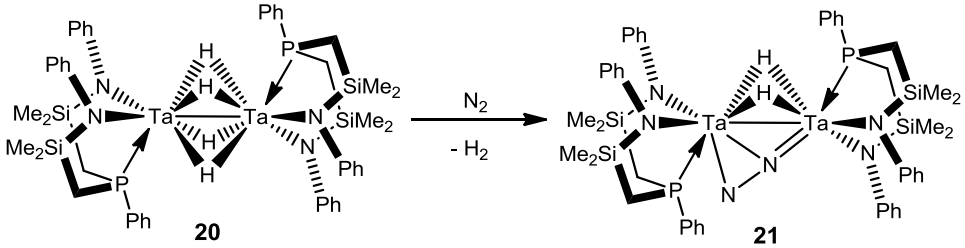

Scheme 5: Formation of a side-on, end-on dinitrogen complex following the reductive elimination of hydrogen as reported by Fryzuk and co-workers.

In an effort to investigate metal dependent trends for N_2 activation, Fryzuk and co-workers reacted the related less bulky $[NPN]^{2-}$ ligand, $PhP(CH_2SiMe_2NPh)_2$, with

$TaMe_3Cl_2$ as a means of synthesizing Group 5 analogs having a similar degree of metal coordinative saturation. Upon hydrogenolysis of the resulting trimethyl complex, [NPN]$TaMe_3$ (**19**), a bridging tetrahydride complex {[NPN]Ta}$_2$(μ-H)$_4$ (**20**) was formed. Under a N_2 atmosphere **20** was found to undergo reaction with N_2 following the reductive elimination of H_2 for the formation of a novel side-on, end-on dinitrogen complex, {[NPN]Ta}$_2$(μ-H)$_2$(μ-η^1:η^2-N_2) (**21**). Structural and computational analysis of **21**, predicted multiple M-N bond character for the end-on bound nitrogen atom as well two single M-N bonds for the terminal side-on bound nitrogen atom, suggesting the localization of significant amounts of electron density on the terminal side-on bound nitrogen atom.

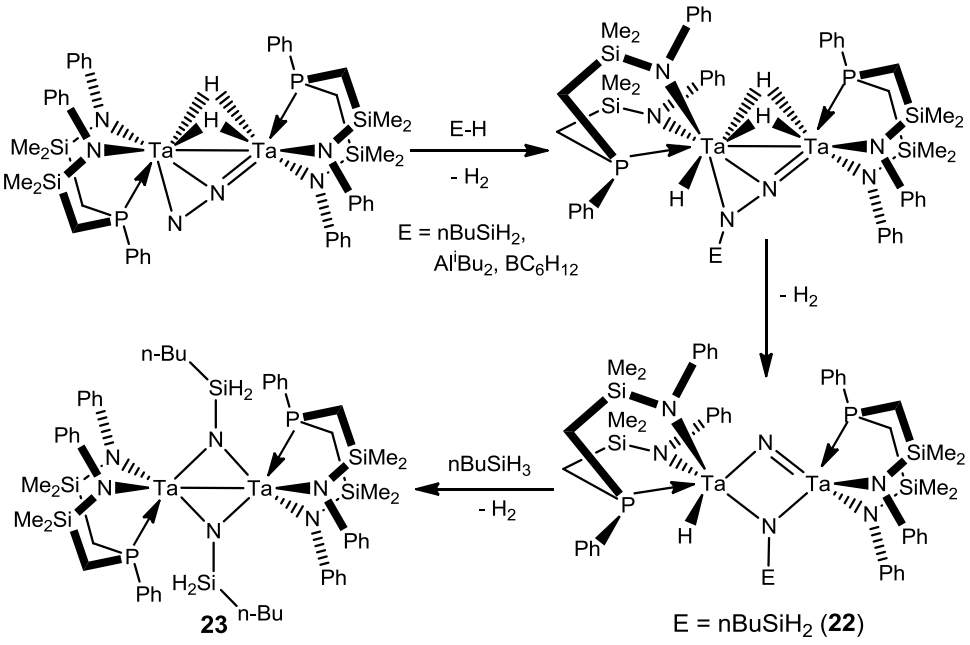

Scheme 6: Reaction of the side-on, end-on dinitrogen complex reported by Fryzuk and co-workers with Lewis acidic hydride reagents.

The unexpected formation of **21** is of significance in that it represents the first known formation of a dinitrogen complex without the need for an external reducing agent

(e.g. potassium graphite, sodium amalgam). Provided the localization of electron density on the terminal nitrogen atom of **21**, it was theorized that a catalytic cycle for the formation of either N_2H_4 or NH_3 could be achieved through 1, 2-addition of electrophilic hydrides across the M-N bonds of **21** for the regeneration of **20**. Through a survey of reactivity, various electrophilic hydrides (e.g. 9-BBN, aluminum hydrides, silanes) were found to undergo 1, 2-addition across the M-N bond of the terminal nitrogen atom of **21** followed by an unexpected cleavage of the final N-N bond upon reductive elimination of the remaining bridging hydrides as depicted in Scheme 6. While phenyl silane and $nBuSiH_3$ were observed to undergo clean reactions with **20**, boron and aluminum hydride reaction products were found to undergo further reactions with the supporting NPN ligand framework. Moreover, reaction of the n-butyl silylated N-N cleavage complex {[NPN]Ta(H)}(μ-N)(μ-$nBuSiH_2N$){[NPN]Ta} (**22**) with an additional equivalent of $nBuSiH_3$ was found to provide the bridging imido complex {[NPN]Ta(μ-$nBuSiH_2N$)}$_2$ (**23**) although further reaction of this complex with excess $nBuSiH_3$ only resulted in decomposition thereby precluding the theorized catalytic cycle.

1.4.3 Activation of Dinitrogen in Group 4 Metallocenes

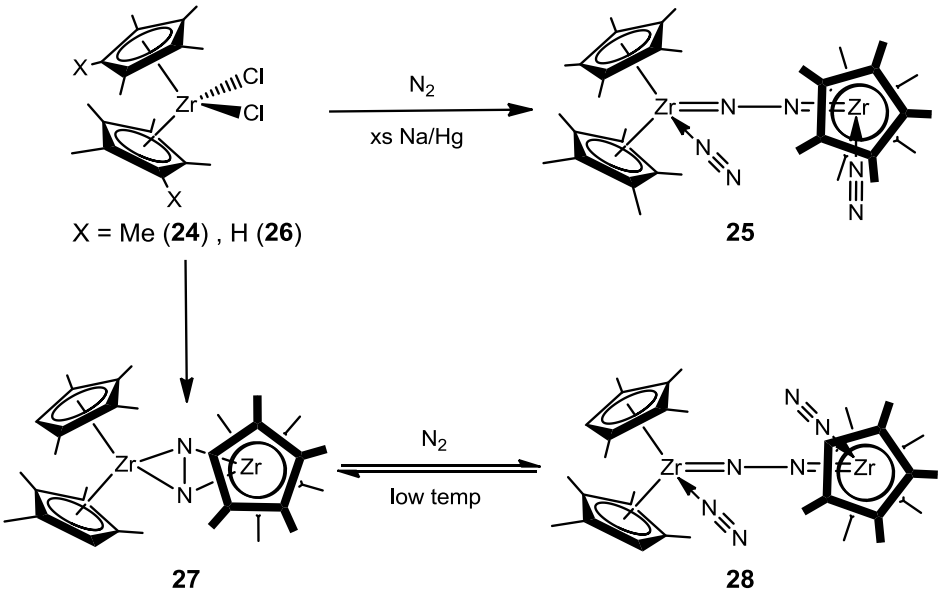

Scheme 7: Comparison of side-on versus end-on dinitrogen bonding motifs in tetramethylcyclopentadienyl and pentamethylcyclopentadienyl metallocene dinitrogen complexes respectively synthesized by Chirik and Bercaw.

Provided the reactivity of side-on dinitrogen ligands having electron density localized on nitrogen atoms, various groups sought to synthesize and investigate the reactivity of side-on dinitrogen complexes. One particular target of interest included the development of side-on dinitrogen complexes for the ubiquitous metallocene supporting ligand framework. In early work by Bercaw and co-workers, reduction of the zirconium metallocene dichloride complex,$Cp^*_2ZrCl_2$ (**24**) in the presence of N_2 was found to yield a complex, $\{Cp^*_2Zr(N_2)\}_2(\mu\text{-}\eta^1\text{:}\eta^1\text{-}N_2)$ (**25**), containing weakly activated end-on and end-on bridged dinitrogen ligands. In contrast to this result, the related *ansa*-metallocene framework was found to yield a side-on dinitrogen complex $[Zr\{rac\text{-}Me_2Si(C_5H_2\text{-}2\text{-}SiMe_3\text{-}4\text{-}^tBu)_2\}]_2(\mu\text{-}\eta^2\text{:}\eta^2\text{-}N_2)$, following the reductive elimination of H_2 from the precursor complex $Zr\{rac\text{-}Me_2Si(C_5H_2\text{-}2\text{-}SiMe_3\text{-}4\text{-}^tBu)_2\}(H)_2$. Suspecting side-on

coordination as a result of reduced sterics, Chirik and co-workers substituted the pentamethylcyclopentadienyl ligand (Cp^*) for the less bulky tetramethylcyclopentadienyl (Cp') ligand with reduction of the dichloride complex Cp'_2ZrCl_2 (**26**) providing the desired side-on dinitrogen complex $\{Cp'_2Zr\}_2(\mu\text{-}\eta^2\text{:}\eta^2\text{-}N_2)$ (**27**) exhibiting an strongly activated N-N bond length of 1.377(3) Å. Interestingly, upon the cooling of solutions of **27** to low temperature in the presence of N_2, this complex was found to form a dinitrogen complex, $\{Cp'_2Zr(N_2)\}_2(\mu\text{-}\eta^2\text{:}\eta^2\text{-}N_2)$ (**29**), containing both end-on and end-on bridged dinitrogen ligands analogous to complex **24** reported by Bercaw. These low temperature studies suggested the thermodynamic stability **28** with this complex potentially having a transient presence in solution.

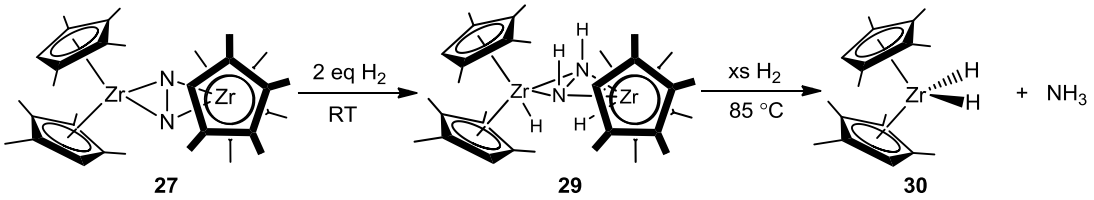

Scheme 8: Reaction of hydrogen with the side-on dinitrogen ligand in the tetramethylcyclopentadienyl metallocene complex reported by Chirik and co-workers.

Given substantial N-N bond elongation, complex **27** was reacted with an excess of H_2 at room temperature to provide the bridged diazene dihydride complex $\{Cp'_2Zr(H)\}_2(\mu\text{-}\eta^2\text{:}\eta^2\text{-}N_2H_2)$ (**29**) as the result of the reaction with two equivalents of H_2. Moreover, when **29** was gently warmed to 85 ˚C in the presence of H_2, small amounts of NH_3, yield = 10-15%, were found to be produced along with the corresponding dihydride complex Cp'_2ZrH_2 (**30**). Although the formation of NH_3 from **29** occurs by an unknown mechanism, computational analysis of the structure of **27** suggests significant overlap between metal centered orbitals and the perpendicular π* molecular orbital for the side-

on dinitrogen ligand. The result is substantial M-N multiple bond character that is then believed to facilitate 1,2-addition reactivity similar to that observed for the π-loaded mononuclear zirconocene imido complexes reported by Bergman and co-workers.[21] However, provided the believed presence of a transient end-on bridged dinitrogen complex in solution as well as the ability for end-on bridged bis(indenyl) zirconium dinitrogen complexes to experience similar reactivity with H_2, it is not conclusively known whether **27** or a transient end-on bridged dinitrogen species is responsible for the observed reactivity.[22]

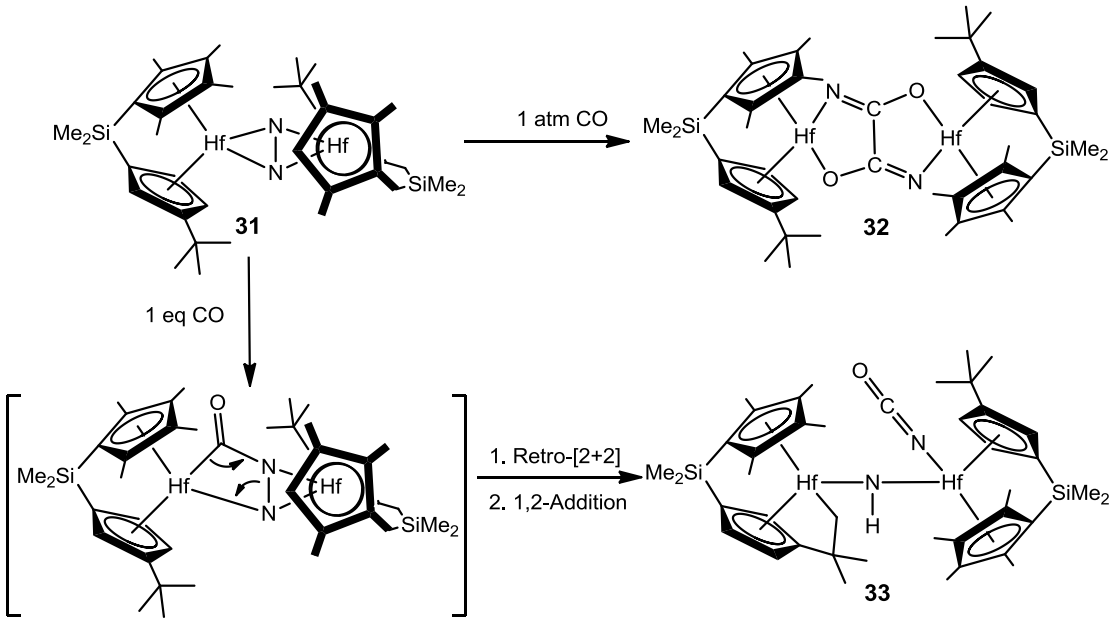

Scheme 9: Ligand-mediated cleavage of the final N-N bond of a side-on dinitrogen ligand through insertion of carbon monoxide followed by retro [2+2] cycloaddition.

Regardless of the reactivity of **27** with H_2, due to the Group 4 nature of the metal centers, this complex lacks the requisite six electrons required to cleave the final N-N bond of dinitrogen. Despite this lack of electrons, when the hafnium hybrid *ansa*-metallocene side-on dinitrogen complex $[Hf\{Me_2Si(C_5Me_4)(C_5H_3\text{-}3\text{-}^tBu)\}]_2(\mu\text{-}\eta^2\text{:}\eta^2\text{-}N_2)$

(**31**) was reacted with carbon monoxide (CO) at atmospheric pressure a hafnium bridging oxamide complex [Hf{$Me_2Si(C_5Me_4)(C_5H_3$-3-$^tBu)$}]$_2$(μ-$N_2C_2O_2$) (**32**) was discovered to form. To probe the origin of this apparent simultaneous N-N cleavage coupled with N-C bond formation, **31** was reacted with 1 equivalent of CO for the formation of a dinuclear NH-bridged hafnium "tuck-in" complex {Hf[$Me_2Si(C_5Me_4)(C_5H_3$-3-$^tBu)$}](NCO)(μ-NH)[Hf{$Me_2Si(C_5Me_4)(C_5H_3$-3-$CMe_2CH_2)$}] (**33**). The formation of **33** is rationalized to occur through the insertion of CO into the M-N bond of the side-on dinitrogen ligand followed by a retro-[2+2] cycloaddition for the formation of an isocyanate ligand and a bridging nitrido ligand that undergoes 1, 2-addition involving a C-H bond from the *ansa*-metallocene *tert*-butyl substituent.[23] This finding represents a fundamental new way to cleave N_2 through its coordination and activation by a metal center followed by "ligand-mediated dinitrogen cleavage" and suggests the potential for more diverse means of performing nitrogen atom functionalization.

1.5 Substitution of Cyclopentadienyl Ligands for Amidinate Ligands

With a rich array of N_2 activation and functionalization chemistry having been demonstrated by Chirik and co-workers through comparatively minor changes in the sterics and electronics of the metallocene ligand framework, the impact of a slightly more significant change to the supporting ligand framework is of particular interest. In the case of Sita and co-workers, the substitution of a cyclopentadienyl ligand for an amidinate ligand has provided analogous reactivity (e.g. olefin polymerization, hydrozirconation)

for Group 4 cyclopentadienyl amidinate (CpAm) complexes relative to their Group 4 metallocene analogs.[24, 25] Therefore similar studies on dinitrogen complexes derived from CpAm supporting ligands were of particular interest for use in investigations of N_2 activation and functionalization.

1.5.1 Comparison of Cyclopentadienyl and Amidinate Ligands

Cyclopentadienyl ligands have been shown to serve as ubiquitous spectator ligands capable of binding various metals. Specifically, cyclopentadienyl ligands are known to serve as monoanionic ligands which in most instances donate six electrons to a metal center through one σ and two π interactions via a η^5-binding motif. However, in the case of either ligand competition for donation of electron density to the metal center or the absence of available orbitals, the cyclopentadienyl ligand can assume either η^1- or η^3-binding motifs which respectively make this ligand a two and four electron donor.[26] Amidinate ligands by comparison have likewise been shown to serve as inert spectator ligands capable of binding a single metal center in a multidentate fashion, although examples of bridging amidinate ligands have been previously observed.[27, 28] Similar to cyclopentadienyl ligands, amidinate ligands have been hypothesized to serve as monoanionic two, four, or six electron donors through respective one σ, two σ, or two σ and one π interactions with the metal center as seen in Figure 4. However, in comparative bonding analysis of amidinate versus cyclopentadienyl ligands by Teuben and co-workers, the amidinate ligand was found to lack any significant π interaction with the metal center suggesting that amidinates principally serve as four electron donors through two σ interactions with a metal.[29] As a result, metal centers with amidinate supporting

ligands should be able to accommodate the donation of additional electron density to the metal center or the formation of additional bonds to the metal center versus corresponding metallocene complexes. Moreover, in comparing the composition of cyclopentadienyl versus amidinate ligands, the presence of harder Lewis basic nitrogen atoms versus carbon atoms in cyclopentadienyl ligands should make CpAm complexes more electron deficient relative to their metallocene analogs.

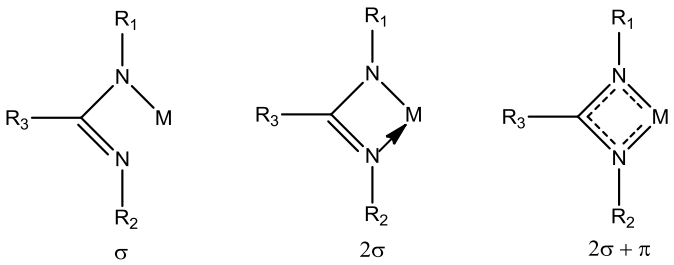

Figure 4: Hypothesized bonding motifs for amidinate ligands.

With regard to configurational stability, despite the formation of stable organometallic complexes, cyclopentadienyl ligands exhibit extremely low barriers to internal rotation about the metal-centroid axis resulting in the apparent equivalence of cyclopentadienyl substituents by such techniques as NMR. Likewise amidinates can undergo fluxional processes, although at much slower rates, for the exchange of the nitrogen atom substituents as the result of either "ring-flipping" or transient nitrogen atom dissociation from the metal center.[30] Finally, in contrast to the cyclopentadienyl ligand, the sterics of amidinates are highly modular as the result of the ability of amidinates to be synthesized from carbodiimides of variable sterics and symmetry.[31] Such modularity is believed to be of significant utility in determining the effects of sterics on the modes and extent of N_2 activation as demonstrated by Chirik.

Chapter 2: Group 6 CpAm Dinitrogen Complexes as Molecular Synthons

2.1 Introduction and Background

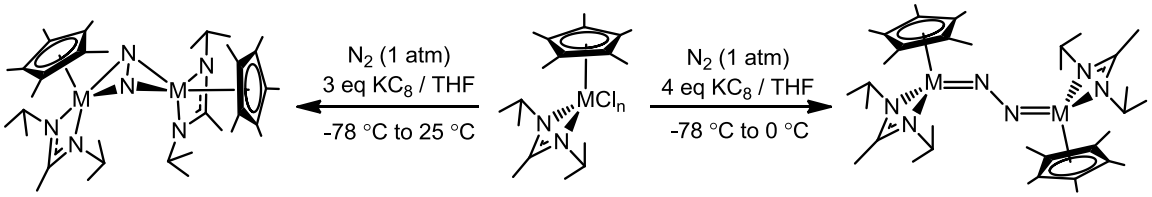

Scheme 10: Synthesis of CpAm non-planar side-on bridged, **37** and **38**, and linear end-on bridged, **39**, dinitrogen complexes through the reduction of CpAm metal chloride precursors with potassium graphite.

Previously, reduced Group 4 and 5 metal centers having the supporting CpAm ligand framework were found to bind and activate N_2. Stark periodic differences were observed in this research when comparing the reduction of Cp*M[N(^{i}Pr)C(Me)N(^{i}Pr)]Cl_2, where M = Zr (**34**) and M = Hf (**35**), versus Cp*Ta[N(^{i}Pr)C(Me)N(^{i}Pr)]Cl_3 (**36**), by potassium graphite (KC_8) in the presence of N_2. Specifically, the reduction of **34** and **35** served to provide the dinuclear non-planar side-on bridged dinitrogen complexes, {Cp*M[N(^{i}Pr)C(Me)N(^{i}Pr)]}$_2$(μ-η^2:η^2-N_2), where M = Zr (**37**) and M = Hf (**38**), while the reduction of **36** was found to yield the dinuclear linear end-on bridged dinitrogen complex, {Cp*Ta[N(^{i}Pr)C(Me)N(^{i}Pr)]}$_2$(μ-η^1:η^1-N_2) (**39**).[32, 33] In contrast to **37** and **38**, complex **39**, having the requisite six electrons needed for complete N_2 cleavage, was found to be thermally unstable with temperatures above 0 ˚C providing the bridging nitrido complex {Cp*Ta[N(^{i}Pr)C(Me)N(^{i}Pr)](μ-N)}$_2$ (**40**).[33]

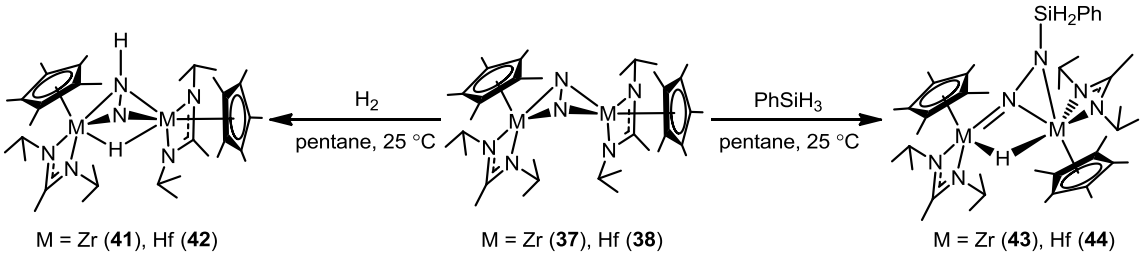

M = Zr (**41**), Hf (**42**) M = Zr (**37**), Hf (**38**) M = Zr (**43**), Hf (**44**)

Scheme 11: Reaction of **37** and **38** with hydrogen and phenylsilane.

Despite the ability of these reported CpAm complexes to bind, activate, and cleave small molecules, to date there has been no demonstrated reactivity of the early transition metal heteroatomic bonds formed concomitantly with small molecule activation and cleavage. In the case of **37** and **38**, nitrogen-atom functionalization was observed through reaction with hydrogen (H_2) and phenylsilane ($PhSiH_3$) to produce the dinuclear non-planar side-on bridged dinitrogen complexes $\{Cp^*M[N(^iPr)C(Me)N(^iPr)]\}_2(\mu\text{-}H)(\mu\text{-}\eta^2\text{:}\eta^2\text{-}N_2H)$, where M = Zr (**41**) and Hf (**42**), and $\{Cp^*M[N(^iPr)C(Me)N(^iPr)]\}_2(\mu\text{-}H)(\mu\text{-}\eta^1\text{:}\eta^2\text{-}N_2SiH_2Ph)$, where M = Zr (**43**) and Hf (**44**).[32] Likewise for the Group 5 dinitrogen complexes **39** and **40**, only metal-centered 1,4-addition was observed when **39** was reacted with H_2 and $PhSiH_3$ to give $\{Cp^*Ta[N(^iPr)C(Me)N(^iPr)](H)\}\{Cp^*Ta[N(^iPr)C(Me)N(^iPr)](X)\}(\mu\text{-}\eta^1\text{:}\eta^1\text{-}N_2)$, where X = H (**45**) and X = SiH_2Ph (**46**), while **40** was found to exclusively react with $PhSiH_3$ to give the σ-bond metathesis product $\{Cp^*Ta[N(^iPr)C(Me)N(^iPr)](H)\}(\mu\text{-}N)\{Cp^*Ta[N(^iPr)C(Me)N(^iPr)](NSiH_2Ph)\}$ (**47**).[33] In all of these complexes, 1,2-addition chemistry for the M-N bonds derived from N_2 appeared to be prohibited, precluding the release of these dinitrogen derived nitrogenous ligands as nitrogen-containing organic products in a catalytic process. Given the stability of these M-N bonds, we sought to

develop model CpAm complexes by which heteroatom transfer reactions could be researched in an effort to develop catalytic processes for the fixation of small molecules.

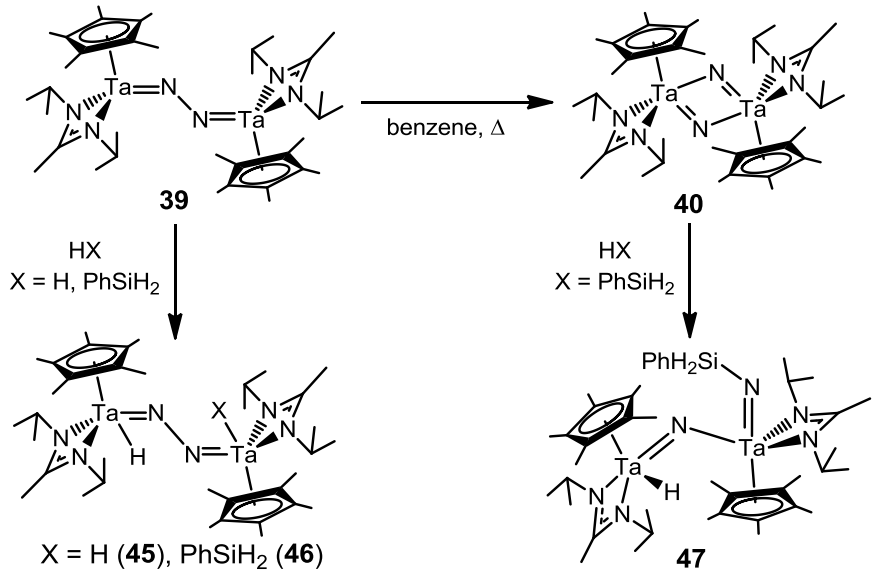

Scheme 12: Thermal N-N bond cleavage of **39** to yield **40** and the reactivity of these complexes with hydrogen and phenylsilane.

In an effort to further demonstrate the periodic trends associated with dinitrogen activation, isostructural CpAm M(IV, d^2), Cp*M[N(^{i}Pr)C(Me)N(^{i}Pr)]Cl_2 where M = Mo (**48**) and M = W (**49**), and M(V, d^1), Cp*M[N(^{i}Pr)C(Me)N(^{i}Pr)]Cl_3 where M = Mo (**50**) and M = W (**51**), metal chloride complexes were developed by Dr. Phil Fontaine of the Sita Group. Upon the reduction of **48** and **51** with KC_8 in the presence of N_2, diamagnetic yellow-brown and dark green crystalline materials could respectively be isolated. Through single crystal X-Ray diffraction and elemental analysis, the isolated dark green material from the reduction of **51** was found to be the Group 6 end-on bridged dinitrogen complex, {Cp*W[N(^{i}Pr)C(Me)N(^{i}Pr)]}$_2$(μ-η^1:η^1-N_2) (**52**) whose structure and relevant geometric parameters are provided in Figure 5.[34] Of particular note is the substantially shorter N-N bonded length, 1.277(8) Å, for the bridging dinitrogen ligand relative to the

previously characterized Group 5 end-on bridged dinitrogen complex, **39**, for which N3-N3a = 1.313(4) Å. This shortened bond length suggests a bridging dinitrogen ligand having increased multiple bond character that approaches the diazene (N_2^{2-}), 1.247 Å, versus hydrazine (N_2^{4-}), 1.470 Å, activation limit.[7] Although single crystals representative of the bulk material from the reduction of **48** could not be obtained, on the basis of elemental analysis as well as similarity of reactivity and ^{1}H NMR resonances (*vide infra*), the resulting crystalline material was assigned to be the analogous complex $\{Cp^*Mo[N(^iPr)C(Me)N(^iPr)]\}_2(\mu\text{-}\eta^1\text{:}\eta^1\text{-}N_2)$ (**53**).[34]

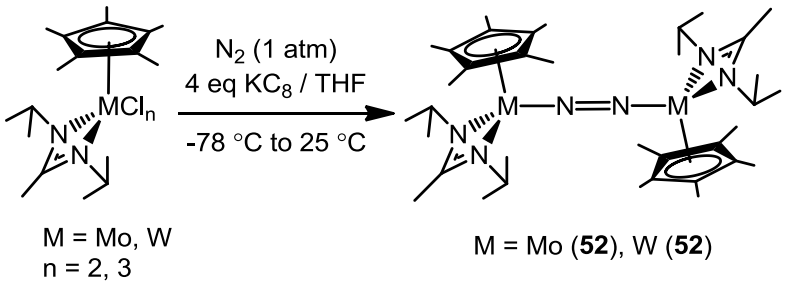

Scheme 13: Synthesis of Group 6 CpAm end-on bridged dinitrogen complexes using potassium graphite as the reducing agent.

Intriguingly, in previous work by Arnold and coworkers, the bisguanidinate and bisamidinate end-on bridged dinitrogen complexes, $\{Ti[N(^iPr)C(NMe_2)N(^iPr)]_2\}_2(\mu\text{-}\eta^1\text{:}\eta^1\text{-}N_2)$ and $Ti[N(SiMe_3)C(Ph)N(SiMe_3)]_2\}_2(\mu\text{-}\eta^1\text{:}\eta^1\text{-}N_2)$, exhibiting similar extents of dinitrogen activation, ~1.28 Å, were found to serve as synthons for the production of multiply bonded metal-ligand species (e.g. oxos, imidos).[35] Provided this reactivity, it was postulated that similar displacement of a weakly activated dinitrogen ligand in favor of stronger ligands should occur in **52** and **53** allowing for the use of these complexes in the divergent synthesis of model complexes for the study of heteroatom transfer reactions.

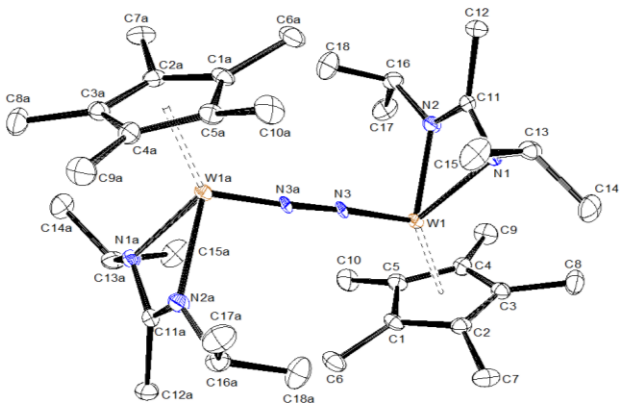

Figure 5: Molecular structure (30% thermal ellipsoids) of **53**. Hydrogen atoms have been removed for the sake of clarity. Selected bond lengths (Å) and bond angles (°) for **53**: W1-N3 1.816(4), N3-N3a 1.277(8), W1-N1 2.172(4), W1-N2 2.182(4), N2-W1-N1 61.43(15), W1-N3-N3a 176.7(5).

2.2 Scaled-Up Synthesis of Group 6 CpAm Dinitrogen Complexes

As a prerequisite to the proposed utilization of Group 6 CpAm dinitrogen complexes **52** and **53** for the production of multiply bonded metal-ligand complexes, a new synthetic route for the scalable production of these complexes was needed. Specifically, the previous synthetic route used KC_8 as a reducing agent requiring the use of extreme reaction conditions (-78 ˚C), pressurized reaction vessels, and the handling of starting materials under an argon atmosphere, all of which served to limit reaction scales to less than 150 mg. Given the relatively small difference in the reduction potential of potassium compared with sodium, $K^+ + e^{-1} \rightarrow K(s)$, $E^\circ = -3.0401$ V versus $Na^+ + e^{-1} \rightarrow Na(s)$, $E^\circ = -2.931$ V, it was reasoned that sodium amalgam (Na/Hg) could potentially be used as a milder reducing agent for the synthesis of **52** and **53**. To test this theory, **50** was reacted at -30 ˚C with four equivalents of 0.5% (w/w) Na/Hg in the presence of N_2 to give a brown colored solution that following standard work-up procedures gave a yellow-

brown crystalline material in good yield (77%). Through ^{1}H NMR, this crystalline material was confirmed to be the desired diamagnetic molybdenum end-on bridged dinitrogen complex, **53**. Likewise, reaction of **51** with four equivalents of 0.5% (w/w) Na/Hg under similar reaction conditions was found to give a dark green solution that following work-up gave dark green crystals in high yield (92%). As in the case of the reaction of **50** with Na/Hg, ^{1}H NMR of the isolated green crystals revealed this material to be the desired diamagnetic complex **52**, confirming the potential of Na/Hg to serve as a reducing agent for the synthesis of both **52** and **53**.

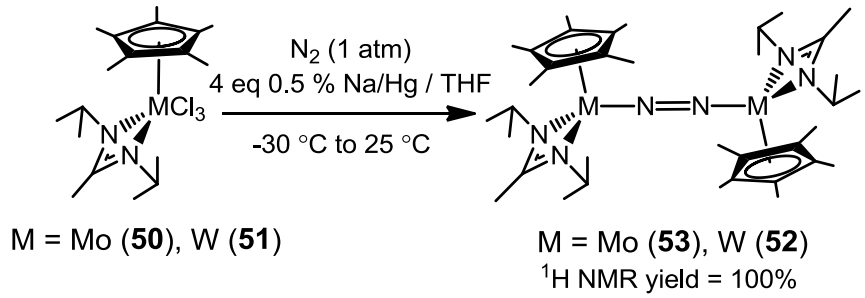

Scheme 14: Synthesis of Group 6 CpAm end-on bridged dinitrogen complexes using sodium amalgam as a reducing agent.

2.3 Group 6 CpAm Dinitrogen Complexes as M(II) Synthons

2.3.1 Group 6 CpAm Bis(Carbonyl) Complexes

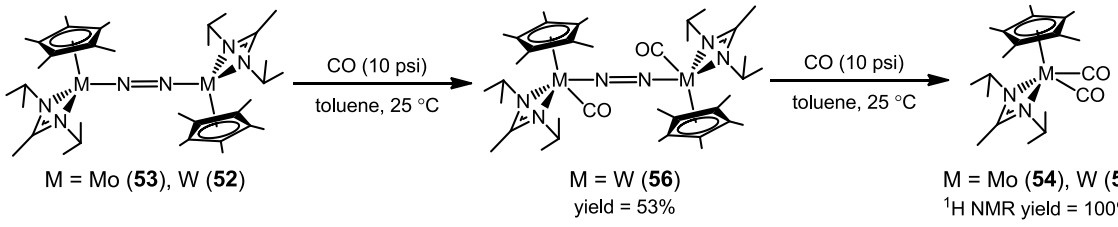

Scheme 15: Synthesis of **54** and **55** through the reaction of **52** and **53** with excess carbon monoxide via the bis(carbonyl) end-on bridged dinitrogen intermediate **56**.

Provided the weakly activated bridging dinitrogen ligand in the crystallographically characterized complex **52**, we sought to investigate N_2 displacement for complexes **52** and **53**. Toward this end, **53** was reacted with excess carbon monoxide (CO), a more π-acidic isolobal analog of N_2, in toluene at room temperature to provide a diamagnetic red-orange crystalline material in good yield (71%). Single crystal and elemental analysis of this material served to confirm the assignment of this material as the bis(carbonyl) complex Cp*Mo[N(^{i}Pr)C(Me)N(^{i}Pr)](CO)$_2$ (**54**). Structurally, **54** exhibited C_s symmetry with elongated C-O bond lengths, C19-O1 = 1.1625(16) Å and C20-O2 = 1.1625(16) Å versus1.128 Å for free CO, consistent with donation of electron density from the metal center into the π* molecular orbital of the carbon monoxide ligands. This back donation is likewise supported by the solid-state infrared spectra (KBr) for **54** that exhibits two reduced vibrational bond stretching modes associated with the CO ligands, ν_{CO} = 1909 and 1806 cm^{-1} versus 2143 cm^{-1} for the free carbon monoxide ligand. The observed extent of metal back donation moreover supports the formal M(II, d^4) assignment of the metal center in **54** when compared to the previously reported M(IV, d^2) complex [Cp$_2$Mo(CO)$_2$][BF$_4$]$_2$, ν_{CO} = 2139 and 2108 cm^{-1}, and the formal M(II, d^4) complex CpMo(η^3-C$_5$H$_5$)(CO)$_2$, ν_{CO} = 1950 and 1854 cm^{-1}.[36] In an analogous manner, **52** was found to react with excess CO in toluene at room temperature to give a red solution that when crystallized from pentane gave red-orange crystals in moderate yield (59 %). Using X-Ray diffraction and elemental analysis, the isolated material was found to be the bis(carbonyl) complex Cp*W[N(^{i}Pr)C(Me)N(^{i}Pr)](CO)$_2$ (**55**) having nearly identical geometric parameters, as detailed in Figure 8, and metal back donation, as seen by the solid-state (KBr) stretching frequencies ν_{CO} = 1892 and 1788 cm^{-1} (*c.f.* ν_{CO} = 2133 and

2087 cm^{-1} for $Cp_2W(CO)_2][BF_4]_2$ and ν_{CO} = 1955 and 1872 cm^{-1} for $CpW(\eta^3\text{-}C_5H_5)(CO)_2$), when compared to **54**.[36]

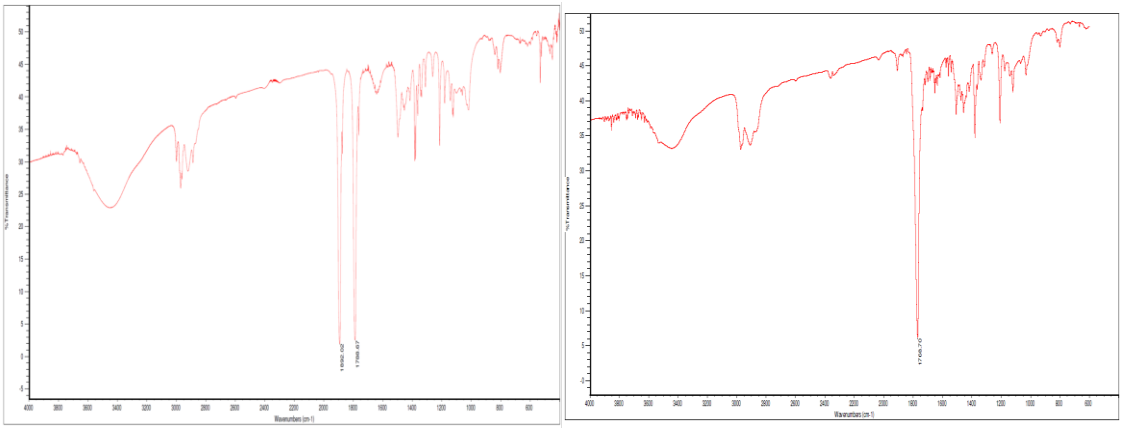

Figure 6: Solid-state (KBr) infrared spectra of **55** (left) and **56** (right).

On the basis of the observed ability of CO to displace N_2 from **52** and **53**, the displacement mechanism for N_2 was proposed to occur through competitive back donation by the metal center. As a means of probing the mechanism of N_2 displacement, we sought to investigate the presence of intermediate species leading to the formation of the bis(carbonyl) complexes **54** and **55**. For this investigation, **52** was reacted in benzene with a limiting amount of CO using a J Young tube to cause the formation of a C_1 symmetric complex in addition to the bis(carbonyl) complex **55** as observed by ^1H NMR. Importantly, in the presence of an excess amount of CO, the observed C_1 symmetric complex was found to quantitatively convert into the bis(carbonyl) complex **55** as seen in Figure 7. Seeking to identify the observed C_1 symmetric intermediate, the products resulting from the reaction of **52** with a limiting amount of CO were carefully crystallized from a mixture of pentane and toluene to provide green crystals in moderate yield (53%). Analysis of these crystals by X-Ray diffraction determined this intermediate species to be

the bis(carbonyl) end-on bridged dinitrogen complex $\{Cp^*W[N(^iPr)C(Me)N(^iPr)](CO)\}_2(\mu\text{-}\eta^1\text{:}\eta^1\text{-}N_2)$ (**56**) which exhibited C-O bonds of similar length to the bis(carbonyl) complex **55**, C19-O1 = 1.171(2) Å versus C19-O1 = 1.1680(17) for **56**, and a substantially shortened N-N bond length when compared with **52**, N3-N3a = 1.144(3) Å versus N3-N3a = 1.277(8) Å in **56**. In support of competitive metal back donation to the carbon monoxide ligand, the solid-state infrared spectrum of **56** shows a bond stretching frequency of ν_{CO} = 1768 cm^{-1}. Surprisingly, attempts to synthesize a molybdenum complex that is analogous to **56** failed to yield any observed C_1 symmetric intermediates with only a mixture of **53** and **54** resulting in ^1H NMR studies.

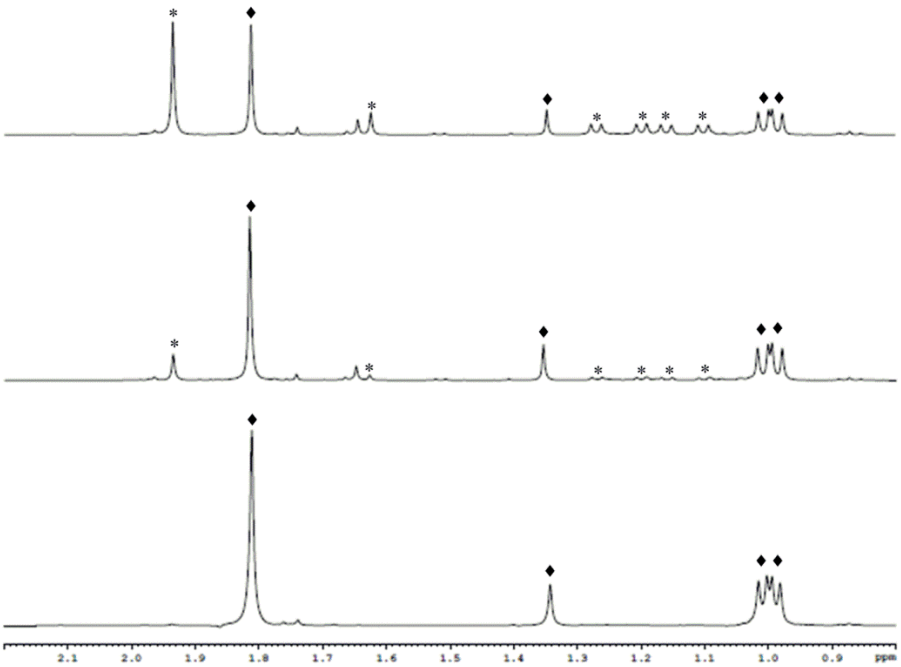

Figure 7: ^1H NMR for the reaction of **52** in the presence of a limiting amount of carbon monoxide after 24 h (top) and an added excess of carbon monoxide after 18 h (middle) and 66 h (bottom) for the formation the intermediate complex **56** (asterisks) and bis(carbonyl) complex **55** (diamonds).

Collectively, these results support a mechanism of N_2 displacement through a competitive back donation process involving the Group 6 metal center. In particular, the substantial shortening of the N-N bond length in **56** versus **52** indicates the potential for Lewis acidic ligands to compete for back donation by the metal center. This competitive process is enabled by the relatively weak π-acidic nature of N_2. Moreover, given the weak σ-donor nature of N_2, this ligand is easily displaced from the metal center in the absence of significant back donation. With regard to the inability to synthesize the molybdenum analog of **56**, the instability of an analogous complex having a weakly activated end-on bridged dinitrogen ligand is presumed to result from the smaller metal orbitals of molybdenum relative to tungsten.

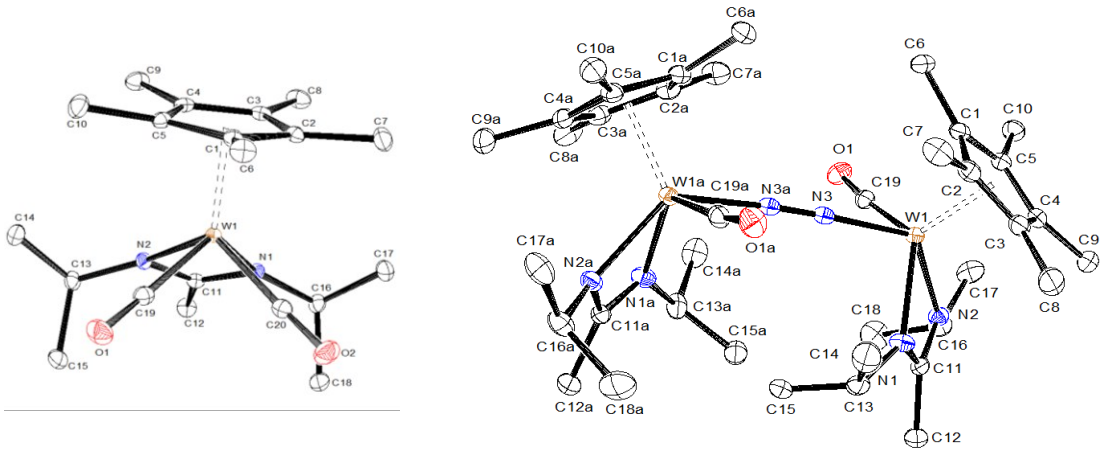

Figure 8: Molecular structure (30% thermal ellipsoids) of **55** (left) and **56** (right). Hydrogen atoms have been removed for the sake of clarity. Selected bond lengths (Å) and bond angles (°) for **55**: W1-N1 2.1802(11), W1-N2 2.1802(11), W1-C19 1.9488(14), W1-C20 1.9488(14), C19-O1 1.1680(17), C20-O2 1.1680(17), N2-W1-N1 60.08(6), C19-W1-C20 74.80(8), W1-C19-O1 175.14(12), W1-C20-O2 175.14(12). Selected bond lengths (Å) and bond angles (°) for **56**: W1-N3 2.0231(15), N3-N3a 1.144(3), W1-N1 2.1571(15), W1-N2 2.2038(16), W-C19 1.932(2), C19-O1 1.171(2), N2-W1-N1 59.87(6), W1-N3-N3a 176.69(9), N3-W1-C19 79.64(7), W1-C19-O1 173.29(17).

2.3.2 Group 6 CpAm Bis(Isocyanide) Complexes

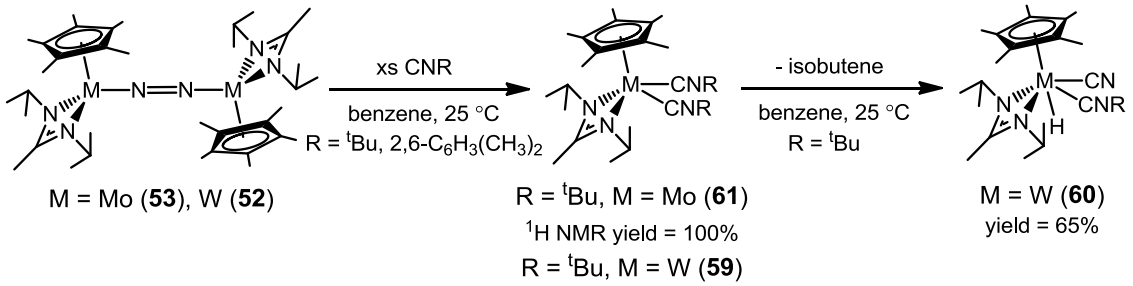

Scheme 16: Synthesis of Group 6 CpAm bis(isocyanide) complexes through the reaction of **52** and **53** with excess 2,6-dimethylphenyl and *tert*-butyl isocyanide and subsequent δ-hydride elimination to form the cyano isocyanide hydride complex **60**.

Having demonstrated the synthesis of bis(carbonyl) complexes from **54** and **55**, we sought to demonstrate the generality of this competitive metal back donation process through the reaction of **52** and **53** with isocyanides, isolobal analogs of CO. Toward this end, in research performed by Dr. Phil Fontaine, **52** and **53** were reacted with excess 2,6-dimethylphenyl isocyanide to produce the corresponding bis(isocyanide) complexes, Cp*M[N(^{i}Pr)C(Me)N(^{i}Pr)](2,6-CNC$_6$H$_3$(CH$_3$)$_2$)$_2$, where M = Mo (**57**) and W (**58**), as confirmed by single-crystal X-Ray diffraction and elemental analysis.[3] However, provided conjugation of the isocyanide functional group with the aromatic ring in 2,6-dimethylphenyl isocyanide, effectively increasing the π-acidity of this ligand, we sought to further demonstrate the generality of this displacement mechanism through the reaction **52** and **53** with a non-conjugated alkyl isocyanide, *tert*-butyl isocyanide (CN^{t}Bu). To begin, when the reaction of **52** with CN^{t}Bu was monitored by ^{1}H NMR a complex mixture of species was observed. Included in this mixture was the starting material **52** in addition to a second complex whose peaks integrated to the expected bis(isocyanide) reaction product Cp*W[N(^{i}Pr)C(Me)N(^{i}Pr)](CN^{t}Bu)$_2$ (**59**) but that procedure failed to yield any solid material following work-up. However, as detailed in Figure 10, before the formation of **59** was complete, a new C_1 symmetric complex having

a distinctive hydride resonance with tungsten satellites, ^{1}H NMR (400 MHz, benzene-d_6): 11.01 ppm ($J^{1}_{1H\text{-}183W}$ = 13.4 Hz), was observed by ^{1}H NMR. When this solution was heated, the observed C_1 symmetric complex having a hydride resonance was found to be formed in quantitative yield by ^{1}H NMR. Through careful crystallization of crude reaction mixtures from pentane yellow single crystals could be obtained. X-Ray diffraction of these single crystals allowed for this material to be identified as the cyanide isocyanide hydride complex, Cp*W[N(^{i}Pr)C(Me)N(^{i}Pr)](H)(CN)(CN^{t}Bu) (**60**), whose molecular structure and geometric parameters are provided in Figure 11. Like the bis(carbonyl) complexes, **60** exhibited a significant degree of metal back donation as evidenced by the presence of elongated C-N cyanide and isocyanide bond lengths, C19-N3 = 1.157(2) and C20-N4 = 1.189(2) respectively, and weaker C-N bond stretching frequencies, ν_{CN} = 2096 cm^{-1}, ν_{CNtBu} = 1955 cm^{-1} versus free organic isocyanides (*c.f.* CN^{t}Bu = 2136 cm^{-1}). Due to the observation of the diamagnetic bis(isocyanide) intermediate **59**, the formation of **59** is presumed to be the result of δ-hydride elimination involving a CN^{t}Bu ligand as has been previously reported in literature.[37]

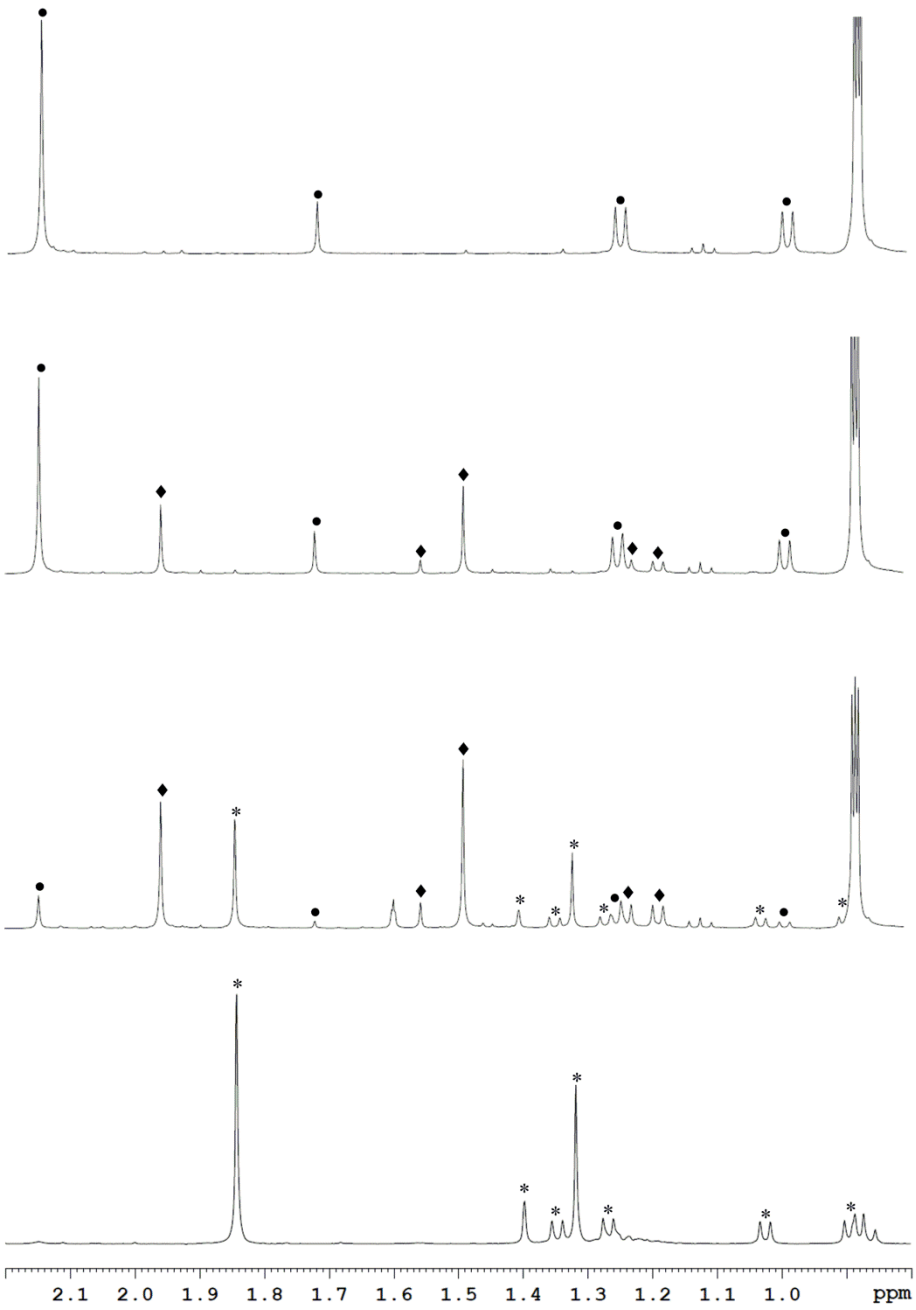

Figure 9: Reaction of **52** (circles) with excess *tert*-butyl isocyanide after 0 h (top), 20 h (top middle), and 9 d (bottom middle) for the formation of the bis(isocyanide) complex **59** (diamonds) and the δ-hydride elimination product **60** (asterisks). ^{1}H NMR reference spectrum of isolated **60** (bottom) (Note: Septet region of spectrum not shown for greater clarity of spectra.)

In practical terms, **59** was produced in larger quantities and moderate yield (65%) through the reaction of **52** with excess CN^tBu at 25 ˚C for ~3 d followed by heating of the solution at 80 ˚C overnight and crystallization from pentane at -30 ˚C. Contrasting the observed instability of **59**, attempted synthesis of the molybdenum analog, $Cp^*Mo[N(^iPr)C(Me)N(^iPr)](CN^tBu)_2$ (**61**), by Dr. Jon Reeds of the Sita research group resulted in the formation of a dark red diamagnetic complex by ^1H NMR which appeared indefinitely stable at room temperature, but which failed to produce any solid materials following work-up. The relative stability of **61** compared with **59** is believed to result from the larger metal orbitals of tungsten versus molybdenum that provide access to the hydride elimination side reaction.

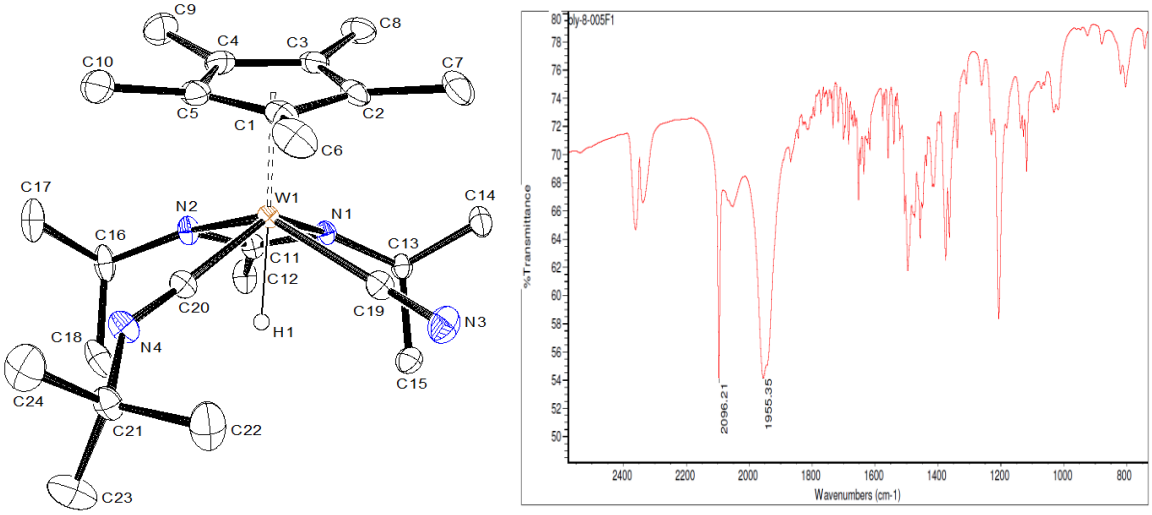

Figure 10: Molecular structure (30% thermal ellipsoids) (left) and solid-state (KBr) spectrum (right) of **60**. Most hydrogen atoms have been removed for the sake of clarity except for selected ones which are represented by spheres of arbitrary size. Selected bond lengths (Å) and bond angles (°) for **60**: W1-C19 1.9906(18), W1-C20 2.1166(18), C19-N3 1.157(2), C20-N4 1.189(2), W1-H1 1.60(2), W1-N1 2.1678(14), W1-N2 2.1689(13), N2-W1-N1 60.69(5), W1-C19-C20 87.64(7), W1-C19-N3 179.37(18), W1-C20-N4 175.10(15), C20-N4-C21 143.00(18).

2.4 Group 6 CpAm Dinitrogen Complexes as M(IV) Synthons

2.4.1 Group 6 CpAm Oxo Complexes

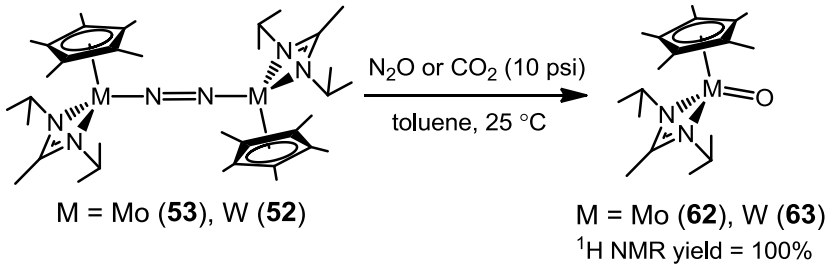

Scheme 17: Synthesis of Group 6 CpAm mononuclear oxo complexes through the reaction with either excess nitrous oxide or carbon dioxide.

With the ability to displace N_2 from **52** and **53** through competitive metal back donation into the π^* molecular orbitals of N_2 and a competing π-acidic ligand (e.g. CO, isocyanides), we wondered whether similar competitive metal back donation could occur between the π^* molecular orbital of N_2 and the σ^* molecular orbital of a competing ligand. Provided that this σ^* molecular orbital is of sufficiently low energy, back-donation by the metal center would allow for the formation of a multiply bonded metal-ligand species having a formal M(IV, d^2) oxidation state. Previously, nitrous oxide (N_2O) has shown the propensity to bind transition metal centers in a η^1-fashion through its oxygen atom followed by back-donation by the metal center leading to the extrusion of N_2 and the formation of metal-oxygen bonds.[38] Therefore, **53** was reacted with N_2O (10 psi) in toluene for 16 h to provide diamagnetic dark purple crystalline material in moderate yield (50%) following work-up. From single crystal X-Ray diffraction, the structure of this isolated crystalline material was found to be the mononuclear CpAm oxo complex Cp*Mo[N(^{i}Pr)C(Me)N(^{i}Pr)](O) (**62**) having a Mo1-O1 bond length of 1.7033(19) Å. Comparing this bond length to the Mo-O bond length of $Mo(O)Cl_4$,

1.670(12) Å, having a formal M(VI, d^0) oxidation state and assumed bond order of 2, the longer bond length of **62** is suggestive of a formal bond order greater than two.[39] However, in comparison to the Mo-O bonds in previously reported mononuclear metallocene oxo complexes, Cp^*_2MoO where Mo-O = 1.720(2) Å and $(CpMe)_2MoO$ where Mo-O = 1.721(2) Å), which have an estimated bond order between two and three, **62** appears to exhibit a slightly shorter Mo-O bond length indicative of greater multiple bond character and therefore lesser nucleophilicity than these previously characterized complexes.[40] Likewise to **53**, the reaction of **52** with N_2O under similar reaction conditions was found to give diamagnetic orange crystals in moderate yield (54%). X-Ray diffraction studies in addition to elemental analysis were subsequently used to confirm the identity of the isolated product to be the expected mononuclear oxo complex, Cp*W[N(^{i}Pr)C(Me)N(^{i}Pr)](O) (**63**), with the geometric parameters and structure of this complex provided in Figure 11. Similar to **62,** the W-O bond length of **63**, 1.7234(17) Å, was found to be greater than a formal bond order of two (c.f. $W(O)Cl_4$ where W-O = 1.684(15) Å) but still shorter than the reactive metallocene oxo complex $(CpMe)_2W(O)$, W-O = 1.744(5) Å, suggestive of its lesser nucleophilicity.[39, 40] Upon further investigation it was found that **62** and **63** could likewise be obtained in moderate yield (63%) through reaction of **52** and **53** with carbon dioxide (CO_2) (10 psi) in toluene. This result mirrors the previously reported ability of the dinitrogen complex *cis*-$Mo(N_2)_2(PMe_3)_4$ to displace weakly activated dinitrogen ligands with CO_2 for the eventual formation of a dimeric carbonate complex, $[Mo(CO_3)(CO)(PMe_3)_3]_2$, following oxygen atom abstraction from CO_2. Moreover, the observed oxygen atom abstraction reaction is consistent with that of other early transition metal complexes including that of

Mayer and co-workers who demonstrated the ability for $WCl_2(PMePh_2)_4$ to yield the tungsten oxo, carbonyl complex, $W(O)(CO)Cl_2(PMePh_2)_2$, involving a similar M(II, d^4) to M(IV, d^2) formal redox couple, upon exposure to CO_2.[41, 42]

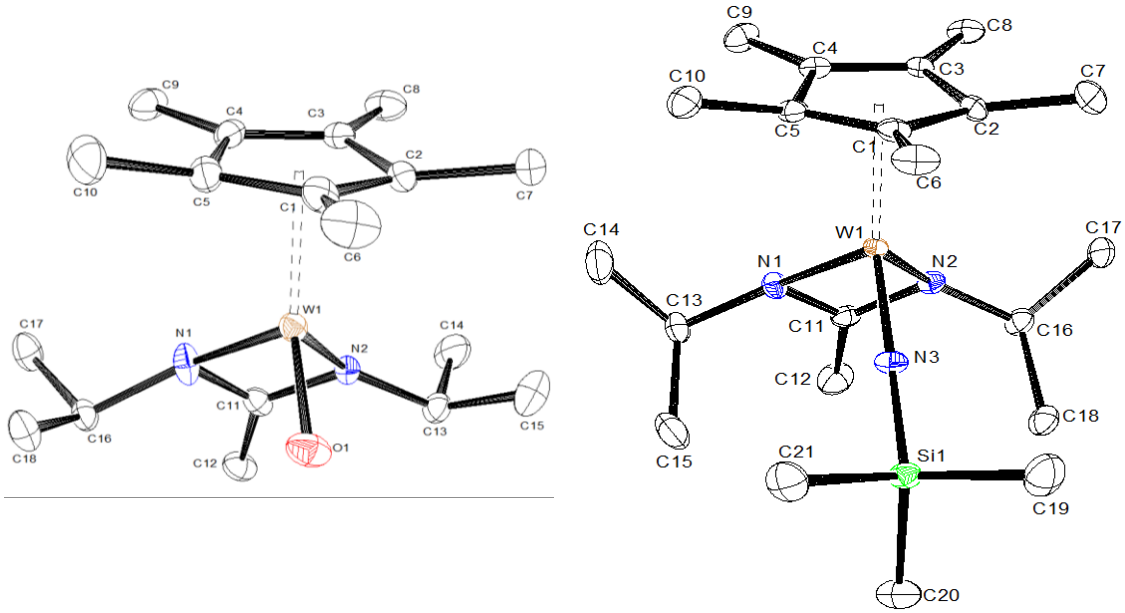

Figure 11: Molecular structure (30% thermal ellipsoids) of **63** (left) and **65** (right). Hydrogen atoms have been removed for the sake of clarity. Selected bond lengths (Å) and bond angles (°) for **63**: W1-O1 1.7234(17), W1-N1 2.1219(19), W1-N2 2.1298(18), N2-W1-N1 61.80(8). Selected bond lengths (Å) and bond angles (°) for **65**: W1-N3 1.763(4), N3-Si1 1.726(4), W1-N1 2.138(4), W1-N2 2.148(5), N2-W1-N1 61.79(19), W1-N3-Si1 175.0(3).

2.4.2 Group 6 CpAm Imido Complexes

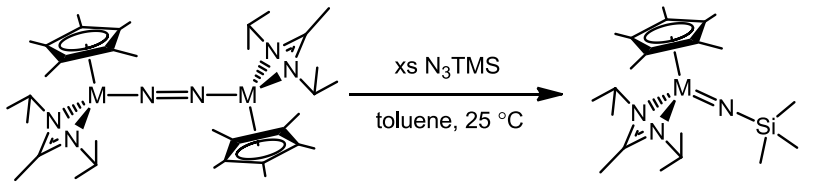

M = Mo (**53**), W (**52**)

M = Mo (**64**), W (**65**)
^{1}H NMR yield = 100%

Scheme 18: Synthesis of Group 6 CpAm mononuclear trimethylsilyl imido complexes, **64** and **65**, through reaction of **52** and **53** with excess trimethylsilyl azide.

Next, we sought to extend the M(IV) synthon chemistry of **52** and **53** to the synthesis of isoelectronic mononuclear imidos given the ability of these complexes to serve as precursors for the synthesis of mononuclear oxos. With the ability of N_2O to form mononuclear oxo complexes, it was reasoned that azides, which are isoelectronic with N_2O, should facilitate analogous multiple metal-nitrogen bond formation. Such analogous chemistry was been widely demonstrated with various weakly activated dinitrogen complexes having been found to react with organic azides for the formation of imidos.[43] Toward this end, in research that was performed in conjunction with Dr. Phil Fontaine, **53** was reacted with an excess of trimethylsilyl azide (N_3SiMe_3) in toluene for the formation of a black crystalline material in moderate yield (40%). Through a combination of X-Ray diffraction and elemental analysis, this crystalline material was found to be the expected mononuclear trimethylsilyl imido complex Cp*Mo[N(^{i}Pr)C(Me) N(^{i}Pr)](NSiMe$_3$) (**64**), having a Mo1-N3 bond length of 1.758(3) Å and Mo1-N3-Si1 bond angle of 175.1(2)˚. Comparison of this M-N bond length to Mo(NPhMe)Cl_4(THF), a mononuclear imido complex having a formal M(VI, d^0) oxidation state, for which Mo-N = 1.717(3) Å with an assumed formal bond order of two, the imido ligand of **64** appears to exhibit a formal bond order greater than two.[44] Moreover when this complex is evaluated against with the previously reported mononuclear metallocene imido complex Cp_2Mo(N^{t}Bu), having a Mo1-N3 bond length of 1.738(2) Å, **64** exhibits a comparatively lower bond order and therefore greater presumed nucleophilicity.[45] In a similar manner, the reaction of **52** with excess N_3SiMe_3 in toluene yielded dark red crystalline material in excellent yield (97%) following standard work-up procedures. Using elemental analysis and X-Ray diffraction this crystalline material was found to be the analogous

mononuclear imido complex Cp*W[N(^{i}Pr)C(Me)N(^{i}Pr)](NSiMe$_3$) (**65**), whose molecular structure and geometric parameters are provided in Figure 11. Although crystallographic structures for tungsten metallocene imido complexes, in addition to the analogous M(VI, d^0) complex W(NPhMe)Cl$_4$(THF), are conspicuously absent from literature, the measured M-N bond length of **65**, W1-N3 = 1.763(4) Å, appears to be only slightly longer than the previously detailed M-N bond length in **64**. Such differences in bond lengths are consistent with expected trends in transition metal covalent radii and suggest similar formal M-N bond orders in **64** and **65**.[46]

Chapter 3: Steric Deprotonation and Isomerization of CpAm Complexes for the Synthesis of Mononuclear Imido Complexes

3.1 Introduction and Background

Despite having demonstrated the ability to utilize Group 6 CpAm end-on bridged dinitrogen complexes, **52** and **53**, as M(IV) synthons for the synthesis of mononuclear Group 6 CpAm trimethylsilyl imido complexes, **64** and **65**, through the reaction with N_3SiMe_3, we sought to develop a more general synthetic route to mononuclear imido complexes given the limited commercial availability and potential safety hazards of organic azides. Previous research has demonstrated the potential to convert amido ligands into imido ligands through α-hydrogen abstraction routes involving an amido ligand and an adjacent alkyl/amido ligand through thermolysis, metal oxidation, or the addition of neutral two electron donor ligands.[47] From a synthetic perspective, the principle advantage of these routes are the ease with which early transition metal amido complexes can be generated from the metathesis of metal halide precursors with lithium amide salts. Moreover, lithium amide salts of variable steric and electronic substitution can be readily synthesized through the reaction organolithium reagents (LiR) with commercially available primary amines (H_2NR'), LiR + H_2NR'= → R-H + LiHNR'. Provided the ability to synthesize amido complexes of modular substitution, we sought to develop a novel route to mononuclear imido complexes utilizing an amido precursor to facilitate future research into the mechanisms of nitrogen atom transfer reactions involving Group 6 CpAm complexes (*vide infra)*.

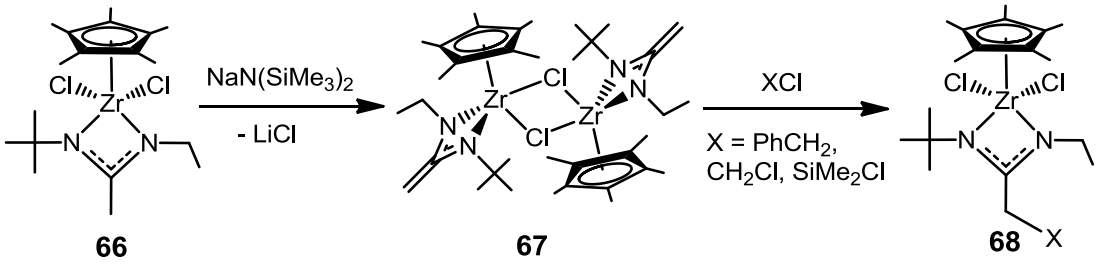

Scheme 19: Steric deprotonation of the Group 4 CpAm dichloride complex **66** with bulky bases and subsequent reaction of the dimeric "enamido" complex, **67**, with electrophiles.

Previously, Sita and co-workers demonstrated the ability to deprotonate the amidinate supporting ligand of Cp*Zr[N(Et)C(Me)N(^{t}Bu)]Cl_2 (**66**) through reaction with sterically bulky bases (e.g. $NaN(SiMe_3)_2$) to yield a dimeric "enamido" complex {Cp*Zr[N(Et)C(CH_2)N(^{t}Bu)](μ-Cl)}$_2$ (**67**). Structural analysis of **67** through X-Ray crystallography revealed significantly shortened M-N, Zr1-N1 = 2.045(4) Å and Zr1-N2 = 2.055(4) Å, and C-C, C11-C12 = 1.332(8) Å, bond lengths for the "enamido" ligand versus related CpAm zirconium complexes, Zr1-N1/Zr1-N2 ≈ 2.20 – 2.30 Å and C11-C12 ≈ 1.50 Å, consistent with the increased dianionic character and formation of a multiple bond in the "enamido" ligand.[48, 49] Moreover, provided the overall C_1 symmetry of **67**, diastereotopic protons for the "enamido" ligand could be observed by ^{1}H NMR. Interestingly, despite being attached to an electropositive metal center, the "enamido" ligand of **67** was found to react with a variety of electrophiles (e.g. alkyl halides, silyl chlorides) for the formation of CpAm dichloride complexes of the general formula Cp*Zr[N(Et)C(CH_2X)N(^{t}Bu)]Cl_2 (**68**) where X = $PhCH_2$, $SiMe_3$, etc… The findings of this research collectively established the ability of steric deprotonation to form an "enamido" ligand that can serve as a distal nucleophilic functional group despite being attached to an electropositive metal center in early transition metal CpAm complexes.

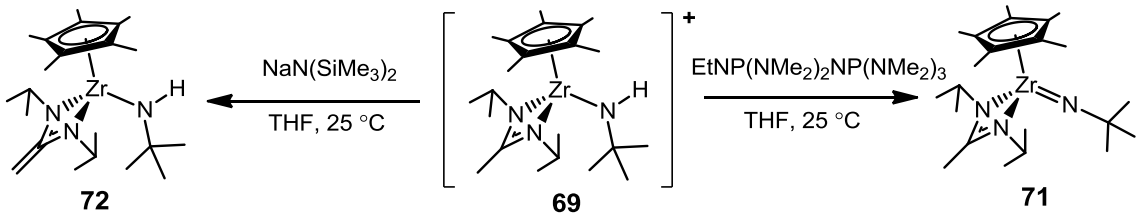

Scheme 20: Chemoselective deprotonation of a cationic Group 4 CpAm amido complex, **69**, to yield imido and "enamido"-amido complexes, respectively **71** and **72**.

Having established the nucleophilicity of "enamido" ligands attached to an early transition metal center, subsequent studies were carried out by Sita and co-workers to determine whether an "enamido" ligand could facilitate the conversion of an amido ligand into the correspond imido ligand. Toward this end, the cationic Group 4 CpAm amido complex $\{Cp^*Zr[N(^iPr)C(Me)N(^iPr)](NH^tBu)\}\{B(C_6F_5)_4\}$ (**69**) was synthesized through amido abstraction of a bis(amido) precursor complex, $Cp^*Zr[N(^iPr)C(Me)N(^iPr)](NH^tBu)_2$ (**70**), upon reaction with trityl tetrakisperfluorophenyl borate, $[Ph_3C][B(C_6F_5)_4]$. Through a survey of various bases of differing steric bulk and substitution, it was noted that reaction of **8** with these bases allowed for the isolation of the isomeric imido, $Cp^*Zr[N(^iPr)C(Me)N(^iPr)](N^tBu)$ (**71**), and "enamido"-amido, $Cp^*Zr[N(^iPr)C(CH_2)N(^iPr)](NHtBu)$ (**72**), complexes through a chemoselective deprotonation step. Similarly to **67**, structural analysis of **72** found that this complex exhibited markedly shorter M-N, Zr1-N1 = 2.0533(16) Å and Zr1-N2 = 2.0631(15) Å, and C-C, C11-C12 = 1.351(3) Å, bond lengths for the "enamido" ligand in addition to a significantly longer M-N bond distance for the sp^2-like *tert*-butyl amido ligand, Zr1-N3 = 2.0533(16) Å and Zr1-N3-C19 = 135.78(13)°, when compared with complex **71** having a sp-like imido ligand, Zr1-N1 = 2.232(2) Å, Zr1-N2 = 2.232(2) Å, C11-C12 = 1.515(4) Å, and Zr1-N3 = 1.839(2) Å, Zr1-N3-C19 = 175.52(18)°. Although

71 and **72** are perceived isomers, it was found that neither addition of base nor increased temperature enabled the conversion of **72** into the perceived more thermodynamically stable complex **71**.[50] Presumably, the kinetic barrier to the interconversion of **71** and **72** is the result of the limited nucleophilicity of the "enamido" ligand in **72** due an inductive effect involving the electropositive zirconium metal center in its highest oxidation state. It was therefore postulated that the synthesis of Group 5 and 6 M(IV) CpAm "enamido"-amido complexes that are isostructural to **72** could potentially facilitate isomerization to a mononuclear imido complex due to the less electropositive nature of such metal centers, thereby providing a more general and modular synthetic route to mononuclear imidos.

3.2 Steric Deprotonation and Isomerization for the Formation of Mononuclear Group 5 CpAm Imido Complexes

To begin, reaction of the previously reported CpAm Ta(IV) dichloride complex Cp*Ta[N(^{i}Pr)C(Me)N(^{i}Pr)]Cl_2 (**73**) with one equivalent of lithium *tert*-butylamide, (LiNH^{t}Bu) in diethyl ether (Et_2O) at -30 °C provided the paramagnetic Ta(IV) amido chloride complex Cp*Ta[N(^{i}Pr)C(Me)N(^{i}Pr)](NH^{t}Bu)Cl (**74**) as a dark red, crystalline material for which elemental analysis was fully consistent with the indicated empirical formula.[51] Single crystals of **74** were further subjected to X-Ray crystallography with the solid-state molecular structure and selected geometric parameters for this compound detailed in Figure 12 and Table 1. With respect to structural parameters of interest for **74**, the Ta1-N3 bond distance of 1.960(2) Å and Ta1-N3-C19 bond angle of 147.82(19)° are consistent with a sp^2-like amido ligand. Various attempts were made to react complex **74** with either an additional equivalent of LiNH^{t}Bu or various organolithium reagents, LiR

(R = Me, Et, and nBu), in an effort to induce α-hydrogen abstraction of the amido ligand for the formation of the desired mononuclear Ta(IV) CpAm imido complex, Cp*Ta[N(^{i}Pr)C(Me)N(^{i}Pr)](N^{t}Bu) (**75**). However, in all cases only intractable oils that failed to give crystalline material resulted.

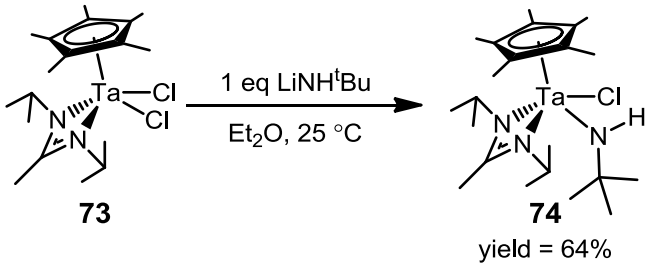

Scheme 21: Synthesis of tantalum(IV) CpAm amido chloride complex, **74**, through the reaction of **73** with one equivalent of lithium *tert*-butyl amide.

Seeking an alternative route to the synthesis of **75**, **74** was reacted with slightly less than one equivalent of lithium diisopropylamide, LiN(^{i}Pr)$_2$, in tetrahydrofuran (THF) at -30 °C to provide in good yield (66%) a dark green crystalline material for which elemental analysis was consistent with the overall loss of HCl from **74**. Single-crystal X-Ray analysis of this green material served to confirm the proposed deprotonation of **74** with the determined structure being Cp*Ta[N(^{i}Pr)C(CH$_2$)N(^{i}Pr)](NH^{t}Bu) (**76**), as depicted in Figure 12 along with the relevant geometric parameters in Table 1, which is isostructural to the previously reported complex **72**. In comparing the structures of **76** and **72**, the former exhibits a small contraction of the metal-ligand bonding distances relative to its Zr(IV) analog as would be expected from a slight contraction of metal covalent radii, for example Ta1-N3 = 1.9804(13) Å versus Zr1-N3 = 2.0533(16) Å. However, in contrast to the inability of **71** to interconvert with **72**, in a 25 ˚C benzene solution, **76** was found to quantitatively convert to **75** after 18 h as evidenced by

diagnostic paramagnetic resonances observed by ^{1}H NMR. Surmounting of this kinetic barrier to amido-imido isomerization for **76** versus **72** is assumed to occur by virtue of a more nucleophilic "enamido" ligand provided the formal M(IV, d^1) metal oxidation state for the former versus a formal M(IV, d^0) oxidation state for the later. To the best of our knowledge, **75** represents the first reported synthesis of a mononuclear tantalum(IV) imido complex with sparse reports of previous tantalum(IV) imido complexes existing as dimeric species having bridging imido ligands and either a M-M single bond or superexchange between two tantalum(IV) metal centers.[52]

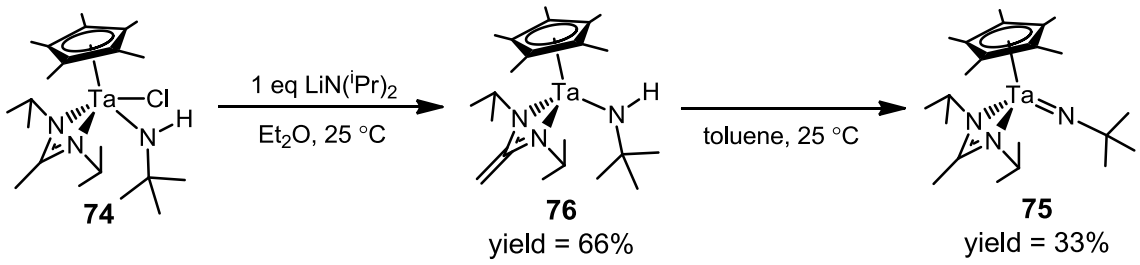

Scheme 22: Steric deprotonation of **74** with lithium diisopropyl amide for the formation of **76** followed by subsequent isomerization to the mononuclear imido complex, **75**.

In practice, a "one-pot" procedure was employed to provide a moderate yield (33%) of **75**, as a red crystalline material, that entailed first treating **74** with a slight excess (1.25 equiv) of LiN(^{i}Pr)$_2$ in THF at -30 °C followed by stirring overnight at room temperature and standard workup. Notably, under these reaction conditions, it is also possible that the isomerization of **76** to **75** is catalyzed by the slight excess of base present. Unequivocal confirmation of the monomeric terminal imido structure of **75** was provided by single-crystal X-Ray analysis with Figure 12 and Table 1 presenting the solid-state molecular structure and selected geometric parameters for this compound. The most notable features of **75** is that, relative to **76**, the C11-C12 bond length of the

amidinate ligand is elongated at 1.499(5) Å while the Ta1-N3 bond distance is shorter at 1.790(3) Å with a sp-like Ta1-N3-C19 bond angle of 177.3(3)° indicating the formation of a multiply-bonded imido versus amido ligand upon isomerization from **76**.

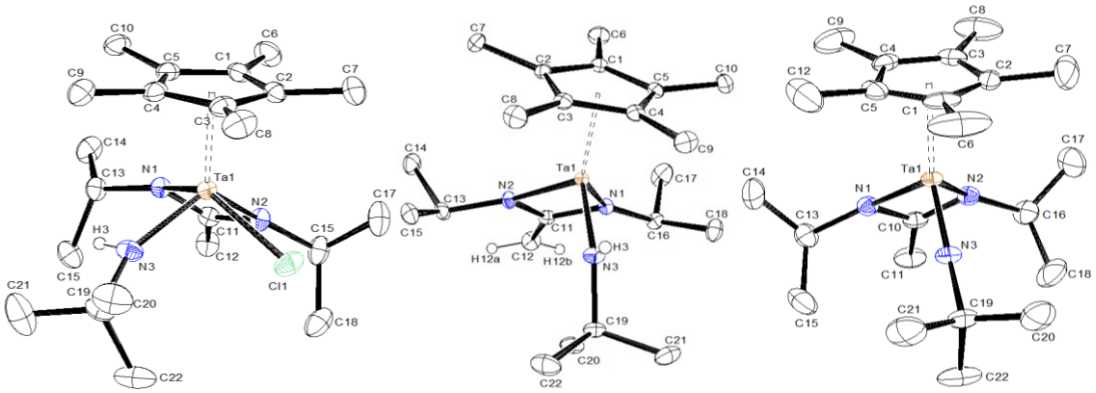

Figure 12: Molecular structures (30% thermal ellipsoids) of **74** (left), **76** (middle), and **75** (right). Hydrogen atoms have been removed for the sake of clarity, except for selected ones for **74** and **76** which are represented by spheres of arbitrary size.

Parameter	**71**	**72**	**75**	**74**	**76**
M1-N3	1.839(2)	2.0533(16)	1.790(3)	1.960(2)	1.9804(13)
M1-N1	2.232(2)	2.0596(15)	2.180(2)	2.1644(18)	2.0432(12)
M1-N2	2.232(2)	2.0631(15)	2.180(2)	2.2050(17)	2.0471(13)
C11-C12	1.515(4)	1.351(3)	1.499(5)	1.506(3)	1.353(2)
C11-N1	1.340(4)	1.417(3)	1.326(3)	1.341(3)	1.406(2)
C11-N2	1.340(4)	1.416(3)	1.326(3)	1.329(3)	1.4009(19)
M1-N3-C19	135.78(13)	135.78(13)	177.3(3)	147.82(19)	136.72(10)

Table 1: Selected geometric parameters for **75**, **74**, and **76** as well as their Group 4 isostructural analogs **71** and **72**.

3.3 Steric Deprotonation and Isomerization for the Formation of Mononuclear Group 6 CpAm Imido Complexes

To assess the generality of the observed isomerization of an amido ligand following the steric deprotonation of supporting amidinate ligands, analogous reaction of the previously reported Group 6 M(IV) CpAm dichloride complexes, Cp*M[N(^{i}Pr)C(Me)N(^{i}Pr)]Cl_2, where M = Mo (**48**) and M = W (**49**), with two equivalents of LiNH^{t}Bu were performed. Toward this end, **49** was reacted with two equivalents of LiNHtBu in Et_2O for 30 m to produce an orange crystalline product in good yield (75%) following standard work-up procedures. Although single crystals of this material could not be obtained, elemental analysis of the isolated product appeared to be fully consistent with the empirical formula for the proposed complex Cp*W[N(^{i}Pr)C(CH_2)N(^{i}Pr)](NH^{t}Bu) (**77**). However, ^{1}H NMR of this elemental analysis sample unexpectedly demonstrated resonances for a metal hydride having diagnostic tungsten satellites, ^{1}H NMR (400 MHz, benzene-d_6): 11.00 ppm ($^2J_{183W\text{-}1H}$ = 43.5 Hz), and diastereotopic protons associated with an "enamido" ligand, ^{1}H NMR (400 MHz, benzene-d_6): 2.95 and 2.99 ($^2J_{1H\text{-}1H}$ = 1.7 Hz). On the basis of elemental analysis as well as the characteristic ^{1}H NMR resonances indicating overall C_1 symmetry of this complex, the molecular structure of the isolated material was conclusively determined to be the imido hydride "enamido" complex Cp*W[N(^{i}Pr)C(CH_2)N(^{i}Pr)](H)(N^{t}Bu) (**78**). Presumably, **78** originates from the oxidative addition of an amido N-H bond in **77** to yield an imido and hydride ligand provided the formal M(IV, d^2) oxidation state of the tungsten metal center. If true, this would represent, to the best of our knowledge, the first known early transition metal-mediated oxidative addition of an N-H bond. Previously, metal-mediated N-H bond activation has only been reported for late transition metals,

however, metal-mediated oxidative 1, 2-migrations for the conversion of early and mid-transition metal carbenes into hydrido carbyne complexes are known.[53, 54]

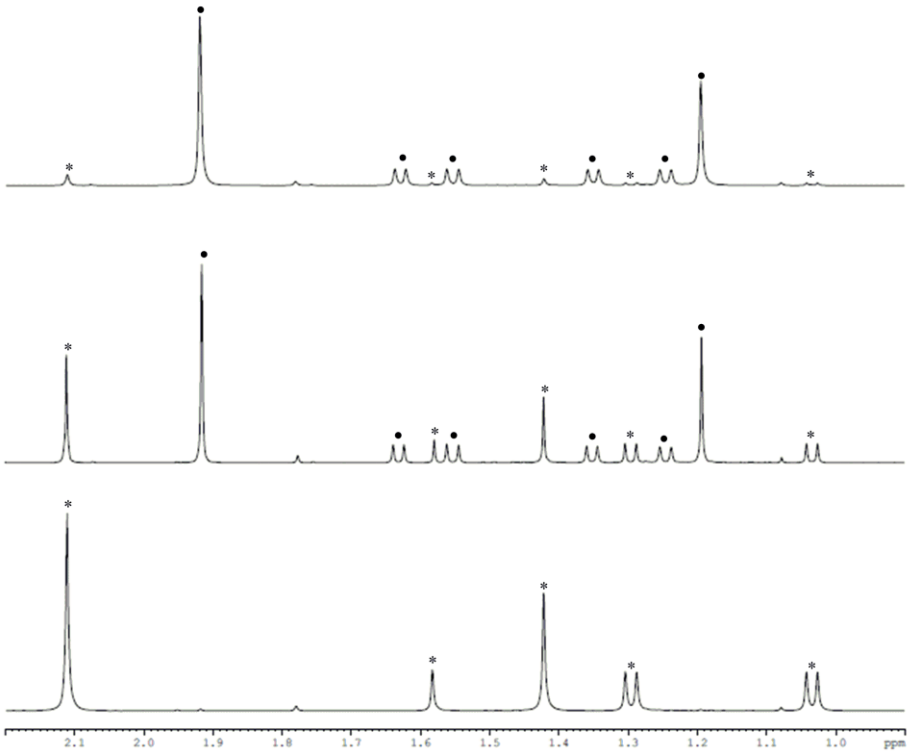

Figure 13: ^{1}H NMR of crystals for **78** (circles) in benzene after 0 h (top), 2 h (middle), and 24 h (bottom) at room temperature to demonstrate the isomerization of **78** to **79** (asterisks). (Note: Septet region of spectra are not shown for greater clarity of spectra.)

Surprisingly, at 25 ˚C, a benzene solution of **78** was found to quantitatively convert into a new dark red diamagnetic species lacking both hydride and "enamido" ligands after 1 d as observed by ^{1}H NMR, Figure 13. Isolation of this new diamagnetic product was achieved through careful crystallization from hexamethyldisiloxane ($O(SiMe_3)_2$). Single crystal X-Ray diffraction of this isolated material in conjunction with elemental analysis was used to unequivocally establish the identity of this complex as the mononuclear Group 6 CpAm imido Cp*W[N(^{i}Pr)C(Me)N(^{i}Pr)](N^{t}Bu) (**79**) whose structure and geometric parameters are provided in Figure 14. With respect to significant

structural parameters for **79**, the imido ligand for this complex was found to exhibit a nearly identical M-N bond length, W1-N3 = 1.753(2) Å, and imido bond angle, W1-N3-C19 = 177.7(2) º, when compared to the analogous mononuclear trimethylsilyl imido complex **65**, W1-N3 = 1.763(4) Å and W1-N3-Si1 = 175.0(3) º. Given the structure of **78** containing a M-H bond, the ability for **78** to isomerize into **79** is somewhat unexpected given the formal M(VI, d^0) oxidation state of the metal center when compared to the isomerization of **76**, having a M(IV, d^1) formal oxidation state. Such a result suggests that periodic trends other than metal oxidation state may dictate the nucleophilicity of the "enamido" ligand and its ultimate role in the isomerization of an amido ligand into an imido ligand.

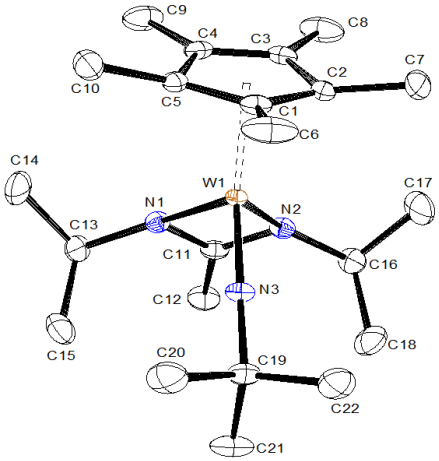

Figure 14: Molecular structure (30% thermal ellipsoids) of **79**. Hydrogen atoms have been removed for the sake of clarity. Selected bond lengths (Å) and bond angles (°) for **79**: W1-N3 1.753(2), N3-C19 1.455(4), W1-N1 2.1558(18), W1-N2 2.1559(18), N2-W1-N1 60.81(11), W1-N3-C19 177.7(2).

In practice, scalable amounts of **79** were prepared in moderate yield (60%) through the synthesis of **78** using standard work-up procedures followed by dissolution of the isolated material in toluene and stirring of the solution at room temperature for 5 d. In research performed by Dr. Jonathan Reeds of the Sita Group, **48** was similarly found to

directly provide the corresponding imido complex Cp*Mo[N(^{i}Pr)C(Me)N(^{i}Pr)](N^{t}Bu) (**80**) following reaction with two equivalents of LiNH^{t}Bu in Et_2O for 1 h. Fortunately, single crystals of **80** suitable for X-Ray diffraction could be obtained in low yield (33%) through crystallization from acetonitrile at -30 ºC with elemental and spectroscopic evidence being consistent with the proposed terminal imido structure. As in the case of **79**, the key geometric parameters of **80**, Mo1-N3 = 1.7428(12) Å and Mo1-N3-C1 = 177.26(10) º, were found to be nearly identical both to **79** as well as the mononuclear trimethylsilyl imido complex **64**, Mo1-N3 1.758(3) Å and Mo1-N3-Si1 175.1(2)°.

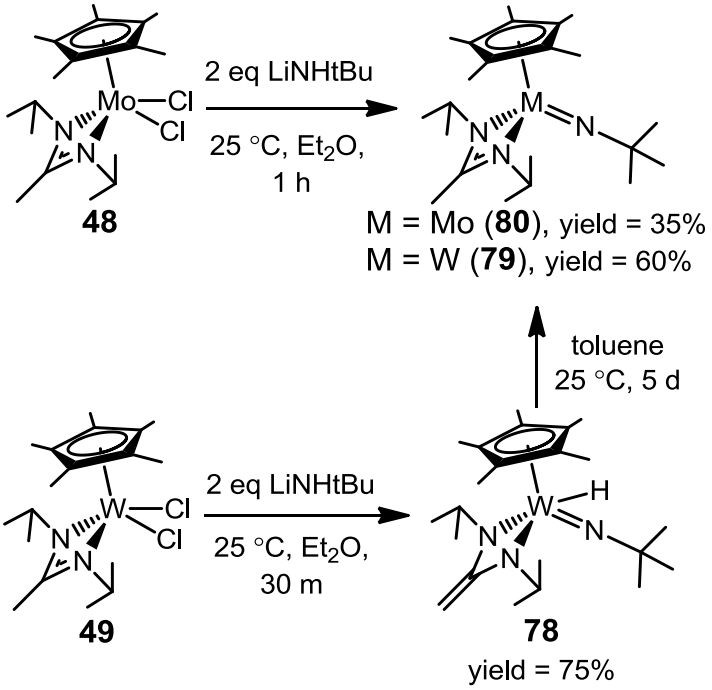

Scheme 23: Synthesis of mononuclear *tert*-butyl imido complexes, **79** and **80**, through steric deprotonation of the amidinate ligand and subsequent isomerization.

Chapter 4: Oxygen Atom Transfer Reactions with Group 6 CpAm Oxos

4.1 Introduction and Background

Nitrous oxide (N_2O) and carbon dioxide (CO_2) represent inexpensive oxidants that are of significant scientific and commercial interest. Specifically, N_2O has the potential to serve as a "green" oxidant whose byproduct, dinitrogen, is an inert and environmentally benign gas. Likewise, although relatively rare, the abstraction of an oxygen atom from CO_2 suggests the potential to use this otherwise ubiquitous inert product of combustion as a cheap industrial feedstock.[55] Recently, the previous academic interest in N_2O as an industrial oxidant has found application in the oxidation of olefins to carbonyls with this chemistry having been successfully demonstrated on the pilot plant scale.[56] Provided the ability to form the mononuclear terminal oxo complexes, **62** and **63**, using N_2O and CO_2, we sought to develop methods for oxygen atom transfer reactions involving Group 6 CpAm complexes as a means of investigating the use of these gases in catalytic oxidation reactions.

Previously, early transition metal complexes were believed to be incapable of heteroatom group transfer chemistry as the result of their presumed inability to undergo stable multielectron changes in the oxidation state of the metal. This inability was believed to preclude the necessary oxidative addition and reductive elimination steps required for the respective transfer of heteroatoms to the metal and release of heteroatomic organic species from the metal in a catalytic cycle. On the basis of this theory, early transition metal centers having redox-active supporting ligands capable of multielectron transformations have been developed by Heyduk and co-workers as a

means of facilitating oxidative addition and reductive elimination processes.[57] To achieve this desired effect, redox-active supporting ligands were designed to be multidentate ligands (e.g. the bis(2-isopropylamido-4-methoxyphenyl)amide = [NNN] in Scheme 23), thereby having stable interactions with the metal center, that exhibit extensive delocalization for the stabilization of the monoanionic ($[NNN]^{1-}$), dianionic ($[NNN]^{2-}$), and trianionic ($[NNN]^{3-}$) forms of the ligand as dictated by the reactivity of the metal center. Utilizing this effect, Heyduk and co-workers have recently reported nitrene transfer reactions for the catalytic synthesis of unsymmetrical carbodiimides from organic azides and isocyanides as described in Scheme 24.

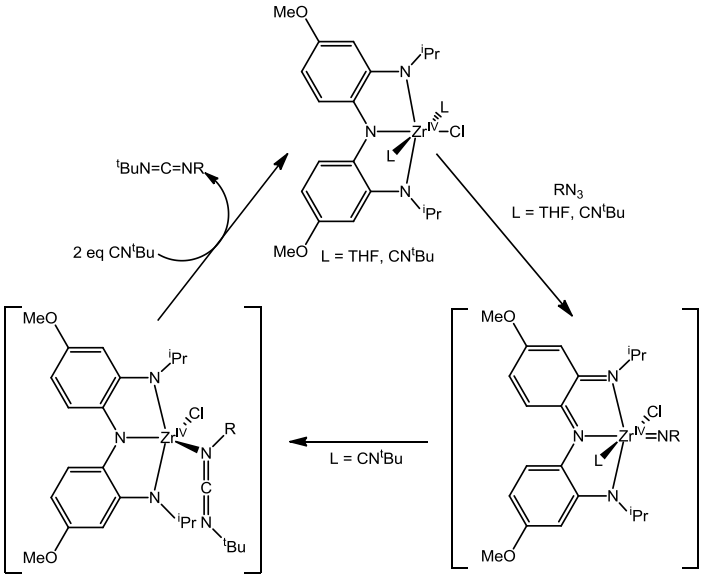

Scheme 24: Catalytic nitrene group transfer for the synthesis of unsymmetrical carbodiimides from organic azides and isocyanides utilizing $Zr[NNN]L_2Cl$, where L = THF or CN^tBu.

Although elegant the use of redox-active ligands is not a requirement for early transition metal heteroatom transfer reactions as demonstrated by reports of tungsten and molybdenum oxotransferase enzymes in biological systems. Through research by Holm

and co-workers, these early transition metal enzymes were found to use a formal M(IV, d^2)/M(VI, d^0) redox couple with dithiolene complexes utilizing the same M(IV, d^2)/M(VI, d^0) couple having been synthesized and used for the oxidation of organic substrates as a means of modeling enzymatic activity.[58] These results collectively suggest that molybdenum and tungsten metal centers, which typically exhibit formal M(IV,d^2) and M(VI, d^0) oxidation states, are capable of undergoing the multielectron transformations needed to facilitate group transfer reactions. Although less commonly observed, stable complexes of molybdenum and tungsten have likewise been observed to exhibit the formal M(II, d^4) oxidation state.[59] Therefore, we wondered whether a related M(II, d^4)/M(IV, d^2) formal redox couple could be exploited for heteroatom group transfer reactions. This was of particular interest given the demonstrated ability to synthesize stable M(II, d^4) and M(IV, d^2) complexes from the end-on dinitrogen complexes **52** and **53**.

$$[M^{IV}]{=}O \rightarrow \text{`}[M^{II}]\text{'} + \text{`O'}$$

$$CO/CNR + \text{`O'} \rightarrow CO_2/OCNR$$

Scheme 25: Proposed half-reactions for oxygen atom transfers involving the Group 6 CpAm mononuclear oxo complexes, **62** and **63**, with either carbon monoxide or isocyanides.

Provided the nucleophilic nature of multiple metal-ligand bonded heteroatomic ligands for early transition metal complexes, it was reasoned that the previously synthesized mononuclear oxo complexes, **62** and **63**, should be reactive toward Lewis acidic compounds. Reactivity with CO and isocyanides were of particular interest given the highly exothermic heats of formation for their corresponding oxidized products (CO

(g) + ½ O_2 (g) → CO_2 (g), ΔH_f = -60 kcal/mol and CNMe (g) + ½ O_2 (g) → OCNMe (g), ΔH_f = -60 kcal/mol). Highly exothermic heats of formation for group transfer reaction products are of significant importance given the inherent strength of M-O bonds in early transition metal complexes and the need to establish overall thermodynamically favorable conditions for reactivity. Moreover the proposed reaction of the mononuclear oxo complexes **62** and **63** with π-acidic ligands such as CO and isocyanides should form κ^2-coordinated ligands via a formally redox neutral process for the metal center as depicted in Scheme 26. The result would be the conversion of the terminal oxo ligand of **62** and **63** into a κ^2-coordinated ligand that is subject to more facile reduction elimination from the metal center in proposed heteroatom group transfer chemistry.

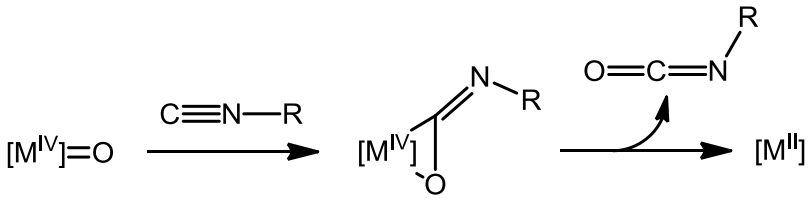

Scheme 26: Proposed formation of a κ^2-isocyanate ligand from mononuclear oxo complexes and subsequent reductive elimination from the metal center.

4.2 Proximal Nucleophilic Attack of π-Acidic Ligands

4.2.1 Reaction with *Tert*-Butyl Isocyanide

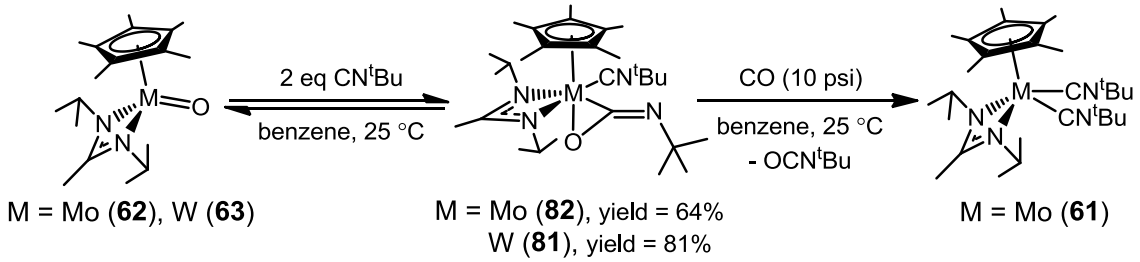

Scheme 27: Reaction of Group 6 CpAm mononuclear oxos, **62** and **63**, with *tert*-butyl isocyanide for the formation of κ^2-*O,C*-*tert*-butyl isocyanate complexes, **81** and **82**, and the subsequent reductive elimination of *tert*-butyl isocyanate from **82**.

To begin, **63** was reacted with two equivalents of CN^tBu in toluene at 25 ˚C for 1 h to give an orange solution that following the removal of volatiles *in vacuo* and crystallization from pentane provided orange crystals in good yield (81%). Single crystals obtained from this material were analyzed by elemental analysis and X-Ray diffraction with the structure of this complex determined to be the κ^2-*O,C*-*tert*-butyl isocyanate (OCN^tBu) complex Cp*W[N(^{i}Pr)C(Me)N(^{i}Pr)](κ^2-*O,C*-OCN^tBu)(CN^tBu) (**81**), whose structure along with relevant bond lengths and angles are provided in Figure 15. Geometric parameters that are of significant note for **81** include the newly formed C-O bond, O1-C19 = 1.329(4) Å, and sp^2-like character for the nitrogen atom of the κ^2-*O,C* isocyanate ligand, C19-N3-C20 118.9(3)˚. Moreover, the solid state infrared spectrum (KBr) of this complex displayed four bond stretching frequencies, ν_{CN} = 2085 and 2054 cm^{-1} for the isocyanide ligand as well as ν_{CN} = 1622 and 1603 cm^{-1} for the κ^2-*O,C* isocyanate ligand, that are consistent with respective back donation by the metal center and formation of a double versus triple bond in the κ^2-*O,C* isocyanate ligand. To the best

of our knowledge, **81** represents the first unequivocally established κ^2-*O,C* binding motif for an isocyanate ligand despite speculation of this structure in previous research.[60]

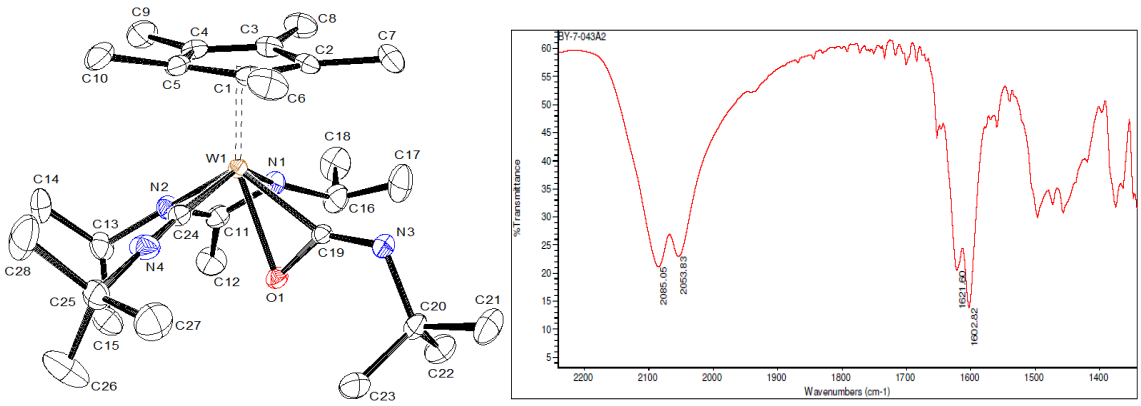

Figure 15: Molecular structure (left) (30% thermal ellipsoids) and solid-state infrared spectrum (right) of **81**. Hydrogen atoms have been removed for the sake of clarity. Selected bond lengths (Å) and bond angles (°) for **81**: O1-C19 1.329(4), W1-O1 2.119(2), W1-C19 2.053(3), W1-C24 2.056(4), C19-N3 1.280(4), C24-N4 1.157(5), W1-N1 2.152(3), W1-N2 2.220(3), C19-N3-C20 118.9(3),W1-C24-N4 177.2(3), C24-N4-C25 176.2(4), N2-W1-N1 60.42(12).

Intriguingly, despite the isolated orange crystals of **81** having been found to be analytically pure by elemental analysis, ^{1}H NMR of the elemental analysis sample in benzene-d_6 was found to proivde a mixture of diamagnetic species. Through comparison with reference spectra, the observed diamagnetic species were identified as being the starting material **63**, CN^{t}Bu, and a C_1 symmetric diamagnetic species whose peaks integrated to the values expected for the structurally characterized complex **81**. Suspecting the establishment of an equilibrium between **63** and **81**, an excess of CN^{t}Bu was added to the ^{1}H NMR sample with resonances of the starting material **63** being quantitatively converted into **81** as observed in Figure 16. Lending further support to this theory of an equilibrium involving **81** with free CN^{t}Bu and **63**, variable temperature (VT) ^{1}H NMR of analytically pure crystals of **81** was found to result in the quantitative

interconversion of **63** and **81** in response to changes in temperature as demonstrated in Figure 17.

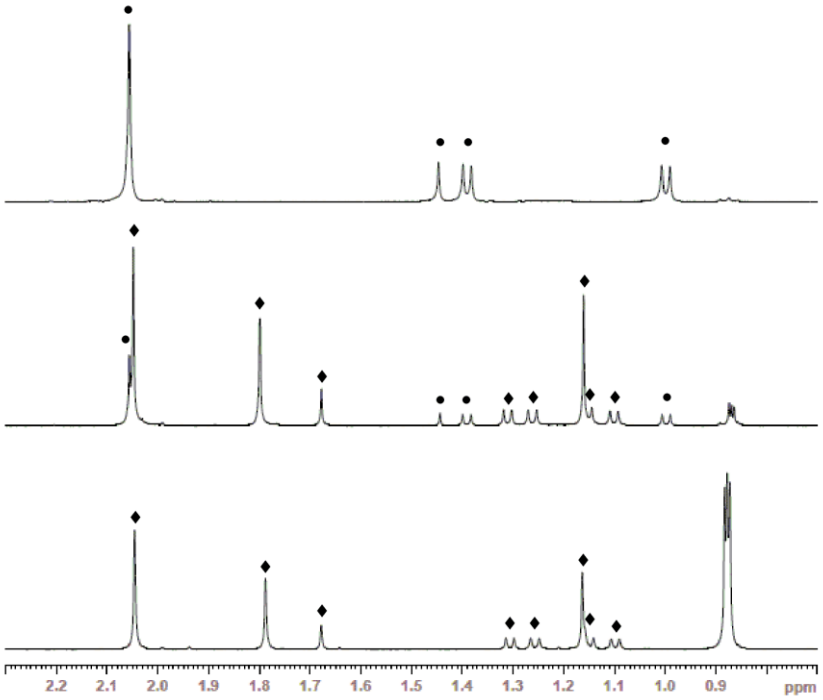

Figure 16: ^{1}H NMR spectrum of complex **63** (circles) (top) and analytically pure crystals of complex **81** (diamonds) in the absence (middle) and presence of excess *tert*-butyl isocyanide (bottom). (Note: Septet region of spectra are not shown for greater clarity of spectra).

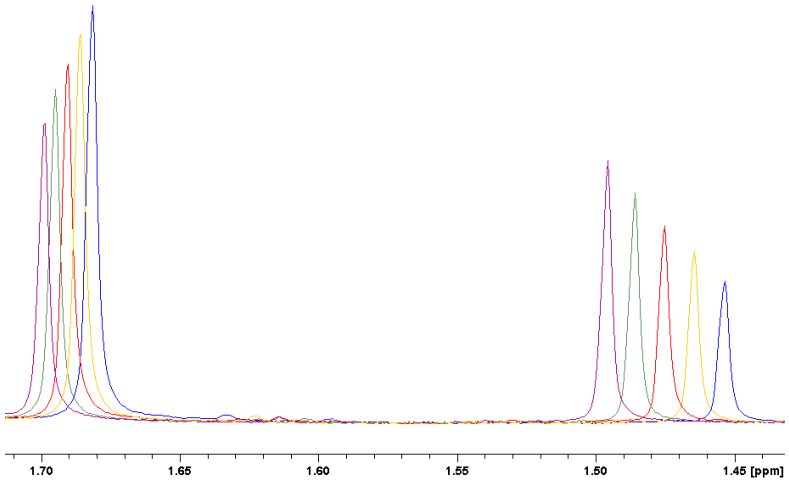

Figure 17: ^{1}H NMR spectrum of the amidinate methyl region for analytically pure crystals of complex **81** at 25 ºC (blue), 30 ºC (yellow), 34.5 ºC (red), 39 ºC (green), and 44 ºC (purple) to demonstrate the reversible thermal interconversion of complexes **81** (left peaks) and **63** (right peaks).

In an attempt to further characterize this thermally reversible equilibrium, analytically pure crystals of **81** were dissolved in a stock solution of durene dissolved in benzene-d_6. Through the use of VT ^{1}H NMR, the concentrations of **63** and **81** at different temperatures could be measured using the durene internal standard to allow for Van't Hoff analysis of this thermally reversible equilibrium, as seen in Figure 18. From this analysis the thermodynamic parameters of the observed equilibrium of **63** and **81** were found to be ΔH^{0}_{dissoc} = 19.9(7) kcal mol^{-1} and ΔS^{0}_{dissoc} = 65.9(3) e.u. resulting in a ΔG^{0}_{dissoc} at 298 K = 0.6(7) kcal mol^{-1} that is consistent with the facile interconversion of **63** and **81** with small changes in temperature. These thermodynamic parameters are furthermore in line with an expected equilibrium having a significant increase in entropy following the release of two equivalents of CN^{t}Bu from **81** and suggest a significant role for the coordination of a second CN^{t}Bu ligand in the formation of **81** as a stable complex.

Given, **81** ←→ **63** + 2 CN^tBu $K_{eq} = ([\mathbf{63}]*[CN^tBu]^2) / [\mathbf{81}]$

where $[CN^tBu] = 2*[\mathbf{63}]$ therefore $K_{eq} = (4*[\mathbf{63}]^3) / [\mathbf{81}]$

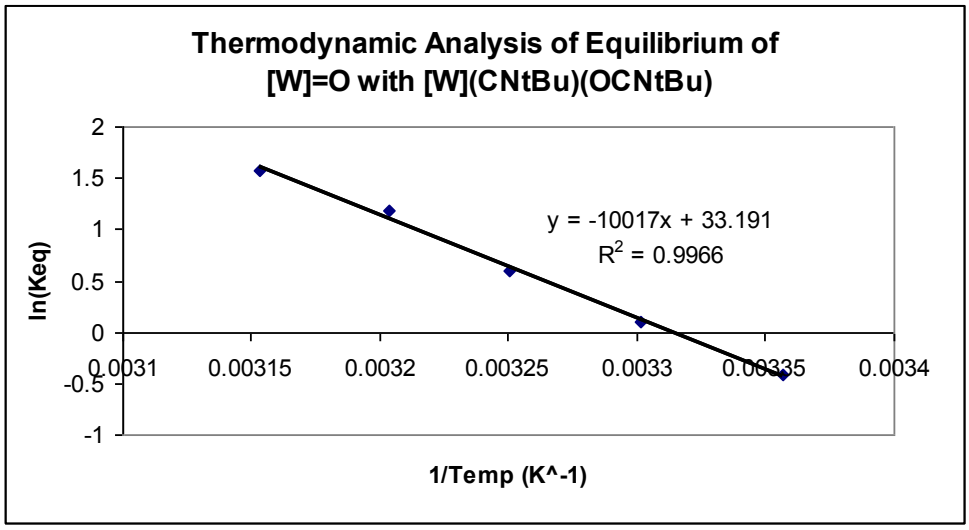

Figure 18: Van't Hoff analysis, 1/T vs. $\ln K_{eq}$, for determination of $\Delta H_{dissoc} = 19.9 \pm 0.7$ kcal/mol and $\Delta S_{dissoc} = 65.9 \pm 0.3$ e.u./mol for the equilibrium of complex **63** with complex **81**. (Note: Error in slope and intercept values were determined from linear regression performed in Excel).

Despite being able to shift the equilibrium of **63** and **81** to completion with the addition of excess CN^tBu, this shifted equilibrium for **81** was found to be incapable of reductively eliminating OCN^tBu with this solution providing a complex mixture of decomposition products when either heated at high temperatures (80 ˚C) or left at room temperature for extended periods of time (>2 wk). Seeking to promote the reductive elimination of OCN^tBu, it was reasoned that the molybdenum analog of **81**, $Cp^*Mo[N(^iPr)C(Me)N(^iPr)](\kappa^2\text{-}O,C\text{-}OCN^tBu)(CN^tBu)$ (**82**), should exhibit a more destabilized formal M(IV, d^2) oxidation state provided the general trend of greater destabilization of higher metal oxidation states for early transition metals when moving up a group. In research performed by Dr. Jon Reeds of the Sita Group, **82** was

synthesized in a similar manner to **81** with this complex having been found to be isostructural to **81** as determined by X-Ray diffraction. Moreover, the solid-state infrared (KBr) spectrum of **82**, was found to exhibit bond stretching frequencies of similar energy to **81**, ν_{CN} = 2112 and 1628 cm^{-1}, that correspond to an activated CN^tBu and κ^2-*O,C-tert*-butyl isocyanate ligand. Likewise to **81**, ^1H NMR of analytically pure crystals **82** in benzene-d_6 were found to exist in a thermally reversible equilibrium with **62** and free CN^tBu, although Van't Hoff analysis of this equilibrium was not performed. However, in contrast to **81**, the shifted equilibrium of **82** with **62** in the presence of excess CN^tBu was found to very slowly produce OCN^tBu and the previously characterized bis(isocyanide) complex **61** after extended periods of time at room temperature.

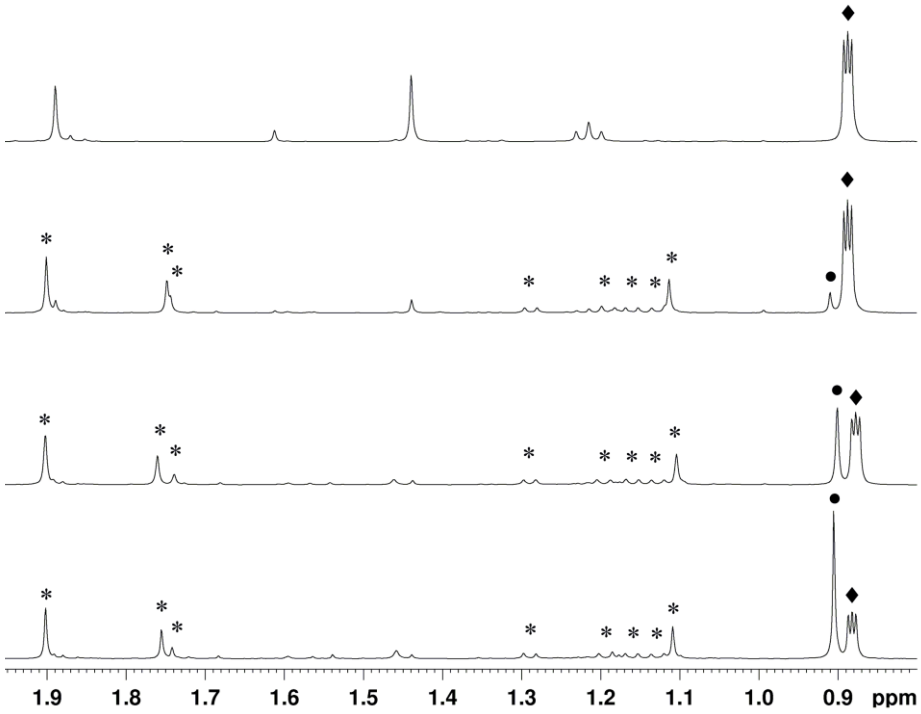

Figure 19: ^1H NMR spectra for the thermal conversion of *tert*-butyl isocyanide (diamonds) into *tert*-butyl isocyanate (circles) using complex **61** in the presence of 5 equivalents of *tert*-butyl isocyanide and nitrous oxide (10 psi) at 25 ˚C after 0 d (top), 2 d (top middle), 2 wk (bottom middle), and 4 wk (bottom). (Note: Septet region of spectra are not shown for greater clarity of spectra).

Having demonstrated the ability to reductively eliminate OCN^tBu from **82** but not **81**, catalytic formation of OCN^tBu was attempted through exposure of a benzene-d_6 solution of **61** to 5 equivalents of CN^tBu under an atmosphere of N_2O (10 psi). When this solution was monitored by ^1H NMR, as seen in Figure 19, the slow and steady production of multiple equivalents of OCN^tBu was observed at a turnover frequency of ~1 equivalent per week. Notably, during catalysis, the only major species observed by ^1H NMR was **82** with only a trace of **61** appearing to be present under catalytic conditions. With the demonstration of **61** as a catalytically competent species as well as its production from the reductive elimination of OCN^tBu from **82** in the presence of excess CN^tBu, the catalytic production of isocyanates from CN^tBu and N_2O is believed to result from an adventitious ligand exchange involving the isocyanide ligand of **61** and N_2O as proposed in Scheme 28. This catalytic production of isocyanates from N_2O and isocyanides, $N_2O + CNR \rightarrow N_2 + OCNR$, represents the first catalytic oxygen atom transfer process involving an early transition metal center and serves to complement previous isocyanate production from oxygen and isocyanides catalyzed by late transition metals.[61] In fact, the findings of this research appear to be in stark contrast to prior research on Group 6 M(IV, d^2) transition metal oxo complexes. Specifically, research by Mayer and co-workers demonstrated the ability to form the oxo, isocyanide complexes, $M(O)[CN\text{-}p\text{-}Tol]Cl_2(PMe_3)_2$ (M = Mo and W) and $W(O)Cl_2(CN^tBu)(PMePh_2)_2$, upon either exposure of $M(PMe_3)_4Cl_2$ to p-tolyl isocyanate (OCN-*p*-Tol) or $W(O)Cl_2(PMePh_2)_3$ to CN^tBu, with both complexes failing to reversibly form and eliminate isocyanate ligands as observed for **81** and **82** respectively.[62] Furthermore, this research serves to contrast previously reported Group 6 metallocene oxo complexes

which exhibit substantially greater nucleophilicity with these complexes having been shown to readily react with heterocumulenes like isocyanates.[63, 64] Therefore, a key aspect of this catalytic cycle is the presumed lesser nucleophilicity of **62** and **63** relative to metallocene oxos, on the basis of bond orders assigned through crystallographic comparisons. This allows for CN^tBu insertion through proximal nucleophilic attack by the oxo ligand following isocyanide coordination to the metal center, but prevents reaction of the oxo ligand with the isocyanate products of catalysis.

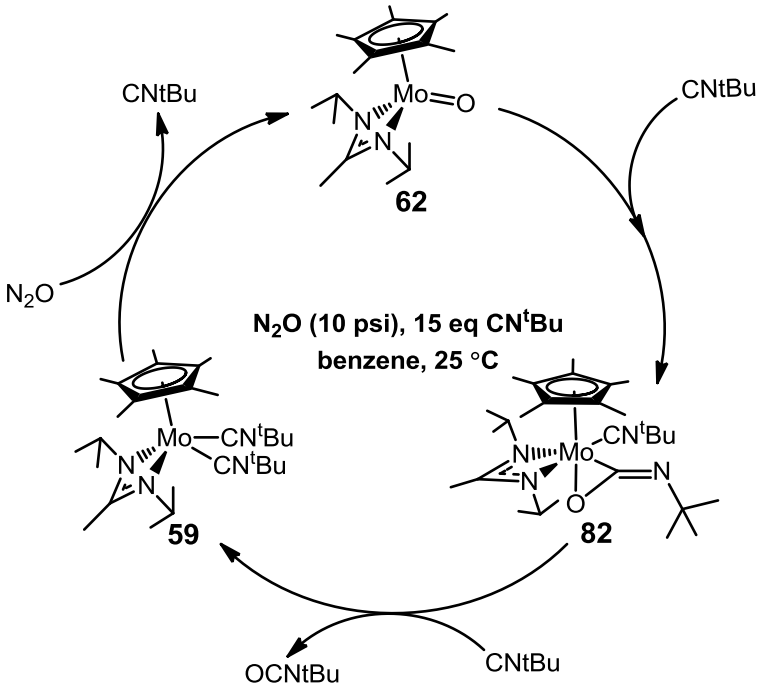

Scheme 28: Proposed catalytic cycle for the formation of *tert*-butyl isocyanate from nitrous oxide and *tert*-butyl isocyanide

4.2.2 Reaction with Carbon Monoxide

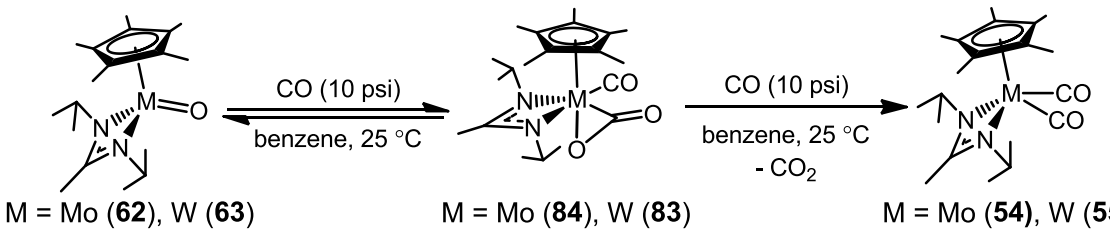

M = Mo (**62**), W (**63**) M = Mo (**84**), W (**83**) M = Mo (**54**), W (**55**)

Scheme 29: Reaction of Group 6 CpAm mononuclear oxos, **62** and **63**, with carbon monoxide for the formation of carbon dioxide and the bis(carbonyl) complexes, **54** and **55**, following reductive elimination of carbon dioxide from the intermediate κ^2-O,C-carbon dioxide complexes, **83** and **84**.

With the reactivity of **62** and **63** with CN^{t}Bu for the formation of κ^2-O,C isocyanate complexes **81** and **82** having been demonstrated, we sought to investigate the analogous reactivity of **62** and **63** with the isolobal carbon monoxide ligand. For this investigation, a benzene-d_6 solution of **63** was transferred into a J Young tube. The headspace of the J Young tube was evacuated and charged with CO (10 psi) to give an orange-colored solution that appeared to consist of a mixture of two diamagnetic species by ^{1}H NMR. As in the case of the reaction of **63** with CN^{t}Bu, through comparison with reference spectra this mixture was found to consist of the starting material **63** and a new C_1 symmetric diamagnetic species as observed in Figure 20. Subjecting this mixture to VT ^{1}H NMR, **63** and the new C_1 symmetric complex were found to quantitatively interconvert with slight changes in temperature as shown in Figure 21. Seeking to probe the identity of this C_1 symmetric species further, a benzene-d_6 solution of **63** was reacted with ^{13}C-labeled carbon monoxide (^{13}CO) (99%) to produce a thermally reversible equilibrium that exhibited two resonances by ^{13}C NMR. On the basis of the presumed similarity in reactivity, these resonances were preliminarily assigned to that of the CO and κ^2-*O,C*-carbon dioxide ligands for the expected product

Cp*W[N(^{i}Pr)C(Me)N(^{i}Pr)](κ^2-*C,O*-CO_2)(CO) (**83**), $^{13}C\{^{1}H\}$ NMR (125.6 MHz, benzene-d_6): 207.8 (W(*C*O), $^{1}J_{13C\text{-}183W}$ = 31.4 Hz, $^{2}J_{13C\text{-}13C}$ = 3.6 Hz), 229.4 (W(η^2-*C*O_2), $^{1}J_{13C\text{-}183W}$ = 67.8 Hz, $^{2}J_{13C\text{-}13C}$ = 3.6 Hz), as seen in Figure 22.

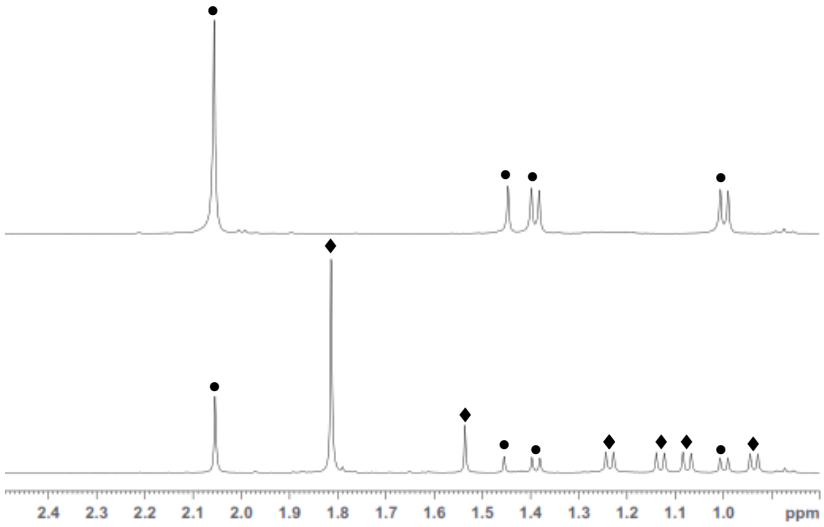

Figure 20: ^{1}H NMR spectra of complex **63** (circles) in the absence (top) and presence of carbon monoxide (bottom) for the formation of an equilibrium mixture with complex **83** (diamonds). (Note: Septet region of spectra are not shown for greater clarity of spectra).

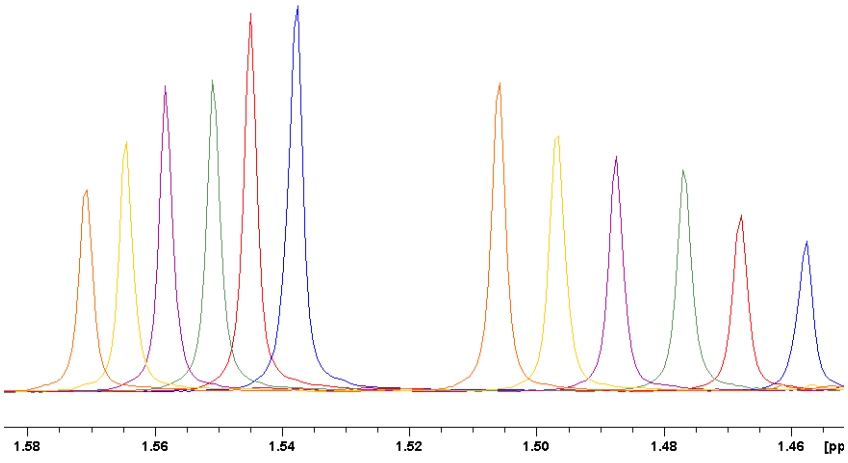

Figure 21: ^{1}H NMR spectra of the amidinate methyl region for an equilibrium mixture of complexes **63** (right peaks) and **83** (left peaks) when complex **63** is in the presence of carbon monoxide at 25 ºC (blue), 30 ºC (orange), 34.5 ºC (green), 39 ºC (purple), 44 ºC (yellow) and 48.5 ºC (orange).

Importantly, through a survey of reaction solvents, it was found that the reaction of a pentane solution of **63** with CO produced fine orange crystals in moderate yield (59%), suggesting the ability of this solvent to shift the equilibrium of **63** and **83** completely to the formation of **83**. Single crystal X-Ray diffraction of this material in conjunction with elemental analysis was subsequently used to definitively assign the structure of the observed C_1 symmetric complex as **83** whose structure and relevant geometric parameters are provided in Figure 23. Structurally, **83** was found to contain a O-C bond, O2-C19 = 1.335(17) Å, and sp^2-like carbon atom, O1-C19-O2= 128.7(12) °, for the κ^2-*O,C*-carbon dioxide ligand in addition to an elongated C-O bond for the coordinated CO ligand, C20-O3 = 1.157(15) Å, suggestive of back donation by the metal center. This crystallographic structure is further supported by the solid-state infrared (KBr) spectrum of **83** which exhibits bond stretching frequencies of 1686 and 1952 cm^{-1} corresponding to the κ^2-*O,C*- carbon dioxide and coordinated CO ligands. The structural parameters of **83** appear to compare favorably with the sparse reports of κ^2-*O,C*-carbon dioxide complexes in literature (c.f. $(CpMe)_2Nb(\kappa^2\text{-}O,C\text{-}CO_2)CH_2Ph$ for which O1-C1 = 1.290(4) Å, O2-C1 = 1.214(5) Å, and O1-C1-O2 131.9(4)°).[65] Provided the analogous reactivity of **63** with CO, we sought to investigate the reductive elimination of CO_2 from **83**. To monitor any potential reductive elimination, **63** was reacted with ^{13}CO (99%) with the resulting equilibrium, as demonstrated in Figure 22, having been found to slowly produce ^{13}C-labeled carbon dioxide ($^{13}CO_2$) and the ^{13}C-labeled bis(carbonyl) species **55** when left a room temperature for extended periods of time (~1 wk). This propensity for CO_2 to reductively eliminate from **83** contrasts the inability of OCN^tBu to reductively

eliminate from **81** suggesting an effect of ligand π-acidity on the reductive elimination of heterocumulene reaction products.

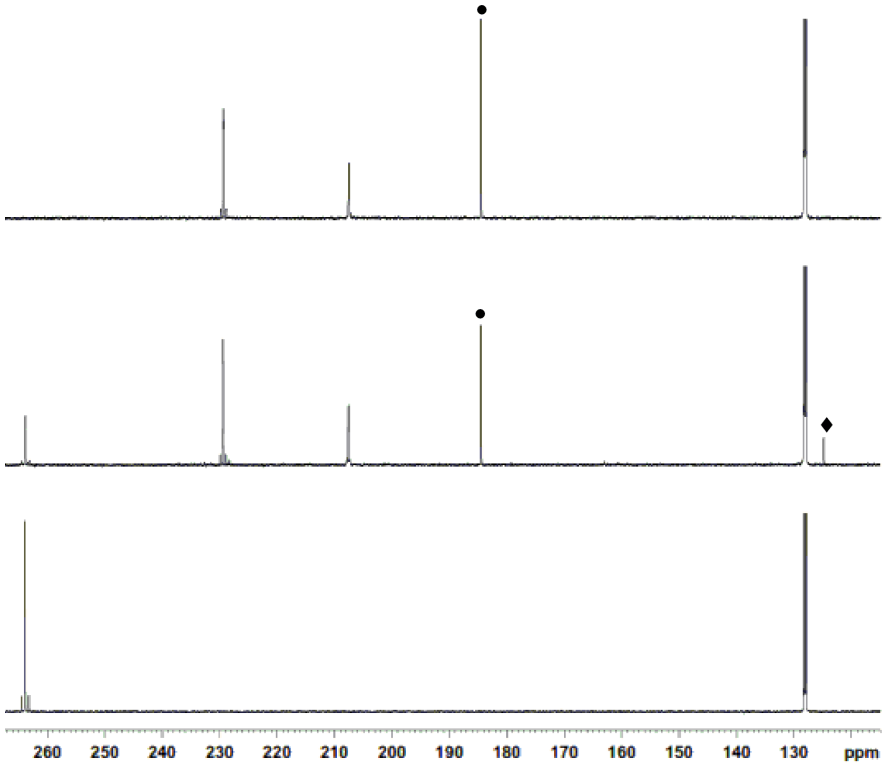

Figure 22: ^{13}C NMR spectra of complex **63** exposed to ^{13}C-labeled carbon monoxide (circles) at 25º C after 1 h (top) and 1 wk (middle) to allow the formation of ^{13}C-labeled complex **55** and ^{13}C-labeled carbon dioxide (diamonds). Reference ^{13}C NMR of ^{13}C-labeled complex **55** (bottom).

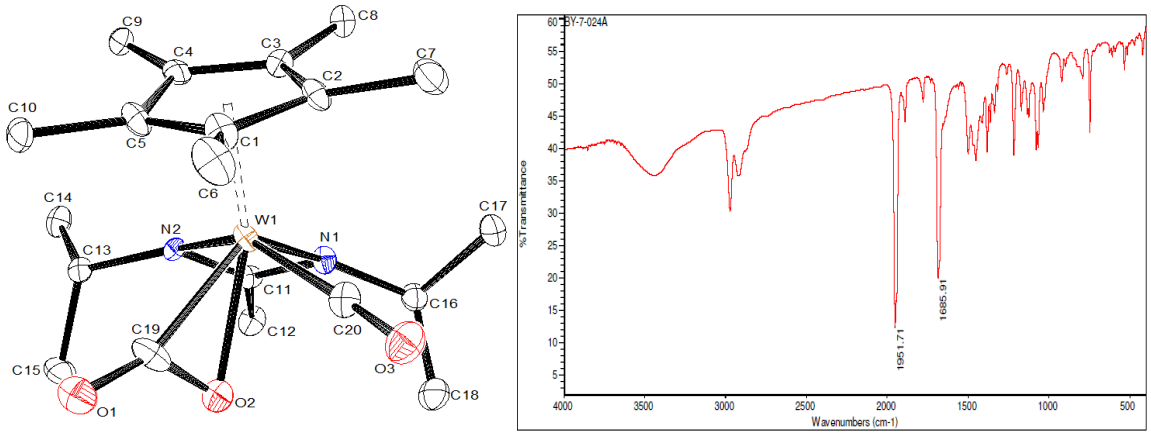

Figure 23: Molecular structure (left) (30% thermal ellipsoids) and solid-state infrared (KBr) spectrum (right) of **83**. Hydrogen atoms have been removed for the sake of clarity. Selected bond lengths (Å) and bond angles (°) for **83**: W1-C19 2.079(12), W1-C20 1.994(13), W1-O2 2.165(9), C19-O1 1.185(16), C19-O2 1.335(17), C20-O3 1.157(15), W1-N1 2.134(9), W1-N2 2.161(10), O1-C19-O2 128.7(12), W1-C20-O3 177.2(11), N2-W1-N1 61.1(3).

Given the ability to reductively eliminate CO_2 from **83**, the analogous reaction of **62** with CO was attempted in research by Dr. Jon Reeds of the Sita group. In this work, it was found that the reaction of **62** with CO resulted in the direct formation of the previously characterized bis(carbonyl) species, **54**, suggesting the immediate elimination of CO_2 upon formation of an analogous intermediate complex Cp*Mo[N(^{i}Pr)C(Me)N(^{i}Pr)](κ^2-*O,C*-CO_2)(CO) (**84**) that was neither observed by ^{1}H nor ^{13}C NMR at room temperature. As a means of confirming the reductive elimination of CO_2, **62** was reacted with ^{13}CO to cause the production of $^{13}CO_2$ at room temperature as confirmed by ^{13}C NMR in Figure 24. This result in combination with the previously observed reductive elimination of OCN^{t}Bu from **81** serves to reinforce the theorized ability to promote heterocumulene reductive elimination from Group 6 CpAm complexes through destabilization of the formal M(IV, d^2) metal oxidation state.

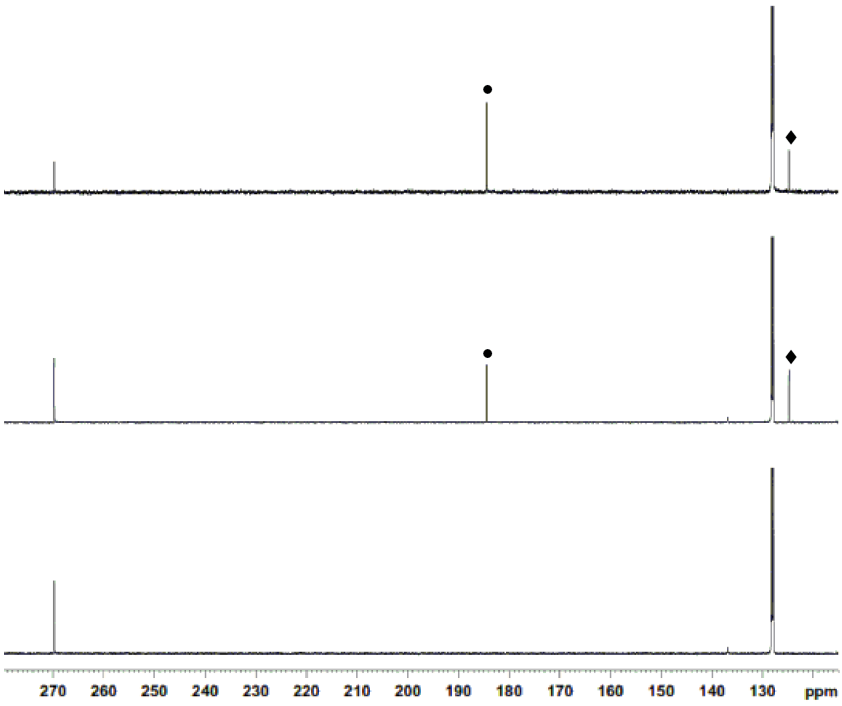

Figure 24: ^{13}C NMR spectra of complex **62** in the presence of ^{13}C-labeled carbon monoxide (10 psi) (circles) at 25º C after 30 m (top) and 18 h (middle) for the evolution of ^{13}C-labeled carbon dioxide (diamonds) and formation of ^{13}C-labeled complex **54**. ^{13}C NMR spectrum of ^{13}C-labeled complex **54** (bottom).

4.3 Light-Mediated Reductive Elimination and Oxidation Processes Involving Group 6 CpAm Oxo Complexes

4.3.1 Light-Mediated Oxidations with Nitrous Oxide

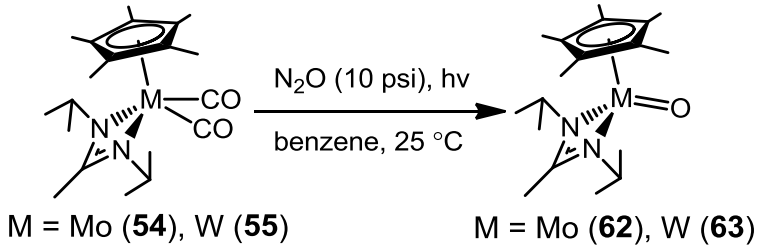

M = Mo (**54**), W (**55**) M = Mo (**62**), W (**63**)

Scheme 30: Light-mediated oxidation of bis(carbonyl) complexes, **54** and **55**, to the corresponding mononuclear oxo complexes, **62** and **63**, by nitrous oxide.

Next we sought to develop a means of oxidizing the bis(carbonyl) reductive elimination products, **54** and **55**, having demonstrated the ability to reductively eliminate CO_2 from **83** and the proposed intermediate **84**, in order to establish conditions for catalytic oxygen atom transfer reactions. As expected, both bis(carbonyl) complexes **54** and **55** were found to be unreactive in the presence of N_2O provided the strong σ-donor and π-acceptor properties of CO. However, provided the well documented photodissociation of carbon monoxide ligands, it was reasoned that exposure of these complexes to UV light could open a coordination site at the metal center for subsequent reaction with oxidants leading to reformation of the oxo complexes **62** and **63**. Toward this end, a benzene-d_6 solution of **55** under a N_2O atmosphere (10 psi) was photolyzed within a Pyrex NMR tube using a Rayonet® carousel of medium pressure Hg lamps. The result seen in Figure 25 was the nearly quantitative formation of the corresponding terminal oxo complex **63** as observed by ^{1}H NMR. Moreover, the photolysis of **54** with N_2O under identical conditions was found to likewise produce the terminal oxo complex **62**, illustrating the ability to oxidize bis(carbonyl) complexes through the photodissociation of CO ligands under oxidizing conditions.

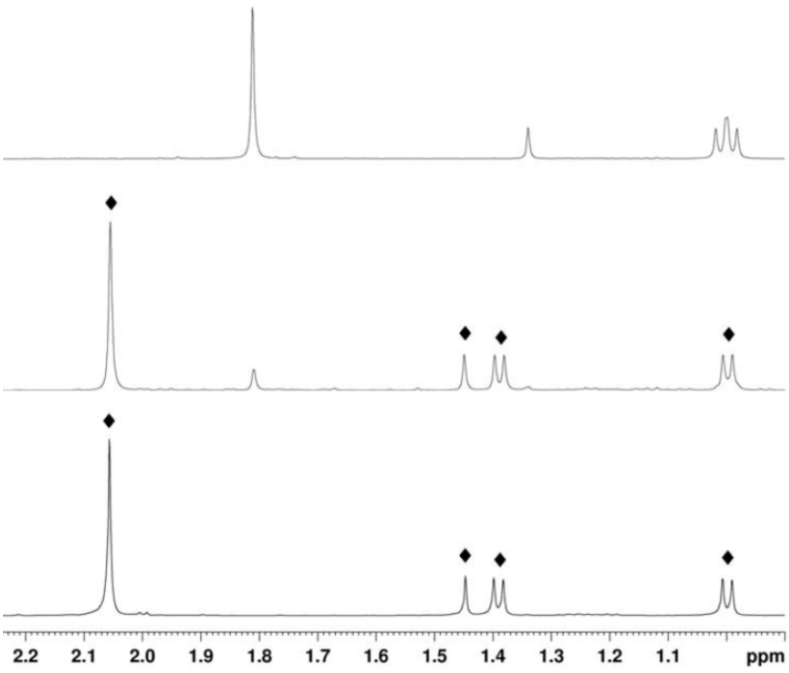

Figure 25: ^{1}H NMR spectra of complex **55** (circles) in the presence of nitrous oxide before (top) and after irradiation with UV light for 3 h (middle) to form complex **63 (**diamonds**)**. Reference ^{1}H NMR spectrum of **63** (bottom). (Note: Septet region of spectra are not shown for greater clarity of spectra).

4.3.2 Light-Mediated Oxidation with Carbon Dioxide

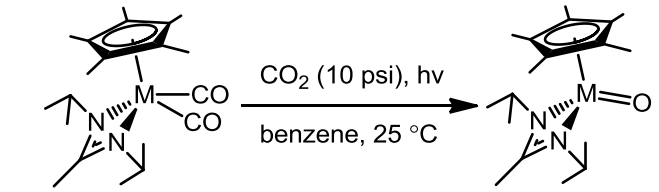

M = Mo (**54**), W (**55**) M = Mo (**62**), W (**63**)

Scheme 31: Light-mediated oxidation of bis(carbonyl) complexes, **54** and **55**, to mononuclear oxo complexes, **62** and **63**, by carbon dioxide.

With the photo-mediated oxidation of **54** and **55** by N_2O, we next sought to determine whether this photo-mediated oxidation process could likewise be extended to the use of CO_2 as an oxidant. To test this theory, a benzene-d_6 solution of **55** in a Pyrex J Young NMR tube was irradiated under an atmosphere of CO_2 (10 psi) with UV light for

6 h to produce the terminal oxo **63** in nearly quantitatively yield along with a small amount of a C_1 symmetric diamagnetic species as observed by ^{1}H NMR. Through comparison with reference spectra this C_1 symmetric species was determined to be the κ^2-*O,C*-carbon dioxide complex **83** as seen in Figure 26. Given the oxidation of this species by CO_2 upon photodissociation of CO, the formation of **83** was presumed to result from the low concentration of CO derived from either CO_2 or the photodissociated carbon monoxide. In an effort to help determine the origin of the CO, ^{13}C-labeled **55** under an atmosphere of unlabeled CO_2 (10 psi) was irradiated with UV light. When the products of this reaction were analyzed by ^{13}C NMR to our surprise the ^{13}C-label appeared to be incorporated in both ^{13}CO and significant amounts $^{13}CO_2$ as seen in Figure 27.

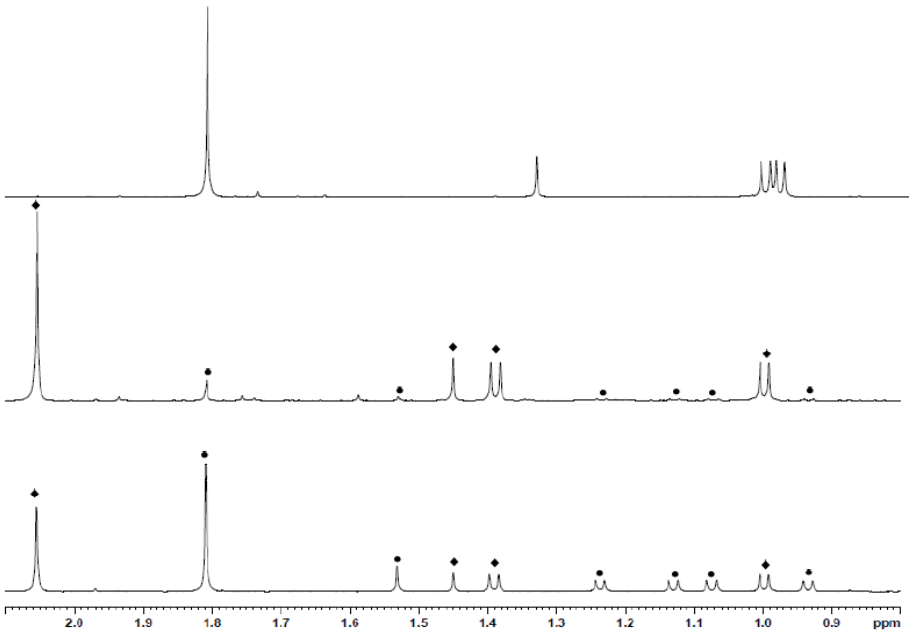

Figure 26: ^{1}H NMR spectra of complex **55** in the presence of carbon dioxide before (top) and after UV irradiation for 6 h (middle) to generate complex **63** (diamonds) and small amounts of complex **83** (circles). ^{1}H NMR spectrum of complex **63** in the presence of carbon monoxide (bottom) to establish an equilibrium with complex **83**. (Note: Septet region of spectra are not shown for greater clarity of spectra.)

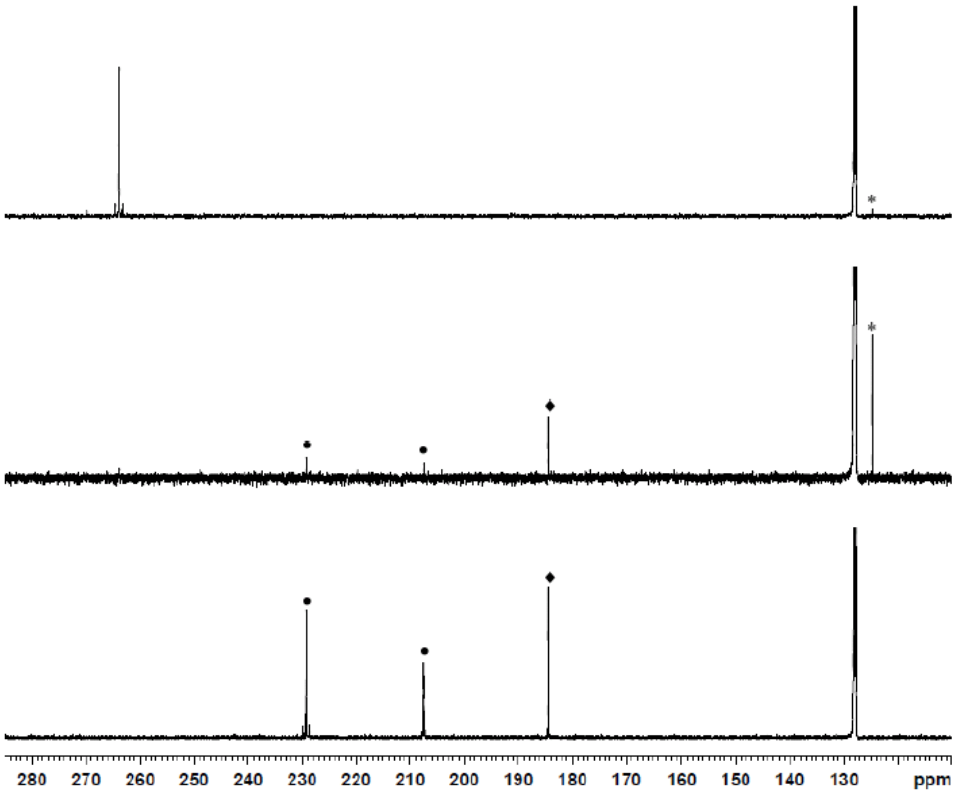

Figure 27: ^{13}C NMR spectra of ^{13}C-labeled complex **55** in the presence of unlabeled carbon dioxide (asterisks) before (top) and after UV irradiation for 3.5 h (middle) to cause evolution of ^{13}C-labeled carbon monoxide (diamonds) and ^{13}C-labeled carbon dioxide (asterisks) as well as the formation of ^{13}C-labeled complex **83** (circles). Reference ^{13}C NMR spectrum of complex **63** in presence of ^{13}C-labeled carbon monoxide to establish an equilibrium with ^{13}C-labeled complex **83** (bottom).

Provided the slow reductive elimination of CO_2 from **83** at room temperature, the migration of the ^{13}C label from the coordinated ^{13}CO ligand of **55** into previously unlabeled CO_2 suggests the potential for the photomediated reductive elimination of CO_2 from **83**. As a means of testing this theory, a benzene-d_6 solution of **63** in a Pyrex J Young NMR tube was placed under an atmosphere of CO to form an equilibrium mixture of **63** and **83**. This equilibrium mixture was then irradiated with UV light to generate in nearly quantitative yield the bis(carbonyl) complex **55**, as observed by ^{1}H NMR in Figure 28, through the presumed reductive elimination of CO_2 from **83**. To confirm this

proposed conversion of **83** to **55** upon the photomediated dissociation of CO_2, a benzene-d_6 solution of **63** was reacted with ^{13}CO (5 psi) for the formation of an equilibrium of ^{13}C-labeled **83** with **63**. Upon the exposure of this equilibrium mixture to UV light, as seen in Figure 29, the ^{13}C-label for this experiment was found to migrate to $^{13}CO_2$ and ^{13}C-labeled **55**, conclusively demonstrating that the conversion of **83** to **55** results from the photomediated dissociation of CO_2.

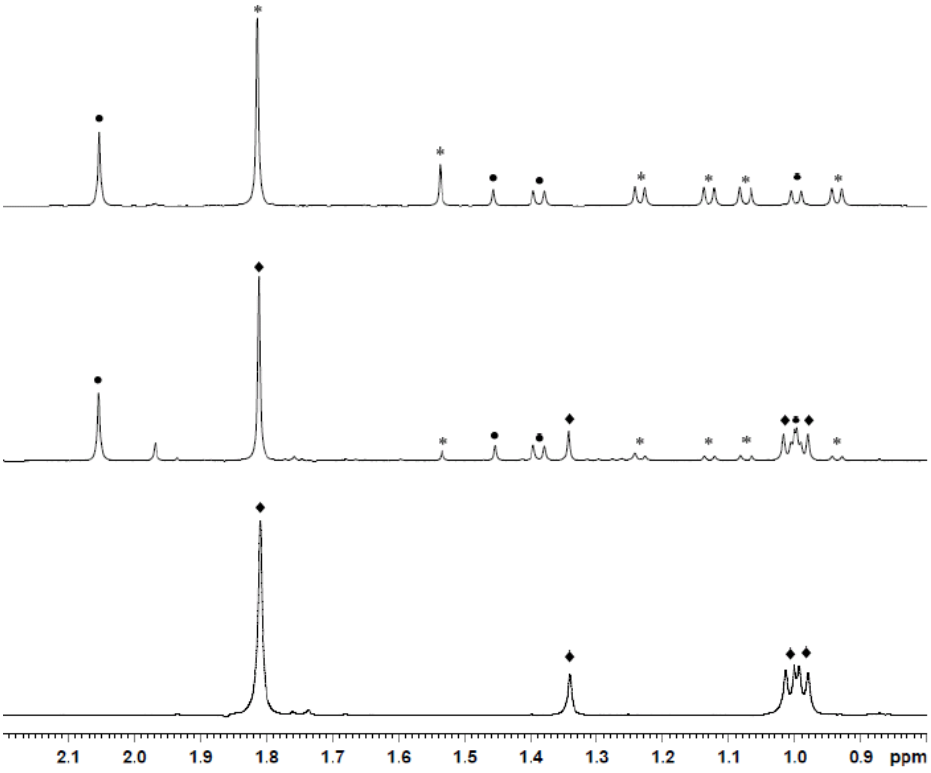

Figure 28: ^1H NMR spectra demonstrating the equilibrium of complex **63** (circles) with complex **83** (asterisks) under a carbon monoxide atmosphere before (top) and after (middle) irradiation with UV for 3 h to generate complex **55** (diamonds) upon the evolution of carbon dioxide. ^1H NMR spectrum of complex **55** (bottom). (Note: Septet region of spectra are omitted for greater clarity of spectra.)

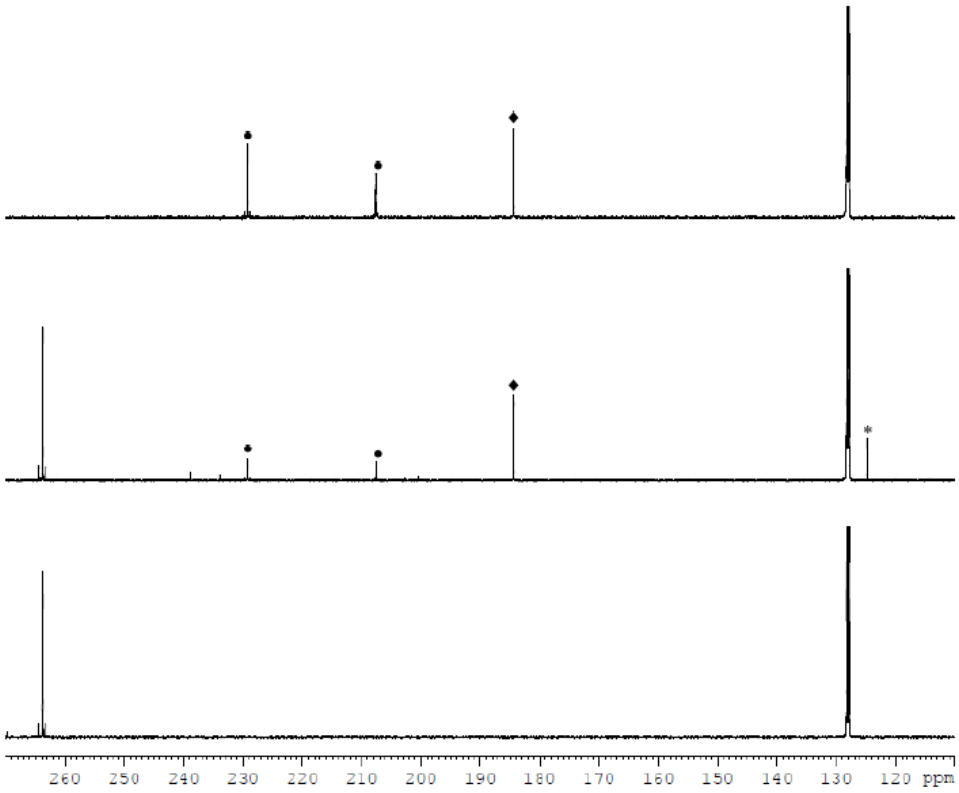

Figure 29: ^{13}C NMR spectra of complex **63** under a ^{13}C-labeled carbon monoxide (diamonds) atmosphere to form complex **83** (circles) before (top) and after (middle) irradiation with UV for 3 h to generate ^{13}C-labeled complex **55** with the evolution of ^{13}C-labeled carbon dioxide (asterisks). Reference ^{13}C NMR spectrum of ^{13}C-labeled complex **55** (bottom).

In a similar manner, through research performed by Dr. Jon Reeds of the Sita group, the irradiation of a benzene-d_6 solution of ^{13}C-labeled **54** under an atmosphere of CO_2 was likewise found to be converted to **62** in a nearly quantitative manner. Unlike ^{13}C-labeled **55** though, the irradiation of ^{13}C-labeled **54** with UV light in the presence of unlabeled CO_2 was found to yield almost exclusively the terminal oxo complex **62** and $^{13}CO_2$. Provided the presence of two equivalents of ^{13}CO ligands for the ^{13}C-labeled starting material, the observed extent of $^{13}CO_2$ conversion from ^{13}CO suggests the possibility of catalytic conversion leading to the selective incorporation of the ^{13}C label

into CO_2 as the result of the presence of stronger C-O bonds in CO_2 versus CO. Notably, provided the ability for **62** to react with CO for the production of CO_2 via its thermal reductive elimination from **84**, it is not known whether a thermal or analogous photodissociative process for the production of $^{13}CO_2$ is operative under the utilized reaction conditions.

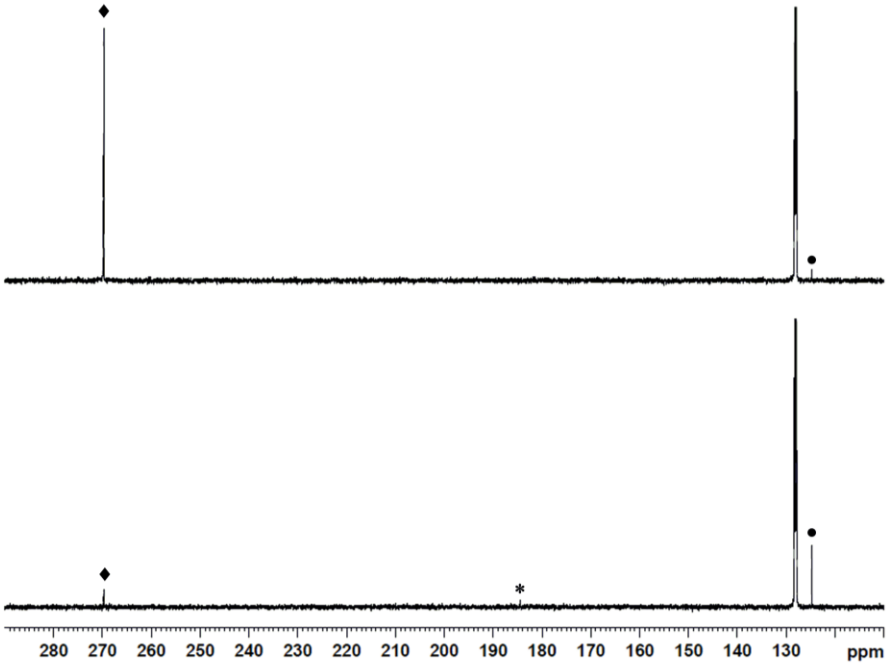

Figure 30: ^{13}C NMR spectra of ^{13}C-labeled complex **54** (diamonds) in the presence of unlabeled carbon dioxide before (top) and after irradiation with UV light for 18 h (bottom) to cause the evolution of ^{13}C-labeled carbon monoxide (asterisks) and ^{13}C-labeled carbon dioxide (circles) upon the formation of **62**.

4.4 Light Mediated Catalytic Oxygen Atom Transfers

4.4.1 Degenerate Oxygen Atom Transfer with Carbon Dioxide

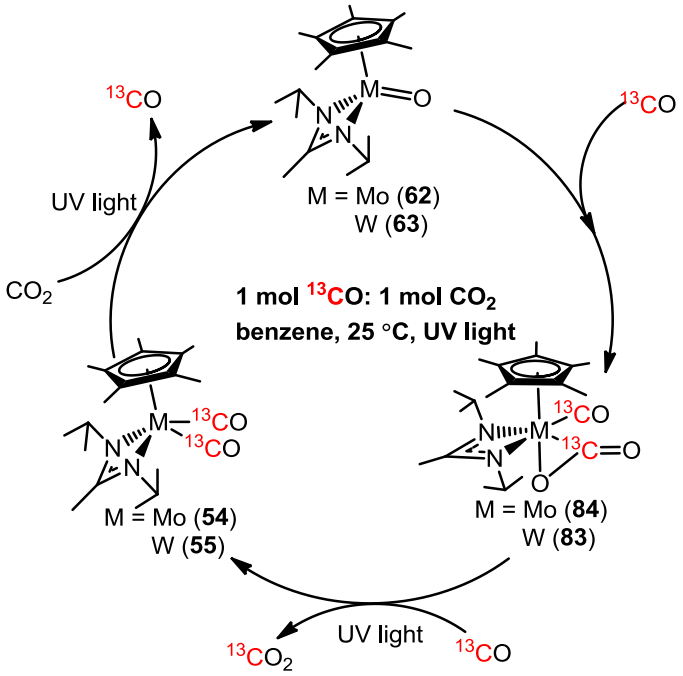

Scheme 32: Proposed light-mediated catalytic cycle for the degenerate oxygen atom transfer reaction involving an equimolar gaseous mixture of ^{13}C-labeled carbon monoxide and unlabeled carbon dioxide.

In principle, all of the fundamental catalytic steps for the transfer of an oxygen atom from CO_2 to CO (i.e. the formation of a κ^2-*C,O*-carbon dioxide complex from the reaction of terminal oxos with CO, the thermal or photomediated reductive elimination of CO_2, and the photomediated oxidation of bis(carbonyl) complexes to terminal oxos) have been demonstrated as stoichiometric reactions with all of the proposed intermediates and reaction products having been isolated and identified. We therefore sought to determine whether the characterized Group 6 CpAm complexes could be used as catalysts for mediating the degenerate transfer of oxygen atoms between ^{13}CO and unlabeled CO_2 through the proposed light-mediated catalytic cycle detailed in Scheme 32. As a means

of investigating this proposed catalytic activity benzene-d_6 solutions of **54** and **55** under an atmosphere (10 psi) of premixed gas containing equimolar amounts of ^{13}CO and CO_2 were irradiated with UV light with progress of the reaction being monitored by ^{13}C NMR. As seen in Figure 31, following irradiation with UV light there is noticeable enrichment of ^{13}C-labeling in CO_2 versus CO when **55** was used as the catalyst, confirming the ability of this complex to mediate degenerate oxygen atom transfer between CO_2 and CO. Moreover, ^{13}C resonances for intermediates **83** and **55** are clearly visible by ^{13}C NMR.

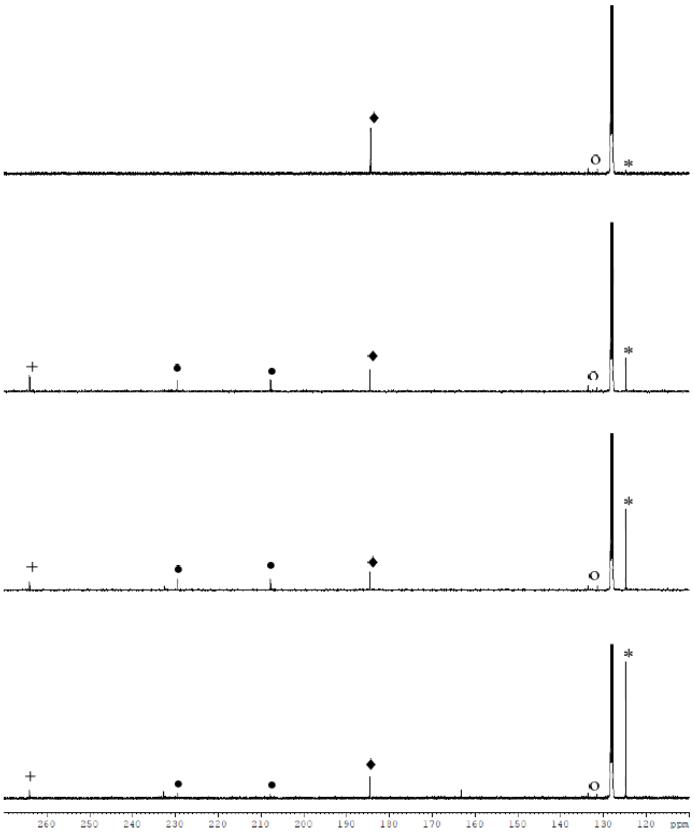

Figure 31: ^{13}C NMR spectra of UV light mediated catalytic reaction of unlabeled complex **55** in the presence of an equimolar mixture of ^{13}C-labeled carbon monoxide (diamonds) and unlabeled carbon dioxide after 0 h (top), 4 h (top middle), 18 h (bottom middle) and 100 h (bottom) for the production of ^{13}C-labeled carbon dioxide (asterisks) and unlabeled carbon monoxide. Identifiable catalytic intermediates include ^{13}C-labeled complex **55** (crosses) and ^{13}C-labeled complex **83** (circles). (Note: Open circles denote ^{13}C resonances of natural abundance from the durene internal standard.)

Surprisingly, when comparing the catalytic activity of **54** and **55** under the same photocatalytic reaction conditions, as depicted in Figure 32, it was found that the tungsten system, mediated by **55**, exhibited substantially greater degenerate oxygen atom transfer activity relative to the molybdenum system mediated by **54**. The basis for this metal dependent effect on catalytic turnover at present is not fully understand although it is suspected that the choice of catalytic initiators (i.e. bis(carbonyl) complexes **54** and **55** versus the terminal oxo complexes **62** and **63**) may have had some effect on the observed relative reaction rates. To the best of our knowledge, the photocatalytic degenerate oxygen atom transfer reactivity observed for **54** and **55** represents the first ever catalytic oxygen atom transfer reaction mediated by an early transition metal. This reactivity is in stark contrast to previous early transition metal complexes for which only stoichiometric oxygen atom transfer reactions involving CO and isocyanides have been observed.[66] This catalytic activity is all the more surprising given the highly exothermic heat of formation for CO_2, $CO\ (g) + \frac{1}{2}\ O_2\ (g) \rightarrow CO_2\ (g)$ where $\Delta H_f = -60$ kcal/mol, which would seem to disfavor the use of CO_2 as an oxidant in the observed catalytic cycle. As such, it seems that this catalytic cycle requires a fine balance of thermodynamic and kinetic barriers to reactivity which at this time is not fully understood.

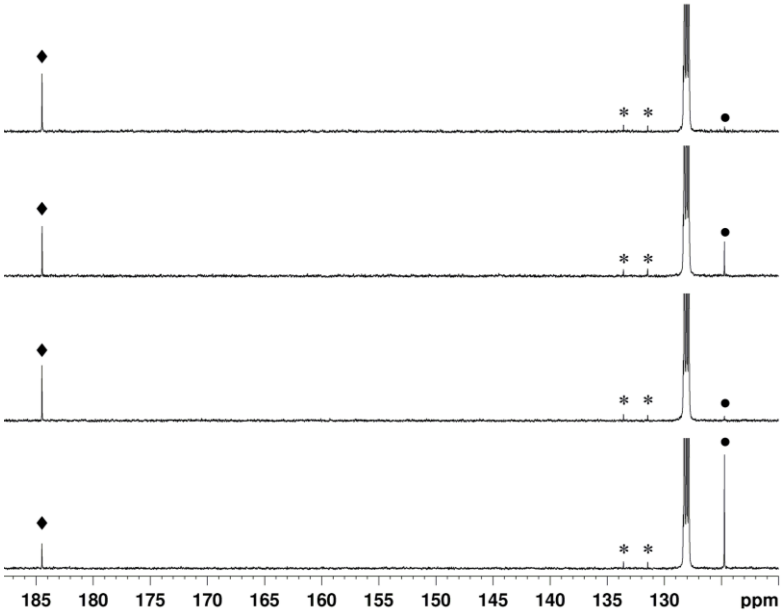

Figure 32: ^{13}C NMR spectra for the photocatalytic scrambling of a ^{13}C-label in an equimolar gaseous mixture of ^{13}CO and unlabeled CO_2 using **54** after 0 h (top) and 18 h (top middle), and **55** after 0 h (bottom middle) and 18 h (bottom). ^{13}C resonances are labeled as CO (diamonds), CO_2 (circles), and a durene internal standard of natural ^{13}C abundance (asterisks).

4.4.2 Non-Degenerate Oxygen Atom Transfer with Nitrous Oxide

With the ability to mediate degenerate oxygen atom transfers involving CO and CO_2 as well as the ability to photolytically oxidize the bis(carbonyl) complexes **54** and **55** to the terminal oxo complexes using N_2O, an alternative photocatalytic non-degenerate oxygen atom transfer process involving N_2O and CO was envisioned. This catalytic cycle, whose proposed mechanism is depicted in Scheme 33, was particularly attractive given the presumed significant thermodynamic driving force for this catalytic cycle involving the formation of inert N_2 and CO_2 gaseous products (N_2O (g) → N_2 (g) + ½ O_2 (g), ΔH_f = -20 kcal/mol and CO (g) + ½ O_2 (g) → CO_2 (g), ΔH_f = -68 kcal/mol).

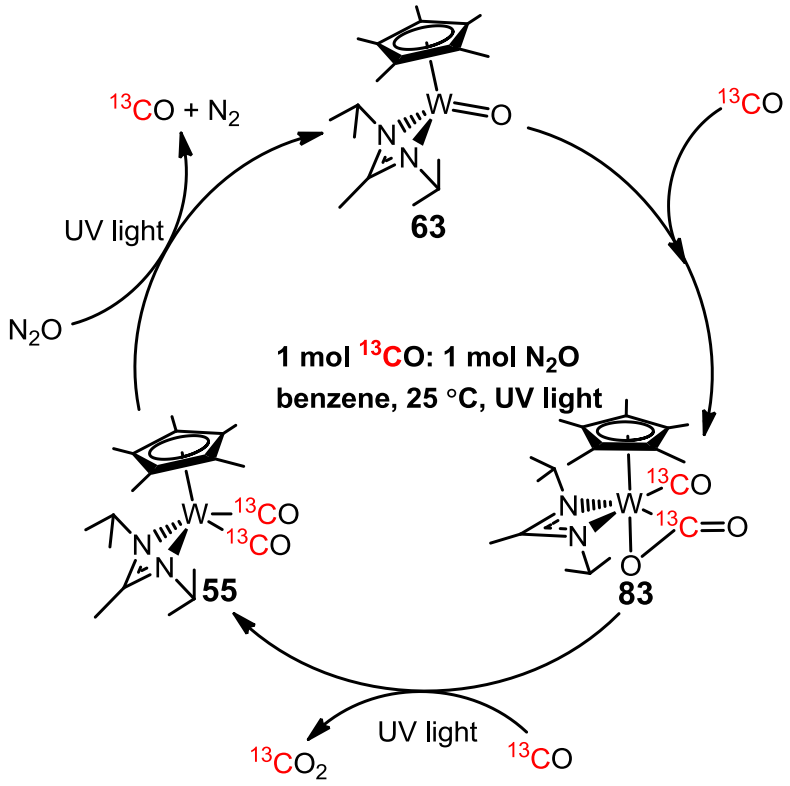

Scheme 33: Proposed light-mediated catalytic cycle for the non-degenerate oxygen atom transfer reaction involving an equimolar gaseous mixture of ^{13}C-labeled carbon monoxide and nitrous oxide.

To assess the feasibility of this proposed catalytic cycle, a benzene-d_6 solution of **55** under an atmosphere (10 psi) of premixed gas containing equimolar amounts of N_2O and ^{13}CO was irradiated with UV light and the progress of the reaction monitored periodically by ^{13}C NMR. As demonstrated in Figure 33, after 16 h the ^{13}C label was found to migrate to $^{13}CO_2$ providing evidence for the proposed non-degenerate oxygen atom transfer from N_2O to CO as mediated by **55**. Despite this observed reactivity, over time under these photocatalytic conditions, **55** was found to be transformed into a complex mixture of decomposition products as the presumed result of the harsh oxidizing conditions. In seeking to demonstrate analogous reactivity with **54**, similar migration of the ^{13}C label into $^{13}CO_2$ was found to occur although at a slower rate as with the

previously characterized photocatalytic degenerate oxygen atom transfer process. However, in contrast to the indistinguishable decomposition of the tungsten system, the catalytic initiator **54** was found to be gradually converted into a nitroso isocyanate complex Cp*Mo[N(^{i}Pr)C(Me)N(^{i}Pr)](NO)(NCO) (**85**) resulting from N-N cleavage of N_2O.[67] Here, the observed non-degenerate photocatalytic oxygen atom transfer chemistry of **54** and **55** was found to complement both the previously detailed degenerate oxygen atom transfer chemistry of these complexes as well as similar reports by Cheng and co-workers on the oxidation of CO to CO_2 by N_2O as mediated by late transition metals.[68]

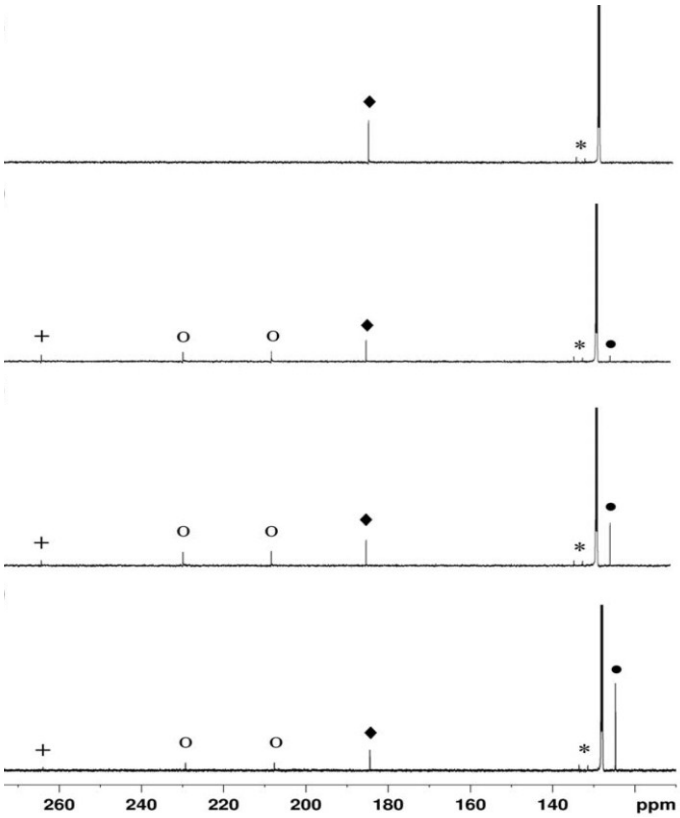

Figure 33: ^{13}C NMR spectra of **55** in the presence of an equimolar mixture of nitrous oxide and ^{13}C-labeled carbon monoxide (diamonds) after 0 h (top), 1 h (top middle), 4 h (bottom middle), and 16 h (bottom) to produce ^{13}C-labeled carbon dioxide (circles). Identifiable catalytic intermediates include ^{13}C-labeled complex **83** (open circles) and ^{13}C-labeled complex **55** (crosses). (Note: Asterisks denote ^{13}C resonances of natural abundance from the durene internal standard.)

Chapter 5: Nitrogen Atom Transfer Reactions with Group 6 CpAm Imidos

5.1 Introduction and Background

A foundational goal of *green* chemistry is the development and introduction of safer, more environmentally-benign chemicals and chemical processes.[69] Isocyanates, RNCO, are important commodity chemicals used in the industrial production of pesticides, herbicides and polyurethane-based materials.[70] However, there is considerable concern over the transportation and on-site storage of large volumes of isocyanates near populated areas, most notoriously, in the case of methyl isocyanate.[71] An attractive alternative, therefore, is the development of highly efficient synthetic transformations that can be used to provide an 'on-demand' source of isocyanates from readily available, inexpensive and innocuous chemical precursors versus traditional synthetic routes involving phosgene gas.[72]

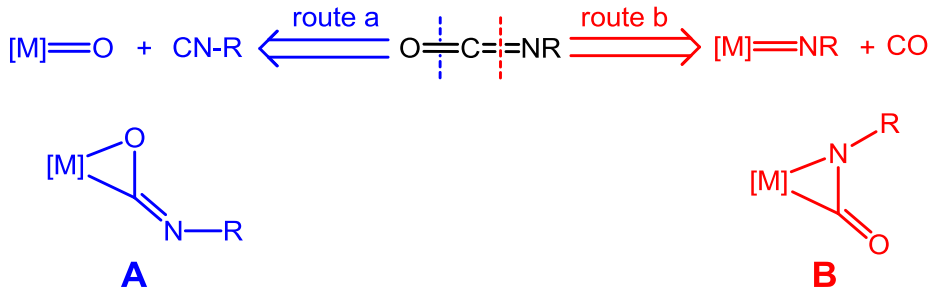

Figure 34: Orthogonal retrosynthetic metal-mediated routes to isocyanates.

Figure 34 presents two retrosynthetic metal-mediated routes to isocyanates that involve an oxygen-atom transfer to an isocyanide (CNR) (*route a*) and nitrene (imido) carbonylation (*route b*).[73, 74, 75] Relevant intermediates for these processes include isomeric κ^2-isocyanate complexes in which the isocyanate fragment is bound to the metal

in either a κ^2-*O,C* fashion in the case of *route a* or through κ^2-*C,N* ligation in the case of *route b* (i.e., structures **A** and **B**, respectively, in Figure 34).[76] For both metal-mediated transformations, a significant challenge is the establishment of reaction energy profiles in which the thermodynamic and kinetic requirements for group transfers to, and from, the metal center can be achieved with catalytic turnover under practical synthetic conditions. Following the success in developing a catalytic process for *route a* that is based on an oxygen atom transfer to isocyanides using N_2O, $N_2O + CNR \rightarrow N_2 + OCNR$, and the novel M(II, d^4)/M(IV, d^2) redox couple for **62** and **63**, we wondered whether *route b* could be established using the terminal imido complexes **64** and **65**. On the basis of identical formal charge and similarity of frontier molecular orbitals, the isolobal terminal imido ligands of **64** and **65** are expected to exhibit similar reactivity to the terminal oxo ligands of **62** and **63**. Therefore, nitrene carbonylation of **64** and **65** is anticipated to provide the isomeric κ^2-*C,N*-isocyanate complexes required for *route b* with the ability to synthesize imidos through the use of organic azides allowing for oxidation of the metal center during catalysis. Extending this analogy of imido versus oxo reactivity, it is hoped that the formation of dinitrogen and isocyanates from organic azides and CO could provide similar thermodynamic conditions that favour catalytic turnover analogous to that previously observed for the non-degenerate oxygen atom transfer involving N_2O and CO. Considered together, such a result would serve to highlight the unique ability of the cyclopentadienyl, amidinate (CpAm) ligand set to support small molecule activation with a novel M(II, d^4)/M(IV, d^2) redox couple serving to facilitate unprecedented early transition metal heteroatom group transfer chemistry. Moreover, direct access to *route a* and *route b* through the use of nearly isostructural oxo and imido complexes is of

considerable academic interest as a means of assessing the relative energetic barriers to these complementary retrosynthetic routes to isocyanates.

5.2 Proximal Nucleophilic Attack of π-Acidic Ligands

5.2.1 Reaction of Trimethylsilyl Imido Complexes with Carbon Monoxide

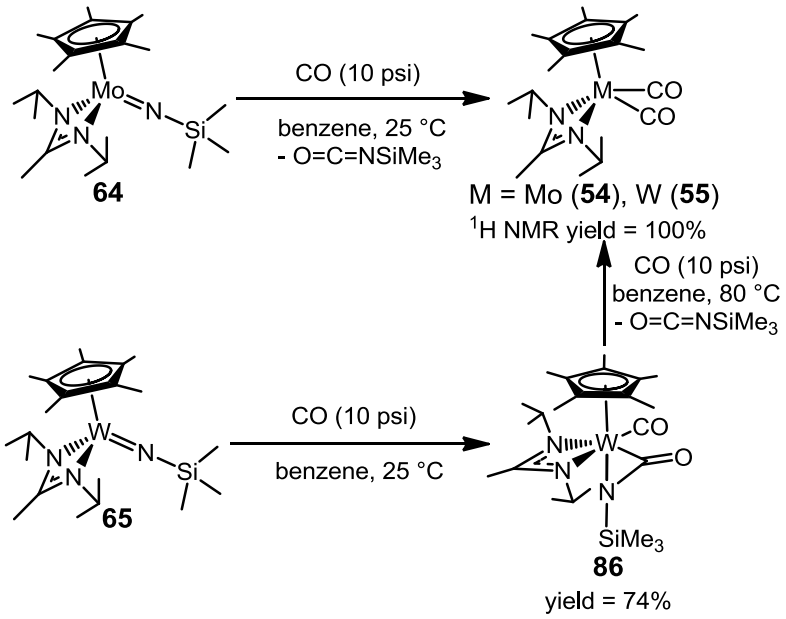

Scheme 34: Reaction of terminal imido complexes **64** and **65** with carbon monoxide for the formation of trimethylsilyl isocyanate.

To begin, **65** was reacted with CO (5 psi) in toluene at 25 ºC to provide orange crystals in good yield (74%). Through a combination of elemental analysis and single crystal X-Ray diffraction, the isolated material was determined to be the κ^2-*C,N*-isocyanate complex Cp*W[N(^{i}Pr)C(Me)N(^{i}Pr)](CO)(κ^2-*C,N*-OCNSiMe$_3$) (**86**) whose molecular structure as well as selected bond lengths and angles are presented in Figure 35. Despite previous literature reports invoking the κ^2-*C,N*- isocyanate binding motif, solid-state structural parameters for early transition metal κ^2-*C,N*-isocyanate complexes

are exceedingly rare.[77] The geometric parameters for **86** that are of note include the elongated N-C bond, N3-C20 = 1.337(2) Å, as well as sp^2-like carbon atom, N3-C20-O2 135.9(2)º, for the κ^2-*C,N*-isocyanate fragment and the elongated C-O bond, C19-O1 = 1.151(3) Å, for the CO ligand that is suggestive of back-donation of electron density from the metal. These structural parameters are consistent with the solid-state infrared spectrum (KBr) for **86** that displays strong absorptions at 1937 cm^{-1} and 1654 cm^{-1} which respectively indicate back donation by the metal center into the CO ligand and the formation of an isocyanate ligand containing a C-O double bond (*cf.* 1721 cm^{-1} for [Nb(η^5-$C_5H_4SiMe_3$)$_2$Cl(κ^2-*C,N*-OCNPh)]).

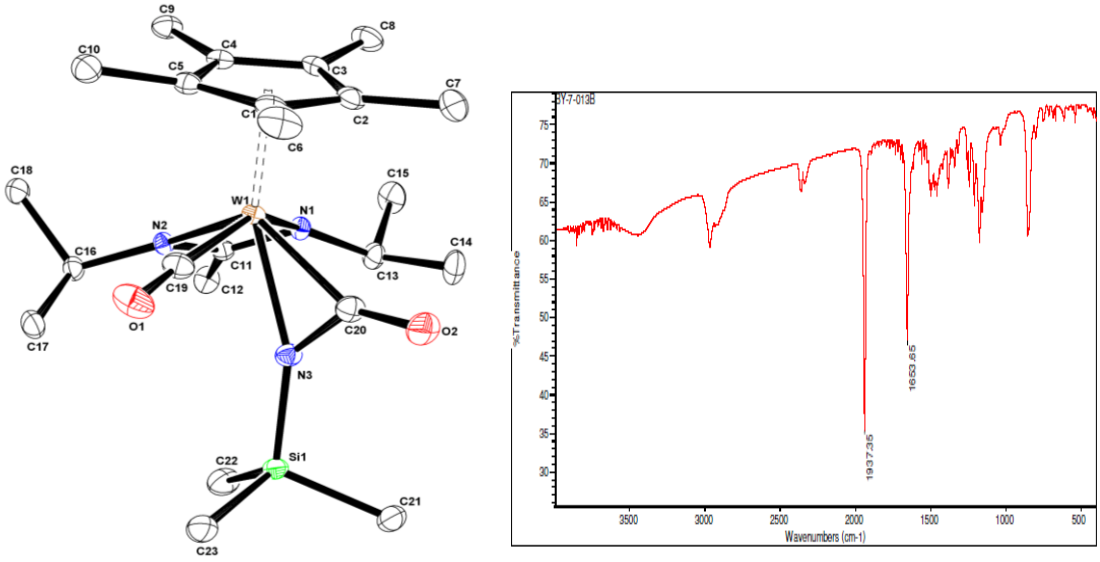

Figure 35: Molecular structure (left) (30% thermal ellipsoids) and solid-state (KBr) infrared spectrum (right) of **86**. Hydrogen atoms have been removed for the sake of clarity. Selected bond lengths (Å) and bond angles (°) for **86**: W1-C20 2.077(2), W1-N3 2.1300(17), C20-N3 1.337(2), C20-O2 1.229(3), W1-C19 1.999(2), C19-O1 1.151(3), W1-N1 2.2224(16), W1-N2 2.1481(16), W1-C19-O1 177.1(2), N1-W1-N2 60.18(6), and N3-C20-O2 135.9(2).

As a means of further characterizing this κ^2-*C,N*-isocyanate complex, **65** was reacted with isotopically labeled ^{13}CO (99%) with the isolated crystalline material of **86**

exhibiting characteristic resonances by ^{13}C NMR, $^{13}C\{^{1}H\}$ NMR (125.6 MHz, benzene-d_6): 209.7 (W(κ^2-*N,C*-O*C*NSiMe$_3$), $^{1}J_{13C\text{-}183W}$ = 23.0 Hz), 228.6 (W(*C*O), $^{1}J_{13C\text{-}183W}$ = 68.0 Hz). Although **86** was found to be stable in solution at 25 °C, at elevated temperatures (*ca* 80 °C) under an atmosphere of CO in a sealed J Young NMR tube, as demonstrated in Figures 36 and 37,^{13}C and ^{1}H NMR revealed the clean conversion of **86** to the previously characterized bis(carbonyl) complex **55** and trimethylsilyl isocyanate (OCNSiMe$_3$) without the observation of additional intermediates (e.g. an isomeric κ^2-*O,C*-isocyanate complex).[78]

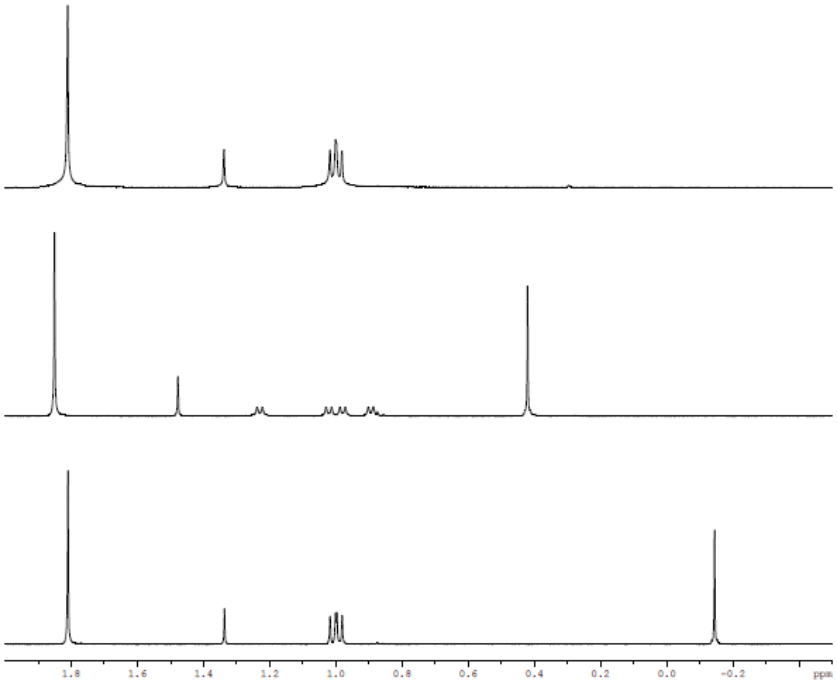

Figure 36: Reference ^{1}H NMR spectrum of complex **55** (top). ^{1}H NMR spectrum of complex **86** at 25 ºC (middle) in the presence of carbon monoxide and after heating at 80 ºC for 2 d (bottom) to cause the release of trimethylsilyl isocyanate and formation of **55**. (Note: Septet region of spectra are not shown for greater clarity of spectra.)

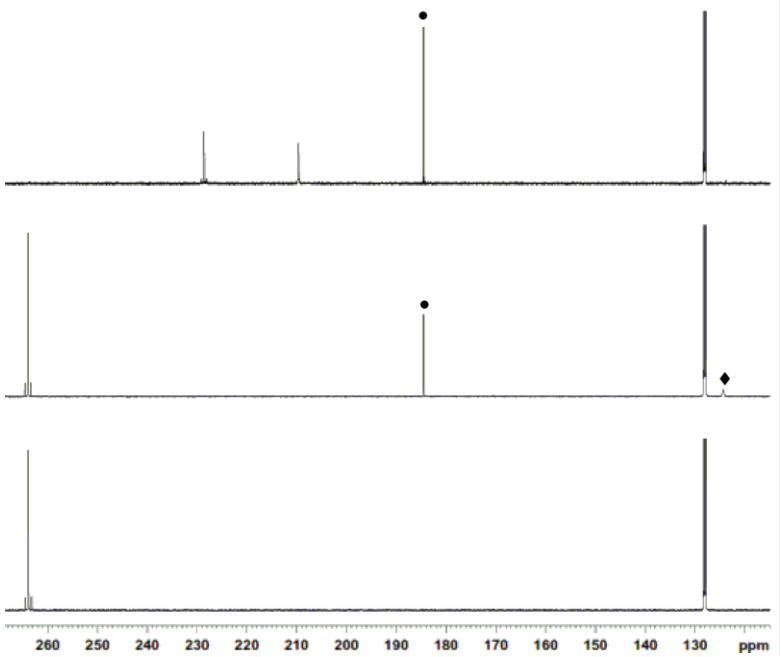

Figure 37: ^{13}C NMR spectrum of ^{13}C-labeled complex **86** at 25 ºC (top) and after heating at 80 ºC for 18 h (middle) in the presence of ^{13}C-labeled carbon monoxide (circles) for the release of ^{13}C-labeled trimethylsilyl isocyanate (diamonds) and the formation of ^{13}C-labeled **55**. Reference ^{13}C NMR of ^{13}C-labeled complex **55** (bottom).

Contrasting this reactivity of **65** is the reactivity of **64** with CO in research performed by Dr. Jonathan Reeds of the Sita Group. As shown in Figure 38, pressurizing a benzene-d_6 solution of the molybdenum analog **64** with CO (10 psi) at 25 °C cleanly provided one equivalent of $OCNSiMe_3$ in addition to the quantitative formation of the bis(carbonyl) **54** after 2 h as determined by ^{1}H NMR. With the previously detailed ability of molybdenum complexes to exhibit lower energetic barriers to the reductive elimination of ligands relative to the analogous tungsten complexes, the conversion of **64** to **54** was believed to occur through the corresponding κ^2-*C,N*-isocyanate complex $Cp^*Mo[N(^iPr)C(Me)N(^iPr)](CO)(\kappa^2$-*C,N*-$OCNSiMe_3)$ (**87**). In an effort to observe this proposed intermediate, low temperature ^{13}C NMR spectroscopy (-25 ˚C) was performed for the reaction of **64** and ^{13}CO with diagnostic ^{13}C resonances, as seen in Figure 39,

$^{13}C\{^{1}H\}$ NMR (125.6 MHz, toluene-d_8, -25.5 ˚C): 200.2 ($^{2}J_{13C\text{-}13C}$ = 3.4 Hz, Mo(κ^2-*C,N*-O*C*NSiMe$_3$) and 236.5 ($^{2}J_{13C\text{-}13C}$ = 3.4 Hz, Mo(*C*O)), having been observed. Combined the observed low temperature ^{13}C NMR resonances along with the analogous formation of OCNSiMe$_3$ serve to further support the theory of decreased barriers to reductive elimination through the destabilization of the formal M(IV, d^2) oxidation state in molybdenum versus tungsten CpAm complexes.

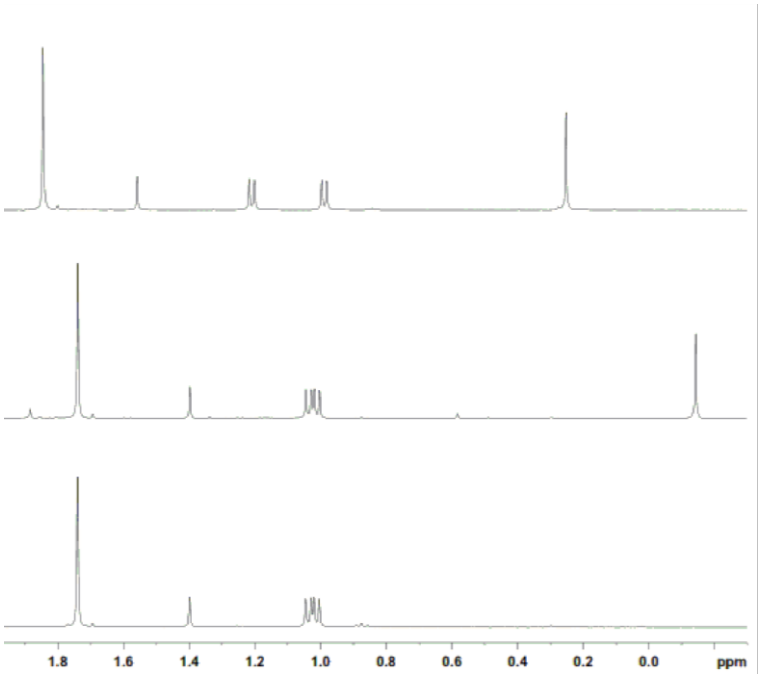

Figure 38: ^{1}H NMR spectrum of complex **64** in the absence (top) and presence (middle) of carbon monoxide (10 psi) at 25 ºC for the production of trimethylsilyl isocyanate and the bis(carbonyl) complex **54**. Reference ^{1}H NMR spectrum of complex **54** (bottom). (Note: Septet region of spectra are not shown for greater clarity of spectra.)

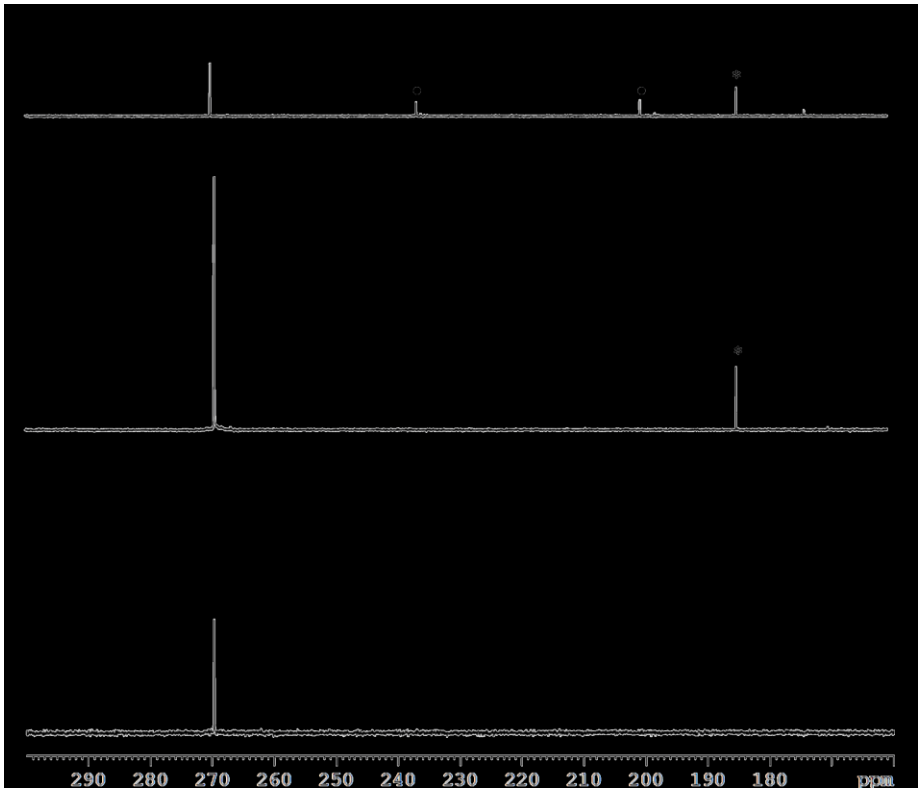

Figure 39: ^{13}C NMR spectrum of complex **64** in the presence of ^{13}C-labeled carbon monoxide (10 psi) (asterisks) at -25.5 ºC (top) for the formation of a κ^2-*C,N*-$OCNSiMe_3$ intermediate **87** (circles) and the subsequent release of ^{13}C-labeled trimethylsilyl isocyanate with the formation of ^{13}C-labeled **54** at 25 ºC (middle). Reference ^{13}C NMR spectrum of ^{13}C-labeled complex **54** (bottom).

5.2.2 Thermal-Mediated Catalytic Synthesis of Isocyanates

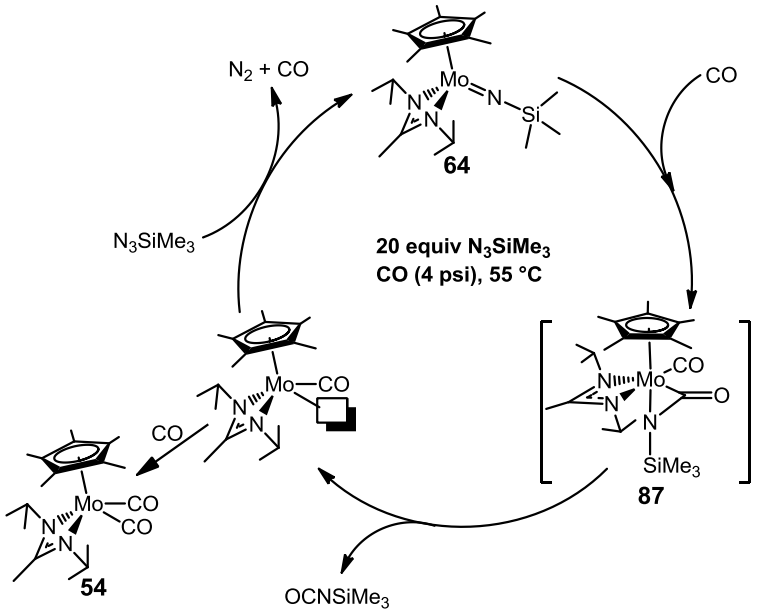

Scheme 35: Proposed *thermal-mediated* catalytic production of trimethylsilyl isocyanate from the reaction of trimethylsilyl azide with carbon monoxide when using **64** as a catalytic initiator.

The ease with which the proposed intermediate **87**, having a less stable M(IV, d^2) formal oxidation state, engages in nitrene carbonylation at even subambient temperatures (-25 °C) is quite surprising. Particularly so for an early transition metal system which typically resists reductive elimination and in the case of M(II, d^4) complexes, where M = Mo and W, has been shown to favor isocyanate decarbonylation in research by Mayer and co-workers.[79] It was, therefore, of interest to determine if these results could provide the basis of a catalytic process for the production of isocyanates involving organic azides and CO. Toward this end, in research performed by Dr. Jonathan Reeds of the Sita group, an analogous photocatalytic cycle to that previously demonstrated for the *light-mediated* oxygen atom transfer reactions involving Group 6 CpAm oxos was envisioned for the

production of isocyanates by Group 6 CpAm imidos. However, while the bis(carbonyl) complex **54** was found to undergo stoichiometric oxidation to **64** through photoirradiation with one equivalent of N_3SiMe_3, as seen by ^1H NMR in Figure 40, the photoirradiation of **54** in the presence of multiple equivalents of N_3SiMe_3 only resulted in decomposition thereby precluding *light-mediated* group transfer catalysis. Despite this result, prior research by our group has established the potential for a coordinatively unsaturated monocarbonyl complex, Cp*Mo[N(^{i}Pr)C(Me)N(^{i}Pr)](CO), that can engage in substrate complexation and the activation and cleavage of strong bonds.[67] Therefore, it was reasoned that, provided the facile thermal reductive elimination of $OCNSiMe_3$, this reactive monocarbonyl complex could still undergo preferential oxidation by N_3SiMe_3 during *thermally-mediated* catalysis versus reaction with gaseous CO to form the otherwise kinetically inert bis(carbonyl) complex, **54**. To test this theory, **64** was heated at 55 ºC in the presence of 20 equivalents of N_3SiMe_3 and CO (4 psi) to produce 4 equivalents of $OCNSiMe_3$ after 18 h when this reaction was monitored by ^1H NMR, Figure 41. Similar to the production of isocyanates and CO_2 using **62** and **63**, the catalytic formation of isocyanates by **64** is believed to occur as the result of the mild nucleophilicity of **3** that precludes its reaction with heterocumulenes (e.g. isocyanates) in contrast to previous observations for other early transition metal imidos.[80]

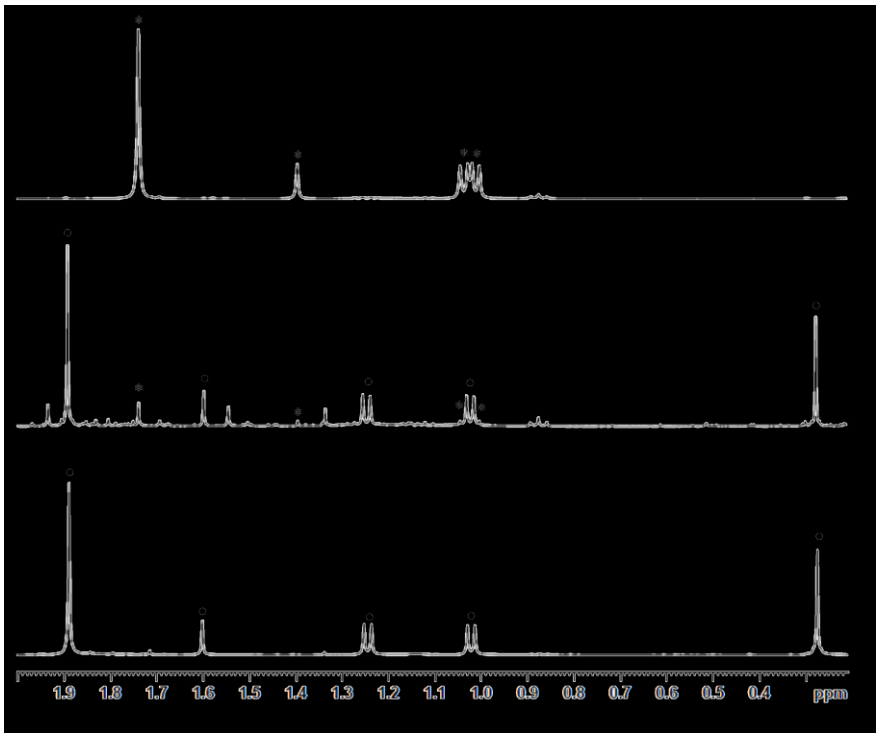

Figure 40: ^{1}H NMR of the photolysis of **54** (asterisks) (top) in the presence of excess trimethylsilyl azide for 1 h leading to the formation of **64** (circles) (middle). Reference ^{1}H NMR spectrum of **64** (bottom). (Note: Septet region of spectra are not shown for greater clarity of spectra.)

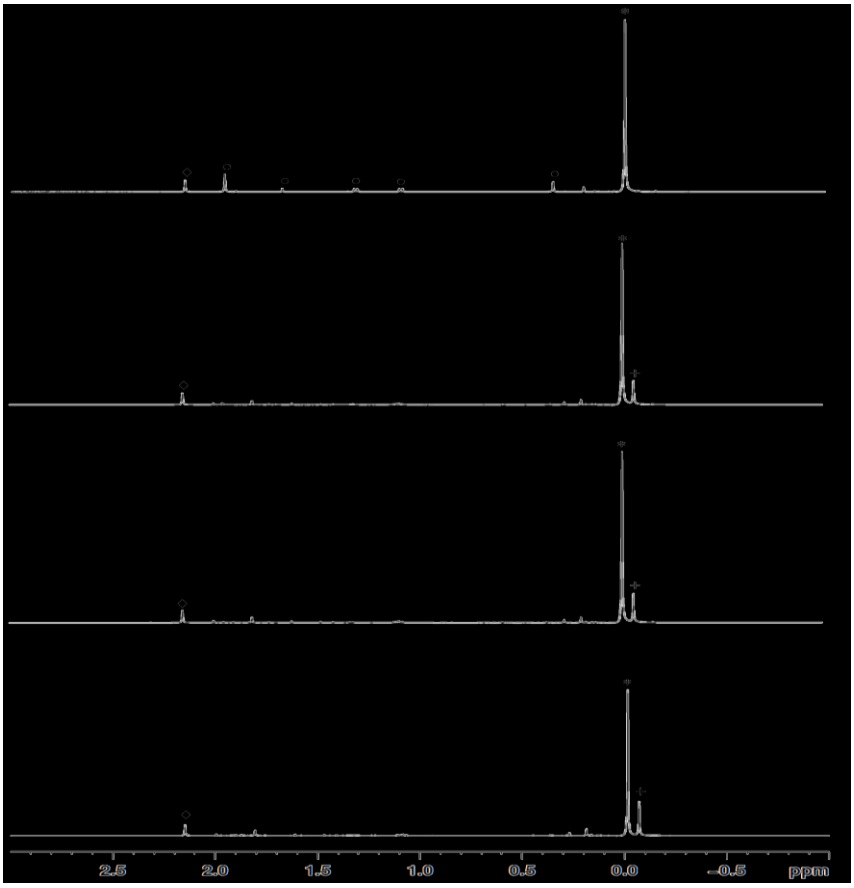

Figure 41: ^{1}H NMR spectra at 0 h (top), 2 h (top middle), 4 h (bottom middle) and 18 h (bottom) for the catalytic synthesis of trimethylsilyl isocyanate (crosses) from 20 equivalents of trimethylsilyl azide (asterisks) and carbon monoxide (4 psi) using **64** (circles) as the catalytic initiator. (Note: Catalytic turnover was assessed through the use of a durene internal standard (diamonds) during the reaction. Septet region of spectra are not shown for greater clarity of spectra.)

5.3 Mechanistic Analysis of Nitrene Group Transfer

5.2.1 Synthesis of a Monocarbonyl Model Complex

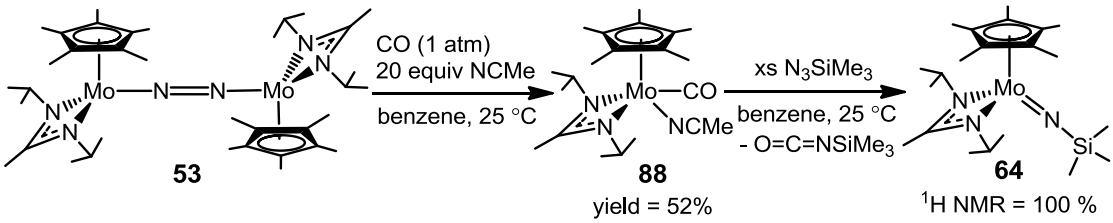

Scheme 36: Synthesis and reactivity of a monocarbonyl model complex, **88**, for investigating the potential intermediacy of a monocarbonyl complex in the catalytic synthesis of isocyanates.

To assess the potential intermediacy of the proposed monocarbonyl complex, Cp*Mo[N(^{i}Pr)C(Me)N(^{i}Pr)](CO)(NCMe) (**88**), which is analogous to the bis(carbonyl) **54** yet has a more labile acetonitrile ligand, was prepared and characterized by Dr. Jonathan Reeds of the Sita group in moderate yield (52%) through the reaction of **53** with acetonitrile and CO. From crystallographic and solid-state infrared (KBr) spectral analysis, as seen in Figure 42, the proposed labile nature of the acetonitrile ligand is supported by the short C-N bond, N1-C2 = 1.1416(16) Å, and sp-like bond angle, N1-C2-C3 = 177.15(14)˚, for this ligand as well as the weak extent of back donation by the metal center as evidenced by a stretching frequency of $\nu_{C\equiv N}$ = 2244 cm^{-1} (*c.f.* 2254 cm^{-1} for free acetonitrile).

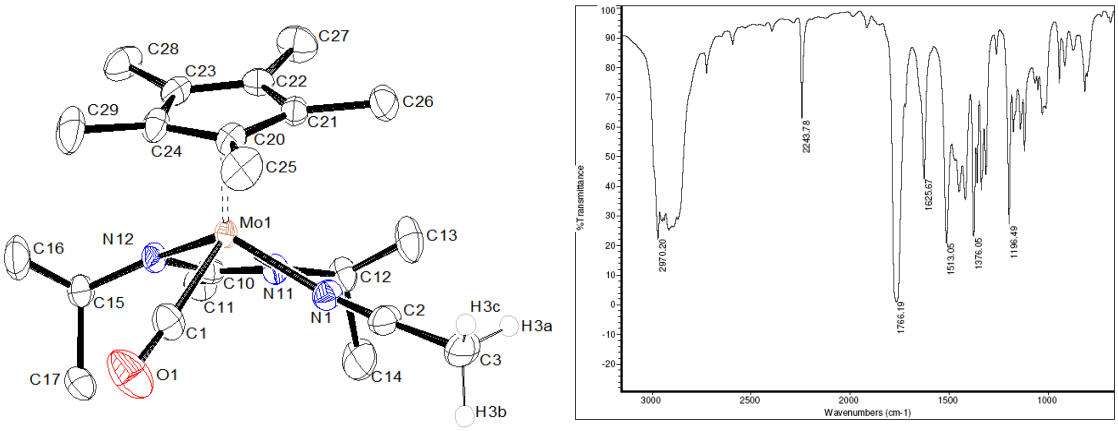

Figure 42: Molecular structure (left) (30% thermal ellipsoids) and solid-state (KBr) infrared spectrum (right) of **88**. Hydrogen atoms have been removed for the sake of clarity. Selected bond lengths (Å) and bond angles (°) for **88**: Mo1-C1 1.8938(13), C1-O1 1.1834(16), Mo1-N1 2.1243(10), N1-C2 1.1416(16), N1-C2-C3 177.15(14).

Due to the labile nature of the acetonitrile ligand, in the reaction of **88** with N_3SiMe_3 this complex was found to quantitatively produce **64** and $OCNSiMe_3$ demonstrating the potential for the proposed monocarbonyl intermediate to be oxidized by N_3SiMe_3 in solution. Moreover, similar *thermally-mediated* catalytic efficiency for

isocyanate synthesis was demonstrated by the use of **88** as a catalytic initiator in the presence of excess N_3SiMe_3 and CO further confirming the intermediacy of the monocarbonyl complex during catalysis.

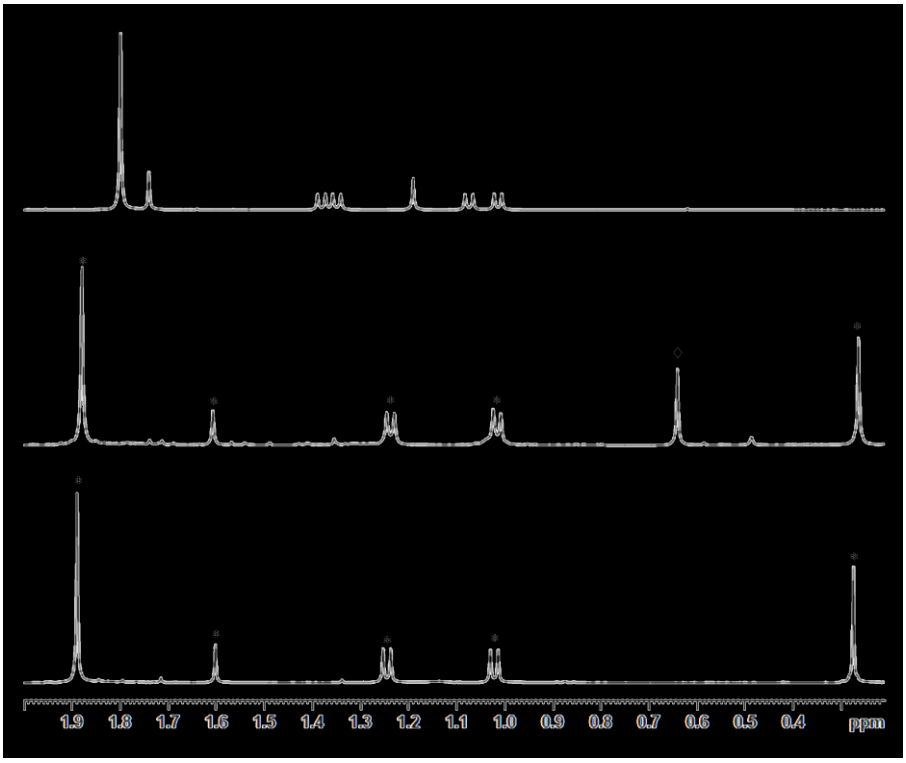

Figure 43: ^{1}H NMR spectra of the reaction of **88** (top) with excess trimethylsilyl azide for the formation of **64** (asterisks) and free acetonitrile (diamonds) (middle) after 2 h at room temperature. Reference ^{1}H NMR spectrum of **64** (bottom). (Note: Septet region of spectra are not shown for greater clarity of the spectra.)

5.2.2 Synthesis of a Cationic Trimethylsilyl Imido Complex

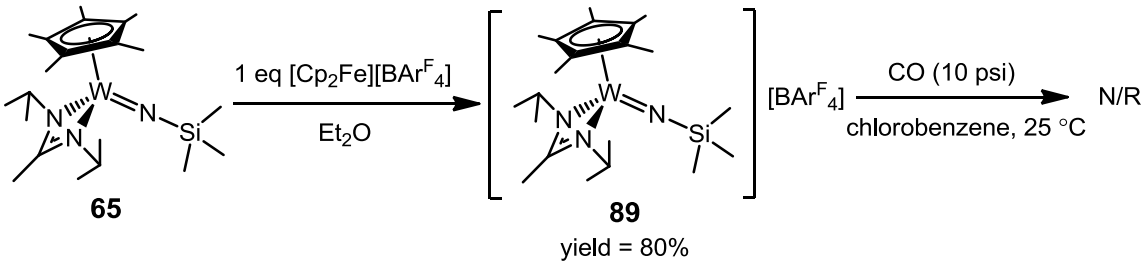

Scheme 37: Synthesis of cationic trimethylsilyl imido complex **89** and its apparent lack of reactivity with carbon monoxide.

To further determine the requirements for the catalytic synthesis of isocyanates from terminal imidos, a cationic imido complex, {Cp*W[N(^{i}Pr)C(Me)N(^{i}Pr)](NSiMe$_3$)}{B[3,5-(CF$_3$)$_2$C$_6$H$_3$]$_4$}$_2$ (**89**) was synthesized in good yield (80%) through the reaction of **65** with 1 equivalent of ferrocenium tetrakis[3,5-bis(trifluoromethyl)phenyl]borate ([Cp$_2$Fe][BAr^F]) in Et$_2$O. Specifically, **89** could be isolated as paramagnetic dark purple crystals that were characterized by elemental analysis and single-crystal X-Ray diffraction with the structure and selected bond lengths and angles for this complex provided in Figure 44. In comparing the molecular structure of **89** with **65** the experimentally-determined geometric parameters for **89**, W1-N3 = 1.746(2) Å and W1-N3-Si1 = 176.88(13)º, were found to be highly isostructural with those of **65**, W1-N3 = 1.763(4) Å and W1-N3-Si1 = 175.0(3)˚, suggesting the presence of a metal centered HOMO having little effect on imido ligand bonding. Surprisingly, despite similar geometric parameters and greater presumed electrophilicty of the metal center, complex **89** was determined to be unreactive toward CO in chlorobenzene. Therefore, the required d^2 metal configuration for reactivity with CO suggests the need to bind the Lewis acidic CO ligand to the metal center prior to a proximal nucleophilic attack by the multiply bonded imido ligand for the formation of a κ^2-*C,N*-isocyanate ligand.

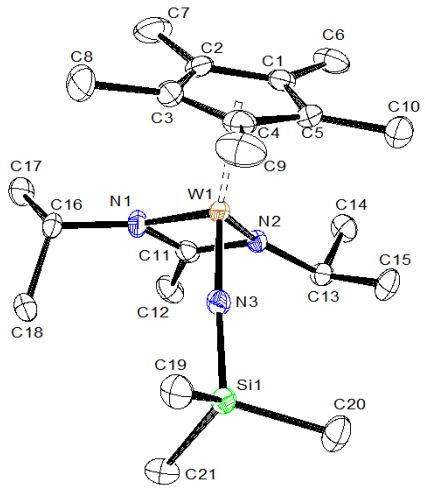

Figure 44: Molecular structure (30% thermal ellipsoids) of **89**. Hydrogen atoms have been removed for the sake of clarity. Selected bond lengths (Å) and bond angles (°) for **89**: W1-N3 1.746(2), N3-Si1 1.773(2), W1-N1 2.077(2), W1-N2 2.097(2), N2-W1-N1 62.87(9), W1-N3-Si1 176.88(13).

5.2.3 Reaction of *Tert*-Butyl Imido Complexes with Carbon Monoxide

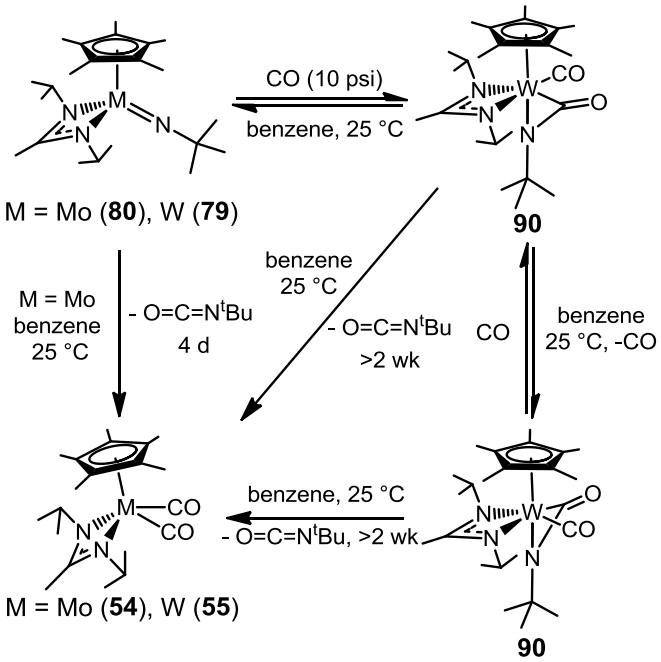

Scheme 38: Reactivity of terminal *tert*-butyl imido complexes, **79** and **80**, with carbon monoxide for the formation of a κ^2-*C,N*-isocyanate complex leading to the gradual reductive elimination of *tert*-butyl isocyanate.

Given the surprisingly facile reductive elimination of $OCNSiMe_3$ from the κ^2-*C,N*-isocyanate complexes **86** and **87** relative to the reductive elimination of *tert*-butyl isocyanate (OCN^tBu) from the κ^2-*O,C*-isocyanate complexes **81** and **82**, we sought to determine whether the Lewis acidic trimethylsilyl groups of **64** and **65** played a role in promoting the reductive elimination of κ^2-coordinated ligands. To test this effect, a benzene-d_6 solution of the previously synthesized terminal tert-butyl imido complex **79** was reacted with CO (10 psi) to give a mixture of diamagnetic complexes observed by ^{1}H NMR that included the starting material **79** and a new fluxional species having an apparent mirror plane of symmetry as depicted in Figure 45. Suspecting a thermally reversible equilibrium reminiscent of the reaction of **63** with CN^tBu, this same NMR sample was subjected to VT ^{1}H NMR to demonstrate the quantitative interconversion of **79** with the fluxional species in which higher temperatures favored the formation of **79** as seen in Figures 45 and 46.

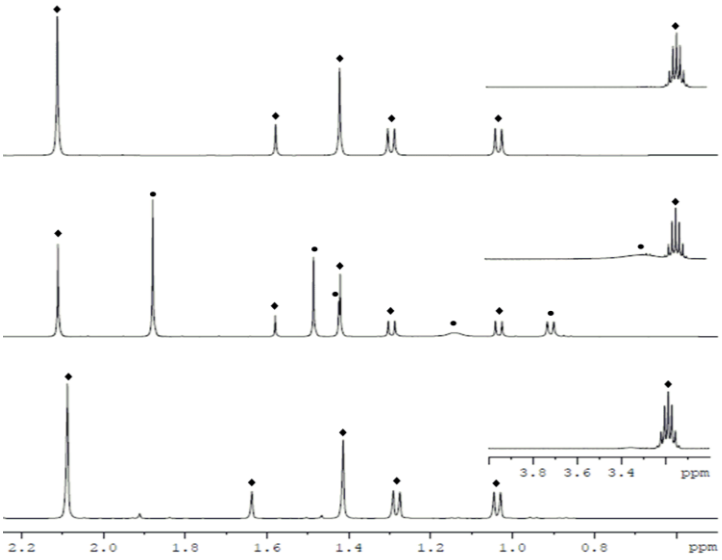

Figure 45: ^{1}H NMR of complex **79** (diamonds) (top) reacted with carbon monoxide (10 psi) at 25 ºC for 2 h to give an equilibrium of **79** with the fluxional species **90** (circles) (middle) and subsequent conversion of **90** to **79** through heating at 70 ºC (bottom). Inset spectra display the amidinate septet regions for **79** and **90**.

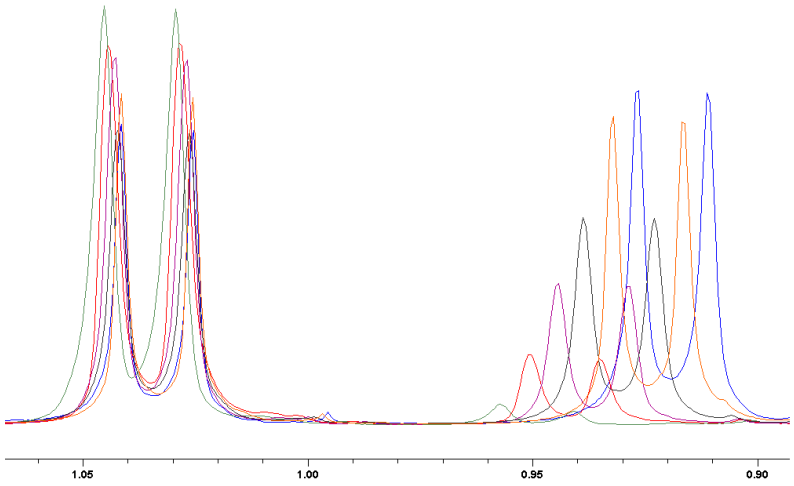

Figure 46: ^{1}H NMR spectra of the amidinate isopropyl region for complex **90** (right peaks) and **79** (left peaks) when complex **79** is in the presence of carbon monoxide at 34 ºC (blue), 40.5 ºC (yellow), 47 ºC (black), 53.5 ºC (purple), 60 ºC (orange) and 66 ºC (green).

Seeking to gain greater insight into the structure of the fluxional species, a toluene-d_8 solution of **79** was reacted with CO to provide an equilibrium of **79** with the new fluxional species. Through low temperature ^{1}H NMR studies, as seen in Figure 47, the fluxionality of the new diamagnetic species having a pseudo mirror plane was found to be frozen out to reveal its underlying C_1 symmetry. With the underlying C_1 symmetry of this fluxional product having been assigned, a toluene-d_8 solution of **79** was reacted with ^{13}CO (99%) to provide extremely weak resonances by ^{13}C NMR. Fortunately, upon cooling of this sample to -70 ˚C the observed ^{13}C NMR resonances were found to sharpen and reveal resonances that are characteristic of a κ^2-*C,N*-isocyanate moiety, $^{13}C\{^{1}H\}$ (125.6 MHz, toluene-d_8, -70 ˚C): 195.3 (W(κ^2-*C,N*-O*C*N^{t}Bu), $^{1}J_{13C\text{-}183W}$ = 15.5 Hz, $^{2}J_{13C\text{-}13C}$ = 1.8 Hz), 228.4 (W(*C*O), $^{1}J_{13C\text{-}183W}$ = 69.4 Hz, $^{2}J_{13C\text{-}13C}$ = 1.8 Hz), as observed in Figure 48. On the basis of the observed ^{13}C NMR resonances the identity of the observed fluxional product is assigned to be the expected κ^2-*C,N*-isocyanate complex Cp*W[N(^{i}Pr)C(Me)N(^{i}Pr)](CO)(κ^2-*C,N*-OCN^{t}Bu) (**90**).

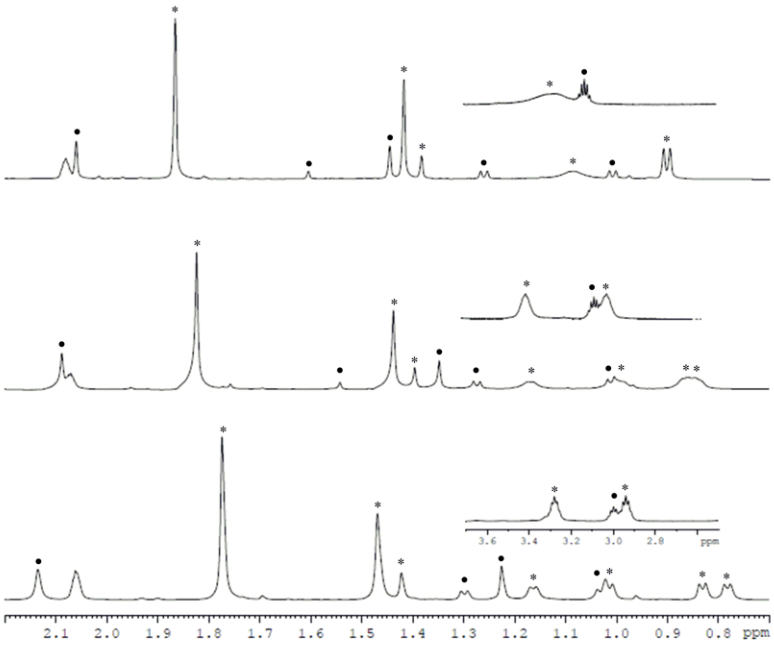

Figure 47: Low temperature ^{1}H NMR for the equilibrium of **90** (asterisks) with **79** (circles) and carbon monoxide at 25 ºC (top), -20 ºC (middle), and -70 ºC (bottom) to reveal the underlying C_1 symmetry of **90** which appears fluxional at room temperature. Inset spectra display the amidinate septet regions for **79** and **90**.

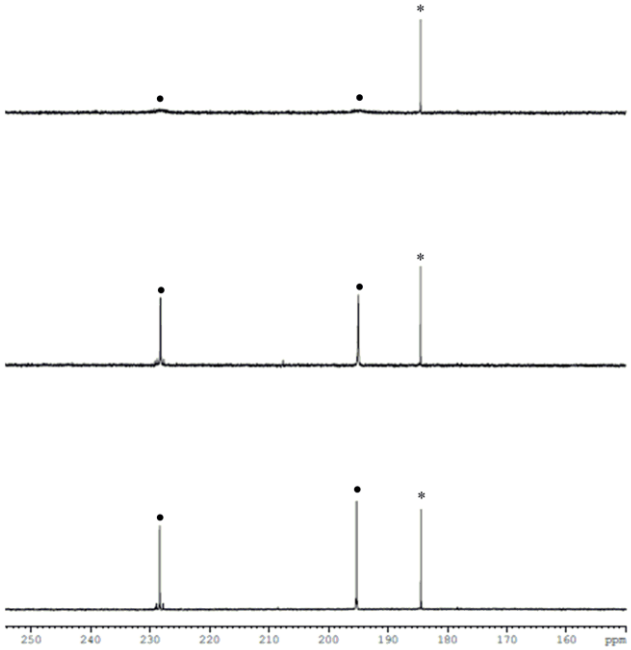

Figure 48: Low temperature ^{13}C NMR for the equilibrium of **90** (circles) with **79** and ^{13}C-labeled carbon monoxide (99 %) (asterisks) at 25 ºC (top), -20 ºC (middle), and -70 ºC (bottom) to reveal diagnostic resonances for a κ^2-*C,N*-isocyanate ligand.

Provided the previously observed thermally reversible equilibrium of **63** with **82** and CN^tBu, the thermally reversible equilibrium of **90** with **79** is presumed to be the result of CO dissociation from the metal center that is promoted at higher temperatures. As further confirmation of this fluxional process involving the dissociation of CO from **90**, **79** was reacted with CO in the presence of excess OCN^tBu with neither resonance averaged peaks nor perturbation of the thermally reversible equilibrium observed by ^1H NMR as seen in Figure 49. This result eliminates the possibility of a κ^2-*C,N* isocyanate ligand undergoing reversible dissociation from the metal center for **90** as the basis for the observed fluxionality provided the absence of rapid exchange with free OCN^tBu.

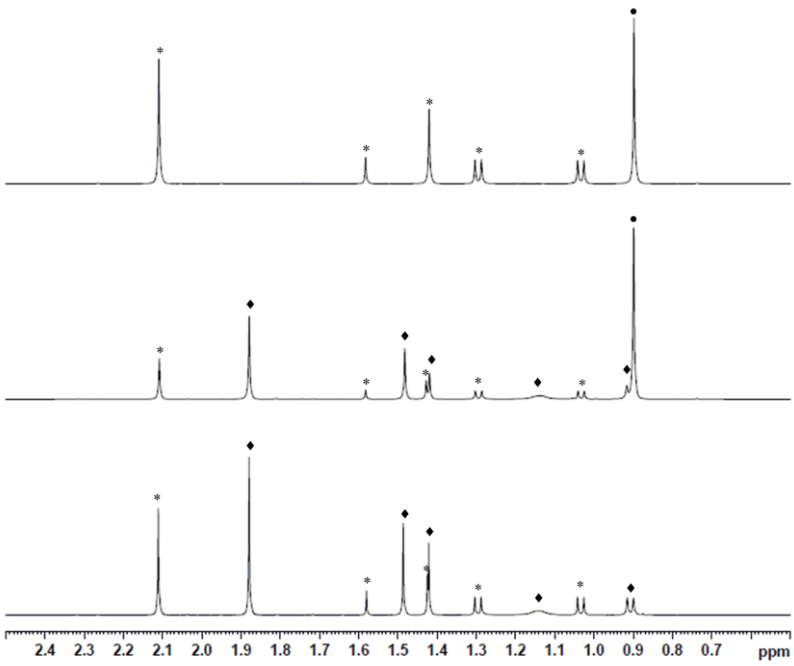

Figure 49: ^1H NMR for the reaction of **79** (asterisks) and excess *tert*-butyl isocyanate with carbon monoxide (circles) (top) to give an equilibrium mixture of **90** (diamonds) and **79** (middle). ^1H NMR spectrum for the observed equilibrium of **90** with **79** and carbon monoxide in the absence of *tert*-butyl isocyanate (bottom). (Note: Septet region of the spectra are not shown for greater clarity of the spectra.)

Although numerous attempts to shift the equilibrium of **90** with **79** to completion through a survey of reaction solvents failed, careful crystallization of the equilibrium mixture from Et_2O was found to give a mixture of crystals that included co-crystallized enantiomers of **90** which were characterized by single-crystal X-Ray diffraction. Notably, the enantiomers of **90** were found to have nearly identical bond lengths and angles and as such the structure of only one enantiomer is depicted in Figure 50 along with selected bond lengths and angles. Comparison of the solid-state structures of **90** and **86** reveal nearly isostructural κ^2-*C,N*-isocyanate complexes with the exception of a more strongly bound κ^2-*C,N*-isocyanate ligand, W1-C20 = 1.987(10) Å and W1-N3 = 2.046(11) Å versus W1-C20 = 2.077(2) Å and W1-N3 = 2.1300(17) Å in **86**, and more weakly bound CO ligand, W1-C19 = 2.176(10) Å versus W1-C19 = 1.999(2) Å in **86**, for **90** in support of the proposed dissociation of CO as the basis for the observed fluxionality. This slight perturbation of ligand bonding in **90** is supported by the solid-sate infrared spectrum (KBr) of the isolated crystalline material that exhibits strong absorptions at 1921, 1936, and 1668 cm^{-1}, nearly the same frequencies as those observed of **86**, 1937 cm^{-1} and 1654 cm^{-1}. This perturbation is theorized to be the result of the Lewis acidic trimethylsilyl group that causes increased back donation by the metal center into the κ^2-*C,N*-isocyanate ligand for **86**. The result is a more electrophilic metal center that is more capable of stably binding CO for the formation of **86** versus an unstable κ^2-*C,N*-isocyanate complex **90** that rapidly decomposes back to CO and **79** through a thermally reversible equilibrium.

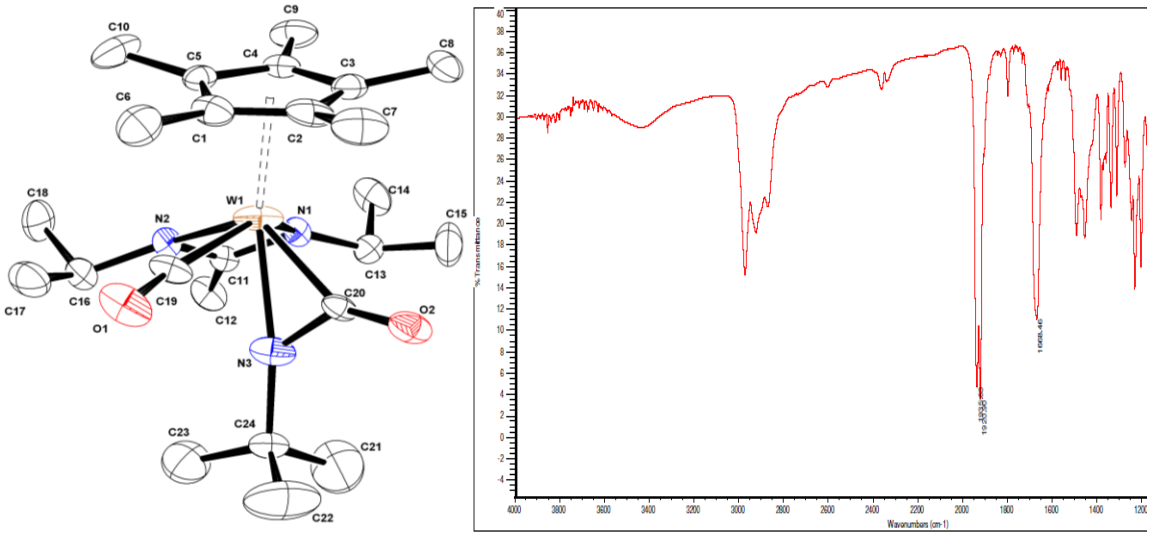

Figure 50: Molecular structure (left) (30% thermal ellipsoids) of **90** and solid-state (KBr) infrared spectrum (right) of isolated solids from the reaction of **79** with CO. Hydrogen atoms have been removed for the sake of clarity. Selected bond lengths (Å) and bond angles (°) for **90**: W1-C20 1.987(10), W1-N3 2.046(11), C20-N3 1.383(14), C20-O2 1.250(11), W1-C19 2.176(10), C19-O1 1.145(11), W1-N1 2.169(12), W1-N2 2.190(12), W1-C19-O1 174.5(13), N1-W1-N2 60.1(3), and N3-C20-O2 135.9(11).

Contrasting the observed reactivity of **79**, the reaction of a benzene-d_6 solution of the analogous molybdenum complex **80** with CO (8 psi) was found by ^{1}H NMR, as shown in Figure 51, to slowly produce the corresponding bis(carbonyl) complex, **54**, and OCN^{t}Bu in quantitative yield after 4 d at room temperature without the observation of any intermediate species. This relatively slow reductive elimination contrasts the immediate formation of **54** upon the exposure of **64** to CO at room temperature. On the basis of the observed equilibrium of **79** with **90** and the absence of an observed κ^2-*C,N* isocyanate intermediate, presumably Cp*Mo[N(^{i}Pr)C(Me)N(^{i}Pr)](CO)(κ^2-*C,N*-OCN^{t}Bu) (**91**), this result suggests that the rate of OCN^{t}Bu reduction elimination for **91** is significantly greater than the rate of formation for **91** due to the lesser ability of **17** to stably bind CO. Seeking to confirm the proposed extrapolation of the observed reactivity for **79** to **90**, a benzene-d_6 solution of **79** was reacted with ^{13}CO at room temperature as a

means of monitoring the products of reductive elimination from the equilibrium mixture of **79** and **90**. When this equilibrium mixture was left at room temperature for 2 weeks a small amount of the corresponding ^{13}C-labeled bis(carbonyl) complex **55** was observed by ^{13}C NMR, Figure 51, confirming the ability of **90** to reductively eliminate OCN^{t}Bu and demonstrating its relevance as a model for the reactivity of **80**.

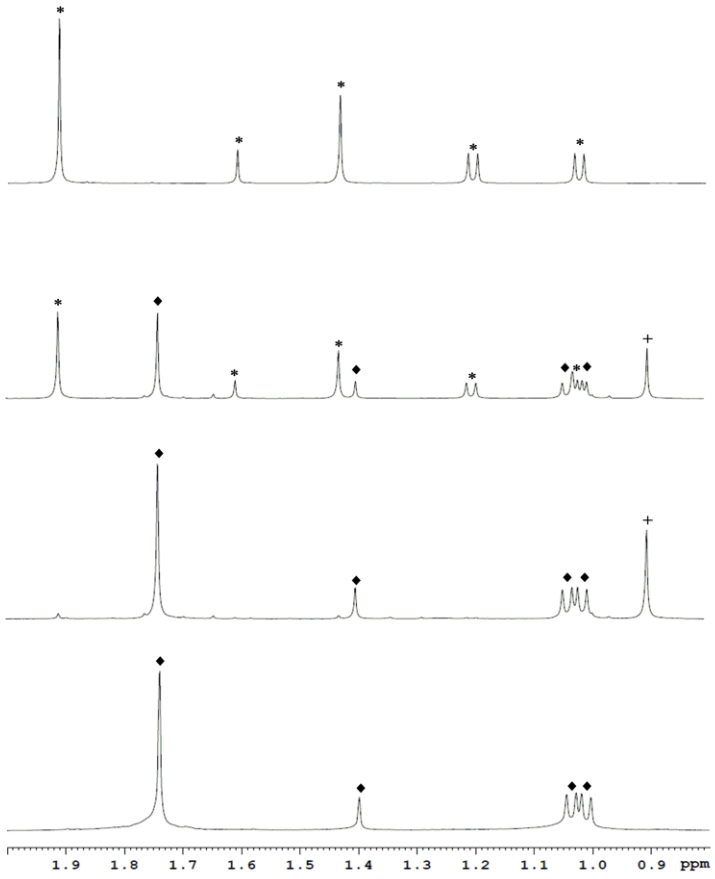

Figure 51: ^{1}H NMR spectrum of **80** (asterisks) in the presence of carbon monoxide (10 psi) at room temperature after 0 h (top), 18 h (top middle), and 4 d (bottom middle) for the quantitative formation of **54** (diamonds) and *tert*-butyl isocyanate (crosses). Reference ^{1}H NMR spectrum of **54** (bottom). (Note: Septet region of spectra are not shown for greater clarity of the spectra.)

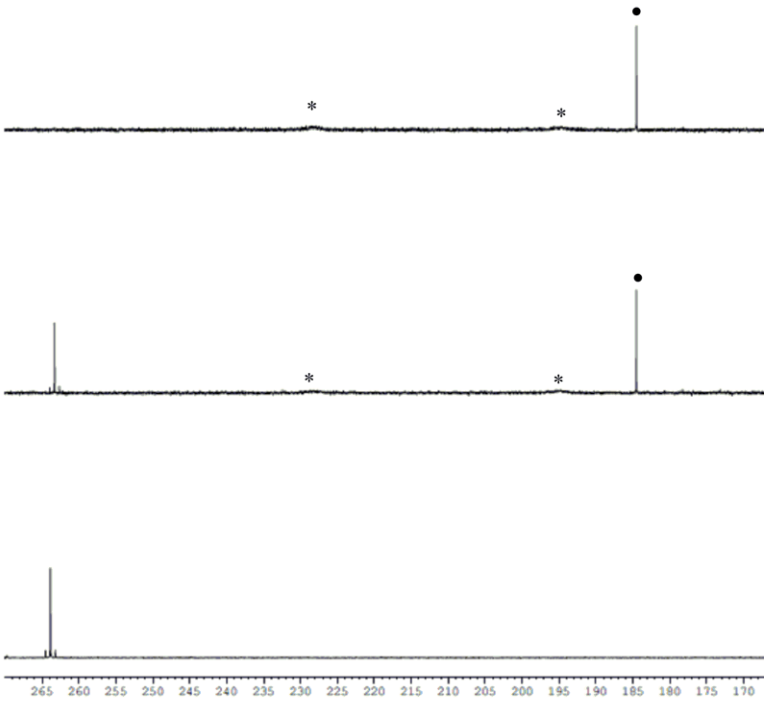

Figure 52: ^{13}C NMR of the equilibrium of **90** (asterisks) with **79** and ^{13}C-labeled carbon monoxide (99%) (circles) at room temperature for 2 h (top) and 2 wk (middle) to demonstrate the slow reductive elimination of *tert*-butyl isocyanate for the formation of ^{13}C-labeled **55**. Reference ^{13}C NMR spectrum of ^{13}C-labeled **55** (bottom).

Collectively, these studies demonstrate the fine balance of bond energies that must be straddled when seeking to develop unprecedented routes for heteroatom transfer reactions involving early transition metals. In conjunction with the previously reported *light-mediated* catalytic oxygen atom transfers involving Group 6 CpAm oxo complexes, the *thermal-mediated* catalytic nitrene carbonylation reported here serves to detail two paths by which catalytic heteroatom transfer can be achieved for early transition metal CpAm complexes as detailed in Scheme 39.

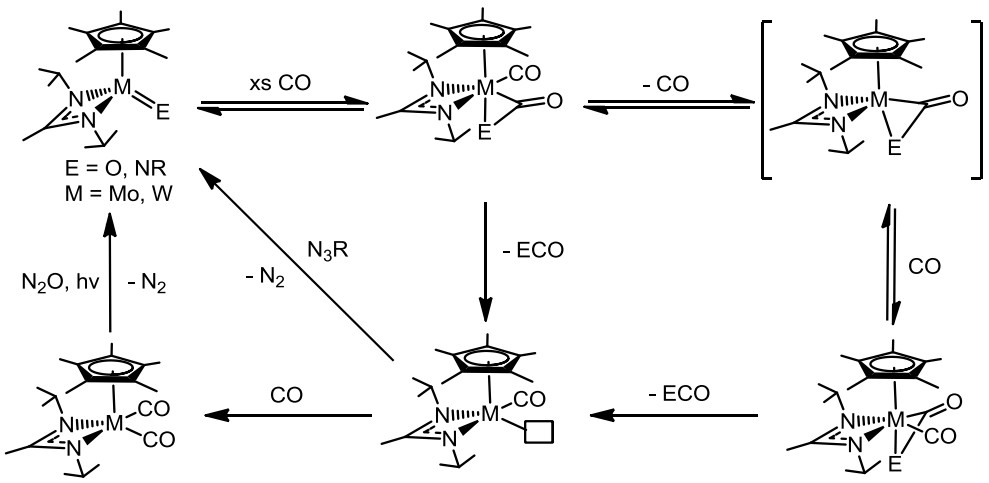

Scheme 39: General overview of catalytic paths for *light-mediated* oxygen atom transfer and *thermally-mediated* nitrene transfer reactions involving Group 6 CpAm complexes.

Chapter 6: Interligand Silyl Transfer Involving Group 6 π-Loaded CpAm Complexes

6.1 Introduction and Background

Multiply bonded ligands (e.g. oxos, imidos, alkylidenes, alkylidynes) attached to metal centers are of significant importance to synthetic, biological, and industrial processes.[81] Such complexes provide routes to novel catalytic transformations while also serving as relevant model complexes for biological and industrial processes. Provided this central role for multiple metal-ligand bonded complexes, novel methods for the formation of multiple metal-ligand bonds is of significant importance. Previously, the reactivity of N-Si bonds has allowed for the use of silyl imido complexes to serve as precursors for the formation multiple M-N bonded species. Specifically, the reaction of terminal silyl imidos with external organic or metal halide donors has been shown to facilitate the formation of nitridos through the loss of organic silyl halides.[82] Of principle importance to this observed reactivity is the Lewis acidic nature of silicon atoms and their ability to form stable hypervalent states, both of which are believed to facilitate reactivity with external nucleophiles.[83]

Related to this reactivity of silicon is the noted ability of silicon atoms to form interligand hypervalent interactions with ligands of substantial negative charge attached to the same metal center.[84] Such interactions are believed to provide the basis for silyl group transfer and abstraction leading to the elimination of organic silyl chlorides and silanes from transition metal complexes with mechanistic evidence supporting the formation of hypervalent silicon intermediates in the transition states of the rate determining steps leading to elimination.[85, 86] Provided the hypothesized ability of

nucleophilic mononuclear terminal oxo, **62** and **63**, and imido, **64** and **65**, complexes to perform proximal nucleophilic attack on Lewis acidic ligands (e.g. isocyanides, CO) coordinated to the metal center, we wondered whether analogous proximal nucleophilic attack could be observed with Lewis acidic silyl substituents. Specifically, we sought to synthesize Group 6 π loaded M(VI, d^0) CpAm complexes containing an oxo and trimethylsilyl imido ligand in effect establishing a competitive process for the attack of the nucleophilic oxygen and nitrogen atoms on the Lewis acidic silyl functional group.

6.2 Investigation of Orthogonal Routes to Group 6 Nitrido Siloxide Complexes

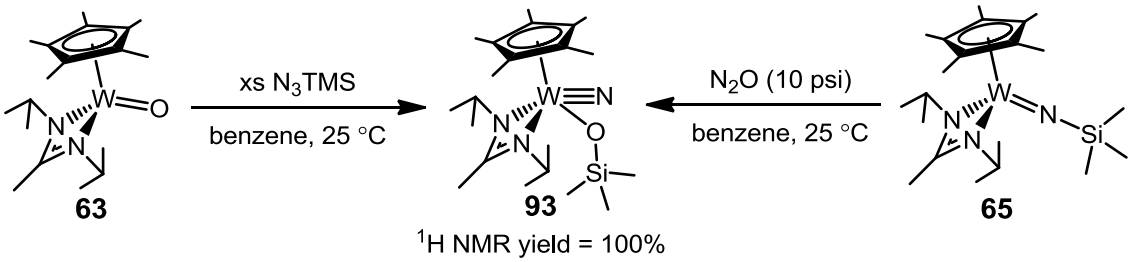

Scheme 40: Orthogonal synthetic routes to the nitrido siloxide complex, **93**, through the reactions of **63** with trimethylsilyl azide and **65** with nitrous oxide.

To begin, a benzene-d_6 solution of **65** was reacted with N_2O (10 psi) for 2 d to produce a colorless C_1 symmetric diamagnetic product having a trimethylsilyl group as observed by ^{1}H NMR in Figure 53. Monitoring this reaction by ^{1}H NMR at room temperature, a transient species, having an apparent mirror plane of symmetry, was observed after 16 h with this species appearing to be quantitatively converted into the final C_1 symmetric product. Despite numerous attempts to isolate the observed C_1

symmetric product from these NMR experiments in all cases these efforts yielded clear intractable oils. In an effort to avoid the formation of intractable oils, a pentane solution of **65** was subsequently reacted with N_2O (10 psi) for 9 d at 25 ˚C to give a similar colorless solution that following crystallization at -30 ˚C provided white crystals of the previously observed diamagnetic product in high yield (99%). Fortunately, single crystals of the isolated material suitable for X-Ray diffraction were obtained with the structure of this complex unequivocally having been determined to be the nitrido siloxide complex Cp*W[N(^{i}Pr)C(Me)N(^{i}Pr)](N)(OSiMe$_3$) (**92**), whose structure and selected bond lengths and angles are provided in Figure 55. Geometric parameters of **92** that are of particular note include the W1-O1, 1.9798(11) Å, and W1-N3, 1.7063(14) Å, bond lengths which are respectively elongated and shortened relative to the corresponding oxo, W1-O1 = 1.7234(17) Å, and imido, W1-N3 = 1.763(4) Å, bond lengths in complexes **63** and **65**. Moreover, complex **92** exhibits significant η^3-bonding character for the cyclopentadienly ligand, as evidenced by W-C bond distances that were found to vary between 2.3819(18) Å and 2.5783(16) Å. Such η^3-bonding character is consistent with competition for π-bonding to the metal center involving the cyclopentadienyl and multiply bonded nitrido ligands in analogy to previously observed competition for π-bonding involving imido and cyclopentadienyl ligands of Group 6 M(VI, d^0) complexes.[87] Collectively, this result implies an increase in bond order upon the conversion of the imido ligand to a nitrido ligand following silyl group transfer involving the imido and oxo ligands in the presumed oxo trimethylsilyl imido intermediate Cp*W[N(^{i}Pr)C(Me)N(^{i}Pr)](O)(NSiMe$_3$) (**93**).

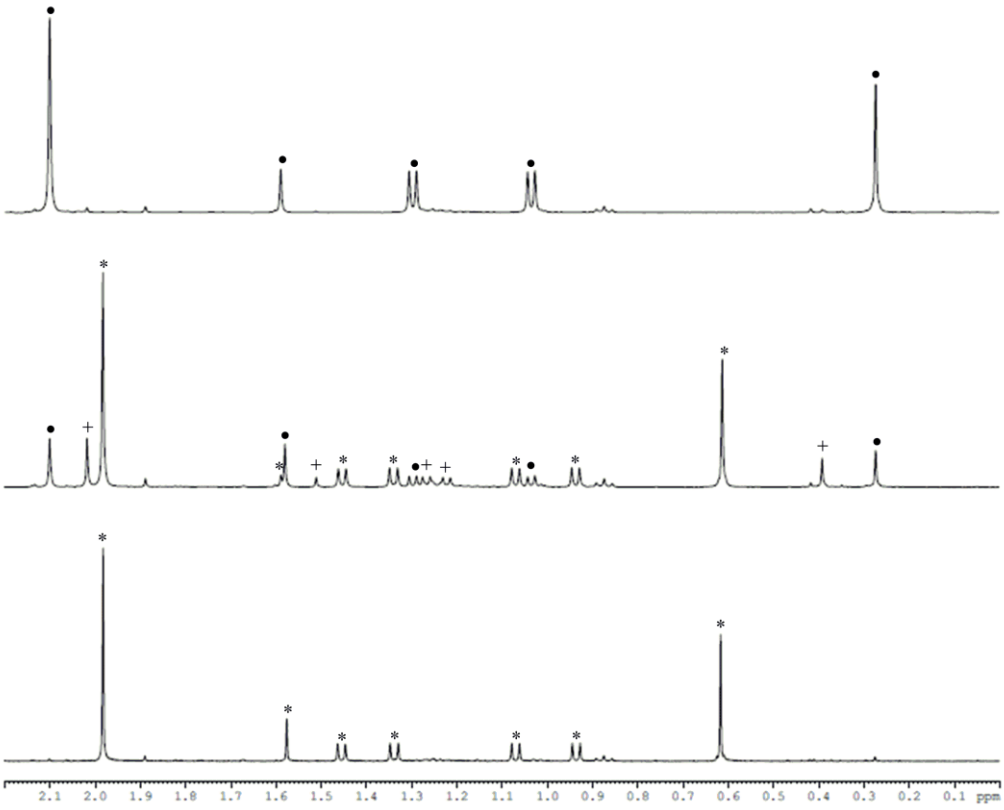

Figure 53: ^{1}H NMR spectra of a benzene solution of **65** (circles) in the presence of nitrous oxide (10 psi) at 0 h (top), 16 h (middle), and 40 h (bottom) for the conversion to **92** (asterisks) through a proposed C_1 symmetric intermediate, Cp*W[N(iPr)C(Me)N(iPr)](NSiMe$_3$)(O) (**93**) (crosses), that is undergoing rapid 'ring flipping' of the amidinate ligand. (Note: Septet region of the spectra are not shown for greater clarity of the spectra).

Seeking further evidence for the presumed intermediacy of **93**, a benzene-d_6 solution of **63** was reacted with an excess of N_3SiMe_3 for the quantitative formation of **92** by ^{1}H NMR, as depicted in Figure 54. However, in contrast to the reaction of **65** with N_2O, when the reaction of **63** with N_3SiMe_3 was monitored by ^{1}H NMR no transient intermediate, tentatively assigned as **93**, was observed despite the presumed intermediacy of this complex in the formation of **92**.

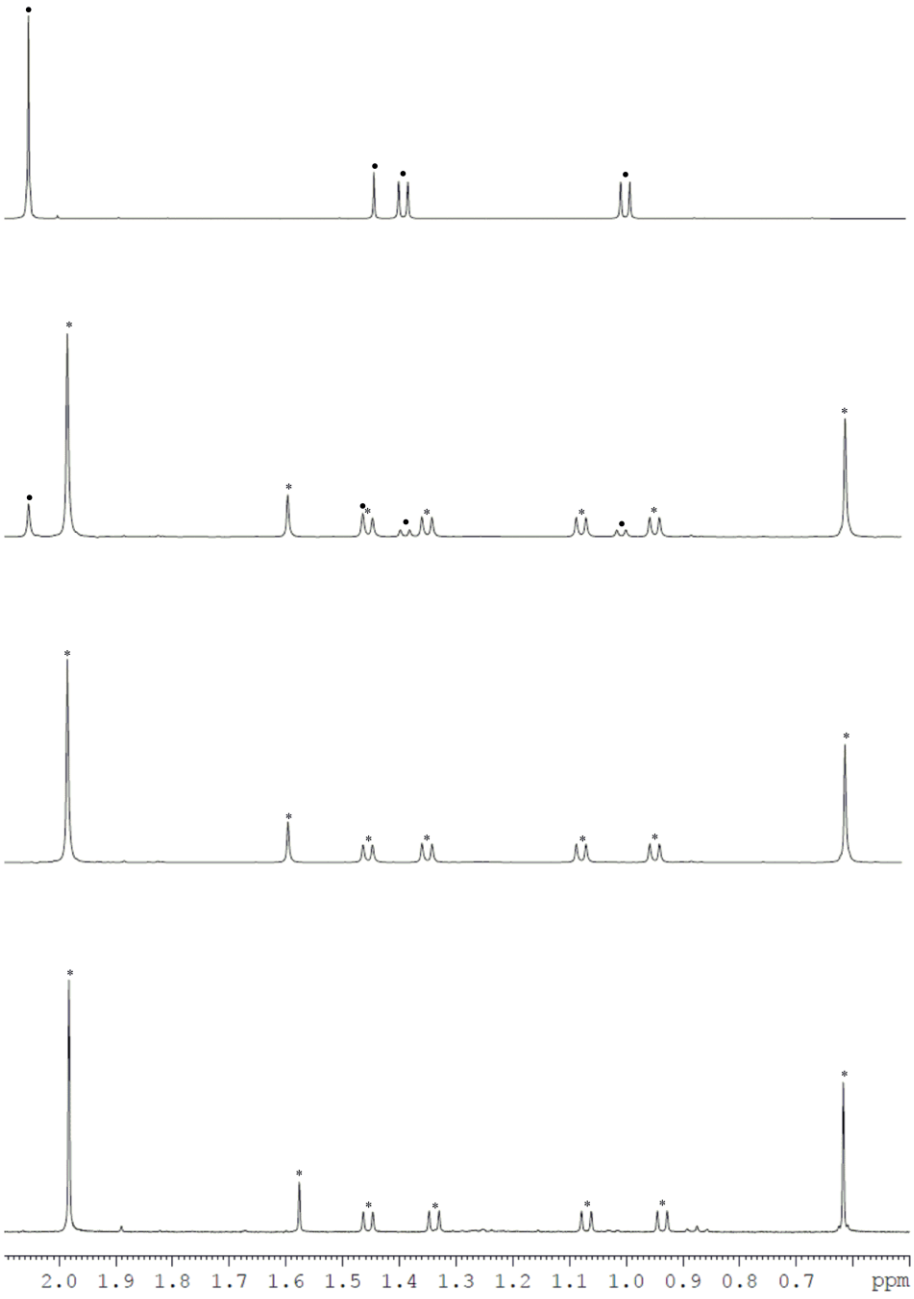

Figure 54: ^{1}H NMR of **63** (circles) (top) in the presence of trimethylsilyl azide after 30 m (top middle) and 16 h (bottom middle) for the generation of **92** (asterisks). Reference ^{1}H NMR spectrum of **92** (bottom). (Note: Septet region of spectra are not shown for greater clarity of the spectra.)

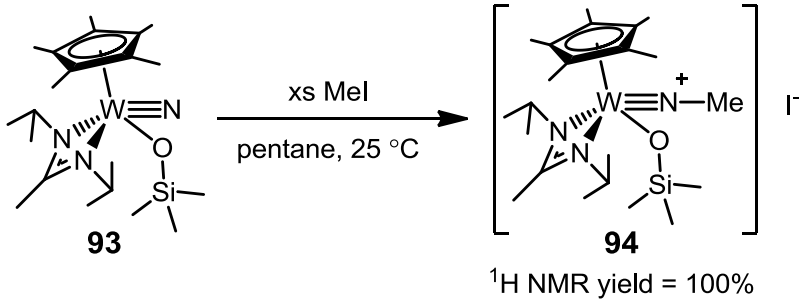

Scheme 41: Reaction of **92** with methyl iodide for the formation of **94**.

Attempts to further characterize **92** through a survey of its reactivity found this complex to be unreactive with silanes, primary alkyl halides, H_2, and CO while reacting quantitatively with methyl iodide to give white crystals in excellent yield (94%) following crystallization from THF and Et_2O at -30 ˚C. Through careful re-crystallization under these conditions, clear crystals of this isolated material suitable for X-Ray diffraction could be obtained with elemental and structural analysis determining the structure of this complex to be the salt {Cp*W[N(^{i}Pr)C(Me)N(^{i}Pr)](OSiMe$_3$)(NMe)}I (**94**), whose structure is depicted in Figure 55. Structurally, the geometric parameters of **94**, W1-N3 = 1.739(2) Å and W1-O1 = 1.9421(19) Å, were found to be similar to that of **92** with the exception of the newly formed linear N-C bond, N3-C22 = 1.442(4) Å and W1-N3-C22 = 169.7(2)˚, resulting in a multiply bonded imido ligand whose bond order is intermediate between that of **92** and **65**. Here, the exclusive reactivity of **92** with unsubstituted alkyl halides is consistent with a high sterically encumbered nucleophilic nitrido ligand that is characteristic of most early transition metal nitridos.[88]

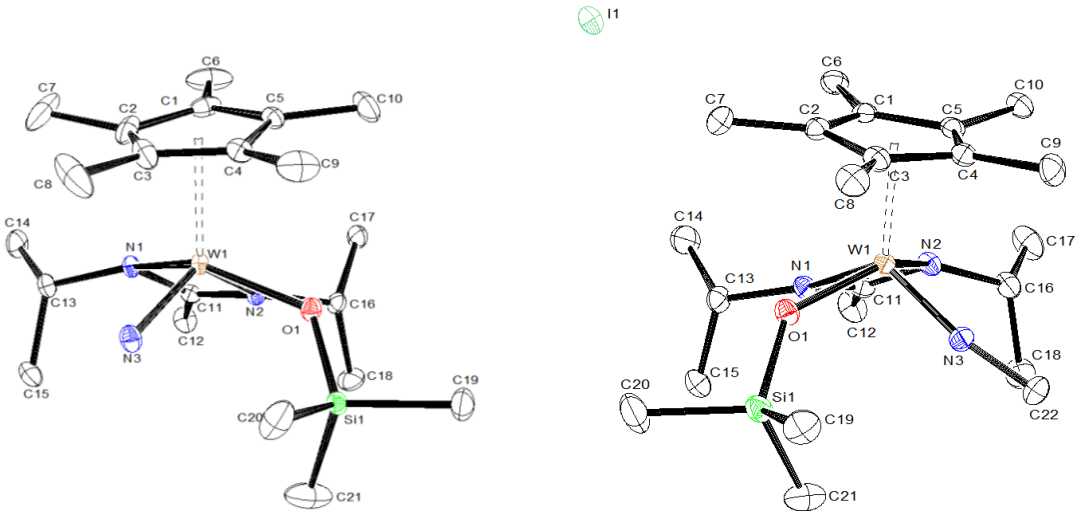

Figure 55: Molecular structure (30% thermal ellipsoids) of **92** (left) and **94** (right). Hydrogen atoms have been removed for the sake of clarity. Selected bond lengths (Å) and bond angles (°) for **92**: W1-N3 1.7063(14), W1-O1 1.9798(11), O1-Si1 1.6357(12), W1-N1 2.1540(13), W1-N2 2.1747(13), N2-W1-N1 59.76(5), N3-W1-O1 99.06(6), W1-O1-Si1 130.85(7). Selected bond lengths (Å) and bond angles (°) for **94**: W1-N3 1.739(2), W1-O1 1.9421(19), O1-Si1 1.642(2), W1-N1 2.139(2), W1-N2 2.153(2), N2-W1-N1 60.22(9), N3-W1-O1 98.14(10), W1-O1-Si1 137.18(12), N3-C22 1.442(4), W1-N3-C22 169.7(2).

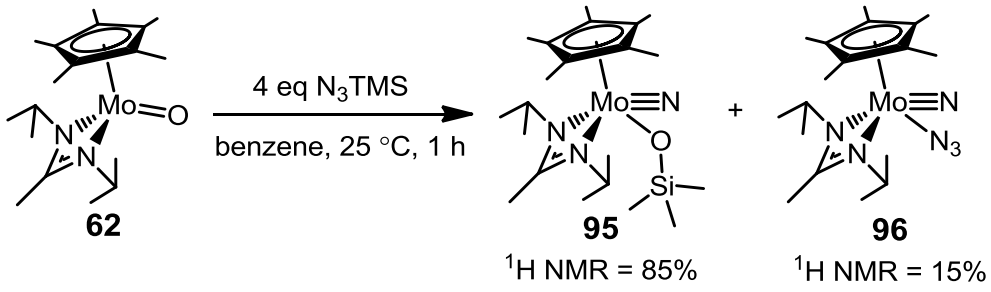

Scheme 42: Reaction of **62** with trimethylsilyl azide for the formation of a mixture of **95** and **96**.

Seeking to investigate the generality of the observed reactivity for **63** and **65**, Dr. Jonathan Reeds of the Sita group sought to test the reactivity of the analogous molybdenum oxo and imido complexes **62** and **64**. Here, in contrast to the reactivity of **65** with N_2O, complex **64** failed to react with N_2O even at elevated temperatures. However, when a benzene-d_6 solution of **62** was reacted with four equivalents of

N_3SiMe_3 for 1 h at 25 ˚C a 5.5:1 mixture of two diamagnetic C_1 symmetric complexes that respectively contained and lacked a trimethylsilyl group was found to be formed as determined by ^{1}H NMR in Figure 56. From careful re-crystallization of the reaction products from pentane, the C_1 symmetric complex containing a trimethylsilyl group was isolated in moderate yield (42%) as pale orange crystals suitable for examination by X-Ray diffraction. Solid-state structural analysis of these crystals revealed the identity of this material to be the analogous π-loaded nitrido siloxide complex, Cp*Mo[N(^{i}Pr)C(Me) N(^{i}Pr)](N)(OSiMe$_3$) (**95**). Here, **95** was found to exhibit an elongated Mo1-O1 bond, 1.9942(9) Å versus 1.7033(19) Å for **62**, consistent with decreased bond order following conversion of the oxo ligand to a siloxide ligand, as well as a Mo1-N3 bond, 1.6728(11) Å, of increased bond order versus the previous reported complex **64**, 1.758(3) Å.

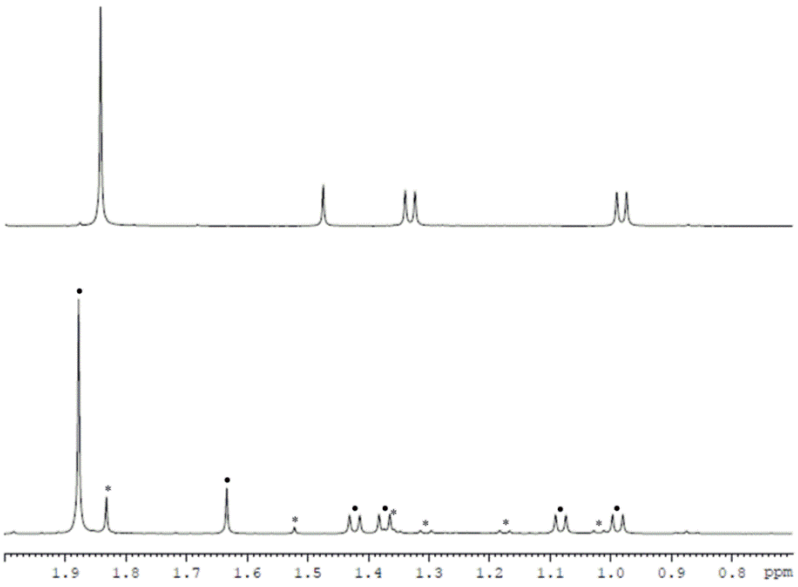

Figure 56: ^{1}H NMR of a benzene solution of **62** (top) in the presence of four equivalents of trimethylsilyl azide after 30 m for the formation of a 5.5:1 mixutre of **95** (circles) and **96** (asterisks) (bottom). (Note: Septet region of the spectra are not shown for greater clarity of the spectra.)

Despite extensive efforts, our group was unable to isolate crystals of the second C_1 symmetric reaction product lacking a trimethylsilyl group. However, analysis of crude solid reaction products isolated from the mother liquor of **95** by ESI-MS allowed for the unambiguous identification of a stable molecular complex having the same isotopic distribution as a complex with the molecular formula $MoN_6C_{18}H_{33}$, as depicted in Figures 57 and 58. This molecular formula and isotopic distribution are consistent with a $(M+H)^+$ peak for the reaction product Cp*Mo[N(^{i}Pr)C(Me)N(^{i}Pr)](N)(N_3) (**96**), which results from the metathesis of the oxo ligand with two equivalents of N_3SiMe_3 leading to the formation hexamethyldisiloxane. Such proposed oxo chemistry has precedence in the related metallocene molybdenum(IV) oxo complex, $Cp^*_2Mo(O)$, previously reported by Parkin and co-workers, which undergoes 1,2-addition chemistry across the M-O bonds with N_3SiMe_3 for the formation of $Cp^*_2Mo(N_3)_2$ and subsequent production of $Cp^*_2Mo(N)(N_3)$ with the loss of N_2.[89]

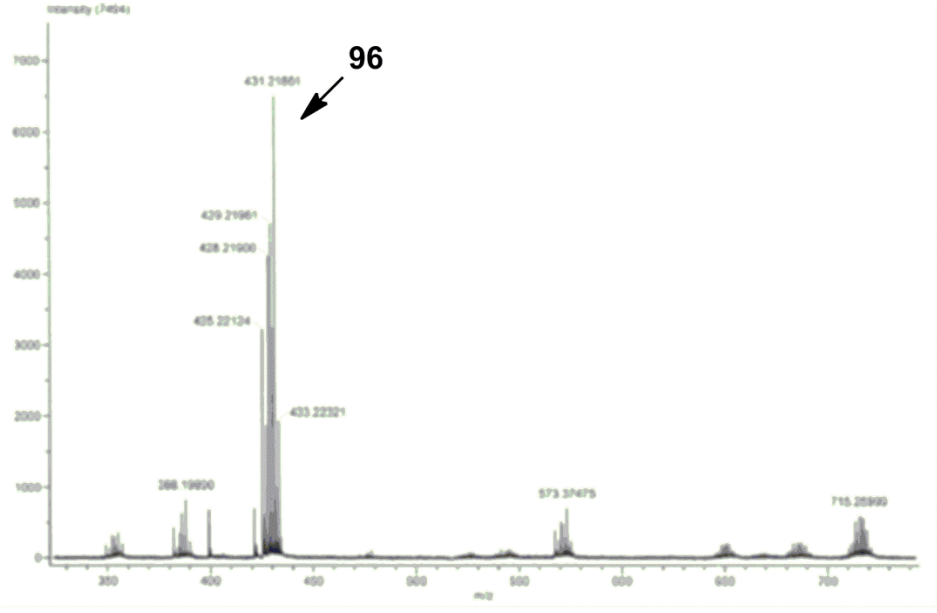

Figure 57: ESI-MS spectrum for the solid material isolated from the mother liquor of **95** to demonstrate the presence of **96** as the predominate species.

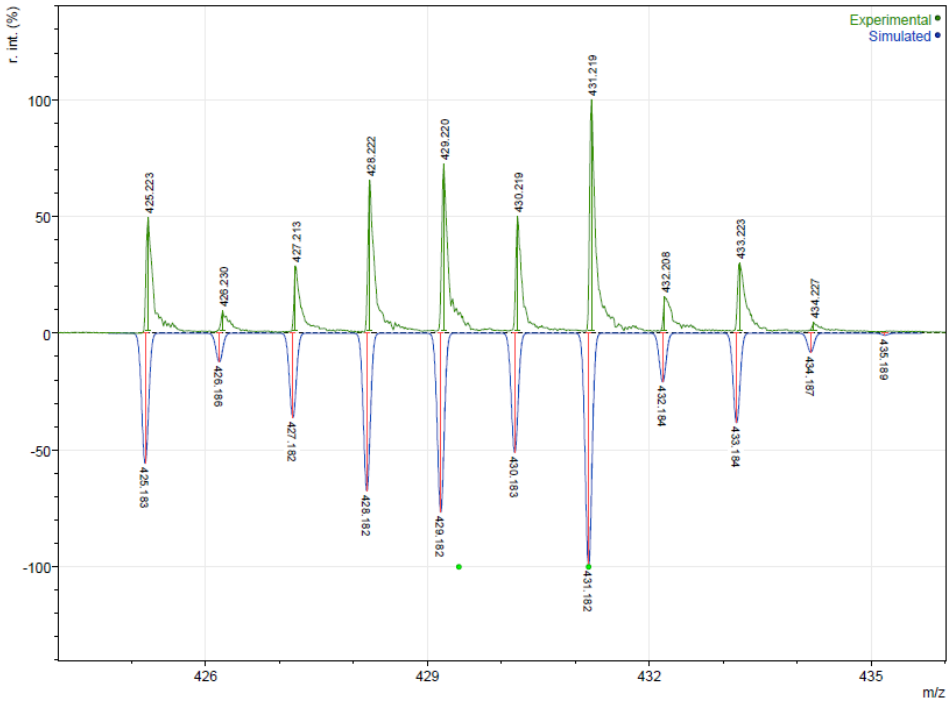

Figure 58: Experimental (top) and simulated (bottom) isotopic distribution for the $(M+H)^+$ peak of a complex having the proposed molecular formula $C_{18}H_{32}N_6Mo_1$.

6.3 Reaction of *Tert*-Butyl Imido with Nitrous Oxide

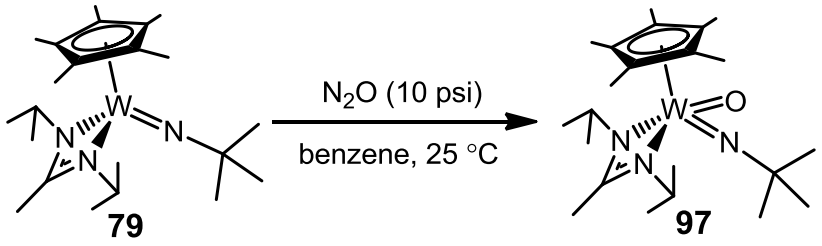

Scheme 43: Proposed reaction product from the reaction of **79** with nitrous oxide.

As a means of identifying the observed transient intermediate from the reaction of **65** with N_2O, attempts were made to independently synthesize a stable *tert*-butyl imido analog of the proposed oxo trimethylsilyl imido intermediate, complex **93**. Toward this goal, a toluene-d_8 solution of the previously reported *tert*-butyl imido complex **79**, was

reacted with N_2O (10 psi) for 3 d at temperatures up to 60 ˚C. When monitored by ^1H NMR, as seen in Figure 59, this reaction was found to give a stable yellow diamagnetic C_1 symmetric product having an apparent mirror plane symmetry similar to the transient intermediate observed in the reaction of **64** with N_2O. On the basis of the similar observed symmetry, this species is tentatively assigned to be the analogous oxo *tert*-butyl imido complex Cp*W[N(^{i}Pr)C(Me)N(^{i}Pr)](N^{t}Bu)(O) (**97**).

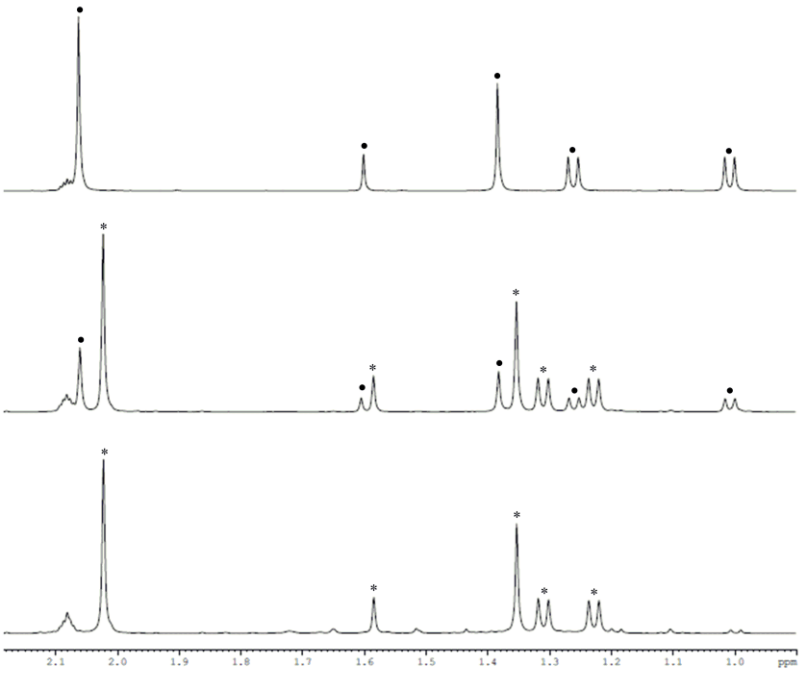

Figure 59: ^1H NMR spectra of a toluene solution of **79** (circles) in the presence of nitrous oxide (10 psi) after 0 h (top) and 2 d (top) followed by heating of the solution at 60 ºC for 16 h (bottom) to give near quantitative conversion to a stable diamagnetic product (asterisks), presumably Cp*W[N(^{i}Pr)C(Me)N(^{i}Pr)](N^{t}Bu)(O) (**97**), having an apparent mirror plane of symmetry due to rapid amidinate "ring flipping". (Note: Septet region of the spectra are not shown for greater clarity of the spectra.)

Despite extensive efforts, the reaction of **79** with N_2O was found to yield intractable oils that failed to give crystalline material following performance of this reaction in various solvents. Moreover, attempts to analyze the observed reaction product

by ESI-MS revealed a stable species having the same isotopic distribution as a complex with the molecular formula $WN_3C_{22}H_{42}$, as would be expected for a $(M+H)^+$ peak for the starting material **79**, as depicted in Figures 60 and 61. Provided the stability and observed C_s symmetry of complexes **65** and **79** as well as the distinctive color change associated with the reaction of **79** and N_2O, the species observed by ESI-MS is believed to be the result of a loss of the oxo ligand from the presumed reaction product **97** under ionizing analysis conditions rather than the product observed by ^1H NMR.[90] However, in the absence of crystallographic confirmation of **97** the presence of the oxo ligand in the observed intermediate would ideally have been confirmed through a complementary analytical method. Principle amongst these methods would be the exposure of **79** to ^{18}O-labeled N_2O for the direct incorporation of an ^{18}O-label in the observed reaction product. Through comparison of the IR spectrum of both these complexes the shifted stretching frequencies for the ^{16}O-labeled versus ^{18}O-labeled oxo ligand could be identified to demonstrate the presence of this ligand in the observed reaction product.

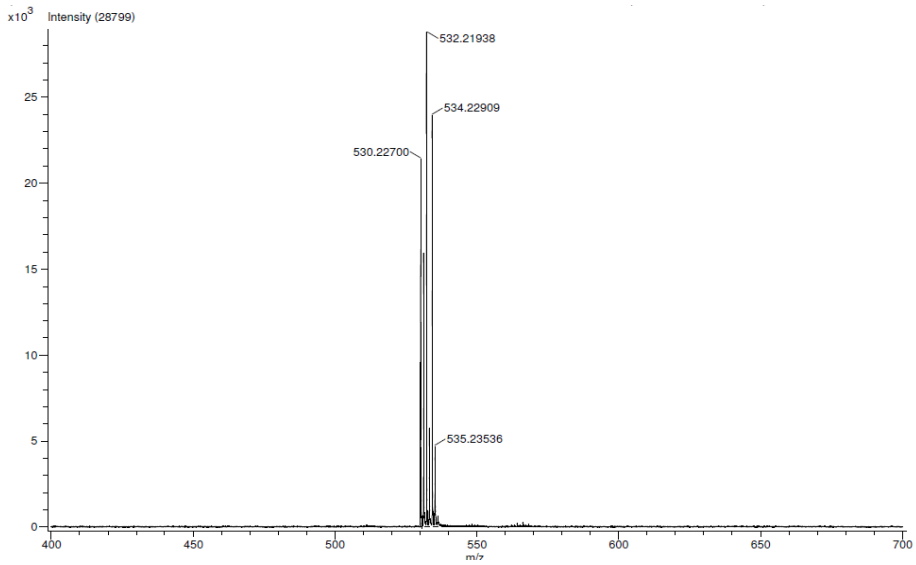

Figure 60: ESI-MS spectrum for the stable yellow diamagntic material produced from the reaction of **79** with nitrous oxide (10 psi).

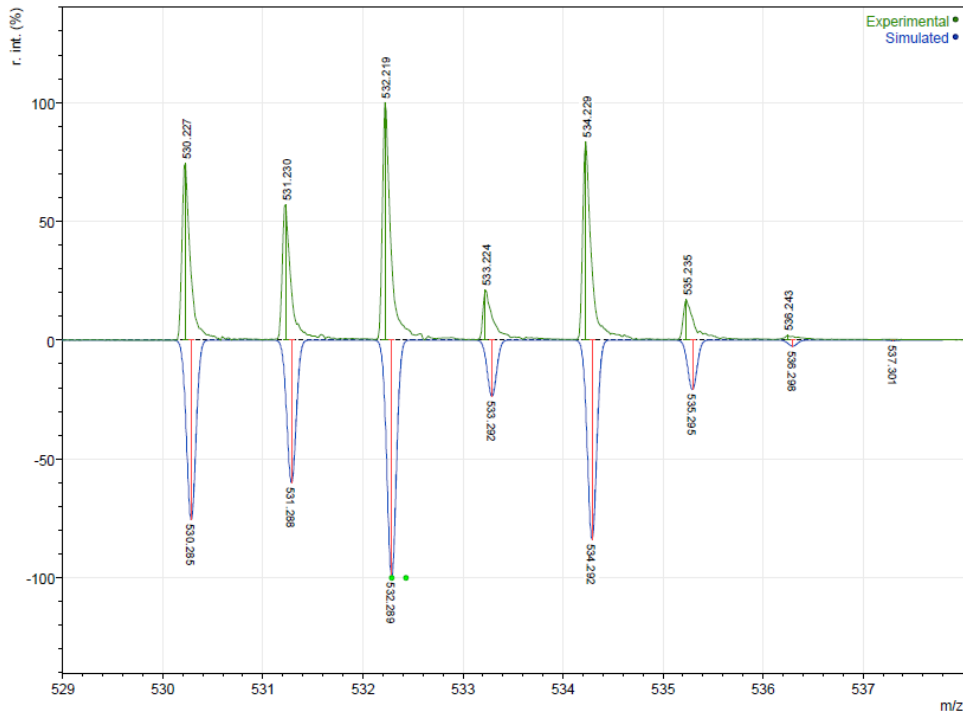

Figure 61: Experimental (top) and simulated (bottom) mass spectrum for the $(M+H)^+$ peak of a complex having the molecular formula $C_{22}H_{41}N_3W_1$.

6.4 Synthesis of Group 6 Bis(oxo) Complex

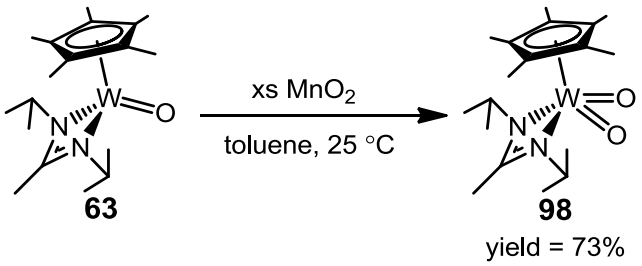

Scheme 44: Synthesis of **98** through the oxidation of **63** with excess manganese dioxide.

In the absence of direct evidence for the proposed reaction product **97**, we sought to probe the origin of the apparent mirror plane of symmetry observed by ^{1}H NMR for the respective transient intermediate and stable product observed from the reaction of **65**

and **79** with N_2O. Specifically, in both cases, despite the proposed overall C_1 symmetry of these complexes, both displayed higher C_s symmetry in solution suggesting the presence of an apparent mirror plane of symmetry for these complexes. Therefore, we sought to synthesize the related bis(oxo) complex Cp*W[N(^{i}Pr)C(Me)N(^{i}Pr)](O)$_2$ (**98**) which should exhibit similar effects from competition of multiply bonded ligands to the metal center provided the isoelectronic nature of terminal oxo and imido ligands. Toward this end, **63** was reacted with excess manganese dioxide (MnO_2) in toluene to provide fine white crystals suitable for analysis by X-Ray diffraction in moderate yield (73%). Structural and elemental analysis of these crystals conclusively identified the isolated product as **98** with the cyclopentadienyl ligand assuming significant η^3-bonding character as evidenced by the W-C bond lengths ranging from 2.292(4) Å to 2.574(4) Å. The origin of this η^3-bonding character is presumed to result from the competition of both oxo ligands for binding the metal center in **98** with the W-O bond lengths, 1.733(3) Å and 1.749(3) Å, indicating a bond order between two and three similar to the previously reported mononuclear oxo complex **63**, W1-O1 = 1.7234(17) Å. Comparison of this structure to its metallocene bis(oxo) analog, (η^1-Cp*)(η^5-Cp*)W(O)$_2$, reported by Bercaw and co-workers, suggests similar competition for π-bonding between the oxo and cyclopentadienyl ligands leading to a η^1-bonding motif for the cyclopentadienyl ligand, although, further reports of the structural details for this complex have yet to be published.[91]

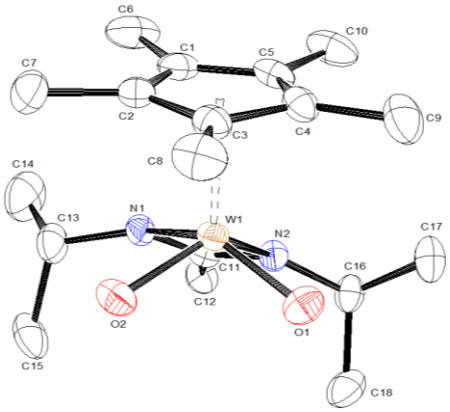

Figure 62: Molecular structure (30% thermal ellipsoids) of **98**. Hydrogen atoms have been removed for the sake of clarity. Selected bond lengths (Å) and bond angles (°) for **98**: W1-O1 1.733(3), W1-O2 1.749(3), W1-N1 2.169(3), W1-N2 2.230(3), N2-W1-N1 58.75(12), O1-W1-O2 99.55(15).

Importantly, analysis of **98** by ^{1}H NMR, as seen in Figure 63, reveals the presence of a single doublet and septet resonance for the isopropyl groups of the amidinate ligand. The full magnetic equivalence of these isopropyl protons, despite the overall C_s symmetry of this complex, as determined by X-Ray crystallography, suggests the rapid exchange of the amidinate isopropyl groups through "ring-flipping" of the amidinate ligand at 25 ˚C. Such "ring-flipping" has previously been reported by our group to occur in square pyramidal Group 4 CpAm complexes through a proposed five coordinate trigonal bipyramidal intermediate.[30a] Provided the presumed structural similarity of the π-loaded complex **98** and proposed oxo imido complexes, Cp*W[N(^{i}Pr)C(Me)N(^{i}Pr)](NR)(O), where R = $SiMe_3$ (**93**) and ^{t}Bu (**97**), these ^{1}H NMR studies support the proposed identity of the transient and stable reaction products of **65** and **79** with N_2O, which exhibit mirror plane symmetry at 25 ˚C in solution despite their lower overall C_1 molecular symmetry.

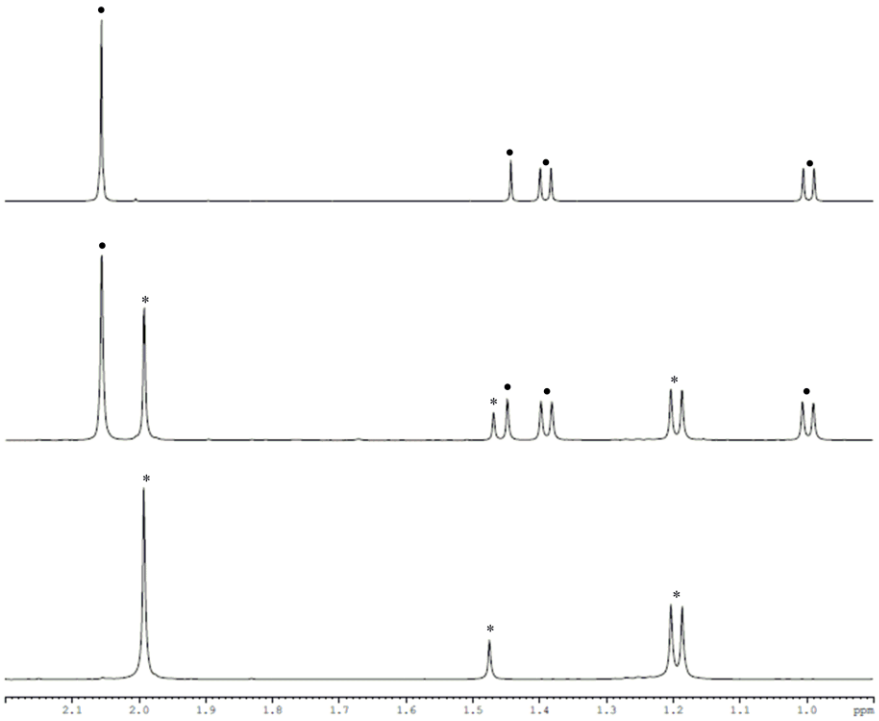

Figure 63: ^{1}H NMR spectrum of **63** (circles) (top) after reaction with two equivalents of manganese dioxide for 1 h (middle) and subsequently four equivalents of additional manganese dioxide for 20 m (bottom) to cleanly give **98** (asterisks). (Note: Septet region of the spectra are not shown for greater clarity of the spectra.)

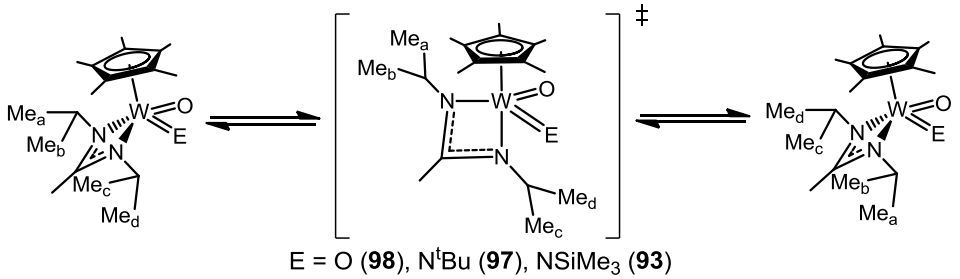

Scheme 45: Mechanism of isopropyl group exchange in **98** and proposed oxo imido complexes, **93** and **97**, through rapid "ring-flipping" of the amidinate ligand.

Collectively, these results suggest the possibility of two reaction paths involving N_3SiMe_3. In the first path, back donation by the metal center leads to the formation of a transient π-loaded oxo trimethylsilyl imido complex, Cp*M[N(^{i}Pr)C(Me)N(^{i}Pr)]

(O)($NSiMe_3$). This transient complex subsequently undergoes interligand silyl group transfer for the formation of a nitrido siloxide complex, Cp*M[N(^{i}Pr)C(Me)N(^{i}Pr)](N)($OSiMe_3$). Given the nucleophilic nature of the oxo ligand, silyl group transfer is believed to occur through a hypervalent silicon transition state resulting from the proximal nucleophilic attack of the oxo ligand on the Lewis acidic silicon atom. Moreover, the direction of this silyl group transfer is presumed to be thermodynamically driven by the formation of inherently stronger Si-O (BDE = 128 kcal/mol for Me_3SiOH) versus Si-N (BDE = 100 kcal/mol for $Me_3SiNHMe$) bonds and the ability to form a stable triply bonded metal nitrido ligand.[92] By contrast, the second reaction path for N_3SiMe_3 involves 1,2-addition across the oxo ligand leading ultimately to the formation of a bis(azide) complex, Cp*M[N(^{i}Pr)C(Me)N(^{i}Pr)](N_3)$_2$, that undergoes subsequent elimination of N_2 to form a nitrido azide complex, Cp*M[N(^{i}Pr)C(Me)N(^{i}Pr)](N)(N_3). Provided the reliance of the first path on metal center back donation into a coordinated N_3SiMe_3 ligand, this pathway is exclusively observed for **63** versus **62** due to the larger metal orbitals of 3rd row transition metals causing favored metal back donation versus 1, 2-addition across the oxo ligand.

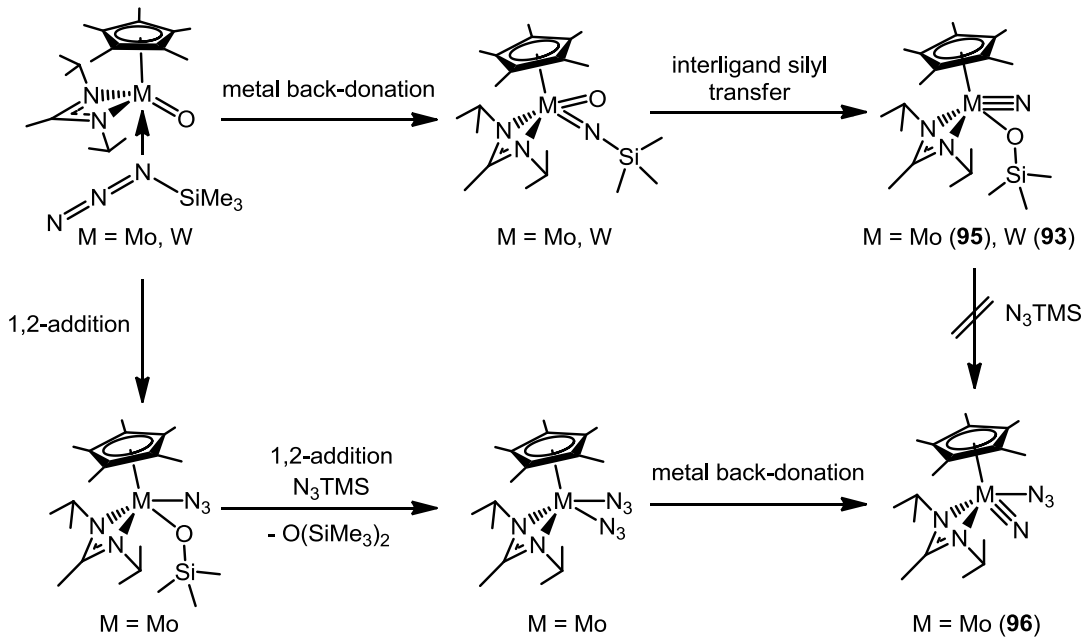

Scheme 46: Proposed mechanisms for the formation of **92**, **95**, and **96** through respective 1,2-addition across an oxo ligand and metal center back donation involving a coordinated N_3SiMe_3 ligand.

Chapter 7: Photolytic Cleavage in Group 6 CpAm Dinitrogen Complexes

7.1 Introduction and Background

Through demonstration of catalytic oxygen atom and nitrene group transfer reactions with Group 6 CpAm oxo and imido complexes, the unusual M(II, d^4)/M(IV, d^2) couple for Group 6 CpAm complexes has proven quite versatile in its ability to form and break metal-heteroatom bonds. While this redox couple was found to directly affect photocatalytic oxygen atom transfers involving the gaseous small molecules N_2O and CO_2, analogous nitrene group transfer required the utilization of organic azides versus the gaseous small molecule dinitrogen. Having established the primacy of these general catalytic routes for heteroatom transfer, we sought to expand the reactivity of Group 6 CpAm complexes with N_2 as a means of developing a generalized method for the binding, activation, and fixation of N_2 in organic compounds of interest. Of principle importance to these efforts is the development of novel methods for the activation and cleavage of the triple bond (BDE = 945 kJ/mol) of N_2.

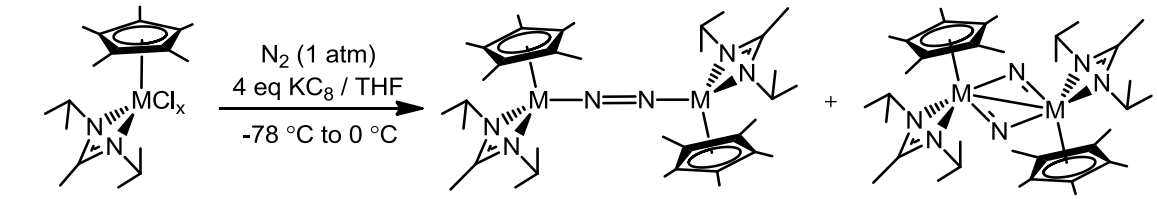

M = Mo, x = 2 (**48**),
W, x = 3 (**51**)

M = Mo (**53**), W (**52**)

M = Mo (**99**)
yield = <5%

Scheme 47: Adventitious isolation of the molybdenum CpAm N-N cleavage complex, **99**, from the potassium graphite reduction of Group 6 CpAm chloride precursors, **48** and **51**, for the synthesis of end-on bridged dinitrogen complexes, **52** and **53**.

Various research groups have reported the ability to cleave N_2 through the use of dinuclear organometallic complexes at ambient temperature.[14, 93] With regard to the CpAm supporting ligand framework, previously Sita and co-workers have found the Group 5 CpAm end-on bridged dinitrogen complex **39** to be thermally unstable at temperatures above 0 ˚C to produce the bridging nitrido N-N cleavage complex **40**.[33] Contrasting the observed thermal instability of **39**, the isostructural Group 6 CpAm end-on bridged dinitrogen complexes **52** and **53**, synthesized from the reduction of the metal halide precursors **50** and **51** with Na/Hg, were found to be thermally stable at temperatures exceeding 100 ˚C.[34] This observed thermal stability for **52** and **53** is consistent with the lesser extent of activation and increased multiple bond character for the end-on bridged dinitrogen ligands of these complexes. Moreover, in research by Dr. Phil Fontaine of the Sita research group, it was found that similar reduction of **48** and **51** with KC_8 provided **52** and **53**. However, in the case of the reduction of **48** with KC_8, it was consistently found that trace amounts, <5%, of a paramagnetic material that formed black single crystals suitable for X-Ray diffraction could be obtained when the products of this reaction were crystallized from Et_2O. Through elemental and structural analysis of these black crystals, the identity of this material was surprisingly revealed to be a N-N cleavage complex, $\{Cp^*Mo[N(^iPr)C(Me)N(^iPr)](\mu\text{-}N)\}_2$ (**99**), containing a four-membered ring with planar geometry having Mo1-N3 and Mo1-N3a bond distances of 2.010(5) and 2.011(5) Å as well as a transannular N•••N non-bonding distance of 3.017 Å. Given that the reduction of **50** with Na/Hg was found provide **53** in quantitative yield by ^1H NMR, the adventitious isolation of **99** from the reaction of **48** with KC_8 is thought

to result from an otherwise unidentified process that is only accessible under KC_8 reduction conditions.

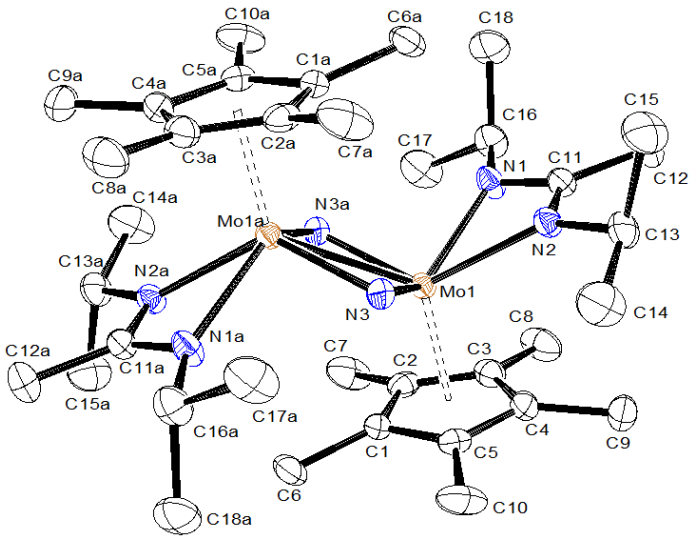

Figure 64: Molecular structure (30% thermal ellipsoids) of **99**. Hydrogen atoms have been removed for the sake of clarity. Selected bond lengths (Å) and bond angles (°) for **99**: Mo1-N3 2.010(5), Mo1a-N3a 2.011(5), Mo1-Mo1a 2.6586(10), N3a-N3 3.017, Mo1-C1 2.345(5), Mo1-C2 2.412(5), Mo1-C3 2.474(6), Mo1-C4 2.479(6), Mo1-C5 2.392(6), Mo1-N1 2.242(5), Mo1-N2 2.247(4), N3a-Mo1-N3 97.21(19), N2-Mo1-N1 58.73(17).

Having reproducibly isolated the N-N cleavage complex **99**, despite the noted thermal stability of **53**, we sought to undertake the task of investigating novel methods for the cleavage of the end-on bridged dinitrogen ligand in **52** and **53** to produce **99** and its presumed tungsten analog $\{Cp^*W[N(^iPr)C(Me)N(^iPr)](\mu\text{-}N)\}_2$ (**100**). Although thermal methods have been the focus of most N_2 cleavage research involving discrete organometallic complexes, various groups have reported the fixation of N_2 through the use of heterogeneous catalysts requiring the use of light.[94] To the best of our knowledge, only two research groups, Cummins and Floriani, have demonstrated light-mediated N-N bond cleavage reactions in discrete organometallic dinitrogen complexes.[15a, 95] In the case of Cummins' work, light mediated N-N cleavage was found to occur at low temperatures

in the otherwise thermally unstable Group 6 trisamido end-on bridged dinitrogen complex, $\{Mo[N(^tBu)Ar]_3\}_2(\mu\text{-}\eta^1\text{:}\eta^1\text{-}N_2)$ (**11**) where Ar = 3,5-$C_6Me_2H_3$, for the formation of equimolar amounts of $Mo[N(^tBu)Ar]_3$ (**10**) and $NMo[N(^tBuAr]_3N$ (**12**). Contrasting this finding, and of specific interest to our research, is the work of Floriani and co-workers which demonstrated light-mediated N-N cleavage in the otherwise thermally stable trimesityl end-on bridged dintirogen complex, $\{Mo(Mes)_3\}_2(\mu\text{-}\eta^1\text{:}\eta^1\text{-}N_2)$ (**101**) where Mes = 2,4,6-$C_6Me_3H_2$, with a bridged nitrido complex, $(\mu\text{-}N)\{Mo(Mes)_3\}_2$ (**102**), being formed following exposure to UV light. In both cases, the observed products can be rationalized to form as the result of light-mediated N_2 extrusion and scission pathways upon irradiation with UV light.[96]

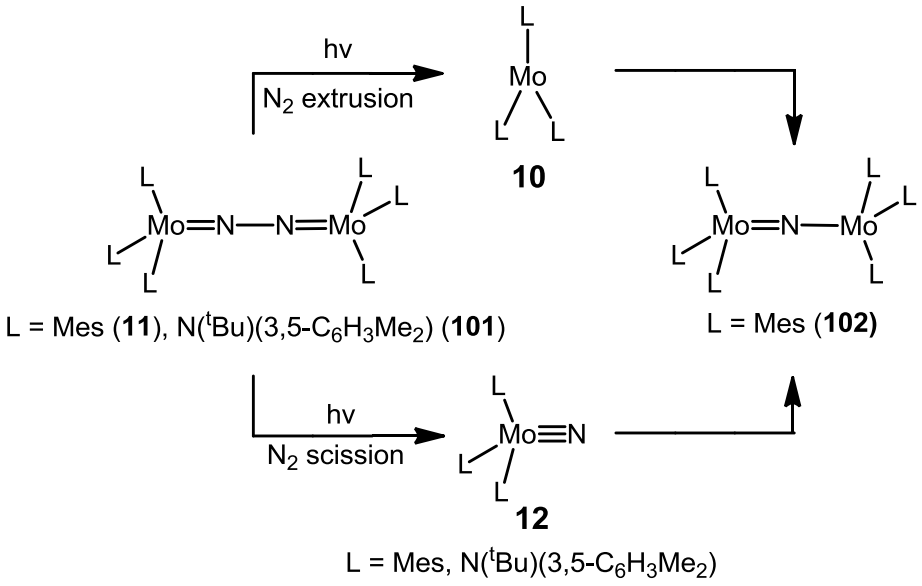

Scheme 48: Light mediated N-N cleavage previously reported by Cummins and Floriani.

With this demonstrated ability to cleave N_2 through UV light exposure, we sought to determine whether similar exposure of the thermally stable dinitrogen complexes **52** and **53** to UV light could be used to facilitate N_2 activation and cleavage. If achieved this

would prove to be a crucial step to toward the application of the unprecedented heteroatom group transfer chemistry for Group 6 CpAm complexes to the activation, cleavage, and fixation of the gaseous small molecule N_2.

7.2 Independent Synthesis of Group 6 CpAm N-N Cleavage Complexes

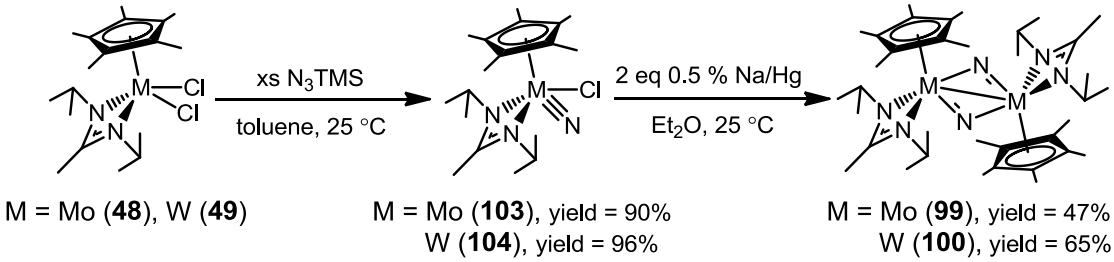

Scheme 49: Independent synthesis of Group 6 CpAm N-N cleavage complexes, **99** and **100**, through sodium amalgam reduction of the nitrido chloride complexes, **103** and **104**, derived from the metal dichloride precursors, **48** and **49**.

In order to determine the efficacy of proposed light-mediated N-N bond cleavage in **52** and **53**, it was reasoned that spectroscopic standards of the N-N cleavage complex **99** and its proposed tungsten analog, **100**, would first need to be independently synthesized. Here, the Group 6 CpAm dichloride precursor **48** was reacted with N_3SiMe_3 for the formation of a diamagnetic complex that provided yellow crystals in excellent yield (90%) following crystallization from toluene. Fortunately, single crystals of this product suitable for X-Ray diffraction were obtained with elemental analysis and structural characterization revealing the product to be the mononuclear nitrido chloride CpAm complex, Cp*Mo[N(^{i}Pr)C(Me)N(^{i}Pr)](N)Cl (**103**).[97] Analysis of the geometric parameters for **103** indicate a relatively short metal-nitrogen bond, Mo1-N3 = 1.674(3) Å,

for the nitrido ligand and a cyclopentadienyl ligand having moderate η^3- versus η^5-bonding character, as evidenced by metal carbon bond lengths ranging from 2.390(4) to 2.569(4) Å. Similar to **48**, the reaction of **49** with N_3SiMe_3 was found to provide white crystals of a diamagnetic product whose elemental and spectroscopic analysis were consistent with the proposed reaction product CpW[N(^{i}Pr)C(Me)N(^{i}Pr)](N)Cl (**104**) when the crude reaction material was crystallized from toluene. With care, single crystals of **104** were obtained for X-Ray diffraction with the determined geometric parameters, W1-N3 = 1.782(13) and W-C bonds for the cyclopentadienyl ligand ranging from 2.338(9) to 2.585(18) Å, indicating a similar structure to **103** with the exception of the cyclopentadienyl ligand for **104** exhibiting substantially greater η^3- versus η^5-bonding character. As such only the structure of **104** is shown in Figure 65 along with selected bond lengths and angles.

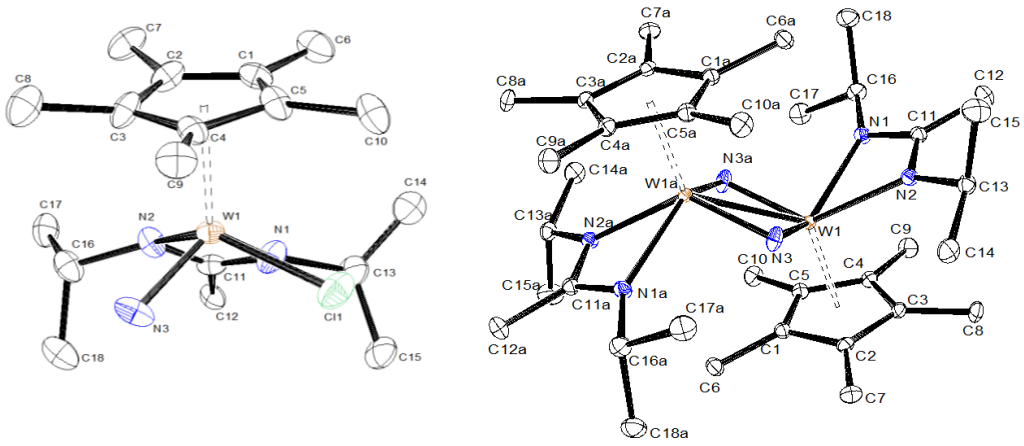

Figure 65: Molecular structure (30% thermal ellipsoids) of **104** (left) and **100** (right). Hydrogen atoms have been removed for the sake of clarity. Selected bond lengths (Å) and bond angles (°) for **104**: W1-N3 1.782(13), W1-C1 2.585(18), W1-C2 2.575(16), W1-C3 2.494(19), W1-C4 2.338(9), W1-C5 2.42(2), W1-Cl1 2.367(6), W1-N1 2.134(10), W1-N2 2.172(10), N2-W1-N1 57.7(5). Selected bond lengths (Å) and bond angles (°) for **100:** W1-N3 1.912(2), W1-N3a 1.908(2), W1-W1a 2.6560(3), N3a-N3 2.747, W1-C1 2.308(3), W1-C2 2.430(3), W1-C3 2.561(3), W1-C4 2.553(3), W1-C5 2.429(3), W1-N1 2.223(2), W1-N2 2.228(2), N3a-W1-N3 91.92(10), N2-W1-N1 59.04(9).

Subsequently, **103** was reacted with Na/Hg in a mixture of THF and Et_2O for 16 h at 25 ˚C to give a dark brown solution that following work-up and crystallization of the crude reaction products from pentane gave a brown crystalline paramagnetic material in moderate yield (47%). Using a combination of single crystal X-Ray diffraction and elemental analysis this material was determined to be the N-N cleavage complex **99**. In a similar manner, the reaction of **104** with Na/Hg in Et_2O for 16 h at 25 ˚C was found to provide a dark brown solution that following work-up and crystallization from THF and Et_2O allowed for the isolation of a black crystalline material in moderate yield (65%). Through single crystal and elemental analysis this isolated material was conclusively determined to be the expected N-N cleavage complex **100** whose structure and selected geometric parameters are shown in Figure 65. In a like manner to the nitrido chloride complexes, **103** and **104**, complex **100** was found to be nearly isostructural to **99** with the exception of shorter M-N bonds for the bridging nitrido ligands, W1a-N3 = 1.912(2) Å and W1a-N3a = 1.908(2) Å, counter to the expected trend for M-N bonding down a group, and substantially greater η^3- versus η^5-bonding character for the cyclopentadienyl ligand having W-C bonds ranging from 2.308(3) to 2.561(3) Å.

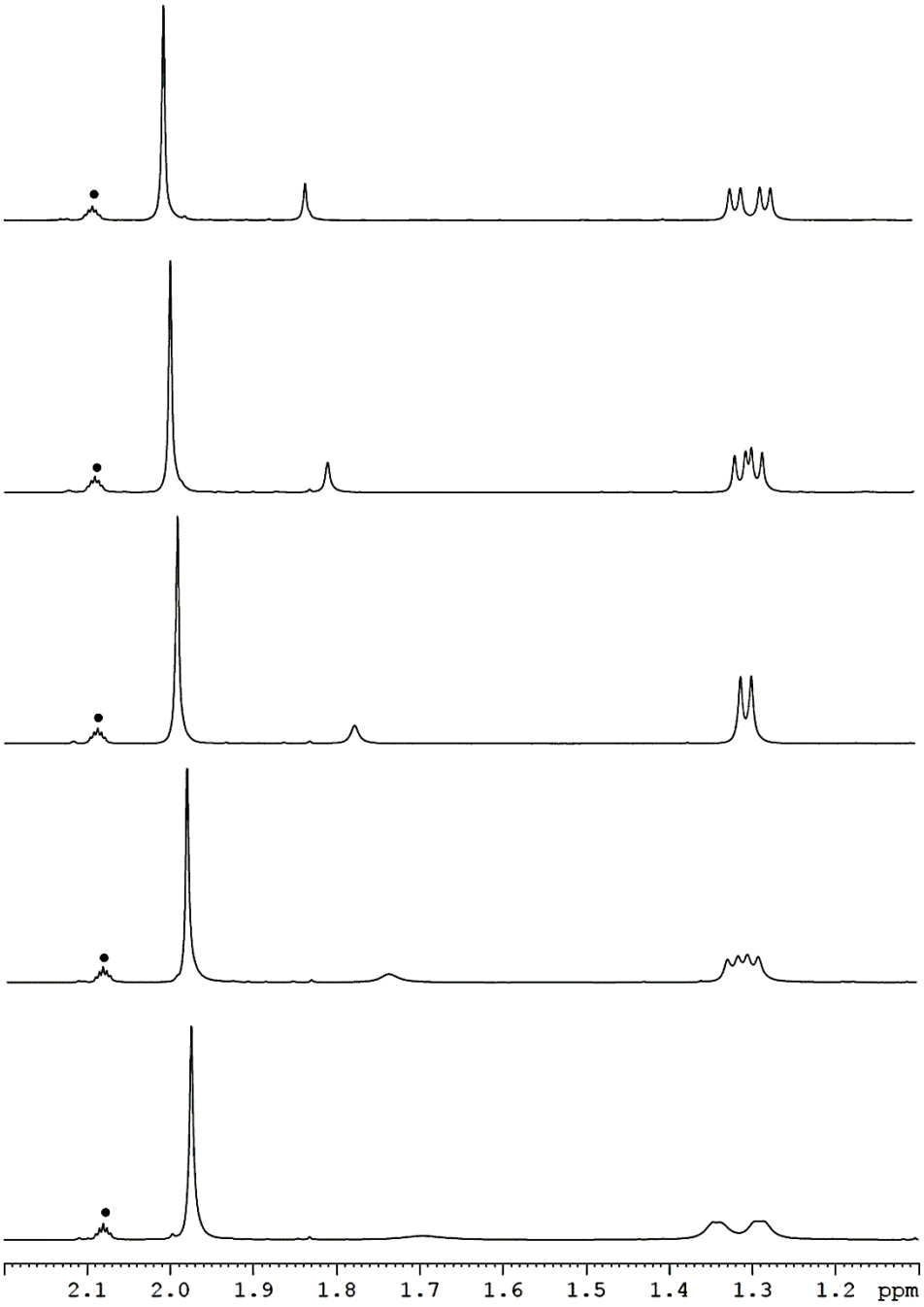

Figure 66: High temperature VT ^{1}H NMR studies of **100** in toluene-d_8 (circles are residual solvent peaks) with spectra obtained at 81.5 ˚C (top), 65 ˚C (top middle), 51 ˚C (middle), 35.5 ˚C (bottom middle), and 25 ˚C (bottom). (Note: Septet region of the spectra are not shown for greater clarity of the spectra.)

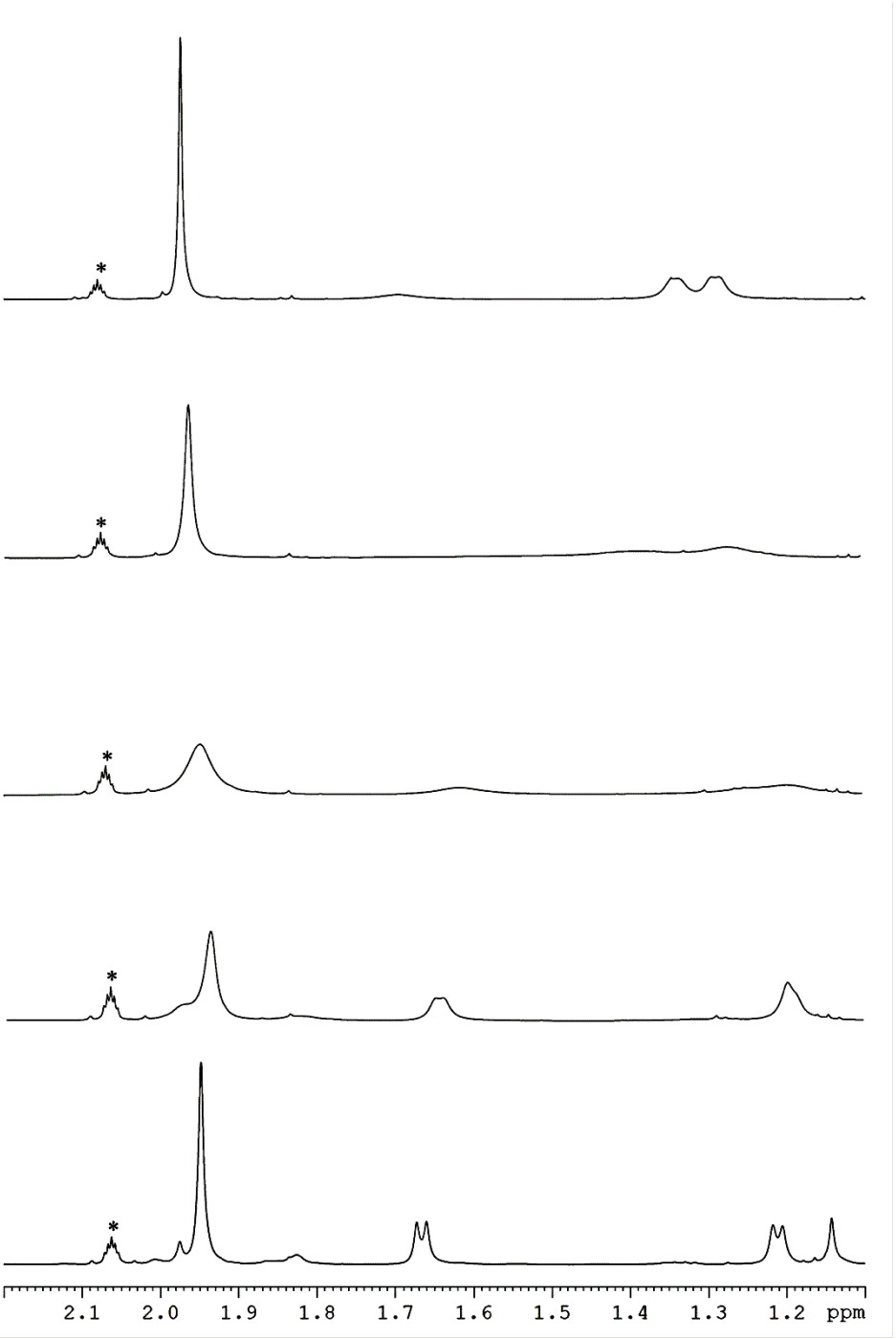

Figure 67: Low temperature VT ^{1}H NMR studies of **100** in toluene-d_8 (asterisks are residual solvent peaks) with spectra obtained at 25 ˚C (top), - 0.5 ˚C (top middle), -26.5 ˚C (middle), -42 ˚C (bottom middle), and -64.5 ˚C (bottom). (Note: Septet region of the spectra are not shown for greater clarity of the spectra.)

Furthermore, in contrast to **99**, ^{1}H NMR of the isolated crystalline material for **100** revealed this complex to be diamagnetic with substantial fluxionality being observed in benzene-d_6 and toluene-d_8 solutions by ^{1}H NMR. The observed diamagnetism of **100** is believed to be the result of the larger metal orbitals of tungsten in **100** versus molybdenum in **99** that yield either a formal M-M bond or superexchange between the two M(V, d^1) metal centers despite the nearly identical intermetallic distances for **99** and **100**, respectively 2.6586(10) and 2.6560(3) Å. In an attempt to investigate the observed fluxionality further, a toluene-d_8 solution of **100** was subjected to both high and low temperature VT ^{1}H NMR as seen in Figures 66 and 67. Although no mechanistic origin for the fluxionality of **100** could be discerned from these studies the observation of diamagnetism at both the high and low temperature limits suggests that the interaction between the metal centers remains intact thereby excluding the possibility of a monomer-dimer equilibrium. Therefore, due to the intact nature of the M_2N_2 core, fluxionality for **100** is presumed to result from processes (e.g. haptic shifts, metal migrations, ring flipping) associated with the supporting cyclopentadienyl and amidinate ligands as the result of their direct competition with the nitrido ligands for π-donation to the metal center.[98, 99]

7.3 Photolytic Cleavage of Group 6 CpAm Dinitrogen Complexes

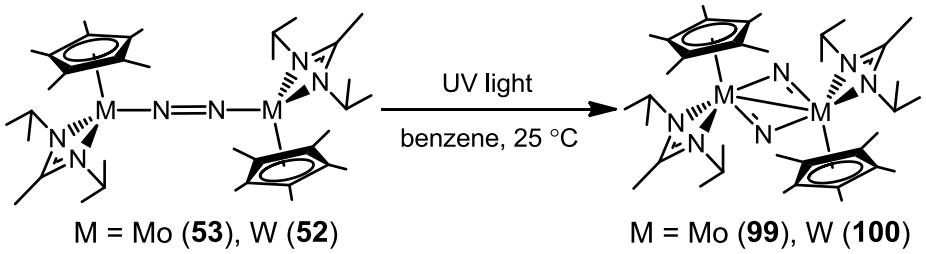

Scheme 50: Photolytic cleavage of Group 6 CpAm end-on bridged dinitrogen complexes, **52** and **53**, for the formation of the Group 6 CpAm N-N cleavage products, **99** and **100**.

With these independent synthetic routes to the proposed N-N cleavage complexes **99** and **100** developed, we sought to utilize these complexes as spectroscopic standards for the investigation of novel N-N cleavage processes. Toward this end, a benzene-d_6 solution of **53** in a Pyrex J Young NMR tube was exposed to UV light for 48 h in a Rayonet® Photochemical Reactor containing medium pressure mercury lamps with the reaction being monitored periodically by ^{1}H NMR to demonstrate the quantitative conversion of **53** to paramagnetic material as seen in Figure 68. Through the careful crystallization of the crude photolysis reaction products of **53** in Et_2O at -30 ˚C, single crystals having the same geometric parameters as the single crystals of **99** isolated from the KC_8 reduction of **48** could be isolated. In contrast to the photolysis of **53**, the analogous photolysis of a benzene-d_6 solution of **52** was found to produce small amounts of the N-N cleavage complex **100,** as evidenced by the presence of diagnostic resonances in Figure 69, after irradiation of the sample with UV light for 48 h.

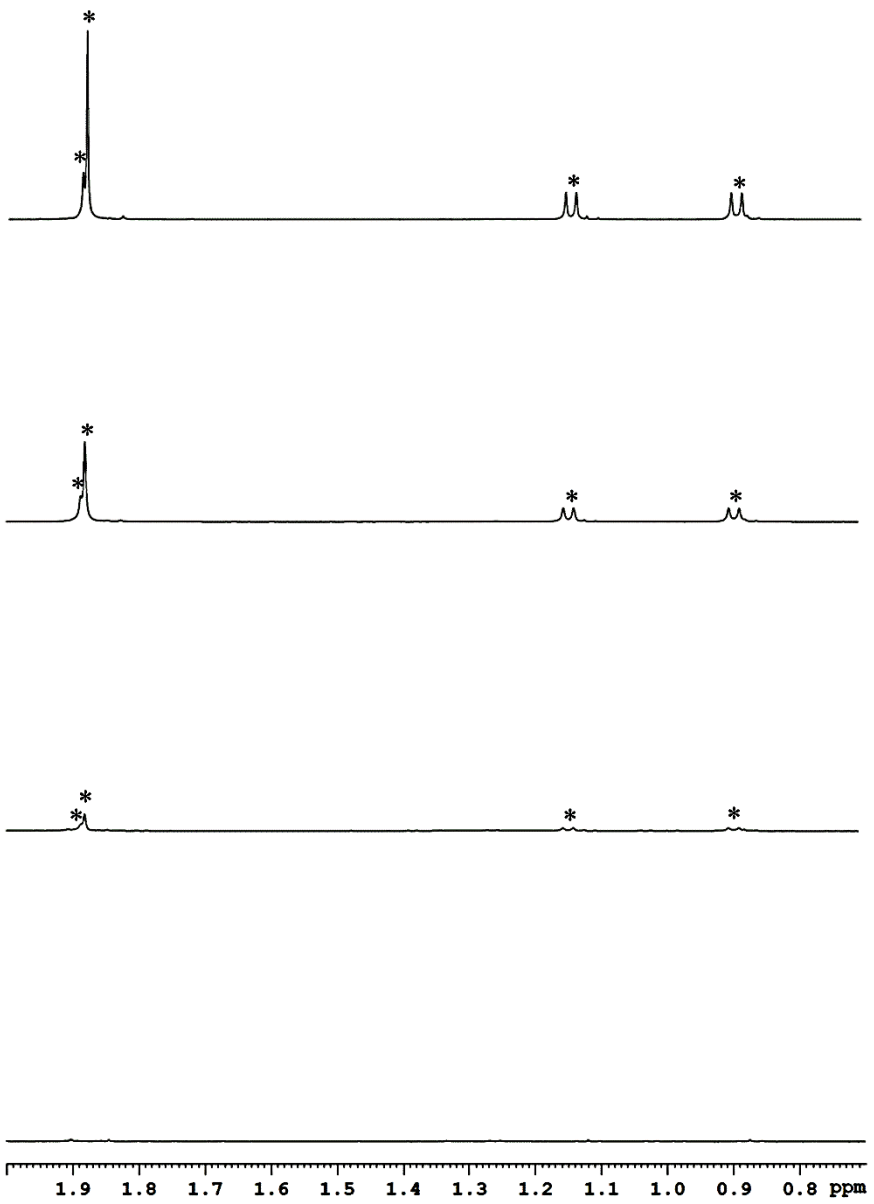

Figure 68: ^{1}H NMR of a benzene-d_6 solution of **53** (asterisks) exposed to UV light after 0 h (top), 4 h (top middle), 24 h (bottom middle), and 48 h (bottom). (Note: Septet region of the spectra are not shown for greater clarity of the spectra.)

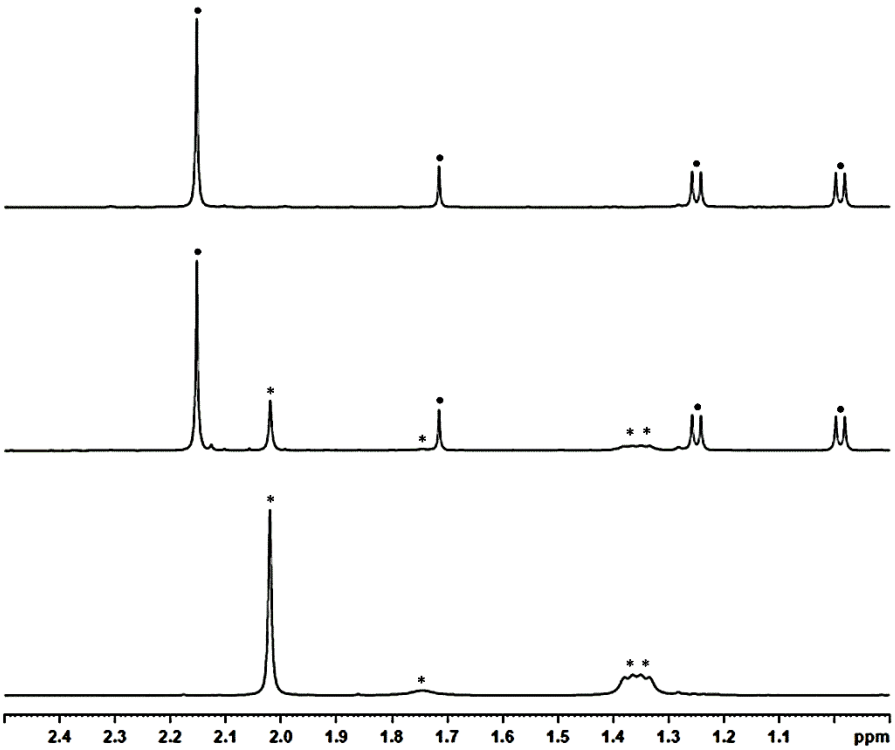

Figure 69: ^{1}H NMR of a benzene-d_6 solution of **52** (circles) exposed to UV light after 0 h (top) and 48 h (middle) for the formation of **100** (asterisks). Reference ^{1}H NMR spectrum of **100** in benzene-d_6 (bottom). (Note: Septet region of the spectra are not shown for greater clarity of the spectra.)

In an effort to further characterize the observed photolysis process for the conversion of **52** and **53** to **99** and **100**, the electronic spectra of these complexes were obtained in Reagent-Plus methylcyclohexane. Of particular interest were UV absorption bands provided the stability of **52** and **53** under prolonged exposure to visible light. As can be seen in Figures 70 and 71 the end-on bridged dinitrogen complexes **53** and **52** exhibit strong absorption bands in the UV region, λ (nm) (ε) = 337 (58,455) and 261 (53,916) for **53** versus λ (nm) (ε) = 309 (49,675) and 253 (49,942) for **52**, with the molybdenum complex **53** exhibiting red-shifted absorption bands relative to **52**. Provided the red-shifted nature of the absorption bands for **53** and the use of a polychromatic UV light source, is it unknown at this time whether the greater N-N cleavage rate for **53**

versus **52** is the result of the relative M-N bond strengths for tungsten versus molybdenum or simply the result of the Pyrex J Young tube selectively filtering out the higher energy wavelengths of UV light needed for the cleavage of **52**. By contrast, in Figures 72 and 73, the N-N cleavage complexes **99** and **100** exhibit comparatively weak absorption bands at λ (nm) (ε) = 583 (705), 453 (1,455), and 371 (2,459) for **99** versus λ (nm) (ε) = 446 (1,979), 336 (6,698), and 290 (10,859) for **100** with similar red-shifting of the molybdenum versus tungsten complexes observed. However, although regions of spectral overlap for the end-on bridged dinitrogen and N-N cleavage complexes clearly exist, the significant differences in the extinction coefficients for these complexes at the wavelengths responsible for N-N photolysis (*vide infra*) suggest minimal $_{\text{inhibition}}$ of photoconversion by the generated N-N cleavage complexes.

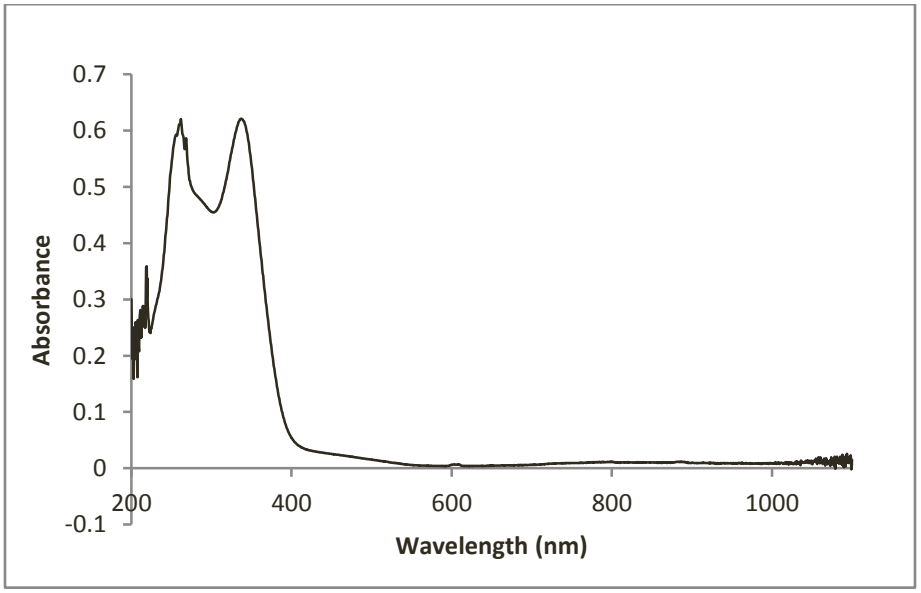

Figure 70: Electronic spectra of **53** in methylcyclohexane. λ (nm) (ε): 831 (925), 458 (1,930), 337 (58,500), 261 (53,900).

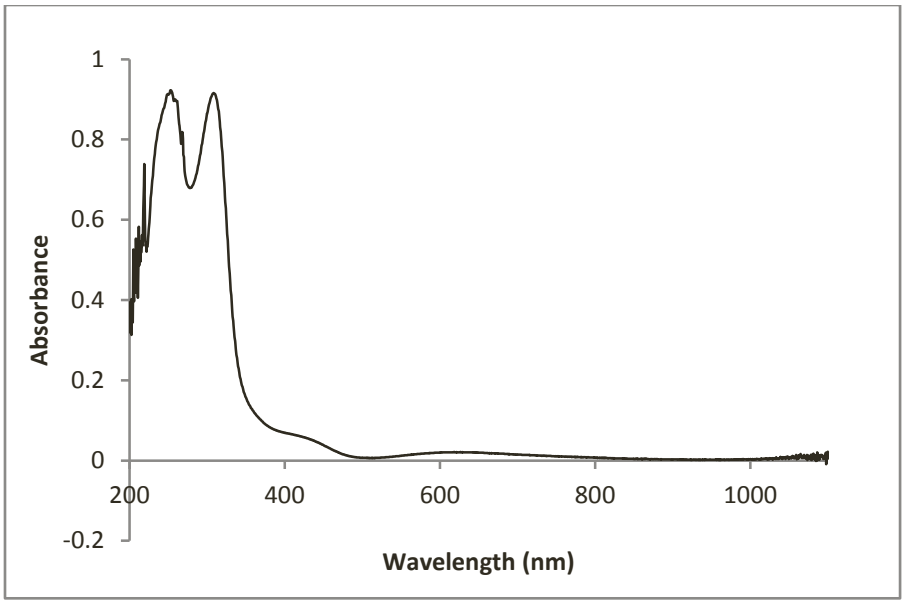

Figure 71: Electronic spectra of **52** in methylcyclohexane. λ (nm) (ε): 618 (1,240), 431 (3,090), 309 (49,700), 253 (49,900).

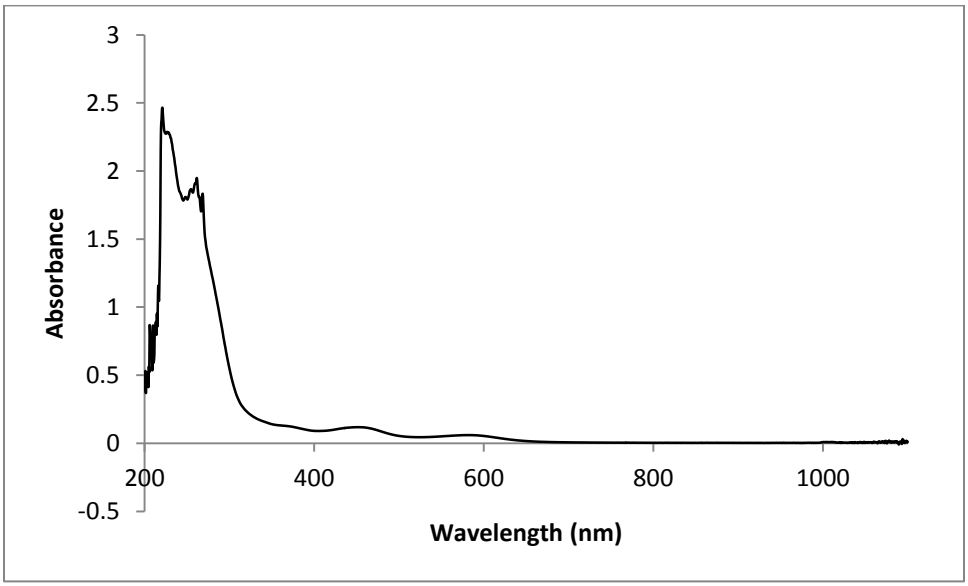

Figure 72: Electronic spectra of **99** in methylcyclohexane. λ (nm) (ε): 583 (705), 453 (1,460), 371 (2,460).

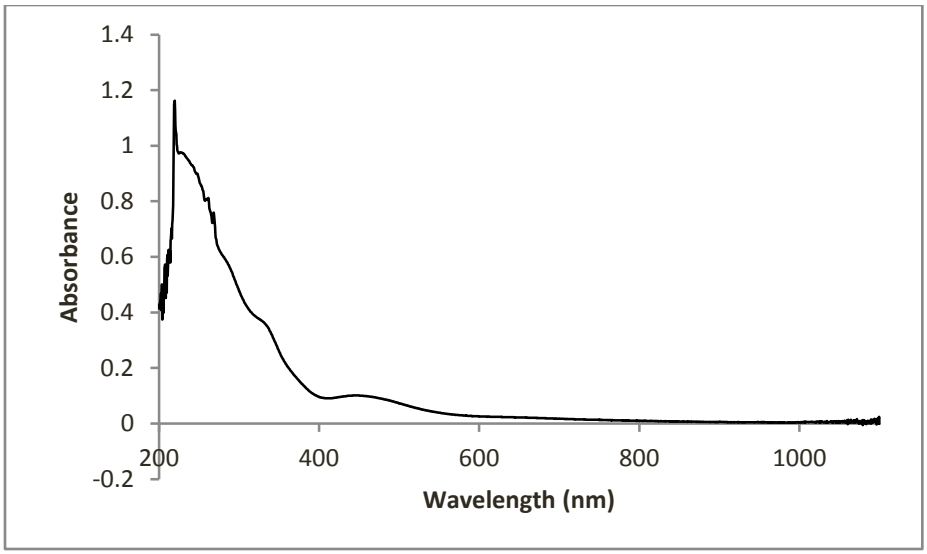

Figure 73: Electronic spectra of **100** in methylcyclohexane. λ (nm) (ε): 446 (1,980), 336 (6,700), 290 (10,900).

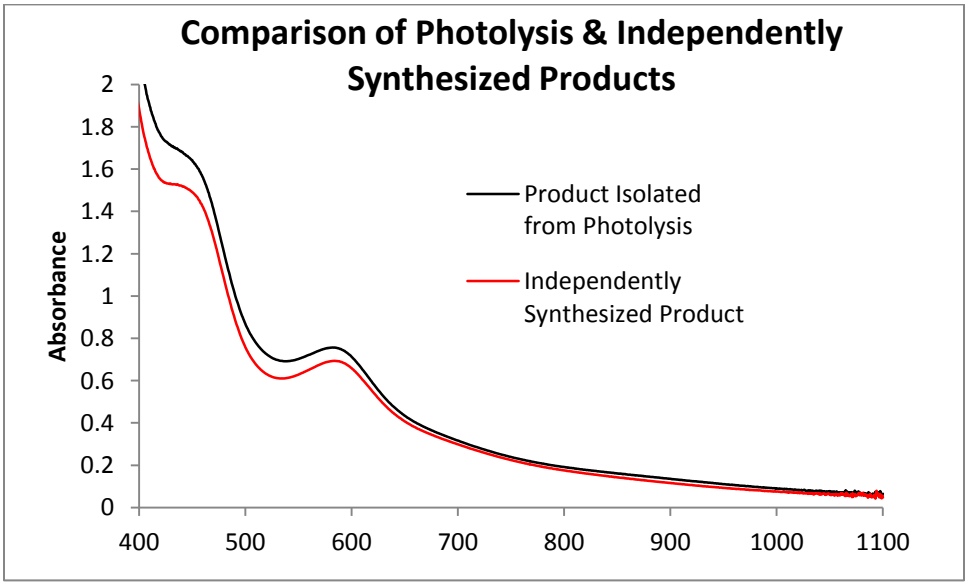

Figure 74: Comparison of electronic spectra for the crystalline material isolated from the photolysis of **53** (black) and **99** (red), which was independently synthesized from the reduction of **103**, in methylcyclohexane for further confirmation of the proposed photoconversion of **53** to **99**.

Utilizing the electronic spectra of **53** and **99** as spectrophotometric references, as seen as in Figure 75, the photolysis of a methylcyclohexane solution of **53** in a quartz cuvette, having a Telfon valved stopper for the exclusion of air, was monitored

periodically by UV-Vis following exposure of this solution to specific wavelengths of UV light through the use of a Xe/Hg lamp and grating monochromator. From these wavelength selective photolysis experiments, the photolysis of **53** was found occur with irradiation of the sample at 337 nm. Upon irradiation for extended periods of time, as seen Figure 76, the characteristic visible absorption for **53** at 831 nm was found to progressively decrease while absorption bands characteristic of **99** at 583 and 453 nm progressively increased. This result provides clear evidence for the photolysis of **53** to **99** through UV-light mediated photolysis. Here, this ability to photolyze the Group 6 CpAm end-on bridged dinitrogen complexes **52** and **53** represents the first example of the same supporting ligand framework serving to facilitate two distinctly different N-N cleavage mechanisms for different transition metal dinitrogen complexes.

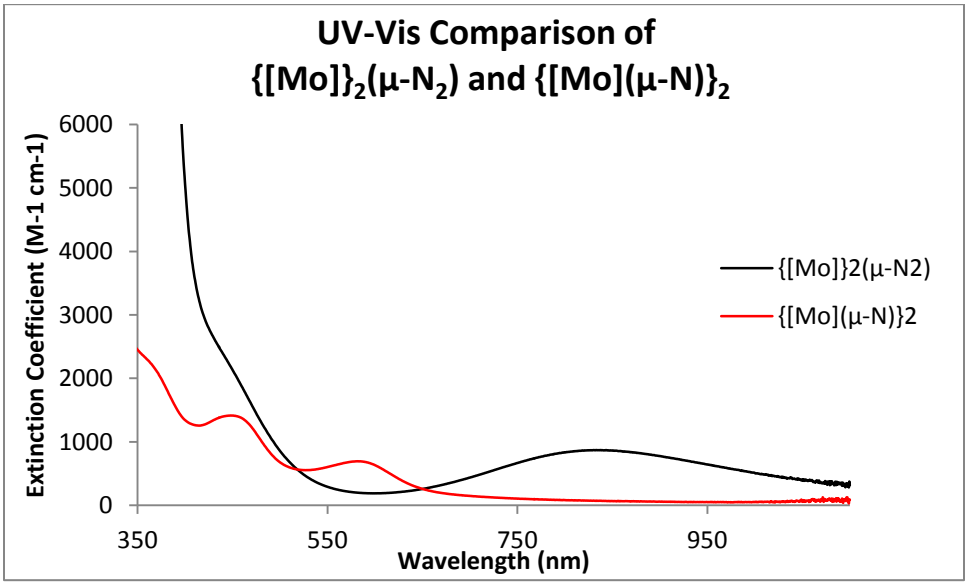

Figure 75: Overlayed electronic spectra of **53** (black) and **99** (red) in methylcyclohexane.

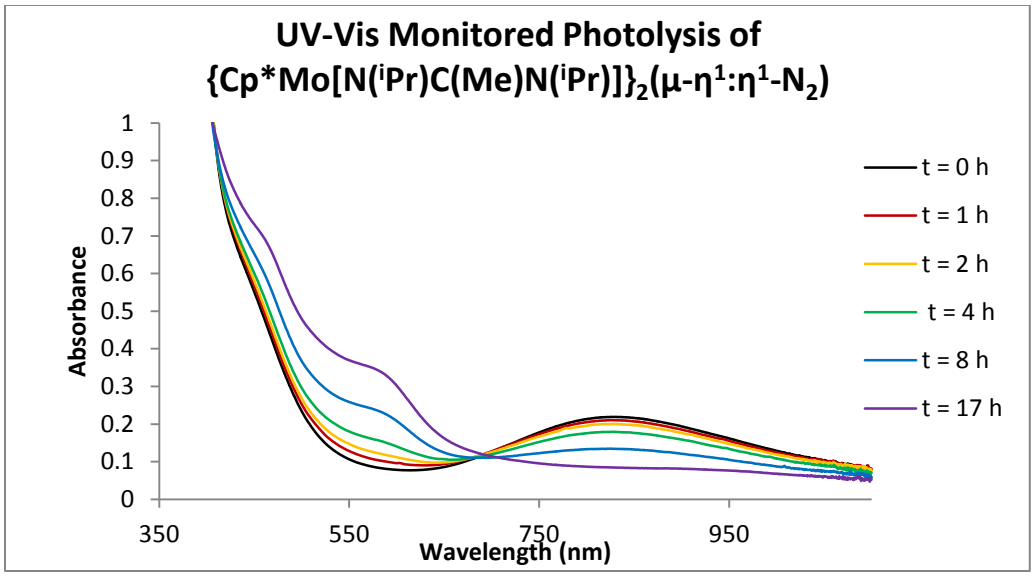

Figure 76: UV-Vis monitored photolysis of **53** at 337 nm in methylcyclohexane.

7.4 Electrochemical Investigation of Group 6 CpAm Dinitrogen Complexes

7.4.1 Cyclic Voltammetry of Group 6 CpAm End-On Dinitrogen Complexes

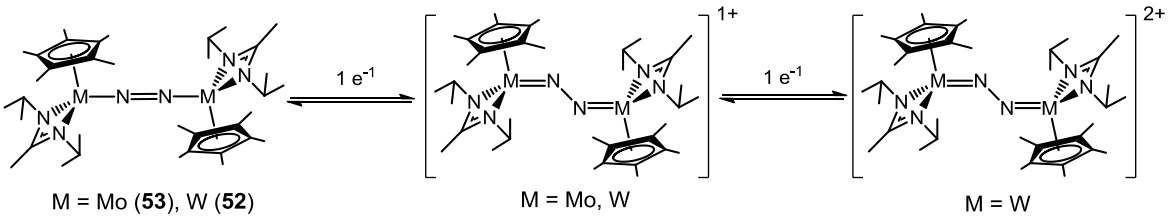

Scheme 51: Cyclic voltammetry studies of Group 6 CpAm end-on bridged dinitrogen complexes, **52** and **53**, for the synthesis of dicationc Group 6 CpAm end-on bridged dinitrogen complexes that are isoelectronic with **39**.

Having established the ability of Group 6 CpAm end-on bridged dinitrogen complexes to photolyze the final N-N bond of the bridged dinitrogen ligand for **52** and **53** we wondered whether this photolytic N-N cleavage process was related to the previously observed thermal N-N cleavage observed for the Group 5 CpAm end-on bridged dinitrogen complex **39**. Of particular relevance is the previous report of photoredox

mediated N_2 cleavage for $\{[(NH_3)_5Os^{II}(N_2)Os^{III}(NH_3)_5]\}$ $(CF_3SO_3)_5$ by Volger and co-workers.[100] Provided the formal M(IV, d^1) oxidation state of the Group 5 metal center in **39**, an analogous photoredox process for the Group 6 metals in **52** and **53** could potentially provide an effectively isoelectronic metal center to that observed for **39** allowing for the thermal mediated N-N cleavage of the bridging dinitrogen ligand of **52** and **53**.[101] In support of this theory, are the extinction coefficients for the UV absorption bands of **52** and **53** which are responsible for N-N photolysis and all have magnitudes of ~50,000 $M^{-1}cm^{-1}$ suggesting their potential identity as metal-to-ligand charge transfer (MLCT) bands. Specifically, these theorized MLCT absorption bands could potentially involve the aromatic cyclopentadienyl ligand which has previously been shown to participate in MLCT processes.[102] Therefore, to study the potential relation of the photocleavage of **52** and **53** to the thermal cleavage of **39** we sought to synthesize isoelectronic analogs of complex **39**. Provided the polycationic nature of the desired isostructural Group 6 end-on bridged dinitrogen complexes, preliminary cyclic voltammetry studies of **52** and **53** were carried out in 0.1 M THF solutions of the weakly coordinating electrolyte $[N(n\text{-}Bu)_4][B(C_6F_5)_4]$ previously reported by Geiger and co-workers using a three electrode setup with a glassy carbon working electrode and silver pseudo-reference electrode.[103] In these studies, **53** was found to exhibit a reversible redox couple at -757 mV relative to the $Cp^*_2Fe/Cp^*_2Fe^+$ couple when decamethylferrocene (Cp^*_2Fe) used as an internal standard, or -1363 mV relative to the Cp_2Fe/Cp_2Fe^+ redox couple when ferrocene (Cp_2Fe) was used as an internal standard, as well as a second irreversible redox couple at more oxidizing potentials as seen in Figure 77. This result suggests the stability of the proposed monocationic complex

$\{Cp^*Mo[N(^iPr)C(Me)N(^iPr)]\}_2(\mu\text{-}\eta^1\text{:}\eta^1\text{-}N_2)^{1+}$ and the instability of the dicationic $\{Cp^*Mo[N(^iPr)C(Me)N(^iPr)]\}_2(\mu\text{-}\eta^1\text{:}\eta^1\text{-}N_2)^{2+}$. In contrast to **53**, cyclic voltammetry of the tungsten analog **52** was found to exhibit two fully reversible redox couples, -1382 and -701 mV relative to the Cp_2Fe/Cp_2Fe^+ redox couple, indicating the stability of the dicationic complex, $\{Cp^*W[N(^iPr)C(Me)N(^iPr)]\}_2(\mu\text{-}\eta^1\text{:}\eta^1\text{-}N_2)^{2+}$, as observed in Figure 78. While the origin of the instability of the molybdenum dicationic complex versus the tungsten dicationic complex in unknown comparison of the first reversible redox couple for **52** and **53** follow the expected trend for electron ionization energies down a group. Moreover, a similar trend for the stability of dicationic tungsten versus molybdenum end-on bridged dinitrogen complexes having the chelating trisamidoamine supporting ligand, $\{[(^tBuC_6H_4)NCH_2CH_2)_3N]M\}_2(\mu\text{-}\eta^1\text{:}\eta^1\text{-}N_2)$, where M = Mo and W, has been reported by Schrock and co-workers as the result of proposed stronger M-N bonds for third versus second row transition metals.[104] However, extrapolation of the instability for the trisamidoamine complexes reported by Schrock should be tempered given the presumed decomposition through extrusion of N_2 versus N-N cleavage in dicationic Group 6 trisamidoamine dinitrogen complexes.

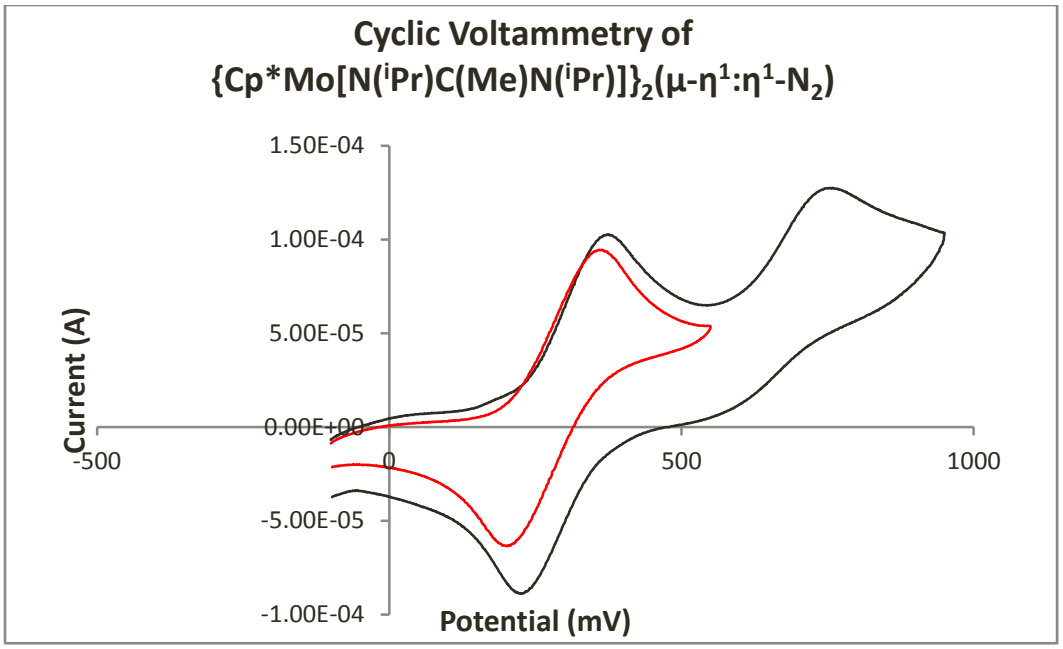

Figure 77: Cyclic voltammetry of **53** at a scan rate of 100 mV/s in a 0.1 M $[N(n\text{-}Bu)_4][B(C_6F_5)_4]$ solution of THF using a glassy carbon working electrode to reveal a reversible redox couple at -757 mV (red) relative to the decamethylferrocene/decamethylferrocenium redox couple and a second irreversible redox couple (black) for **53** at more oxidizing potentials.

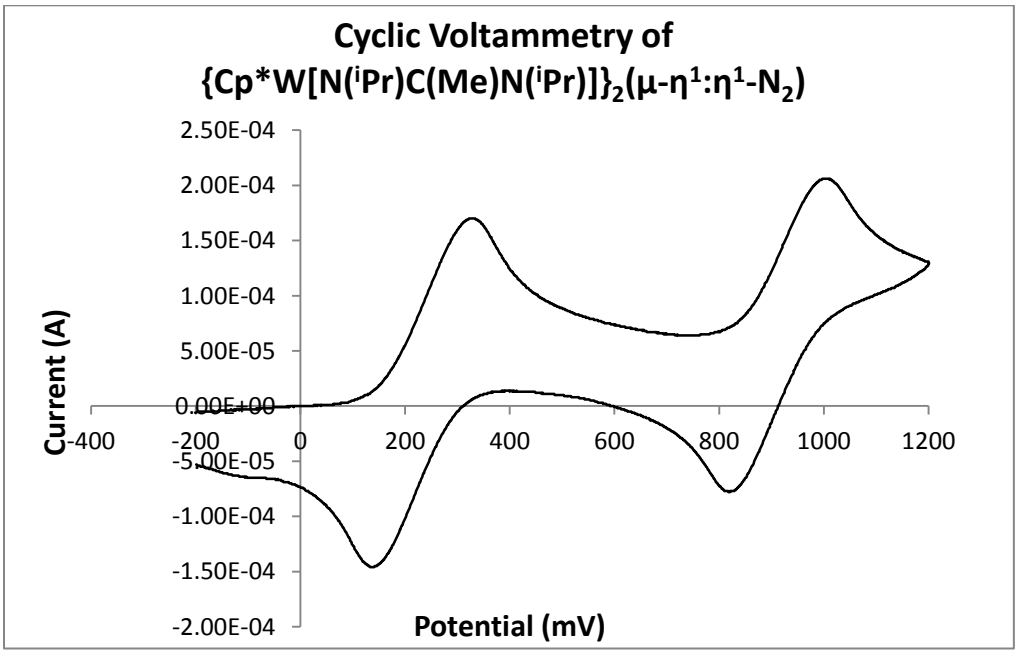

Figure 78: Cyclic voltammetry of **52** in a 0.1 M $[N(n\text{-}Bu)_4][B(C_6F_5)_4]$ solution of THF using a glassy carbon working electrode to reveal two reversible redox couples at -1382 mV and -701 mV relative to the ferrocene/ferrocenium redox couple.

Provided the presence of the two fully reversible redox couples for **52** at less oxidizing potentials versus the Cp_2Fe/Cp_2Fe^+ couple, it was reasoned that the stable dicationic form of **52** could be synthesized through reaction with two equivalents of ferrocenium oxidation reagents. Towards this end, **52** was reacted with two equivalents of $[Cp_2Fe][BAr^F]$ in Et_2O to provide a black paramagnetic solid in excellent yield (88%). Through careful crystallization of the crude product from a mixture of THF and Et_2O, black single crystals suitable for X-Ray diffraction could be obtained. Here, structural analysis in conjunction with elemental analysis determined the structure of this crystalline material to be that of the stable dicationic CpAm end-on bridged dinitrogen complex $\{Cp^*W[N(^iPr)C(Me)N(^iPr)]\}_2(\mu\text{-}\eta^1\text{:}\eta^1\text{-}N_2)$ $\{B[3,5\text{-}(CF_3)_2C_6H_3]_4\}_2$ (**105**). Interestingly, **105** exhibits a more activated N-N bond, N3-N3a = 1.319(8) Å, as well as shorter M-N bonds, W1-N3 = 1.763(4) Å, and a more acute M-N-N bond angle, W-N3-N3a = 166.4(6)˚, as compared with **52** whose selected structural parameters are listed in Table 2 along with the corresponding values from complexes **105** and **39**. When compared with the isoelectronic analog **39**, N3-N3a = 1.313(4) Å, Ta1-N3 = 1.807(2) Å, and Ta1-N3-N3a = 172.7(3)˚, the structural parameters of **105** suggests that the lowest energy configuration of this complex is intermediate between that observed for **52** and **39** with **105** having a more acute M1-N3-N3a angle that may make this complex more prone to N-N cleavage.[16] Moreover the observed paramagnetism of **105** suggests isolation of the formal M(V, d^1) metal centers linked by the bridging dinitrogen ligand similar to the paramagnetism observed in **39**. In general this increased activation of N_2 for **105** is presumed to be the result of the depopulation of a HOMO having increased N-N bond character on moving to the formal M(IV, d^1) oxidation state for the metal centers.

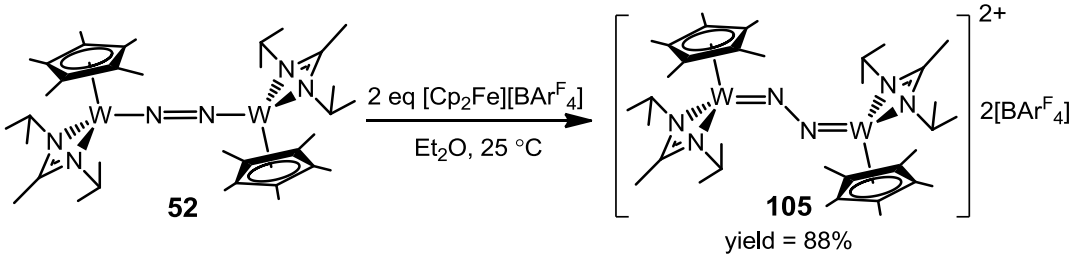

Scheme 52: Synthesis of **105** through the reaction of **52** with two equivalent of $[Cp_2Fe][Bar^F]$.

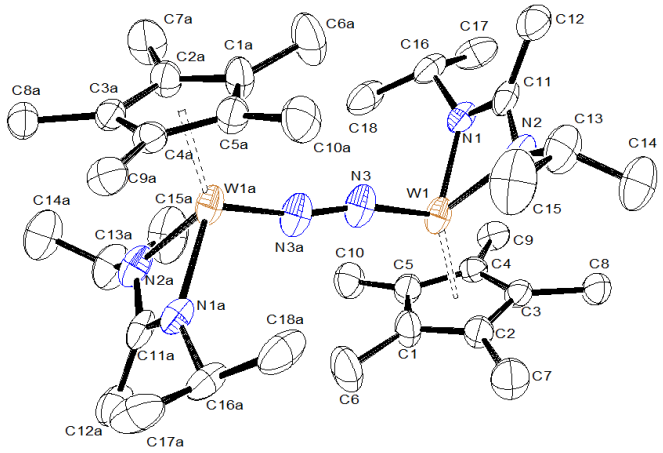

Figure 79: Molecular structure (30% thermal ellipsoids) of **105**. Hydrogen atoms have been removed for the sake of clarity. Selected bond lengths (Å) and bond angles (°) for **105**: W1-N3 1.763(4), N3-N3a 1.319(8), W1-N1 2.079(5), W1-N2 2.103(4), N2-W1-N1 62.60(17), W1-N3-N3a 166.4(6).

Parameter	**52**	**105**	**39**
N3-N3a	1.277(8)	1.319(8)	1.313(4)
M1-N3	1.816(4)	1.763(4)	1.807(2)
M1-N1	2.172(4)	2.079(5)	2.185(2)
M1-N2	2.182(4)	2.103(4)	2.186(2)
M1-N3-N3a	176.7(5)	166.4(6)	172.7(3)
N1-M1-N2	61.43(15)	62.60(17)	60.53(9)

Table 2: Selected structural parameters of comparison for complexes **52**, **105**, and **39**.

7.4.2 Cyclic Voltammetry of Group 6 CpAm N-N Cleavage Complexes

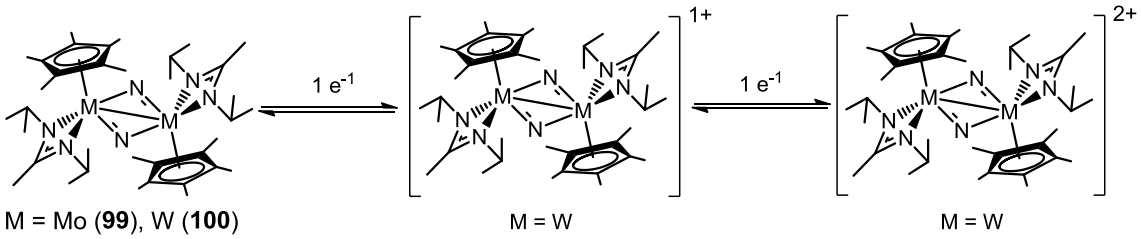

Scheme 53: Cyclic voltammetry studies of Group 6 CpAm end-on bridged dinitrogen complexes, **99** and **100**, for the synthesis of the dicationic Group 6 CpAm N-N cleavage complex **106**, that is isoelectronic with **40**.

Having assessed the stability of the dicationic form for the end-on bridged dinitrogen complexes **52** and **53**, we next sought to determine whether isoelectronic analogs of **40** could be synthesized from the corresponding Group 6 CpAm N-N cleavage complexes, **99** and **100**. Toward this end, analogous cyclic voltammetry studies were performed on **99** in a THF solution of $[N(n\text{-}Bu)_4][B(C_6F_5)_4]$ with only a single irreversible oxidation of this complex having been observed as seen in Figure 80. Again, contrasting this observed instability for the molybdenum analog, the analogous investigation of **100** by cyclic voltammetry revealed the presence of two fully reversible redox couples at -1590 mV and -446 mV relative to the Cp_2Fe/Cp_2Fe^+ redox couple. These reversible redox couples when compared to the generation of the dicationic form of **52**, were found to respectively occur at less oxidizing and more oxidizing potentials indicating the lesser stability of the dicationic form of **100** potentially due to the closer proximity of the cationic metal centers.

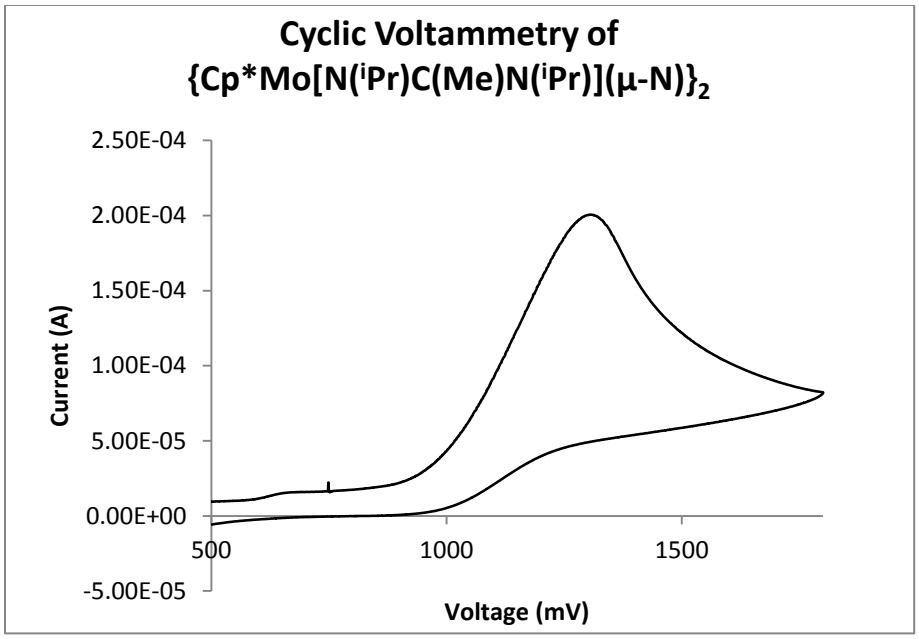

Figure 80: Cyclic voltammetry of **99** at a scan rate of 100 mV/s in a 0.1 M $[N(n\text{-}Bu)_4][B(C_6F_5)_4]$ solution of THF using a glassy carbon working electrode to reveal an irreversible redox couple for **99**.

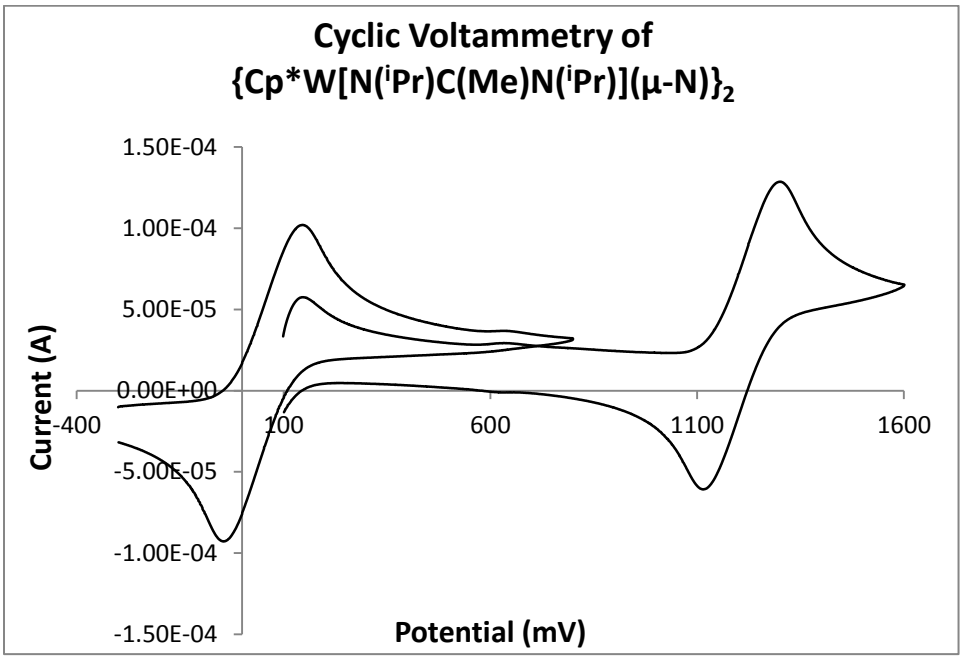

Figure 81: Cyclic voltammetry for **100** at a scan rate of 100 mV/s in a 0.1 M $[N(n\text{-}Bu)_4][B(C_6F_5)_4]$ solution of THF using a glassy carbon working electrode at 25 ˚C for the demonstration of two fully reversible redox couples at -1590 mV and -446 mV relative to the ferrocene/ferrocenium redox couple.

Again, provided the presence of the two fully reversible redox couples for **100** at less oxidizing potentials versus the Cp_2Fe/Cp_2Fe^+ couple, it was reasoned that the stable dicationic form of **100** could be synthesized through reaction with two equivalents of ferrocenium oxidation reagents. Therefore, **100** was reacted with two equivalents of $[Cp_2Fe][BAr^F]$ in Et_2O to provide a brown diamagnetic solid in excellent yield (85%). Through crystallization of the crude product from a mixture of THF, Et_2O, and pentane, single crystals suitable for n diffraction could be obtained. Here, structural analysis in conjunction with elemental analysis confirmed the structure of this material to be the presumed dicationic CpAm N-N cleavage complex $\{Cp^*W[N(^iPr)C(Me)N(^iPr)](\mu\text{-}N)\}_2\{B[3,5\text{-}(CF_3)_2C_6H_3]_4\}_2$ (**106**). Interestingly, **106** exhibits smaller N••••N, N3-N3a = 2.557 Å, and longer M••••M internuclear distances, W1-W1a = 2.8037(3) Å, as well as shorter M-N bonds and a more asymmetric M_2N_2 core, W1-N3 = 1.817(3) Å and W1-N3a = 1.972(3) Å, as compared with **100** whose selected structural parameters are listed in Table 3 with the corresponding values for complexes **106** and **40**. When compared with the isoelectronic analog **40**, N3-N3a = 2.574 Å, Ta1-Ta1a = 2.8144(4)Å, Ta1-N3 = 1.883(3) Å, and Ta1-N3a = 1.923(3) Å, the structural parameters of **106** further confirm that as expected the lowest energy configuration of this complex is closer to **40** versus **52.**

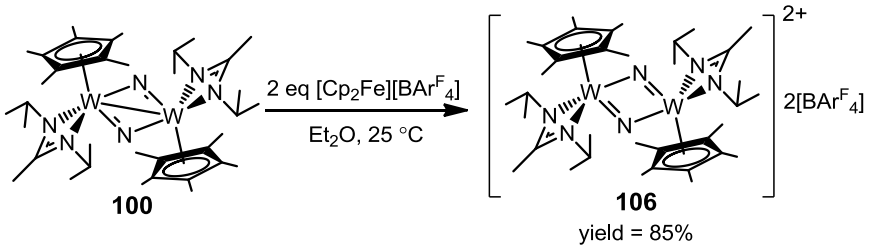

Scheme 54: Synthesis of **106** through the reaction of **100** with two equivalent of $[Cp_2Fe][Bar^F]$.

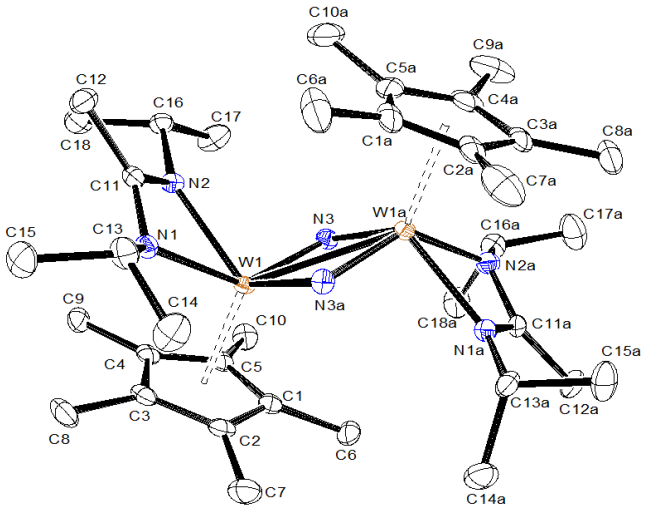

Figure 82: Molecular structure (30% thermal ellipsoids) of **106**. Hydrogen atoms and counterions have been removed for the sake of clarity. Selected bond lengths (Å) and bond angles (°) for **106**: W1-N3 1.817(3), W1-N3a 1.972(3), N3-N3a 2.557, W1-W2 2.8037(3), W1-N1 2.122(3), W1-N2 2.195(3), N2-W1-N1 60.52(12), N3-W1-N3a 84.76(13).

Parameter	**100**	**106**	**40**
N3-N3a	2.747	2.557	2.574
M1-N3	1.912(2)	1.817(3)	1.883(3)
M1-N3a	1.908(2)	1.972(3)	1.923(3)
M1-N1	2.223(2)	2.122(3)	2.227(4)
M1-N2	2.228(2)	2.195(3)	2.290(3)
M1-M2	2.6560(3)	2.8037(3)	2.8144(4)
N1-M1-N2	59.04(9)	60.52(12)	58.31(12)
N3-M1-N3a	91.92(10)	84.76(13)	84.65(15)

Table 3: Selected structural parameters of comparison for complexes **100**, **106**, and **40**.

Provided the respective the isoelectronic nature and nearly isostructural geometric parameters of **105** and **106** with **39** and **40** in conjunction with the instability of the dicationic form of complex **53** having weaker M-N bonds, we sought to test whether **105** could be thermally converted into **106**. Despite a survey with various solvents, to date **105** and **106** have only been found to be soluble in THF without undergoing further decomposition. Therefore, analytically pure crystals of **105** were dissolved in THF-d_8 and this solution was left to react at room temperature. However, when this solution is left for any extended period at room temperature, **105** polymerizes the THF NMR solvent as the presumed result of its polycationic nature exhibiting significant electrophilicity. As a result, at this time it is not known whether a photoredox process followed by thermal N-N cleavage is the origin of the photolytic cleavage of **52** and **53**, however, such reactivity could potentially be assessed through future studies on the photoemissive properties of **52** and **53**. Specifically, unreactive excited MLCT states must eventually relax to their ground state, one potential relaxation process being fluorescence following relaxation of the complex to the lowest vibrational level of the excited state. With regard to the excited MLCT states for **52** and **53**, this would result in **52** having substantially higher photoemission relative to **53** provided its comparative thermal stability following photoredox thereby confirming N-N cleavage through a photoredox process followed by thermal N-N cleavage of the N_2 ligand.

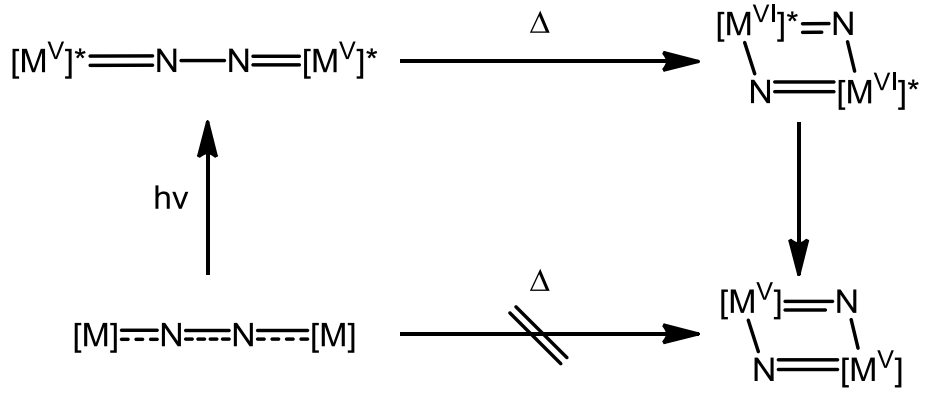

Scheme 55: Proposed photoredox mechanism involving **52** and **53** for the formation **99** and **100** through attainment of excited MLCT states that undergo subsequent thermal N-N cleavage.

Experimentals

All manipulations with air and moisture sensitive compounds were carried out under N_2 or Ar atmospheres using standard Schlenk or glovebox techniques. All solvents were dried (Na for toluene and methylcyclohexane versus Na/benzophenone for pentane, Et_2O, and THF) and distilled under N_2 prior to use. Benzene-d_6, toluene-d_8, and THF-d_8 were dried over Na/K alloy and isolated by vacuum transfer prior to use while chlorobenzene-d_5 was dried over calcium hydride and isolated by vacuum transfer prior to use. Celite was oven dried (150 °C for several days) prior to use. All amines were dried over CaH_2 and distilled by short path distillation while acetonitrile was dried over CaH_2, vacuum transferred, and passed through activated alumina prior to use. Cooling was performed in the internal freezer of a glovebox maintained at -30 ºC. Nitrous oxide (99%), carbon dioxide (99%), carbon monoxide (99%), equimolar gaseous mixtures of ^{13}CO and CO_2, equimolar gaseous mixtures of ^{13}CO and N_2O, $^tBuNH_2$, $HN(^iPr)_2$, trimethylsilyl azide, *tert*-butyl isocyanate, *tert*-butyl isocyanide, methyl iodide, and manganese dioxide were purchased from Sigma Aldrich. All purchased chemicals were used as received unless otherwise noted. Chemicals $LiNH^tBu$, $LiN(^iPr)_2$, $[Cp_2Fe][BAr^F]$, and the tetrabutylammonium tetrakis(pentafluorophenyl)borate electrolyte salts were prepared according to previously reported literature procedures in similar yield and purity. All ^1H NMR and ^{13}C NMR spectra were recorded at either 400 MHz or 500 MHz and 125.6 MHz respectively. Low and high temperature NMR spectrometer data involved respective calibration with methanol and ethylene glycol standards. Cyclic voltammetry studies utilized a standard three-electrode cell with a glassy carbon disk as a working electrode, a platinum flag as the counter electrode, and a silver wire as the

reference electrode. All potentials were recorded relative to either the ferrocene/ferrocenium or decamethylferrocene/decamethylferrocenium redox couple through the addition of these internal standards to samples analyzed by cyclic voltammetry. Light mediated reactions were performed using a Rayonet® Photochemical Reactor containing a carousel of ultraviolet lamps (catalogue number: RPR-3500A) with an output of 300-400 nm. Selective wavelength photoirradiation experiments were performed using a Xe/Hg arc lamp and a grating monochromator having a bandpass of 20 nm. All mass spectra were analyzed on a JEOL AccuTOF-CS mass spectrometer using electron spray ionization in the positive mode for the detection of ions. Elemental analyses were carried out by Midwest Microlab LLC.

{Cp*Mo[N(^{i}Pr)C(Me)N(^{i}Pr)]}$_2$(μ-η^1:η^1-N$_2$) (53)

A solution of **50** (309 mg, 0.70 mmol) in 40 mL of THF was cooled to -30 °C, at which point 0.5% (w/w) of NaHg (13.169 g, 2.86 mmol) was added, and the solution was allowed to warm to room temperature. The reaction mixture was stirred at room temperature for 16 h to yield a yellow-brown colored solution, after which time the volatiles were removed *in vacuo* and the solid residue was taken up in pentane and filtered through Celite. The filtrate was then concentrated and cooled to -30 °C to give yellowish-brown crystals of **53** (208 mg, yield = 77%). ^{1}H NMR (400 MHz, benzene-d_6): 0.88 (12H, d, J = 6.4 Hz, CH(CH_3)$_2$), 1.13 (12H, d, J = 6.4 Hz, CH(CH_3)$_2$), 1.87 (30H, s, C$_5$(CH_3)$_5$), 1.89 (6H, s, NC(CH_3)N), 3.45 (4H, sept, J = 6.4 Hz, CH(CH$_3$)$_2$).

{Cp*W[N(^{i}Pr)C(Me)N(^{i}Pr)]}$_2$(μ-η^1:η^1-N$_2$) (52)

A solution of **51** (307 mg, 0.54 mmol) in 30 mL of THF was cooled to -30 °C, at which point 0.5% (w/w) NaHg (9.964 g, 2.17 mmol) was added and the solution was allowed to warm to room temperature. The reaction mixture was stirred at room temperature for 1.5 h to yield a dark green colored solution, after which time the volatiles were removed *in vacuo* and the solid residue was taken up in pentane and filtered through Celite. The resulting dark green filtrate was then concentrated and cooled to -30 °C to give dark green crystals of **52** (257 mg, yield = 92%). ^{1}H NMR (400 MHz, benzene-d_6): 0.98 (12H, d, J = 6.4 Hz, CH(CH_3)$_2$), 1.24 (12H, d, J = 6.4 Hz, CH(CH_3)$_2$), 1.71 (6H, s, NC(CH_3)N), 2.14 (30H, s, C$_5$(CH_3)$_5$), 3.26 (4H, sept, J = 6.4 Hz, CH(CH$_3$)$_2$).

Cp*Mo[N(^{i}Pr)C(Me)N(^{i}Pr)](CO)$_2$ (54)

Within a Schlenk tube, a solution of **53** (0.142 g, 0.184 mmol) in 6 mL of toluene was charged with 5 psi of carbon monoxide (99%), and the contents of the storage tube were stirred for 40 h at room temperature. The volatiles from the resulting dark red solution were then removed *in vacuo*, and the residue was taken up in pentane and filtered through a pad of Kimwipe placed within a glass pipet. The solvent of the dark red filtrate was removed *in vacuo* to provide a crude product that was recrystallized from pentane at -30 °C to provide dark red crystals of **54** (112 mg, yield = 71%). For **54**: Anal. Calc'd for C$_{20}$H$_{32}$N$_2$O$_2$Mo: C, 56.05; H, 7.53; N, 6.54; Found: C, 56.57; H, 7.38; N, 6.54. ^{1}H NMR (400 MHz, benzene-d_6) 0.99 (6H, d, J = 6.3 Hz, CH(CH_3)$_2$), 1.03 (6H, d, J = 6.3 Hz, CH(CH_3)$_2$), 1.42 (3H, s, NC(CH_3)N), 1.74 (15H, s, C$_5$(CH_3)$_5$), 3.48 (2H, sept, J = 6.3 Hz, CH(CH$_3$)$_2$). IR (KBr) ν_{CO} = 1909 and 1806 cm^{-1}.

Cp*W[N(^{i}Pr)C(Me)N(^{i}Pr)](CO)$_2$ (55)

Within a Schlenk tube, a solution of **52** (60 mg, 0.063 *m*mol) in 4 mL of toluene was charged with 5 psi of carbon monoxide (99%), and the contents of the storage tube were stirred for 40 h at room temperature. The volatiles from the resulting dark brown solution were then removed *in vacuo*, and the residue taken up in pentane and filtered through a pad of Kimwipe placed within a glass pipet. The solvent of the dark brown filtrate was removed *in vacuo* to provide a crude product that was recrystallized from a mixture of pentane and toluene at -30 °C to provide orange-red crystals of **55** (39 mg, yield = 59%). For **55**: Anal. Calc'd for $C_{20}H_{32}N_2O_2W$: C, 46.34; H, 6.22; N, 5.40; Found: C, 46.19; H, 6.11; N, 5.37. ^{1}H NMR (400 MHz, benzene-d_6) 0.99 (6H, d, J = 6.4 Hz, CH(CH_3)$_2$), 1.01 (6H, d, J = 6.4 Hz, CH(CH_3)$_2$), 1.34 (3H, s, NC(CH_3)N), 1.81 (15H, s, C$_5$(CH_3)$_5$), 3.35 (2H, sp, J = 6.4 Hz, CH(CH$_3$)$_2$). IR (KBr) ν_{CO} = 1892 and 1788 cm-1.

{Cp*W[N(^{i}Pr)C(Me)N(^{i}Pr)](CO)}$_2$(μ-η^1:η^1-N$_2$) (56)

A solution of **52** (43 mg, 0.045 mmol) in 0.5 mL of benzene-d_6 was transferred into a J Young tube. The headspace of the J Young tube was evacuated, charged with carbon monoxide (8 psi), and reacted at room temperature for 15 h to give a dark green colored solution. Volatiles were removed *in vacuo* to give a dark green oil that was crystallized at -30 ºC from a mixture of pentane and toluene to give dark green crystals for **56** (24 mg, yield = 53%). Anal. calc'd for $W_2O_2N_6C_{38}H_{64}$: C, 45.41; H, 6.42; N, 8.37, Found: C, 45.39; H, 6.22; N, 8.12. ^{1}H NMR (400 MHz, benzene-d_6): 1.11 (3H, d, J = 6.5 Hz,

$CH(CH_3)_2$), 1.17 (3H, d, J = 6.7 Hz, $CH(CH_3)_2$), 1.21 (3H, d, J = 6.7 Hz, $CH(CH_3)_2$), 1.28 (3H, d, J = 6.5 Hz, $CH(CH_3)_2$), 1.62 (3H, s, $N(CH_3)N$), 1.94 (15H, s, $C_5(CH_3)_5$), 3.56 (1H, sept, J = 6.7 Hz, $CH(CH_3)_2$), 3.59 (1H, sept, J = 6.5 Hz, $CH(CH_3)_2$). IR (KBr) $\nu_{C\equiv O}$ = 1768 cm^{-1}.

Cp*W[N(^{i}Pr)C(Me)N(^{i}Pr)](H)(CN)(CN^{t}Bu) (60)

Tert-butyl isocyanide (84 uL, 0.73 mmol) was added dropwise to a solution of **52** (85 mg, 0.090 mmol) in 5 mL of toluene. The solution was stirred at room temperature for 70 h to produce a dark red solution. Volatiles were removed *in vacuo* to give a dark red oil. The red oil was re-dissolved in 4 mL toluene, transferred into a storage tube and heated at 80 ˚C under an argon atmosphere for 14 h to give a yellowish-green solution. Volatiles were removed *in vacuo* and the crude product was dissolved in minimal pentane and cooled to –30º C to produce orange crystals of **60** (61 mg, yield = 64.9%). Anal. Calc'd for $W_1N_4C_{24}H_{42}$: C, 50.51; H, 7.42; N, 9.82; Found: C, 50.61; H, 7.27; N, 9.76. ^{1}H NMR (400 MHz, benzene-d_6): 0.90 (3H, d, J = 6.6 Hz, $CH(CH_3)_2$), 1.03 (3H, d, J = 6.4 Hz, $CH(CH_3)_2$), 1.27 (3H, d, J = 6.4 Hz, $CH(CH_3)_2$), 1.32 (9H, s, $CN(CH_3)_3$), 1.35 (3H, d, J = 6.6 Hz, $CH(CH_3)_2$), 1.40 (3H, s, $NC(CH_3)N$), 1.84 (15H, s, $C_5(CH_3)_5$), 3.35 (1H, sept, J = 6.4 Hz, $CH(CH_3)_2$), 3.46 (1H, sept, J = 6.6 Hz, $CH(CH_3)_2$), 11.01 (1H, s, $J^1_{1H\text{-}183W}$ = 13.4 Hz). Solid state IR (KBr): $\nu_{C\equiv N}$ = 2096 cm^{-1}, $\nu_{C\equiv NtBu}$ = 1955 cm^{-1}.

Cp*Mo[N(^{i}Pr)C(Me)N(^{i}Pr)](O) (62)

A solution of **53** (126 mg, 0.163 mmol) in 6 mL of toluene was transferred to a storage tube with a Teflon valve. The headspace of the storage tube was evacuated and the tube was charged with 10 psi nitrous oxide (99%) at room temperature. The reaction mixture was stirred at room temperature for 16 h to produce a purple colored solution. Volatiles were removed *in vacuo* to give a purple solid. The crude product was dissolved in hexamethyldisiloxane and filtered through a dry pad of Kimwipe placed in a glass pipette tip. The dark purple filtrate was concentrated and cooled to -30 °C to produce dark purple

crystals of **62** (66 mg, yield = 50%). Anal. calc'd for $C_{18}H_{32}N_2OMo$: C, 55.64; H, 8.31; N, 7.21; Found: C, 54.88; H, 7.72; N, 7.45. ^{1}H NMR (400 MHz, benzene-d_6): 0.98 (6H, d, J = 6.3 Hz, CH(CH_3)$_2$), 1.33 (6H, d, J = 6.4 Hz, CH(CH_3)$_2$), 1.47 (3H, s, NC(CH_3)N), 1.84 (15H, s, C$_5$(CH_3)$_5$), 3.24 (2H, sept, J = 6.4 Hz, CH(CH$_3$)$_2$).

Synthesis of Cp*W[N(^{i}Pr)C(Me)N(^{i}Pr)](O) (63) using N_2O

A solution of **52** (302 mg, 0.319 mmol) in 5 mL of toluene was transferred to a storage tube with a Teflon valve. The headspace of the storage tube was evacuated and the tube was charged with 5 psi nitrous oxide (99%) at room temperature. The reaction mixture was stirred at room temperature for 2 h to produce an orange brown colored solution. Volatiles were removed *in vacuo* and the crude product was dissolved in pentane and filtered through a dry pad of Kimwipe placed in a glass pipette tip. The collected red-orange filtrate was concentrated and cooled to -30 °C to produce dark orange crystals of **63** (166 mg, yield = 55%). Anal. calc'd for $C_{18}H_{32}N_2OW$: C, 45.37; H, 6.77; N, 5.88; Found: C, 45.22; H, 6.62; N, 5.77. ^{1}H NMR (400 MHz, benzene-d_6): 0.99 (6H, d, J = 6.3 Hz, CH(CH_3)$_2$), 1.38 (6H, d, J = 6.3 Hz, CH(CH_3)$_2$) 1.46 (3H, s, NC(CH_3)N), 2.04 (15H, s, C$_5$(CH_3)$_5$), 3.17 (2H, sept, J = 6.3 Hz, CH(CH$_3$)$_2$).

Synthesis of Cp*W[N(^{i}Pr)C(Me)N(^{i}Pr)](O) (63) using CO_2

A solution of **52** (46 mg, 0.049 mmol) in 6 mL of toluene was transferred to a storage tube with a Teflon valve. The headspace of the storage tube was evacuated and the tube was charged with 10 psi carbon monoxide (99%) at room temperature. The reaction mixture was stirred at room temperature for 48 h to produce an orange brown colored solution. Volatiles were removed *in vacuo* and the crude product was dissolved in pentane and filtered through a dry pad of Kimwipe placed in a glass pipette tip. The collected red-orange filtrate was concentrated and cooled to -30 °C to produce dark orange crystals of **63** (29 mg, yield = 63%). ^{1}H NMR (400 MHz, benzene-d_6): 0.99 (6H,

d, J = 6.3 Hz, CH(CH_3)$_2$), 1.38 (6H, d, J = 6.3 Hz, CH(CH_3)$_2$) 1.46 (3H, s, NC(CH_3)N), 2.04 (15H, s, C$_5$(CH_3)$_5$), 3.17 (2H, sept, J = 6.3 Hz, CH(CH$_3$)$_2$).

Cp*Mo[N(^{i}Pr)C(Me)N(^{i}Pr)](NSiMe$_3$) (64)

Trimethylsilyl azide (20 μL, 0.15 mmol) was added dropwise to a solution of **53** (58 mg, 0.075 mmol) in 4 mL of toluene. The solution was stirred at room temperature for 1 h to produce a black colored solution. Volatiles were removed *in vacuo* to give a black solid. The crude product was dissolved in pentane and filtered through a dry pad of Kimwipe placed in the tip of a glass pipette. The collected black filtrate was concentrated and cooled to -30 ºC to produce black crystals of **64** (28 mg, yield = 40%). Anal. calc'd for $C_{21}H_{41}N_3Mo_1Si_1$: C, 54.88; H, 8.99; N, 9.14; Found: C, 54.91; H, 8.80; N, 9.24. ^{1}H NMR (400 MHz, benzene-d_6): 0.28 (9H, s, Si(CH_3)$_3$), 1.02 (6H, d, J = 6.3 Hz, CH(CH_3)$_2$), 1.24 (6H, d, J = 6.3 Hz, CH(CH_3)$_2$), 1.60 (3H, s, NC(CH_3)N), 1.89 (15H, s, C$_5$(CH_3)$_5$), 3.22 (2H, sept, J = 6.3 Hz, CH(CH$_3$)$_2$).

Cp*W[N(^{i}Pr)C(Me)N(^{i}Pr)](NSiMe$_3$) (65)

Trimethylsilyl azide (65 μL, 0.49 mmol) was added dropwise to a solution of **52** (70 mg, 0.074 mmol) in 6 mL of toluene. The solution was stirred at room temperature for 3 h to produce a dark red solution. Volatiles were removed *in vacuo* to give a dark red solid. The crude product was dissolved in pentane and filtered through a dry pad of Kimwipe placed in the tip of a glass pipette. The collected dark red filtrate was concentrated and cooled to -30 ºC to produce dark red crystals of **65** (78 mg, yield = 97%). Anal. Calc'd for $W_1Si_1N_3C_{21}H_{41}$: C, 46.06; H, 7.55; N, 7.68; Found: C, 45.79; H, 7.35; N, 7.63. ^{1}H NMR (400 MHz, benzene-d_6): 0.27 (9H, s, Si(CH_3)$_3$), 1.03 (6H, d, J = 6.4 Hz, CH(CH_3)$_2$), 1.30 (6H, d, J = 6.4 Hz, CH(CH_3)$_2$), 1.59 (3H, s, NC(CH_3)N), 2.10 (15H, s, C$_5$(CH_3)$_5$), 3.13 (2H, sept, J = 6.4 Hz, CH(CH$_3$)$_2$).

Synthesis of Cp*Ta[N(^{i}Pr)C(Me)N(^{i}Pr)](NH^{t}Bu)Cl (74)

A solution of LiNH^{t}Bu (74 mg, 0.91 mmol) in 10 mL of Et_2O was cooled to -30 °C and added dropwise to a -30 °C solution of **73** (471 g, 0.891 mmol) in 50 mL of Et_2O over a period of 5 m. The reaction mixture was allowed to warm to room temperature and stirred for 3 h to produce a red-purple colored solution. Volatiles were removed *in vacuo* to yield a red-purple solid. The crude product was dissolved in pentane and filtered through Celite. The collected dark red filtrate was concentrated and cooled to -30 °C to give dark red crystals of **74** (324 mg, yield = 64%). Anal. Calc'd for $C_{22}H_{42}N_3ClTa$: C, 46.75; H, 7.50; N, 7.44; Found: C, 46.94; H, 7.39; N, 7.22.

Synthesis of Cp*Ta[N(^{i}Pr)C(Me)N(^{i}Pr)](N^{t}Bu) (75)

A -30 °C solution of LiN(^{i}Pr)$_2$ (53 mg, 0.496 mmol) in 10 mL of Et_2O was added dropwise to a -30 °C solution of **73** (224 mg, 0.396 mmol) in 20 mL of Et_2O over a period of 5 m. The reaction mixture was allowed to warm to room temperature and stirred for 2 h to produce a green-brown colored solution. Volatiles were removed *in vacuo* to give a brown oil. The oil was dissolved in pentane and filtered through Celite. The collected dark brown filtrate was dried *in vacuo* to give a brown solid that was then dissolved in toluene and left at room temperature for 16 h to produce a dark red colored solution. Solvent was removed *in vacuo* to give a bright red oil. The oil was dissolved in minimal pentane and cooled to -30 °C for 1 wk to give bright red crystals of **75** (76 mg, yield = 33%). Anal. Calcd for $C_{22}H_{41}N_3Ta$: C, 49.97; H, 7.82; N, 7.95; Found: C, 49.76; H, 7.51; N, 7.86.

Synthesis of Cp*Ta[N(^{i}Pr)C(CH_2)N(^{i}Pr)](NH^{t}Bu) (76)

A -30 °C solution of LiN(^{i}Pr)$_2$ (43 mg, 0.402 mmol) in 5 mL of THF was added dropwise to a -30 °C solution of **73** (226 mg, 0.403 mmol) in 15 mL of THF. The reaction mixture was warmed to room temperature and stirred at this temperature for 1 h to produce a dark green colored solution. Volatiles were removed *in vacuo* to yield a dark green solid. The crude product was dissolved in minimal pentane and filtered through Celite. The collected filtrate was concentrated and cooled to -30 °C to give dark green crystals of **76** (140 mg, yield = 66%) Anal. Calc'd for $C_{22}H_{41}N_3Ta$: C, 49.99; H, 7.82; N, 7.95; Found: C, 50.21; H, 7.67; N, 7.93.

Cp*W[N(^{i}Pr)C(CH_2)N(^{i}Pr)](H)(N^{t}Bu) (78)

A –30 ºC solution of lithium tert-butyl amide (66 mg, 0.84 mmol) in 10 mL of Et_2O was added dropwise to a –30 ºC solution of **49**. The solution was allowed to warm to room temperature and stirred for 35 m to give a yellow-orange colored solution. Volatiles were removed *in vacuo* to give a yellow-orange solid. The solid was dissolved in pentane and filtered through a short pad of Cellite on a glass frit to give an orange-red colored filtrate. The filtrate was concentrated and cooled to -30 ºC to give orange crystals of **78** (159 mg, yield = 75%). Anal. Calc'd for $W_1N_3C_{22}H_{41}$: C, 49.70; H, 7.78; N, 7.91; Found: C, 49.82; H, 7.65; N, 7.81. ^{1}H NMR (400 MHz, benzene-d_6): 1.20 (9H, s, NC(CH_3)$_3$), 1.25 (3H, d, J = 6.7 Hz, CH(CH_3)$_2$), 1.35 (3H, d, J = 6.1 Hz, CH(CH_3)$_2$), 1.55 (3H, d, J = 6.1 Hz, CH(CH_3)$_2$), 1.63 (3H, d, J = 6.7 Hz, CH(CH_3)$_2$), 1.92 (15H, s, C$_5$(CH_3)$_5$), 2.95 (1H, d, $^2J_{1H\text{-}1H}$ = 1.7 Hz, NC(CH_2)N), 2.99 (1H, d, $^2J_{1H\text{-}1H}$ = 1.7 Hz,

NC(CH_2)N), 3.84 (1H, sept, J = 6.7 Hz, CH(CH_3)$_2$), 4.22 (1H, sept, J = 6.1 Hz, CH(CH_3)$_2$), 11.00 (1H, s, $^1J_{183W\text{-}1H}$ = 43.5 Hz, WH).

Cp*W[N(^{i}Pr)C(Me)N(^{i}Pr)](N^tBu) (79)

A –30 ºC solution of lithium *tert*-butyl amide (66 mg, 0.84 mmol) in 10 mL of Et_2O was added dropwise to a –30 ºC solution of **49** (212 mg, 0.399 mmol). The solution was allowed to warm to room temperature and stirred for 35 m to give a yellow-orange colored solution. Volatiles were removed *in vacuo* to give a yellow-orange solid. The crude product was dissolved in pentane and filtered through a short pad of Cellite on a glass frit to give an orange-red colored filtrate. The filtrate was concentrated and cooled to -30 ºC to give orange crystals of **78** (159 mg). Crystals of **78** were dissolved in 5 mL of toluene and the solution was stirred for 5 d at room temperature to give a dark red colored solution. Volatiles were removed *in vacuo* to give a dark red solid. The crude product was dissolved in minimal hexamethyldisiloxane and cooled to –30 ºC to give dark red crystals of **79** (127 mg, yield = 60%). Anal. Calc'd for $W_1N_3C_{22}H_{41}$: C, 49.70; H, 7.78; N, 7.91; Found: C, 50.06; H, 7.84; N, 7.81. ^{1}H NMR (400 MHz, benzene-d_6): 1.03 (6H, d, J = 6.5 Hz, CH(CH_3)$_2$), 1.29 (6H, d, J = 6.5 Hz, CH(CH_3)$_2$), 1.42 (9H, s, NC(CH_3)$_3$), 1.58 (3H, s, NC(CH_3)N), 2.11 (15H, s, C_5(CH_3)$_5$), 3.14 (2H, sept, J = 6.5 Hz, CH(CH_3)$_2$).

Cp*Mo[N(^{i}Pr)C(Me)N(^{i}Pr)](N^tBu) (80)

A -30 ºC solution of lithium *tert*-butyl amide (11.2 mg, 0.014 mmol) in 10 mL of Et_2O was added dropwise to a -30 ºC solution of **48** (30 mg, 0.07 mmol). The solution

was allowed to warm to room temperature and stirred for 1 h to give a red colored solution. Volatiles were removed *in vacuo* to give a red solid. The crude product was dissolved in pentane, passed through a pad of Cellite in the tip of a pipette, and volatiles were removed *in vacuo*. The red solid was dissolved in minimal acetonitrile and cooled to -30 ºC to give dark red crystals of **80** (10.4 mg, yield = 35%). Anal. Calc'd for $Mo_1N_3C_{22}H_{41}$: C, 59.56; H, 9.32; N, 9.48; Found: C, 59.63; H, 9.21; N, 9.44. ^{1}H NMR (400 MHz, benzene-d_6): 1.02 (6H, d, J = 6.4 Hz, CH(CH_3)$_2$), 1.20 (6H, d, J = 6.4 Hz, CH(CH_3)$_2$), 1.43 (9H, s, NC(CH_3)$_3$), 1.61 (3H, s, NC(CH_3)N), 1.61 (15H, s, C_5(CH_3)$_5$), 3.17 (2H, sept, J = 6.4 Hz, CH(CH$_3$)$_2$).

Cp*W[N(^{i}Pr)C(Me)N(^{i}Pr)](κ^2-*O,C*-OCN^{t}Bu)(CN^{t}Bu) (81).

Tert-butyl isocyanide (41 µL, 0.38 mmol) was added dropwise to a solution of **63** (83 mg, 0.18 mmol) in 6 mL of toluene. The solution was stirred at room temperature for 1 h to produce a yellow-orange solution. Volatiles were removed *in vacuo* to give an orange colored oil. The crude product was dissolved in minimal pentane and cooled to – 30º C to produce red-orange crystals of **81** (91 mg, yield = 81%). Anal. Calc'd for $W_1O_1N_4C_{28}H_{45}$: C, 52.32; H, 7.85; N, 8.72; Found: C, 52.29; H, 7.80; N, 8.69. ^{1}H NMR (400 MHz, benzene-d_6): 1.11 (3H, d, J = 6.4 Hz, CH(CH_3)$_2$), 1.15 (3H, d, J = 6.4 Hz, CH(CH_3)$_2$), 1.16 (9H, s, CN(CH_3)$_3$), 1.26 (3H, d, J = 6.4 Hz, CH(CH_3)$_2$), 1.31 (3H, d, J = 6.4 Hz, CH(CH_3)$_2$), 1.68 (3H, s, NC(CH_3)N), 1.79 (9H, s, CN(CH_3)$_3$), 2.05 (15H, s, C_5(CH_3)$_5$), 3.35 (1H, sp, J = 6.4 Hz, CH(CH$_3$)$_2$), 3.71 (1H, sp, J = 6.4 Hz, CH(CH$_3$)$_2$), IR (KBr) $\nu_{isocyanide}$ = 2085 cm^{-1}, 2054 cm^{-1}; $\nu_{C=N}$ = 1622 cm^{-1}, 1603 cm^{-1}.

Cp*Mo[N(^{i}Pr)C(Me)N(^{i}Pr)](κ^2-*O,C*-OCN^{t}Bu)(CN^{t}Bu) (82)

Tert-butyl isocyanide (15 µl, 0.13 µmol) was added to a solution of **62** (54 mg, 13 µmol) in 5 mL of toluene. The solution was stirred at room temperature for 6 h to give an orange-brown solution. Volatiles were removed *in vacuo* to give a brown solid. The crude product was dissolved in pentane and filtered through a plug of Celite. The collected brown filtrate was concentrated and cooled to -30 C overnight to produce orange crystals of **82** (48 mg, yield = 64%). Anal. calc'd for $C_{28}H_{50}N_4MoO$: C, 60.61; H, 9.09; N, 9.94; Found: C, 60.87; H, 9.34; N, 9.94. ^{1}H NMR (400 MHz, benzene-d_6): 1.10 (9H, s, OCNC(CH_3)$_3$), 1.13 (3H, d, J = 6.4 Hz, CH(CH_3)$_2$), 1.17 (3H, d, J = 6.4 Hz, CH(CH_3)$_2$), 1.21 (3H, d, J = 6.4 Hz, CH(CH_3)$_2$), 1.30 (3H, d, J = 6.4 Hz, CH(CH_3)$_2$), 1.74 (3H, s, N_2CCH_3), 1.78 (9h, s, CNC(CH_3)$_3$), 1.91 (15H, s, C_5(CH_3)$_5$), 3.31 (1H, sp, J = 6.4 Hz, CH(CH$_3$)$_2$), 3.74 (1H, sp, J = 6.4 Hz, CH(CH$_3$)$_2$). IR (KBr) $\nu_{isocyanide}$ = 2112 cm^{-1}; $\nu_{C=N}$ = 1628 cm^{-1}.

Cp*W[N(^{i}Pr)C(Me)N(^{i}Pr)](κ^2-*O,C*-CO_2)(CO) (83)

A solution of **63** (29 mg, 0.061 mmol) in 1.5 mL of pentane was transferred into a J Young NMR tube. The headspace of the J Young NMR tube was evacuated and charged with carbon monoxide (10 psi) at room temperature. The J Young NMR tube was left at room temperature for 4 days to allow product crystallization. The mother liquor was decanted from the J Young tube to give bright orange crystals of **83** (19 mg, yield = 59%). Anal. Calc'd for $W_1O_3N_2C_{20}H_{32}$: C, 45.11; H, 6.06; N, 5.26; Found: C,

45.10; H, 6.02; N, 5.31. ^{1}H NMR (400 MHz, benzene-d_6): 0.94 (3H, d, J = 6.4 Hz, CH(CH_3)$_2$), 1.08 (3H, d, J = 6.7 Hz, CH(CH_3)$_2$), 1.13 (3H, d, J = 6.7 Hz, CH(CH_3)$_2$), 1.24 (3H, d, J = 6.4 Hz, CH(CH_3)$_2$), 1.54 (3H, s, NC(CH_3)N), 1.81 (15H, s, C$_5$(CH_3)$_5$), 3.30 (1H, sp, J = 6.7 Hz, CH(CH$_3$)$_2$), 3.54 (1H, sp, J = 6.4 Hz, CH(CH$_3$)$_2$). ^{13}C{^{1}H} NMR (125.6 MHz, benzene-d_6): 207.8 (W(*C*O), $^{1}J_{13C\text{-}183W}$ = 31.4 Hz, $^{2}J_{13C\text{-}13C}$ = 3.6 Hz), 229.4 (W(η^2-*C*O$_2$), $^{1}J_{13C\text{-}183W}$ = 67.8 Hz, $^{2}J_{13C\text{-}13C}$ = 3.6 Hz).IR (KBr) $\nu_{C=O}$ =1686 cm^{-1}; $\nu_{C\equiv O}$ = 1952 cm^{-1}.

Cp*W[N(i Pr)C(Me)N(i Pr)](*κ*^{2}-*C,N*-OCNSiMe$_3$)(CO) (86)

A solution of **65** (50 mg, 0.089 mmol) in 6 mL of toluene was transferred to a storage tube with a teflon valved stopper. The headspace of the storage tube was evacuated and the tube was charged with carbon monoxide (5 psi). The reaction mixture was stirred at room temperature for 14 h to produce a bright orange colored solution. Volatiles were removed *in vacuo* to give a bright orange solid. The crude product was dissolved in pentane and filtered through a dry pad of Kimwipe placed in a glass pipette tip. The collected orange filtrate was concentrated and cooled to -30 °C to produce bright orange crystals of **86** (45 mg, yield = 74%). Anal. calc'd for $W_1Si_1O_2N_3C_{21}H_{41}$: C, 46.09; H, 7.55; N, 7.67; Found: C, 45.79; H, 7.35; N, 7.63. ^{1}H NMR (400 MHz, benzene-d_6): 0.42 (9H, s, Si(CH_3)$_3$), 0.89 (3H, d, J = 6.4 Hz, CH(CH_3)$_2$), 0.98 (3H, d, J = 6.4 Hz, CH(CH_3)$_2$), 1.02 (3H, d, J = 6.4 Hz, CH(CH_3)$_2$), 1.23 (3H, d, J = 6.4 Hz, CH(CH_3)$_2$), 1.48 (3H, s, NC(CH_3)N), 1.85 (15H, s, C$_5$(CH_3)$_5$), 3.19 (1H, sp, J = 6.4 Hz, CH(CH$_3$)$_2$), 3.60 (1H, sp, J = 6.4 Hz, CH(CH$_3$)$_2$). ^{13}C{^{1}H} NMR (125.6 MHz, d^6-benzene): 209.7 ($^{1}J_{13C\text{-}183W}$ = 23.0 Hz, W(*κ*^{2}-*C,N*-O*C*NSiMe$_3$), 228.6 ($^{1}J_{13C\text{-}183W}$ = 68.0 Hz, W(*C*O)). IR (KBr) $\nu_{C\equiv O}$ = 1937 cm^{-1}; $\nu_{C=O}$ = 1653 cm^{-1}.

Cp*Mo[N(^{i}Pr)C(Me)N(^{i}Pr)](NCMe)(CO) (88)

A solution of **52** (29.8 mg, 0.0390 mmol) in 0.5 mL of benzene was transferred into a J Young tube. Twenty equivalents of acetonitrile (41 ul, 0.79 mmol) were added to the J Young tube with a microsyringe and the headspace of the tube was evacuated and charged with CO (~1 atm). The contents of the tube were shaken and reacted at 25 ºC for 8 h to give a red colored solution. Volatiles were removed *in vacuo* to give a red residue. The crude product was washed with pentane, dissolved in toluene and filtered through a dry pad of Celite in the tip of a pipette. The dark red filtate was concentrated and cooled to -30 °C to give red crystals of **88** (17.6 mg, yield = 52%). Anal. calc'd for $C_{21}H_{35}N_3MoO$: C, 57.11; H, 7.99; N, 9.52; Found: C, 56.73; H, 7.94; N, 9.52. ^{1}H NMR (400 MHz, benzene-d_6): 1.02 (3H, d, J = 6.5 Hz, CH(CH_3)$_2$), 1.08 (3H, d, J = 6.5 Hz, CH(CH_3)$_2$), 1.15 (3H, s, NCCH_3), 1.36 (3H, d, J = 6.5 Hz, CH(CH_3)$_2$), 1.39 (3H, d, J = 6.5 Hz, CH(CH_3)$_2$), 1.75 (3H, s, NC(CH_3)N), 1.81 (15H, s, C$_5$(CH_3)$_5$), 3.73 (1H, sept, J = 6.5 Hz, CH(CH$_3$)$_2$), 3.84 (1H, sept, J = 6.5 Hz, CH(CH$_3$)$_2$). IR (KBr) $\nu_{C\equiv O}$ = 1766 cm^{-1}; $\nu_{C\equiv N}$ = 2244 cm^{-1}.

{Cp*W[N(^{i}Pr)C(Me)N(^{i}Pr)](NSiMe$_3$)} {B[3,5-(CF$_3$)$_2$C$_6$H$_3$]$_4$} (89)

A solution of {Cp$_2$Fe} {B[3,5-(CF$_3$)$_2$C$_6$H$_3$]$_4$} (132 mg, 0.126 mmol) in 10 mL of Et$_2$O was cooled to -30 ºC and added dropwise to a -30 ºC solution of **65** (76 mg, 0.126 mmol) in 10 mL of Et$_2$O over a period of 10 m to give a dark purple colored solution. Volatiles were removed *in vacuo* to concentrate the solution. Pentane was added to the concentrated solution and the solution was cooled to -30 ºC to give a dark purple powder. The crude product was washed with additional -30 ºC pentane, dissolved in minimal Et$_2$O and cooled to -30 ºC to give dark purple crystals of **89** (157 mg, yield = 80%). Anal. Calc'd for $W_1N_3Si_1B_1C_{53}H_{53}F_{24}$: C, 45.10; H, 3.79; N, 2.98; Found: C, 45.22; H, 4.00; N, 3.02. (**note: Complex **89** is paramagnetic with diagnostic resonances observed by ^{1}H NMR in chlorobenzene-d_5.)

Cp*W[N(^{i}Pr)C(Me)N(^{i}Pr)](CO)(κ^2-*C,N*-OCN^{t}Bu) (90)

A solution of **79** (38 mg, 0.072 mmol) in 6 mL of toluene was transferred into a storage tube with a teflon valved stopper. The headspace of the storage tube was evacuated and charged with carbon monoxide (16 psi). The tube contents were stirred at room temperature for 3 d with the removal of volatiles *in vacuo* giving a red oil. The oil was quickly transferred using Et_2O into a vial and volatiles were immediately removed *in vacuo*. The red oil was dissolved in minimal pentane and crystallized at -30 ºC to give a mixture of red crystals of **79** and **90** (16 mg). (Note: ^{1}H NMR resonances for **90** were assigned on the basis of the observed thermally reversible equilibrium m with **79** in the presence of carbon monoxide.) ^{1}H NMR (400 MHz, benzene-d_6): 0.91 (6H, d, J = 6.7 Hz, CH(CH_3)$_2$), 1.14 (6H, br, CH(CH_3)$_2$), 1.42 (3H, s, NC(CH_3)N), 1.49 (9H, s, NC(CH_3)$_3$), 1.88 (15H, s, C$_5$(CH_3)$_5$), 3.29 (2H, br, CH(CH$_3$)$_2$). ^{13}C{^{1}H} NMR (125.6 MHz, d^8-*toluene*, -70 ºC): 195.3 ($^1J_{13C\text{-}183W}$ = 15.5 Hz, $^2J_{13C\text{-}13C}$ = 1.8 Hz, W(κ^2-*C,N*-O*C*N^{t}Bu)), 228.4 ($^1J_{13C\text{-}183W}$ = 69.4 Hz, $^2J_{13C\text{-}13C}$ = 1.8 Hz, W(*C*O)). IR (KBr) $\nu_{C\equiv O}$ = 1921 cm^{-1}, 1936 cm^{-1}; $\nu_{C=O}$ = 1668 cm^{-1}.

Cp*W[N(^{i}Pr)C(Me)N(^{i}Pr)](N)(OSiMe$_3$) (93)

A solution of **65** (272 mg, 0.497 mmol) in 8 mL of pentane was transferred into a storage tube with a teflon valved stopper. The headspace of the storage tube was evacuated and the tube was charged with nitrous oxide (15 psi). The storage tube contents were stirred at room temperature for 9 d to give a tan-colored solution. Volatiles were removed *in vacuo* to give a pale yellow solid. The crude product was dissolved in minimal pentane and cooled to -30 ºC to give white crystals of **93** (278 mg, yield = 99%). Anal. Calc'd for $C_{21}H_{41}N_3O_1Si_1W_1$: C, 44.75; H, 7.34; N, 7.46; Found: C, 44.86; H, 7.09; N, 7.27. ^{1}H NMR (400 MHz, benzene-d_6): 0.62 (9H, s, $^2J_{1H\text{-}183W}$ = 3.0 Hz, Si(CH_3)$_3$), 0.94 (3H, d, J = 6.9 Hz, CH(CH_3)$_2$), 1.07 (3H, d, J = 6.9 Hz, CH(CH_3)$_2$), 1.34 (3H, d, J = 6.9 Hz,

$CH(CH_3)_2$), 1.46 (3H, d, J = 6.9 Hz, $CH(CH_3)_2$), 1.58 (3H, s, $NC(CH_3)N$), 1.98 (15H, s, $C_5(CH_3)_5$), 3.67 (1H, sept, J = 6.9 Hz, $CH(CH_3)_2$), 4.11 (1H, sept, J = 6.9 Hz, $CH(CH_3)_2$).

{Cp*W[N(ⁱPr)C(Me)N(ⁱPr)](NCH$_3$)(OSiMe$_3$)}I (94)

Methyl iodide (6 µL, 0.10 mmol) was added dropwise to a solution of **93** (28 mg, 0.050 mmol) in 4 mL of pentane. The solution was stirred at room temperature for 3 h to give a pale yellow colored solution. Volatiles were removed *in vacuo* to give a fine white solid. The crude product was dissolved in minimal THF and crystallized from a mixture of THF and Et_2O at – 30 ºC to give fine white crystals of **94** (33 mg, yield = 94%). Anal. Calc'd for $C_{22.75}H_{44.75}I_1N_3O_1Si_1W_1$: C, 38.20; H, 6.31; N, 5.88; Found: C, 38.07; H, 6.32; N, 5.71. ^{1}H NMR (400 MHz, benzene-d_6): 0.03 (9H, s, $Si(CH_3)_3$), 0.79 (3H, d, J = 6.9 Hz, $CH(CH_3)_2$), 0.81 (3H, d, J = 6.9 Hz, $CH(CH_3)_2$), 1.23 (3H, d, J = 6.9 Hz, $CH(CH_3)_2$), 1.59 (3H, d, J = 6.9 Hz, $CH(CH_3)_2$), 1.70 (3H, s, $NC(CH_3)N$), 2.04 (15H, s, $C_5(CH_3)_5$), 3.48 (1H, sept, J = 6.9 Hz, $CH(CH_3)_2$), 4.45 (1H, sept, J = 6.9 Hz, $CH(CH_3)_2$), 4.93 (3H, $J^2_{1H\text{-}183W}$ = 3.8 Hz, $WN(CH_3)$).

Cp*Mo[N(ⁱPr)C(Me)N(ⁱPr)](N)(OSiMe$_3$) (95)

Trimethylsilyl azide (18.6 uL, 0.141 mmol) was added to a solution of **64** (49.8 mg, 0.128 mmol) in 2 mL of toluene and stirred at room temperature for 16 h to give an orange colored solution. Volatiles were removed *in vacuo* to give an orange oil. The crude product was dissolved in pentane and cooled to –30 ˚C to give orange crystals of **95**

(25.7 mg, yield = 42%). Anal. Calc'd for $C_{21}H_{41}N_3O_1Si_1Mo_1$: C, 53.03; H, 8.69; N, 8.84; Found: C, 52,82; H, 8.49; N, 8.73. ^{1}H NMR (400 MHz, benzene-d_6): 0.61 (9H, s, Si(CH_3)$_3$), 0.99 (3H, d, J = 6.8 Hz, CH(CH_3)$_2$), 1.08 (3H, d, J = 6.8 Hz, CH(CH_3)$_2$), 1.37 (3H, d, J = 6.9 Hz, CH(CH_3)$_2$), 1.43 (3H, d, J = 6.9 Hz, CH(CH_3)$_2$), 1.62 (3H, s, NC(CH_3)N), 1.88 (15H, s, C$_5$(CH_3)$_5$), 3.62 (1H, sept, J = 6.8 Hz, CH(CH$_3$)$_2$), 4.01 (1H, sept, J = 6.9 Hz, CH(CH$_3$)$_2$).

Cp*Mo[N(^{i}Pr)C(Me)N(^{i}Pr)](N)(N$_3$) (96)

Volatiles for the mother liquor from the synthesis of **95** removed *in vacuo*. The crude material was dissovled in minimal Et_2O and cooled to -30 ˚C to give a brown amorphous solid (4.1 mg, yield = 7%) whose crude ^{1}H NMR corresponded to the reaction product **96**. This solid was subsequently analyzed by ESI-MS to identify the molecular formula of the primary product as $C_{18}H_{32}N_6Mo_1$. ^{1}H NMR (400 MHz, benzene-d_6): 1.02 (3H, d, J = 6.6 Hz, CH(CH_3)$_2$), 1.18 (3H, d, J = 6.6 Hz, CH(CH_3)$_2$), 1.30 (3H, d, J = 7.0 Hz, CH(CH_3)$_2$),1.37 (3H, d, J = 7.0 Hz, CH(CH_3)$_2$), 1.50 (3H, s, NC(CH_3)N), 1.83 (15H, s, C$_5$(CH_3)$_5$), 3.42 (1H, sept, J = 6.6 Hz, CH(CH$_3$)$_2$), 3.54 (1H, sept, J = 7.0 Hz, CH(CH$_3$)$_2$).

Reaction of 79 with N_2O for Synthesis of Cp*W[N(^{i}Pr)C(Me)N(^{i}Pr)](N^{t}Bu)(O) (97)

A solution **79** (5 mg, 0.09 mmol) in 0.5 mL of toluene-d_8 was transferred into a J Young tube. The headspace of the J Young tube was evacuated and charged with nitrous oxide (10 psi). Contents of the J Young tube were reacted at room temperature for 40 h and

subsequently heated at 60 ˚C for 16 h to give a yellow solution with progress of the reaction monitored periodically by ^{1}H NMR. ^{1}H NMR (400 MHz, toluene-d_8): 1.23 (6H, d, J = 6.6 Hz, CH(CH_3)$_2$), 1.31 (6H, d, J = 6.6 Hz, CH(CH_3)$_2$), 1.35 (9H, s, C(CH_3)$_3$), 1.59 (3H, s, NC(CH_3)N), 2.02 (15H, s, C$_5$(CH_3)$_5$), 3.63 (2H, sept, J = 6.6 Hz, CH(CH$_3$)$_2$).

Cp*W[N(^{i}Pr)C(Me)N(^{i}Pr)](O)$_2$ (98)

A solution of **63** (57 mg, 0.12 mmol) in 4 mL of pentane was stirred at room temperature with manganese dioxide (31 mg, 0.36 mmol) for 4 h to give an orange-yellow solution with suspended black particles. The suspension was passed through a Kimwipe in the tip of a pipette to remove the solids. The resulting orange filtrate was concentrated to 5 mL *in vacuo* and an additional amount of manganese dioxide (31 mg, 0.36 mmol) was added to the solution. The solution was pipetted up and down for 10 m to give a clear yellow solution containing black suspended particles. The suspension was passed through a Kimwipe in the tip of a glass pipette to give a pale yellow filtrate. Volatiles were removed *in vacuo* to give a pale yellow solid. The crude product was dissolved in minimal pentane and cooled to -30 ºC to give colorless crystals of **98** (43 mg, yield = 73%). Anal. Calc'd for $C_{18}H_{32}N_2O_2W_1$: C, 43.89; H, 6.55; N, 5.69; Found: C, 44.10; H, 6.20; N, 5.60. ^{1}H NMR (400 MHz, benzene-d_6): 1.20 (12H, d, J = 6.7 Hz, CH(CH_3)$_2$), 1.47 (3H, s, NC(CH_3)N), 1.99 (15H, s, C$_5$(CH_3)$_5$), 3.67 (1H, sept, J = 6.7 Hz, CH(CH$_3$)$_2$).

{Cp*Mo[N(^{i}Pr)C(Me)N(^{i}Pr)](μ-N)}$_2$ (99)

Sodium amalgam (0.5% w/w) (2.223 g, 0.4830 mmol) was added to a -30 ˚C solution of **103** (185 mg, 0.439 mmol) in 15 mL of a 1:1 mixture of THF and Et_2O. The solution was allowed to warm to room temperature and stirred for 16 h to give a black-brown colored solution. Volatiles were removed *in vacuo* to give a brown-black solid. The crude product was dissolved in pentane and passed through Cellite in the tip of a pipette. The black filtrate was concentrated and cooled to -30 ˚C to give black crystals of **99** (79 mg, yield = 47%). Anal. Calc'd for $C_{36}H_{64}N_6Mo_2$: C, 55.93; H, 8.35; N, 10.88; Found: C, 55.98; H, 8.35; N, 10.72. UV (methylcyclohexane) λ (nm) (ε): 583 (705), 453 (1,455), 371 (2,459). (Note: Complex **99** is paramagnetic with diagnostic resonances observed by ^{1}H NMR in benzene-d_6.)

{Cp*W[N(^{i}Pr)C(Me)N(^{i}Pr)](μ-N)}$_2$ (100)

Sodium amalgam (0.5% w/w) (1.139 g, 0.2480 mmol) was added to a -30 ˚C solution of **104** (120 mg, 0.235 mmol) in 15 mL of Et_2O. The solution was allowed to warm to room temperature and stirred for 16 h to give a black-brown colored solution. Volatiles were removed *in vacuo* to give a brown-black solid. The crude product was dissolved in toluene and passed through Cellite in the tip of a pipette. Volatiles were removed *in vacuo* and the resulting solid was dissolved in a mixture of THF and Et_2O and cooled to -30 ˚C to give black crystals of **104** (73 mg, yield = 65%). Anal. Calc'd for $C_{36}H_{64}N_6W_2$: C, 45.56; H, 6.80; N, 8.86; Found: C, 45.77; H, 6.63; N, 8.65. ^{1}H NMR (400 MHz, benzene-d_6): 1.34 (6H, d, J = 6.4 Hz, CH(CH_3)$_2$), 1.37 (6H, d, J = 6.4 Hz, CH(CH_3)$_2$), 1.75 (3H, br, NC(CH_3)N), 2.02 (15H, s, C$_5$(CH_3)$_5$), 3.65 (2H, br, CH(CH$_3$)$_2$). UV (methylcyclohexane) λ (nm) (ε): 446 (1,979), 336 (6,698), 290 (10,859).

Cp*Mo[N(^{i}Pr)C(Me)N(^{i}Pr)](N)Cl (103)

Trimethylsilyl azide (0.081 mL, 0.62 mmol) was added to a solution of **48** (228 mg, 0.515 mmol) in 15 mL of toluene and stirred at room temperature for 18 h to give a yellow-brown solution. Volatiles were removed *in vacuo* to give a yellow-brown solid. The crude product was dissolved in toluene and fltered through a Kimwipe in the tip of a glass pipette. The yellow-brown filtrate was concentrated and cooled to -30 ˚C to give yellow crystals of **103** (195 mg, yield = 90%). Anal. Calc'd for $C_{18}H_{32}N_3Cl_1Mo_1$: C, 51.23; H, 7.65; N, 9.96; Found: C, 51.33; H, 7.49; N, 10.01. ^{1}H NMR (400 MHz, benzene-d_6): 1.19 (3H, d, J = 6.7 Hz, CH(CH_3)$_2$), 1.25 (3H, d, J = 6.7 Hz, CH(CH_3)$_2$), 1.34 (3H, d, J = 6.7 Hz, CH(CH_3)$_2$), 1.44 (3H, d, J = 6.7 Hz, CH(CH_3)$_2$), 1.60 (3H, s, NC(CH_3)N), 1.89 (15H, s, C$_5$(CH_3)$_5$), 3.67 (1H, sept, J = 6.7 Hz, CH(CH$_3$)$_2$), 3.69 (1H, sept, J = 6.7 Hz, CH(CH$_3$)$_2$.

Cp*W[N(^{i}Pr)C(Me)N(^{i}Pr)](N)Cl (104)

Trimethylsilyl azide (0.20 mL, 1.50 mmol) was added to a solution of **49** (528 mg, 0.994 mmol) in 15 mL of toluene and stirred at room temperature for 1 h to give a dark green solution. Volatiles were removed *in vacuo* and to give a pale green solid. The crude product was dissolved in toluene and filtered through a Kimwipe in the tip of a glass pipette. The dark green filtrate was concentrated and cooled to -30 ˚C to give white crystals of **104** (484 mg, yield = 96%). Anal. Calc'd for $C_{18}H_{32}N_3Cl_1W_1$: C, 42.39; H, 6.33; N, 8.24; Found: C, 42.60; H, 6.10; N, 8.27. ^{1}H NMR (400 MHz, benzene-d_6): 1.12 (3H, d, J = 6.8 Hz, CH(CH_3)$_2$), 1.16 (3H, d, J = 6.8 Hz, CH(CH_3)$_2$), 1.30 (3H, d, J = 6.8

Hz, CH(CH_3)$_2$), 1.48 (3H, d, J = 6.8 Hz, CH(CH_3)$_2$), 1.53 (3H, s, NC(CH_3)N), 2.00 (15H, s, C$_5$(CH_3)$_5$), 3.76 (1H, sept, J = 6.8 Hz, CH(CH$_3$)$_2$), 3.85 (1H, sept, J = 6.8 Hz, CH(CH$_3$)$_2$).

{Cp*W[N(^{i}Pr)C(Me)N(^{i}Pr)]}$_2$(μ-η^1:η^1-N$_2$) {B[3,5-(CF$_3$)$_2$C$_6$H$_3$]$_4$}$_2$ (105)

A –30 ˚C solution of {Cp$_2$Fe} {B[3,5-(CF$_3$)$_2$C$_6$H$_3$]$_4$} (135 mg, 0.129 mmol) in 10 mL of Et$_2$O was added dropwise to a –30 ˚C solution of **52** (61 mg, 0.064 mmol) in 10 mL of Et$_2$O over a period of 5 m. The solution was allowed to warm to room temperature and stirred for 1 h to give a black suspension. The suspension was concentrated *in vacuo* and washed with -30 ˚C pentane. The crude product was dissolved in minimal THF and filtered through a Kimwipe. The filtrate was concentrated *in vacuo* and crystallized from a mixture of THF and Et$_2$O to give fine black crystals of **105** (152 mg, yield = 88%). Anal. Calc'd for C$_{100}$H$_{88}$N$_6$F$_{48}$B$_2$W$_2$: C, 44.87; H, 3.32; N, 3.14; Found: C, 44.81; H, 3.35; N, 3.36. (Note: Complex **105** is paramagnetic with diagnostic resonances observed by ^{1}H NMR in tetrahydrofuran-d_8.)

{Cp*W[N(^{i}Pr)C(Me)N(^{i}Pr)](μ-N)}$_2$ {B[3,5-(CF$_3$)$_2$C$_6$H$_3$]$_4$}$_2$ (106)

A –30 ˚C solution of {Cp$_2$Fe} {B[3,5-(CF$_3$)$_2$C$_6$H$_3$]$_4$} (79 mg, 0.075 mmol) in 10 mL of Et$_2$O was added dropwise to a –30 ˚C solution of **100** (35 mg, 0.037 mmol) in 20 mL of Et$_2$O over a period of 5 m. The solution was allowed to warm to room temperature and stirred for 30 m to give a brown suspension. The suspension was concentrated *in vacuo* and washed with -30 ˚C pentane. The crude product was dissolved in minimal THF and filtered through a Kimwipe. The filtrate was concentrated *in vacuo* and crystallized from

a mixture of THF and Et_2O to give fine black crystals of **106** (84 mg, yield = 85%). Anal. Calc'd for $C_{100}H_{88}N_6F_{48}B_2W_2$: C, 44.87; H, 3.32; N, 3.14; Found: C, 44.64; H, 3.30; N, 3.24. ^{1}H NMR (400 MHz, THF-d_8): 1.25 (6H, d, J = 6.6 Hz, CH(CH_3)$_2$), 1.44 (6H, d, J = 6.6 Hz, CH(CH_3)$_2$), 2.45 (3H, s, NC(CH_3)N), 2.57 (15H, s, C$_5$(CH_3)$_5$), 4.08 (2H, sept, J = 6.6 Hz, CH(CH$_3$)$_2$), 7.58 (8H, s, C$_6H_3$(CF$_3$)$_2$), 7.79 (16H, s C$_6H_3$(CF$_3$)$_2$).

Appendix: Yonke, B. Y.; Keane, A. J.; Zavalij, P. Y.; Sita, L. R. *Organometallics* 2012 *31*, 345-355

References

1) (a) Shi, Z.; Zhang, C.; Tang, C.; Jiao, N. *Chem. Soc. Rev.* **2012**, *41*, 3381-3430. (b) Punniyamurthy, T.; Velusamy, S.; Iqbal, J. *Chem. Rev.* **2005**, *105*, 2329-2363. (c) Sheldon, R. A.; Arends, I. W. C. E.; Brink, G.-J. T.; Dijksman, A. *Acc. Chem. Res.* **2002**, *35*, 774-781.

2) (a) Schlogl, R. *Angew. Chem. Int. Ed.* **2004**, *42*, 2004-2008. (b) Catalytic Ammonia Synthesis: Fundamentals and Practice, Jennings, J. R. Ed.; Plenum Press: New York, 1991.

3) Burgess, B. K.; Lowe, D. J. *Chem. Rev.* **1996**, *96*, 2983-3011.

4) (a) Lancaster, K. M.; Roemelt, M.; Ettenhuber, P.; Hu, Y.; Ribbe, M. W.; Neese, F.; Bergmann, U.; DeBeer, S. *Science*, **2011**, *334*, 974-977. (b) Spatzal, T.; Aksoyoglu, M.; Zhang, L.; Andrade, S. L. A.; Schleicher, E.; Weber, S.; Rees, D. C.; Einsle, O. *Science* **2011**, *334*, 940 (c) Einsle, O.; Tezcan, F. A.; Andrade, S. L. A.; Schmid, B.; Toshida, M.; Howard, J. B.; Rees, D. C. *Science*, **2002**, *297*, 1696-1700. (d) Howard, J. B.; Rees, D. C. *Chem. Rev.* **1996**, *96*, 2965-2982.

5) Eady, R. R. *Chem. Rev.* **1996**, *96*, 3013-3030.

6) Sellman, D.; Suuter, J. *Acc. Chem. Res.* **1997**, *30,* 460-469.

7) Demaison, J.; Hegelund, F.; Burger, H.; *J. Mol. Struct.* **1997**, *413*, 447-456.

8) Blomberg, M. R. A.; Siegbahn, P. E. M. *J. Am. Chem. Soc.* **1993**, *115*, 6908-6915.

9) Liu, H. I.; Burgess, B. K.; Natoli, C. R.; Filiponni, A.; Gavini, N.; Hedman, B.; Cicco, A. D.; Hodgson, K. O. *J. Am. Chem. Soc.* **1994**, *116*, 2418-2423.

10) Hidai, M.; Mizobe, Y. *Chem. Rev.* **1995**, *95*, 1115-11333.

11) (a) Hidai, M.; Mizobe, Y. *Pure Appl. Chem.* **2001,** *73*, 261-263. and references therein (b) Hidai, M *Coord. Chem. Rev.* **1999**, *185-186*, 99-108. and references therein

12) Shih, K.-Y.; Schrock, R. R.; Kempe, R. *J. Am. Chem. Soc.* **1994**, *116*, 8804-8805.

13) Schrock, R. R. *Acc. Chem. Res.* **2005**, *38*, 955-962. and reference therein

14) Gambarotta, S.; Scott, J. *Angew. Chem. Int. Ed.* **2004**, *43*, 5298-5308. and references therein

15) (a) Curley, J. J.; Cook, T. R.; Reece, S. Y.; Muller, P.; Cummins, C. C. *J. Am. Chem. Soc.* **2008**, *130*, 9394-9405. (b) Laplaza, C. E.; Cummins, C. C. *Science*. **1995**, *268*, 861-863.

16) (a) Laplaza, C. E.; Johnson, M. J. A.; Peters, J. C.; Odom, A. L.; Kim, E.; Cummins, C. C.; George, G. N.; Pickering, I. J. *J. Am. Chem. Soc.* **1996**, *118*, 8623-8638. (b) Cui, Q.; Musaev, D. G.; Svensson, M.; Sieber, S.; Morokuma, K. *J. Am. Chem. Soc.* **1995**, *117*, 12366-12367.

17) Laplaza, C. E.; Johnson, A. R.; Cummins, C. C. *J. Am. Chem. Soc.* **1996**, *118*, 709-710.

18) Curley, J. J.; Sceats, E. L.; Cummins, C. C. *J. Am. Chem. Soc.* **2006**, *128*, 14036-14037.

19) Fryzuk, M. D.; Love, J. B.; Rettig, S. J.; Young, V. G. *Science* **1997**, *275*, 1445-1447.

20) Fryzuk, M. D. *Acc. Chem. Res.* **2009**, *42*, 127-133. and references therein

21) Chirik, P. J. *Dalton Trans.* **2007**, 16-25. and references therein

22) (a) Pun, D.; Bradley, C. A.; Lobkovsky, E.; Keresztes, I.; Chirik, P. J. *J. Am. Chem. Soc.* **2008**, *130*, 14046-14047. (b) Pun, D.; Lobkovsky, E.; Chirik, P. J. *J. Am. Chem. Soc.* **2008**, *130*, 6047-6054.

23) (a) Knobloch, D. J.; Lobkovsky, E.; Chirik, P. J. *Nat. Chem.* **2010**, *2*, 30-35. (b) Knobloch, D. J.; Lobkovsky, E.; Chirik, P. J. *J. Am. Chem. Soc.* **2010**, *132*, 10553-10564.

24) (a) Kaminsky, W.; Kuelper, K.; Brintzinger, H. H.; Wild, F. R. W. P. *Angew. Chem. Int. Ed.* **1985**, *97*, 507-508. (b) Sinn, H.; Kaminsky, W.; Vollmer, H. J.; Woldt, R. *Angew. Chem. Int. Ed.* **1980**, *92*, 396-402. (c) Schwartz, J.; Labinger, J. A. *Angew. Chem. Int. Ed.* **1976**, *15*, 333-340.

25) (a) Sita, L. R. *Angew. Chem. Int. Ed.* **2009**, *48*, 2464-2472. (b) Zhang, Y.; Keaton, R. J.; Sita, L. R. *J. Am. Chem. Soc.***2003**, *125*, 8746-8747.

26) O'Connor, J. M.; Casey, C. P. *Chem. Rev.* **1987**, *87*, 307-318.

27) Edelmann, F. T; Anthony, F. H.; Mark, J. F. *Adv. Organomet. Chem.* **2008**, *57*, 183-352.

28) (a) Zinn, A.; Weller, F.; Dehnicke, K. *Z. Allg. Anorg. Chem.* **1991**, *594*, 106. (b) Fenske, D.; Baum, G.; Zinn, A.; Dehnicke, K. *Z. Naturforsch.* **1990**, *45b*, 1273. (c) Maier, S.; Hiller, W.; Strahle, J.; Ergezinger, C.; Dehnicke, K. *Z. Naturforsch.* **1988**, *43b*, 1628.

29) Duchateau, R.; van Wee, C. T.; Meetsma, A.; van Duijnen, P. T.; Teuben, J. H. *Organometallics*, **1996**, *15*, 2279-2290.

30) (a) Koterwas, L. A.; Fettinger, J. C.; Sita, L. R. *Organometallics*, **1999**, *18*, 4183-4190. (b) Wedler, M.; Knosel, F.; Edelmann, F. T.; Behrens, U. *Chem. Ber.* **1992**, *125*, 1313.

31) Babcock, J. R.; Sita, L. R. *J. Am. Chem. Soc.* **1998**, *120*, 5585-5586.

32) Hirotsu, M.; Fontaine, P. P. Zavalij, P. Y.; Sita, L. R. *J. Am. Chem. Soc.* **2007**, *129*, 12690-12692.

33) Hirotsu, M.; Fontaine, P. P.; Epshteyn, A. E.; Zavalij, P. Y.; Sita, L. R. *J. Am. Chem. Soc.* 9284-9285.

34) Fontaine, P.P.; Yonke, B. Y.; Zavalij, P. Y.; Sita, L. R. *J. Am. Chem. Soc.*, **2010**, *132*, 12273-12285.

35) (a) Mullins, S. M.; Duncan, A. P.; Bergman, R. G.; Arnold, J. *Inorg. Chem.* **2001**, *40*, 6952-6963. (b) Hagadorn, J. R.; Arnold, J. *Inorg. Chem.* **1997**, *36*, 2928-2929.

36) (a) Goncalves, I. S.; Romao, C. C. *J. Organomet. Chem.* **1995**, *48*, 155-161. (b) Ascenso, J. R.; de Azevedo, C. G.; Goncalves, I. S.; Herdtweck, E.; Moreno, D. S.; Pessanha, M.; Romao, C. C. *Organometallics*, **1995**, *14*, 3901-3919.

37) (a) Herrmann, W. A.; Menjón, B.; Herdtweck, E. *Organometallics* **1991**, *10*, 2134-2141. (b) Jones, W. D.; Kosar, W. P. *Organometallics* **1986**, *5*, 1823-1829. (c) Giamdomenico, C. M.; Hanau, L. H.; Lippard, S. J. *J. Organomet. Chem.* **1982**, *1*, 142-148.

38) Tolman, W. B. *Angew. Chem. Int. Ed.* **2010**, *49*, 1018-1024. and references therein

39) Iijima, K.; Shibata, S. *Chem. Lett.* **1972**, 1033-1036.

40) (a) Shin, J. H.; Churchill, D. G.; Bridgewater, B. M.; Pang, K.; Parkin, G. *Inorg. Chim. Acta* **2006**, *359*, 2942-2955. (b) Luo, L.; Lanza, G.; Fragala, I. L.; Stern, C.

L.; Marks, T. J. *J. Am. Chem. Soc.* **1998**, *120*, 3111-3122. (c) Bridgeman, A. J.; Davis, L.; Dixon, S. J.; Green, J. C.; Wright, I. N. *J. Chem. Soc. Dalton Trans.***1995**, 1023-1027. (d) Parkin, G. E.; Bercaw, J. E. *J. Am. Chem. Soc.* **1989**, *111*, 391-393. (e) Silavwe, N. D.; Bruce, M. R. M.; Philbin, C. E.; Tyler, D. R. *Inorg. Chem.* **1988**, *27*, 4669-4676. (f) Silavwe, N. D.; Chiang, M. Y.; Tyler, D. R. *Inorg. Chem.***1985**, *24*, 4219-4221. (g) Green, M. L. H.; Lynch, A. H.; Swanwick, M. G. *J. Chem. Soc. Dalton Trans*. **1972**, 1445-1447.

41) Alvarez, R.; Atwood, J. L.; Carmona, E.; Perez, P. J.; Poveda, M. L.; Rogers, R. D. *Inorg. Chem.* **1991**, *30*, 1493-1499.

42) (a) Ohnishi, T.; Seino, H.; Hidai, M.; Mizobe, Y. *J. Organomet. Chem.* **2005**, *690*, 1140-1146. (b) Hsu, S.-H.; Chang, J.-C.; Lai, C.-L.; Hu, C.-H.; Lee, H. M.; Lee, G.-H.; Peng, S.-M.; Huang, J.-H. *Inorg. Chem.***2004**, *43*, 6786-6792. (c) Fu, P.-F.; Khan, M. A.; Nicholas, K. M. *J. Organomet. Chem.* **1996**, *506*, 49-59. (d) Hall, K. A.; Mayer, J. M. *J. Am. Chem. Soc.* **1992**, *114*, 10402-10411. (e) Fu, P.-F.; Khan, M. A.; Nicholas, K. M. *Organometallics*, **1992**, *11*, 2607-2613. (f) Fu, P.-F.; Khan, M. A.; Nicholas, K. M. *Organometallics*, **1991**, *10*, 382-384. (g) Bryan, J. C.; Geib, S. J.; Rheingold, A. L.; Mayer, J. M. *J. Am. Chem. Soc.* **1987**, *109*, 2826-2828.

43) (a) Monillas, W. H.; Yap, G. P. A.; Theopold, K. H. *Inorg. Chim. Acta* **2011**, *369*, 103-119. (b) Moret, M.-E.; Peters, J.C. *Angew. Chem. Int. Ed.* **2011**, *50*, 2063-2067. (c) Mankad, N. P.; Muller, P.; Peters, J. C. *J. Am. Chem. Soc.* **2010**, *132*, 4083-4085. (d) Bart, S. C.; Lobkovsky, E.; Bill, E.; Chirik, P. J. *J. Am. Chem. Soc.* **2006**, *128*, 5302-5303. (e) Eckert, N. A.; Vaddadi, S.: Stoian, S.; Lachicotte, R. J.; Cundari, T. R.; Holland, P. L. *Angew. Chem. Int. Ed.* **2006**, *45*, 6868-6871. (f) Hanna, T. E.;

Keresztes, I.; Lobkovsky, E.; Bernskoetter, W. H.; Chirik, P. J. *Organometallics*, **2004**, *23*, 3448-3458.

44) Chou, C. Y.; Huffman, J. C.; Maatta, E. A. *J. Chem. Soc. Chem. Comm.* **1984**, 1184-1185.

45) Green, J. C.; Green, M. L. H.; James, T.; Konidaris, P. C.; Maunder, G. H.; Mountford, P. *J. Chem. Soc. Chem. Comm.* **1992**, 1361-1365.

46) Cordero, B.; Gomez, V.; Platero-Prats, A. E.; Reves, M.; Echeverria, J.; Cremades, E.; Barragan, F.; Alvarez, S. *Dalton Trans.* **2008**, 2832-2838.

47) (a) Mindiola, D. J. *Acc. Chem. Res.* **2006**, *39*, 813-821. and references therein (b) Morrison, D. L.; Rodgers, P. M.; Chao, Y.-W.; Bruck, M. A.; Grittini, C.; Tajima, T. L.; Alexander, S. J.; Rheingold, A. L.; Wigley, D. E. *Organometallics*, **1995**, *14*, 2435-2446. (c) Walsh, P. J.; Hollander, F. J.; Bergman, R. G. *Organometallics*, **1993**, *12*, 3705-3723. (d) Zambrano, C. H.; Profilet, R. D.; Hill, J. E.; Fanwick, P. E.; Rothwell, I. P. *Polyhedron*, **1993**, *12*, 689-709. (e) Cummins, C. C.; Schaller, C. P.; Van Duyne, G. D.; Wolczanski, P.T.; Chan, A. W. E.; Hoffman, R. *J. Am. Chem. Soc.* **1991**, *113*, 2985-2994. (f) Walsh, P. J.; Hollander, F. J.; Bergman, R. G. *J. Am. Chem. Soc.* **1988**, *110*, 8729-8731. (g) Cummins, C. C.; Baxter, S. M.; Wolczanski, P. T. *J. Am. Chem. Soc.* **1988**, *110*, 8731-8733.

48) Zhang, Y.; Kissuonko, D. A.; Fettinger, J. C.; Sita, L. R. *Organometallics*, **2003**, *22*, 21-23.

49) Keaton, R. J.; Koterwas, L. A.; Fettinger, J. C.; Sita, L. R. *J. Am. Chem. Soc.* **2002**, *124*, 5932-5933

50) Kissuonko, D. A.; Epshteyn, A.; Fettinger, J. C.; Sita, L. R. *Organometallics*, **2006**, *25*, 1076-1078.

51) Epshteyn, A.; Zavalij, P. Y.; Sita, L. R. *J. Am. Chem. Soc.* **2006**, *128*, 16052-16053.

52) (a) Hoffman, D. M.; Suh, S. *Chem. Comm.* **1993**, *8*, 714-715.(b) Cotton, F. A.; Matonic, J. H.; Murillo, C. A.; Wang, X.; *Bull. Soc. Chim. Fr.* **1996**, *133*, 711-720. (c) Culmsee, M.; Kurck, T.; Meyer, G.; Wickleder, M. S. *Z. Anorg. Allg. Chem.* **2001**, *627*, 1111-1112. (d) Radius, U.; Schorm, A.; Kairies, D.; Schmidt, S.; Moller, F.; Pritzkow, H.; Sundermeyer, J. *J. Organomet. Chem.* **2002**, *655*, 96-104.

53) (a) van der Vlugt, J. I. *Chem. Soc. Rev.* **2010**, *39*, 2302-2322. and references therein (b) Braun, T. *Angew. Chem. Int. Ed.* **2005**, *44,* 5012-5014. and reference therein

54) (a) Bolano, T.; Castarlenas, R.; Esteruelas, M. A.; Modrego, F. J.; Onate, E. *J. Am. Chem. Soc*. **2005**, *127*, 11184-11195. (b) Esteruelas, M. A.; Gonzalez, A. I.; Lopez, A. M.; Onate, E. *Organometallics,* **2003,** *22*, 414-425. (c) Jacobsen, H. *J. Organomet. Chem.* **2003**, *674*, 50-55. (d) Caulton, K. *J. Organomet. Chem.* **2001**, *617-618*, 56-64. (e) Bannwart, E.; Jacobsen, H.; Furno, F.; Berke, H. *Organometallics*, **2000**, *19*, 3605-3619.

55) Yin, X.; Moss, J. R. *Coord. Chem. Rev.* **1999**, *181*, 27-59.

56) Parmon, V. N.; Panov, G. I.; Uriarte, A.; Noskov, A. S. *Catal. Today* **2005**, *100*, 115-131.

57) (a) Heyduk, A.F.; Zarkesh, R. A.; Nguyen, A. I. *Inorg, Chem.* **2011**, *50*, 9849-9863. (b) Nguyen, A. I.; Zarkesh, R. A.; Lacy, D. C.; Thorson, M. K.; Heyduk, A. F. *Chem. Sci.,* **2011**, ***2***, 166-169. (c) Blackmore, K. J.; Lal, N. Ziller, J. W.; Heyduk, A. F. *Eur. J. Inorg. Chem.* **2009**, 735-743. (d) Blackmore, K. J.; Lal, N.; Ziller, J. W.;

Heyduk, A. F. *J. Am. Chem. Soc.* **2008**, *130*, 2728-2729. (e) Haneline, M. R.; Heyduk, A. F. *J. Am. Chem. Soc.* **2006**, *128*, 8410-8411. (f) Blackmore, K. J.; Ziller, J. W.; Heyduk, A. F. *Inorg. Chem.* **2005**, *44*, 5559-5561.

58) (a) Holm, R. H.; Solomon, E. I.; Majumdar, A.; Tenderholt, A. *Coord. Chem. Rev.* **2011**, *255*, 993-1015. (b) Donahue, J. P.; Goldsmith, C. R.; Nadiminti, U.; Holm, R.H. *J. Am. Chem. Soc.* **1998**, *120*, 12869-12881. (c) Lorber, C.; Donahue, J. P.; Goddard, C. A.; Norlander, E.; Holm, R. H. *J. Am. Chem. Soc.* **1998**, *120*, 8102-8112. (d) Holm, R. H. *Chem. Rev.* **1987** *87*, 1401-1449.

59) Earnshaw, A.; Greenwood, N. Chemistry of the Elements, 2nd Ed.; Butterworth-Heinemann: Burlington, MA, 1997.

60) (a) Braunstein, P.; Nobel, D. *Chem. Rev.* **1989**, *89*, 1927-1945. (b) Minzoni, F.; Pelizzi, C.; Predieri, G. *J. Organomet. Chem*. **1982**, *231*, C6-C8.

61) (a) T. J. Deming, B. M. Novak, *J. Am. Chem. Soc.* **1993**, *115*, 9101.(b) S. Nemeth, L. I. Simandi, *Inorg. Chim. Acta* **1982**, *64*, L21-L22. (c) S. Otsuka, A. Nakamura, Y. Tatsuno, *Chem. Commun*. **1967**, 836.

62) (a) Hall, K. A.; Mayer, J. M. *J. Am. Chem. Soc.* **1992**, *114*, 10402-10411. (b) Su, F.-M.; Cooper, C.; Geib, S. J.; Rheingold, A. L.; Mayer, J. M. *J. Am. Chem. Soc.* **1986**, *108*, 3545-3547.

63) (a) Shin, J. H.; Churchill, D. G.; Bridgewater, B. M.; Pang, K.; Parkin, G. *Inorg. Chim. Acta*, **2006**, *359*, 2942-2955. (b) Pilato, R. S.; Rubin, D.; Geoffroy, G. L.; Rheingold, A. L. *Inorg. Chem.* **1990**, *29*, 1986-1900.

64) Pilato, R. S.; Housmekerides, C. E.; Jernakoff, P.; Rubin, D.; Geoffroy, G. L. *Organometallics,* **1990**, *9*, 2333-2341.

65) (a) T.-F. Wang, C.-C. Hwu, C.-W. Tsai, K.-J. Lin, *Organometallics* **1997**, *16*, 3089-3090. (b) P.-F. Fu, M. A. Khan, K. M. Nicholas, *J. Organomet. Chem*. **1996**, *506*, 49-59. (c) P.-F. Fu,.M. A. Khan, K. M. Nicholas, *J. Am. Chem. Soc*. **1992**, *114*, 6579-6580.

66) (a) Kim, Y.; Rende, D. E.; Gallucci, J. D.; Wojcicki, A. *J. Organomet. Chem.* **2003**, *68*, 85-101. (b) Kim, Y.; Gallucci, J.; Wojcicki, A. *J. Am. Chem. Soc.***1990**, *112*, 8600-8602.

67) Reeds, J. P.; Yonke, B. L.; Zavalij, P. Y.; Sita, L. R. *J. Am. Chem. Soc.* **2011**, *133*, 18602-18605.

68) (a) Li, C.-S.; Sun, K.-S., Cheng, C.-H. *J. Chem. Soc. Dalton Trans.***1992**, 1025-1029. (b) Lee, J.-D.; Fang, W.-P.; Li, C.-S.; Cheng, C.-H. *J. chem. Soc. Dalton Trans.***1991**, 1923-1927.

69) Anastas, P. T.; Warner, J. C. Green Chemistry: Theory and Practice, Oxford University Press: New York, 1998.

70) Kent and Riegel's Handbook of Industrial Chemistry and Biotechnology, 11th ed.; Kent, J.A., Ed.; Springer Science: New York, 2007.

71) Broughton, E. *J. Environ. Health*, **2005**, *4*, 6.

72) Saunders, J. H.; Slocombe, R. J. *Chem. Rev.* **1948**, *43*, 203-218.

73) (a) Angelici, R. J. *J. Organomet. Chem.* **2008**, *693*, 847-856, and references therein. (b) Deming, T. J.; Novak, B. M. *J. Am. Chem. Soc.* **1993**, *115*, 9101-9111. (c) Deming, T. J.; Novak, B. M. *J. Am. Chem. Soc.* **1993**, *115*, 9101-9111. (d) Wu, J.; Fanwick, P. E.; Kubiak, C. P. *Organometallics*, **1987**, *6*, 1805-1807. (e) DeLaet, D. L.; Del Rosario, R.; Fanwick, P. E.; Kubiak, C. P. *J. Am. Chem. Soc.* **1987**, *109*,

754-758. (f) Nemeth, S.; Simandi, L. I. *Inorg. Chim*. *Acta.* **1982**, *64*, L21-L22. (g) Otsuka, S.; Nakamura, A.; Tatsuno, Y. *Chem. Comm.* **1967**, 836.

74) (a) Takemoto, S.; Kobayashi, T.; Ito, T.; Inui, A.; Karitani, K.; Katagiri, S.; Masuhara, Y.; Matsuzaka, H. Organometallics, **2011,** *30*, 2160-2172. (b) Laskowski, C. A.; Miller, A. J. M.; Hillhouse, G. L.; Cundari, T. R. *J. Am. Chem. Soc.* **2011**, *133*, 771-773. (c) Chomitz, W. A.; Arnold, J. *Chem. Comm.* **2008**, 3648-3650. (d) Shay, D. T.; Yap, G. P. A.; Zakharov, L. N.; Rheingold, A. L.; Theopold, K. H. *Angew. Chem. Int. Ed.* **2005**, 44*,* 1508-1510. (e) Kogut, E.; Wiencko, H. L.; Zhang, L.; Cordeau, D. E.; Warren, T. H. *J. Am. Chem. Soc.* **2005**, *127*, 11248-11249. (f) Hanna, T. E.; Keresztes, I.; Lobkovsky, E.; Bernskoetter, W. H.; Chirik, P. J. *Organometallics*, **2004**, *23*, 3448-3458. (g) Brown, S. D.; Betley, T. A.; Peters, J. C. *J. Am. Chem. Soc.* **2003**, *125*, 322-323. (h) Jenkins, D. M.; Betley, T. A.; Peters, J. C. *J. Am. Chem. Soc.* **2002**, *124*, 11238-11239. (i) Ge, Y. W.; Sharp, P. R. *Inorg. Chem.* **1992**, *31***,** 379-384. (j) Glueck, D. S.; Wu, J.; Hollander, F. J.; Bergman, R. G. *J. Am. Chem. Soc.* **1991**, *113*, 2041-2054. (k) Collman, J. P.; Kubota, M.; Vastine, F. D.; Sun, J. Y.; Kang, J. W. *J. Am. Chem. Soc.* **1968**, *90*, 5430-5437.

75) (a) Laskowski, C. A.; Hillhouse, G. L. *Organometallics,* **2009**, *28*, 6114-6120. (b) Cowley, R. E.; Eckert, N. A.; Elhaik, J.; Holland, P. L. *Chem. Comm*. **2009**, 1760-1762.

76) Braunstein, P.; Nobel, D. *Chem. Rev*. **1989**, *89*, 1927-1945.

77) Antinolo, A.; Carrillo-Hermosilla, F.; Otero, A.; Fajardo, M.; Garces, A.; Gomez-Sal, P.; Lopez-Mardomingo, C.; Martin, A.; Miranda, C. *J. Chem. Soc. Dalton. Trans.* **1998**, 59-65.

78) Mindiola, D. J.; Hillhouse, G. L. *Chem. Comm.*, **2002**, 1840-1841.

79) (a) Atagi, L. M.; Mayer, J. M. *Organometallics,* **1994**, *13*, 4794-4803. (b) Hall, K. A.; Mayer, J. M. *J. Am. Chem. Soc.* **1992.** *114*, 10402-10411. (c) Bryan, J. C.; Geib, S. J.; Rheingold, A. L.; Mayer, J. M. *J. Am. Chem. Soc.* **1987**, *109*, 2826-2828.

80) Dunn, S. C.; Hazari, N.; Cowley, A. R.; Green, J. C.; Mountford, P. *Organometallics*, **2006**, *25*, 1755-1770.

81) Nugent, W. A.; Mayer, J. M. Metal–Ligand Multiple Bonds: The Chemistry of Transition Metal Complexes Containing Oxo, Nitrido, Imido, Alkylidene, or Alkylidyne Ligands; Wiley-Interscience; New York, New York, 1988.

82) (a) Schomber, B. M.; Ziller, J. W.; Doherty, N. M. *Inorg. Chem.* **1991**, *30*, 4488-4490. (b) Hoffman, N. W. Prokopuk, N.; Robbins, M. J.; Jones, C. M.; Doherty, N. M. *Inorg. Chem* **1991**, *30*, 4177-4181. (c) Jones, C. M.; Chan, D. M.-T.; Calabrese, J.; Doherty, N. M. *J. Am. Chem. Soc.* **1988**, *110*, 8071-8075. (d) Doherty, N. M.; Critchlow, S. C. *J. Am. Chem. Soc.* **1987**, *109*, 7906-7908. (e) Doherty, N. M.; Critchlow, S. C. *J. Am. Chem. Soc.* **1987**, *109*, 7906-7908.

83) Chuit, C.; Corriu, J. P.; Reye, C.; Young, J. C. *Chem. Rev.* **1993**, *93*, 1371-1448.

84) (a) Ignatov, S. K.; Rees, N. H.; Merkoulov, A. A.; Dubberley, S. R.; Razuvaev, A. G.; Mountford, P.; Nikonov, G. I. *Chem. Eur. J.* **2008**, *14*, 296-310. (b) Nikonov, G. I.; Mountford, P.; Ignatov, S. K.; Green, J. C.; Leech, M. A.; Kuzmina, L. G.; Razzuvaev, A. G.; Rees, N. H.; Blake, A. J.; Howard, J. A. K.; Lemenovskii, D. A. *J. Chem. Soc. Dalton Trans.* **2001**, 2903-2915.

85) (a) Sorenson, K. L.; Lerchen, M. E.; Ziller, J. W.; Doherty, N. M. *Inorg. Chem.* **1992**, *31*, 2678-2679. (b) Jones, C. M.; Lerchen, M. E.; Church, C. J.; Schomber, B.

M.; Doherty, N. M. *Inorg. Chem.* **1990**, *29*, 1679-1682. (c) Burger, U.; Wannagat, U. *Monatsh. Chem.* **1963**, *94*, 761.

86) (a) Sharma, B.; Chen, S.-J.; Abbott, J. K. C.; Chen, X.-T.; Xue, Z.-L. *Inorg. Chem.* **2012**, *51*, 25-27. (b) Gountchev, T. I.; Tilley, T. D. *J. Am. Chem. Soc.* **1997**, *119*, 12831-12841.

87) Radius, U.; Sundermeyer, J.; Peters, K.; von Schnering, H.-G.; *Eur. J. Inorg. Chem.* **2001**, *6*, 1617-1623.

88) Eikey, R. A.; Abu-Omar, M. M. *Coord. Chem Rev.* **2003**, *243*, 82-124.

89) (a) Shin, J. H.; Churchill, D. G.; Bridgewater, B. M.; Pang, K.; Parkin, G. *Inorg. Chim. Acta* **2006**, *359*, 2942-2955. (b) Shin, J. H.; Savage, W.; Murphy, V. J.; Bonanno, J. B.; Churchill, D. G.; Parkin, G. *J. Chem. Soc. Dalton Trans.* **2001**, 1732-1753. (c) Shin, J. H.; Bridgewater, B. M.; Churchill, D. G.; Baik, M.-H.; Friesner, R. A.; Parkin, G. *J. Am. Chem. Soc.* **2001**, *123*, 10111-10112.

90) Henderson, W.; McIndoe, J. Mass Spectrometry of Inorganic and Organometallic Compounds; John Wiley & Sons; West Sussex, England, 2005.

91) Parkin, G.; Bercaw, J. E. *J. Am. Chem. Soc.***1989**, *111*, 391-393.

92) Walsh, R. *Acc. Chem. Res.* **1981**, *14*, 246-252.

93) (a) Hinrichsen, S.; Broda, H.; Gradert, C.; Soncksen, L.; Tuczek, *F. Annu. Rep. Prog. Chem., Sect. A: Inorg. Chem.,* **2012**, *108*, 17–47. (c) Shaver, M. P.; Fryzuk, M. D. *Adv. Synth. Cat.* **2003**, *345*, 1061-1076. (d) Fryzuk, M. D.; Johnson, S. A. *Coord Chem. Rev.* **2000**, *200-202*, 379-409. (e) Gambarotta, S. *J. Organomet. Chem.* **1995**, *500*, 117-126.

94) (a) Hoshino, K.; Inui, M.; Kitamura, T.; Kokado, H. *Angew. Chem. Int. Ed.* **2009**, *39*, 2409-2412. (b) Linnik, O. P.; Kisch, H. *Mendeleev Commun.* **2008**, *18*, 10-11.

(c) Rusina, O.; Linnik, O.; Eremenko, A.; Kisch, H. *Chem.-Eur. J.* **2003**, *9*, 561-565. (d) Schrauzer, G. N.; Strampach, N.; Hui, L. N.; Palmer, M. R.; Salehi, J. *Proc. Natl. Acad. Sci.* **1983**, *40*, 3873-3876. (e) Schrauzer, G. N.; Guth, T. D. *J. Am. Chem. Soc.* **1977**, *99*, 7189-7193.

95) Solari, E.; Da Silva, C.; Iacono, B.; Hesschenbrouck, J.; Rizzoli, C.; Scopelliti, R.; Floriani, C. *Angew. Chem. Int. Ed.* **2001**, *40*, 3907-3909.

96) (a) Brummer, J. G.; Crosby, G. A. *Inorg. Chem*. **1985**, *24*, 552-558. (b) Caruana, A.; Hermann, H.; Kisch, H. J. Organomet. Chem. **1980**, *187*, 349-359. (c) Caruana, A.; Kisch, H. *Angew. Chem. Int. Ed*. **1979**, *18*, 328.

97) Haddad, T. S.; Aistars, A.; Ziller, J. W.; Doherty N. M. *Organometallics*, **1993**, *12*, 2420-2422.

98) (a) Jutzi, P. *J. Organomet. Chem.* **1990**, *400*, 1-17. (b) Jutzi, P. *Pure Appl. Chem.* **1990**, *62*, 1035-1038. (c) Jutzi, P. *Adv. Organomet. Chem.* **1986**, *26*, 217-295. (d) Jutzi, P. *Chem. Rev.* **1986**, *86*, 983-996.

99) References for fluxional behavior of amidinate ligand: (a) Koterwas, L. A.; Fettinger, J. C.; Sita, L. R. *Organometallics*, **1999**, *18*, 4183-4190. (b) Stewart, P. J.; Blake, A. J.; Mountford, P. *Organometallics*, **1998**, *17*, 3271-3281. (c) Wedler, M.; Knosel, F.; Edelmann, F. T.; Behrens, U. *Chem. Ber*. **1992**, *125*, 1313-1318.

100) Kunkley, H.; Vogler, A. *Angew. Chem. Int. Ed.* **2010**, *49*, 1591-1593.

101) Vogler, A.; Kunkley, H. *Coord. Chem. Rev.* **1998**, *177*, 81-96.

102) Vogler, A.; Kunkley, H. *Coord. Chem. Rev.* **2001**, *211*, 223-233.

103) (a) LeSeur, R. J.; Buttolph, C.; Geiger, W. E. *Anal. Chem.* **2004**, *76*, 6395-6401. (b) LeSuer, R. J.; Geiger, W. E. *Angew. Chem. Int. Ed.* **2000**, *9*, 248-250.

104) Greco, G. E.; Schrock, R. R. *Inorg. Chem.* **2001**, *40*, 3861-3878.